Macroscopic Quantum Phenomena

A thesis submitted to the University of Waikato
for the degree of
Doctor of Philosophy in Physics
by

William John Munro

May 1994

Abstract

This thesis consists of two parts. Although both are concerned with macroscopic quantum phenomena, I choose to present the two parts quite separately.

Macroscopic Quantum Phenomena: Tests of Quantum Mechanics

The correctness of quantum mechanics has been verified in numerous situations. A particularly strong test of quantum mechanics was suggested by Bell, who showed that the predictions of all classical theories, based as they are on the assumptions of local realism, contradict those of quantum mechanics. Later work by Greenberger, Horne, and Zeilinger showed that the GHZ phenomena also contradicts all classical theories. Experimental tests of Bells inequality performed to date support quantum mechanics (No experimental test of the GHZ phenomenon has yet been attempted). However, such tests have been so far restricted to microscopic systems in the sense that one particle is at a detector at a time.

Our interest here in the first part of this thesis is in tests of quantum mechanics against local realistic theories in macroscopic or mesoscopic systems where there is a significant number of particles incident on each analyser. The states considered in the first two chapters are not simple quantum superpositions of macroscopically distinct states, but we nevertheless show how one can obtain tests of quantum mechanics in situations involving large numbers of particles. A more elementary macroscopic quantum state, and one in which the deviation from classical interpretations is striking, is the *Schrödinger Cat* state considered by Schrödinger in his famous "Schrödinger Cat" paradox. In Chapter Three we consider a scheme for generating such a state.

The Quantum Brownian Motion Master Equation

The second section of this thesis involves an examination of various aspects of the Quantum Brownian Motion Master Equation.

We begin with a discussion of the recent problem occurring from the study of the quantum Brownian motion (QBM) master equation, which can occur because the QBM master equation is not of the Lindblad form. We examine two specific examples, namely the damped free particle and the two level atom. More specifically, in the case of the evolution of a free particle, we show that the equation of motion for the Wigner function (which is exactly the same as the Fokker-Planck equation for classical Brownian motion) gives unphysical results if the initial position distribution is well localised. In the case of the two level atom we show that unphysical results can also occur even in the steady state.

The last chapter of the thesis involves using the quantum Brownian motion master equation to estimate the rate of diagonalisation of the off diagonal elements of a Fermion system. These elements contain the "quantum information" and hence knowledge of how long they exist can determine the type of model required to describe the semiconductor medium. Using a very simplistic approach we can show that there are two main time scales present and for normal parameters one of these is very small. If we neglect electron-electron scattering we can show that the the many electron system solution is simply a product of the one electron solutions.

Acknowledgements

First and foremost I am very grateful to my two supervisors Dr Margaret Reid and Professor Crispin Gardiner for their help, patience, and guidance throughout the last three years and before. I feel privileged to have worked with these people, whose knowledge and insight have inspired me.

The majority of this research in this thesis has taken place at the University of Waikato, but a large contribution has come from the University of Queensland in Australia. The discussions with Professor Peter Drummond, Dr Gerald Milburn, and Dr Howard Wiseman have proved invaluable.

At the University of Auckland,Professor Dan Walls, Dr Mathew Collett, and Dr Sze Tan must be thanked for there immensely beneficial discussions. At the University of Macquarie in Sydney, Dr Barry Sanders help and guidance is expressly appreciated

Thanks must also go to all physics students and staff, both past and present at the University of Waikato, for their help, encouragement, and friendship. Special thanks must be made to our secretary Heidi Eschmann and Chris Humphreys.

I thank the New Zealand Vice Chancellors Committee for its support through a Post Graduate Scholarship and a William Georetti Scholarship and to the School of Science and Information Technology Services for providing a job while this thesis was been written up.

The greatest thanks must go to my wife Tracey for her time, encouragement, and tolerance. Her constant support and willingness to help will always be much appreciated.

Contents

List of Figures

Chapter 1

Introduction

This thesis is divided into three distinct parts. The first two parts contain the main results of the thesis while the third part contains the conclusion and appendices. The first part of this thesis investigates macroscopic phenomena which have no classical description and may be used to differentiate quantum mechanics from classical mechanics. The second part investigates various aspects of the quantum Brownian motion master equation.

1.1 Macroscopic Quantum Phenomena: Tests of Quantum Mechanics

There has always been a keen interest in experiments which distinguish quantitatively between the predictions of quantum mechanics and classical theories. Experiments testing predictions of classical or local realistic theories, against quantum mechanics were originally suggested by Bell [1].

Since 1972 a series of experiments, of increasing precision and making use of various atomic sources and detection arrangements, have been carried out to test the Bell inequality. The first experimental test of the inequality was done by Freedman and Clauser [2] using a $3d4p^1P_1$ state of calcium that produces correlated photons in atomic decay. They found that a clear violation of the Bell inequality is possible and the results are in agreement with the quantum mechanical prediction. The most conclusive tests of Bell inequality to date using atomic sources were performed by Aspect et al [3–6]. It was suggested by Reid and Walls [7] and Horne and Zeilinger [8] that the correlated photon pairs produced in parametric down conversion could be used to demonstrate a violation of Bells inequality. Recent experiments by Alley and Shih [9], Ou and Mandel [10], and Rarity and Tapster [11] using the correlated photon pairs produced in parametric down conversion have observed nonlocal quantum correlations and violations of Bells inequality. However, objections to these conclusions have been raised. Where the efficiency of polarisers is high, the objection by realists have centred on the low efficiency of detectors for photons, which leaves open the possibility that the observed polarisation correlations may be the result of some process of enhancement in the detection process itself [12].

The original results of Bell and the experimental tests done so far have been concerned with microscopic systems as for example, the correlation between two spatially separated photons. In such systems most physicists feel confident of the correctness of quantum mechanics and accept that classical physical intuition (local realism) does not necessary apply to microscopic phenomena. The belief is that predictions of quantum mechanics become those of classical physics as the system becomes macroscopic. Thus we are still confident of the predictions of classical theories at this level and our view of the macroscopic world is one in which local realism holds.

Nevertheless there appears to be no fundamental reason why these non-classical features of quantum mechanics may not be generated on a macroscopic scale. There have been proposals to generate quantum superposition states of two macroscopically distinct states in SQUID rings [13] and also more recently, at least for mesoscopic states, in optical devices [14, 15]. So far there has been no experimental success in generating these states. In each of these cases there is an experimental signature which is used to indicate the existence or otherwise of a macroscopic quantum superposition state.

A problem with many such experimental designs which have been or may be suggested is that, although they support quantum theory against a particular classical theory, it is not often clear whether there are any other classical-type theories which could generate the same results. Our interest in the first part of this thesis is to suggest macroscopic or mesoscopic states predicted by quantum mechanics which, although not necessarily simple macroscopic superposition states, do at least show a clear quantitative contrast with all classical theories in that they violate Bells inequality. Such states have been suggested and discussed in an idealised sense previously by Drummond [16], Mermin [17], and Oliver and Stroud [18], who studied the photons emitted in cooperative, higher spin states and Rydberg atoms in a high Q cavity respectively. More recently Mermin [19] proposed a multiparticle extension of the tests of quantum mechanics versus classical theories suggested by Greenberger, Horne, and Zeilinger [20]. Here only one particle is detected at each detector/analyser. Unfortunately current experimental situations corresponding to these examples fall a long way short of being able to test quantum mechanics against classical theories. Thus for realistic experimental situations the distinction between quantum and classical theories vanishes, at least with respect to the particular test suggested originally by Bell. The question is whether this limit is a fundamental one with the consequence that these more extreme quantum effects are not realisable in any but the most microscopic of systems, or whether this is a limit merely imposed by today's technology. In this thesis we suggest the latter is true and propose an alternative method for generating the macroscopic quantum states, namely parametric amplification and parametric oscillation.

Appropriately, we begin, in chapter 2, by focussing our attention on the use of correlated photon number states produced through parametric down conversion to test quantum mechanics in situations where more than one photon is simultaneously incident on each analyser [16, 21, 22]. There is thus an equivalence to higher spin tests of quantum mechanics. Our calculations are models for extensions of the experiments of Shih and Alley [9], Ou and Mandel [10] and Rarity and Tapster [11]. Numerous Bell inequality tests of quantum theory for higher spin states have been formulated previously [17, 18, 23], but none have been realised experimentally to date.

Initially we consider the weak Bell inequalities where the normalisation is with respect to joint probabilities, rather than the marginal probabilities used in the strong inequalities. This is necessary in photocounting experiments because of the relatively poor efficiency associated with photon detection. The effect of poor efficiencies is particularly relevant in photon counting experiments where more than one photon is detected at a time.

In chapter 2 we consider previous and new formulations of the Bell inequalities as applied to correlated number states, comparing the quantum prediction for the degree of departure from classical predictions in each case. In the first instance we use a simple model interaction Hamiltonian to describe the basic quantum nature of the correlated photon states generated by down conversion. The effect of detection inefficiencies is explicitly modelled. We then present a more complete calculation of the field generated using an optical parametric oscillator, where the down conversion takes place inside an optical cavity. We consider this situation in some detail since the use of a cavity configuration may enable enhancement of the conversion efficiency for signal and idler photons of a particular mode.

Finally in this chapter we consider the situation where we can have high photodetection efficiencies, but poor resolution of the photon number due to electronic noise. This result is part of a preliminary investigation applicable to the recent experiment of Smithey et al [24], where quantum photon number correlations are measured between two macroscopic pulses produced by parametric down conversion. Here the use of photodiodes implies a high detection efficiency. This regime is of particular interest since a strong test of the Bell inequality which is not limited by auxiliary assumptions [25, 26] might be possible. However the new limitation provided by electronic noise which will limit the resolution of photon number detected must be considered.

We point out that the multi-particle tests described here are different to those proposed recently by Greenberger et al [19, 20, 27] and Mermin [28]. In their case the particles are spatially separated so that there is still only one particle incident on each analyser. An extension of the Greenberger-Horne-Zeilinger result as applied to situations of more than one photon per analyser has been considered by us [29] previously and provides the foundation for chapter 3.

In chapter 3 we present a formulation of the *all or nothing* Greenberger-Horne-Zeilinger paradox in terms of boson fields, and suggest how the paradox might be realised using a correlated photon triplet. The suggested experiment might be readily extended to test for the first time, to our knowledge, quantum mechanics against local realism for situations of more than one quanta per wavepacket incident on each measurement apparatus. Thus we have another potential test of macroscopic quantum mechanics.

In a realistic experimental situation the ideal correlations predicted by the GHZ state would not be obtainable and hence the conflict with the classical EPR arguments is not revealed so directly. Mermin [28], however showed that the contradiction with classical theories is still stronger than that of traditional Bell inequalities. In chapter 3 of this thesis, we consider experiments performed using six detectors but where there are arbitrary large number of photons incident simultaneously on each detector. This is in stark contrast to the multiparticle states discussed by Mermin [28] recently where the individual quanta emitted are spatially separated such that only one photon is incident on a detector at a given time.

In chapters 2-3 we have shown a violation of the Bell's inequality and the GHZ phenomenon at the macroscopic level. These are two potential tests of macroscopic quantum mechanics. In both cases we have a macroscopic number of states which are microscopically distinct superposed, so that only some pairs (or triplets for the GHZ phenomena) are macroscopically separated. A more elementary macroscopic quantum state, and one in which the deviation from classical interpretations is striking, was that considered by Schrödinger in his famous *Schrödinger Cat* paradox [30].

Schrödinger considered the consequence of using a quantum mechanical measurement which has two possible outcomes to determine whether or not a gun is fired in the direction of a cat. If the gun is fired the cat will be killed. The whole apparatus is enclosed in a box which is opened at a later time and the state of the cat (live or dead) examined. Now if the object being measured, the quantum measuring device, the lethal arrangement and the cat are not subject to external loss, then the total system can be considered to be a single quantum system. Hence the state of the system would be a linear combination of the state with the cat alive and the state with the cat dead, where the action of examining the contents of the box determines which state the system is in. Hence the quantum system is described as a superposition of two macroscopically distinct states. Now as Schrödinger pointed out the physical interpretation of such a state becomes a problem. For example in the above case, surely the cat must be alive or dead, whether or not one chooses to examine the contents of the box. Surely, macroscopic objects exist in a particular state prior to measurement.

Whether or not these *Schrödinger cat* states exist in a real physical system is still an open question. So far, no macroscopic superposition states have ever been observed experimentally. There have been theoretical schemes suggested [13–15, 31–52]. Leggett and co-workers [36] suggested that SQUID rings may be used to generate macroscopic superpositions states. More recently there have been suggestions to prepare similar states in optical devices [14, 39]. For example Yurke and Stoler [14], and Milburn and Holmes [39] showed that a nonlinear χ^3 medium might be used to generate a "Schrödinger Cat" state. They showed that a coherent state propagating through an amplitude-dispersive medium can evolve into a superposition state of two coherent states which are π out of phase with each other. The calculations of Yurke and Stoler [14] showed that the interference fringes present in one of the quadrature measurements (in conjunction with the observation of twin isolated peaks in the conjugate quadrature phase amplitude) are indicative of "Schrödinger Cat" like states. Such states are analogous to those considered by Schrödinger in his famous "Schrödinger cat" paradox, and hence defy all classical interpretations.

A possible weakness with the design of this type of experiment is that, although certain results, namely the observation of fringes provide evidence for a macroscopic quantum state, it is not clear whether the results exclude all alternative classical theories in the way that a Bell-inequality test does.

In chapter 4 we focus our attention on the use of parametric oscillation to generate "Schrödinger cat" like states. Recent proposals for the generation of superposition states have included the use of both degenerate [31, 32, 38] and nondegenerate [43] parametric oscillation schemes. In this chapter we will only consider degenerate parametric oscillation. Recent work by Reid and Yurke [53] has shown that "Schrödinger Cat" states are not present in the steady state field of the optical degenerate parametric oscillator in the limit where the pump losses are much greater than signal losses. However this is not necessarily the case for other regimes of parametric oscillation, and it has been suggested by Carmichael and Wolinsky [31] that "Schrödinger Cat" states may be present in a transient regime. In order to establish the predicted existence of the Schrödinger cat states and whether the criteria for the macroscopic quantum superposition states can be met experimentally, one needs to model the transient evolution of the quantum parametric oscillator in regimes of large quantum noise. This is the prime objective of chapter 4.

A fundamental problem associated with the observation and formulation of Schrödinger-cat type states it that macroscopic objects are not isolated, but are coupled to their environment. The environment causes the quantum coherences to be destroyed [34] (that is the interference fringes will be washed away). This occurs on a very fast time scale for a macroscopic object [54]. In this case losses to the system make the observations indistinguishable from that expected of a classical mixture of states, and no superposition states are present. Proposals by Mecozzi and Tombesi [33] and Kennedy and Walls [34] have shown that the use of a squeezed vacuum input rather than the usual vacuum input to model the dissipation has distinct advantages in decreasing the rate of decoherence. A large enough degree of squeezing reduces the diagonal dispersion below the vacuum level and provides a means to prepare states with very small diagonal and off-diagonal dispersions in one quadrature [34]. For the degenerate parametric oscillator, signal cavity loss destroys the formation of the "Schrödinger Cat" state. This means experimental realisation is difficult, being limited to systems with sufficiently small loss. The second objective of this chapter is to study the effect of substituting the vacuum input for a signal input/output cavity mirror with a squeezed vacuum input.

1.2 The Quantum Brownian Motion Master Equation

In part (2) of this thesis we examine various aspects of quantum Brownian motion and the quantum Brownian motion master equation.

Master equations have been used extensively in the past thirdly years to study many aspects of damped open quantum systems. There have been two main forms of the master equation used, one is the quantum optical master equation, while the second is the quantum Brownian motion master equation. Both have proved useful in describing many physical problems. However in the past few years it has been realised that the QBM master equation is not of the Lindblad form [55–57], which forces a master equation to preserve positivity. This must lead in the case of the QBM master equation to situations in which an unphysical density operator will arise.

The aim of chapter 5 of this thesis is to gain an understanding of the limitations of the quantum Brownian motion master equation. To do this we first review the derivation of the QBM master equation given by Gardiner [58]. We follow this derivation with several specific examples of the kind of unphysical solution which may be obtained, investigating in particular two extreme cases. The first is a particle for which H_{sys} is purely a kinetic term; this gives the true analogue of classical Brownian motion- in fact the equation of motion for the Wigner function is exactly the same as the Fokker-Planck equation for classical Brownian motion. We can show that unphysical results will be obtained for all temperatures provided the initial distribution corresponds to a sufficiently well localised wavefunction. However, at reasonable temperatures this gives rise to a very rapid and rather small transient. The other model is a simple two level system, which perhaps might model a bistable SQUID system [59, 60]. In particular we show that anomalous results can occur even the steady state.

We use the quantum Brownian motion to model a semiconductor medium. In a semiconductor medium there are electron-phonon interactions. In chapter 6 we specifically model this electron-phonon interaction as being a coupling between electrons and a phonon bath. This allows use to use the quantum Brownian motion master equation to model the time evolution of the system. By specifically coupling the electron probability density to the phonon bath we can examine the rate of decay of the off-diagonal elements of the master equation. We begin by initially considering a one electron system. We show that the single electron solution has two particular time constants, one temperature independent while the second is inversely proportional to the temperature. For realistic semiconductor parameters these time constants are exceedingly small, and hence the quantum effects contained in the off-diagonal elements decay away rapidly. Extending the calculations to a two electron system we show with electron-electron scattering neglected that the two electron solution is simply the product of the one electron solution. More importantly we show that the many electron solution with electron-electron scattering neglected is again simply the product of the one electron solutions. The effect of electron-electron scattering is an important physical effect and hence last in this chapter we provide a brief discussion of how this effect can be modelled.

Most of the original work in the thesis has been published in a series of papers, which, together with the appropriate chapters, are listed as follows:

Chapter 2:

W. J. Munro and M. D. Reid, "Violations of Bell's Inequalities in Multiparticle States generated using Parametric Amplification" Quantum Optics Letter **6**, 1 (1994).

W. J. Munro and M. D. Reid, "Generation via Parametric Down Conversion of Macro-

scopic Quantum States Which Violate a Bell's Inequality," Phys Rev **47**,4412(1992).

W. J. Munro and M. D. Reid, "Higher Spin Tests of Quantum Mechanics using Parametric Down Conversion", Accepted for publication in Phys Rev A.

W. J. Munro and M. D. Reid, "Strong Tests of Quantum Mechanics using Parametric Down Conversion", Being prepared for publication in Phys. Rev. A.

Chapter 3: M .D. Reid and W. J. Munro, "Macroscopic Boson States Exhibiting the Greenberger, Horne and Zeilinger Contradiction with Local Realism", Phys. Rev. Lett **69**,997(1992).

Chapter 4: L. J. Krippner, W. J. Munro and M. D. Reid, "Transient Macroscopic Quantum Superposition States in Degenerate Parametric Oscillation", submitted to Phys. Rev A.

Chapter 5: W. J. Munro and C. W. Gardiner, "Quantum Brownian Motion: The Validity of the Quantum Brownian Motion Master Equation", submitted to Phys. Rev A.

Chapter 6: W. J. Munro and C. W. Gardiner, Being prepared for publication.

Part I

Macroscopic Quantum Phenomena: Tests of Quantum Mechanics

Chapter 2

Multiparticle and Higher Spin Tests of Quantum Mechanics using Parametric Down Conversion

Abstract

We show that various experimental configurations using correlated photon number states are predicted to violate many forms of the Bell inequality. This test is potentially one of macroscopic quantum mechanics in that violations are predicted for situations where large numbers of photons are detected at a single detector at a time. The configurations also allow higher spin tests of quantum mechanics. We indicate how the violations of the Bell inequality might be achieved with both parametric amplification and parametric oscillation. The effect of photodetection inefficiencies is analysed. In order to investigate the potential for Bell-inequality tests in the high intensity regime of recent experiments in which detection efficiencies may be very high, we introduce a simple model for the effect of electronic noise which introduces a poor resolution of the photon number detected. We show that it is impossible to formulate the weak Bell inequality but that it is possible to test the strong inequality.

2.1 Introduction

Bell's theorem [1, 61] provides a way of testing the predictions of quantum mechanics against those of classical (local realism) theories [62]. For certain experiments quantum mechanics allows a violation of the Bell inequality predicted from the assumptions of local realism. To date experiments have shown a violation of the classical Bell inequality in support of quantum mechanics [3, 5]. A number of the recent experiments use parametric down conversion to generate a correlated photon pair [63–65] which exhibits this extreme quantum behaviour [9–11, 66–70]. In these experiments, the photons of each pair are individually incident on one of two spatially separated "analysers" (polarisers or beam splitters or an alternative measuring apparatus). There are thus (assuming each particle is detected) two possible outcomes at each analyser, in analogy with the original spin-$\frac{1}{2}$ formulation of the Bell inequality tests.

In this chapter we focus attention on the use of correlated photon number states pro-

duced through parametric down conversion to test quantum mechanics in situations where more than one photon is simultaneously incident on each analyser [16, 21, 22]. There is thus an equivalence to higher spin tests of quantum mechanics. Our calculations are models for extensions of the experiments of Shih and Alley [9], Ou and Mandel [10] and Rarity and Tapster [11]. Various Bell inequality tests of quantum theory for higher spin states have been formulated previously [17, 18, 23], but have not been realised experimentally to date. In this chapter we consider previous and new formulations as applied to correlated number states, comparing the quantum prediction for the degree of departure from classical predictions in each case. In the first instance we use a simple model interaction Hamiltonian to describe the basic quantum nature of the correlated photon states generated by down conversion. The effect of detection inefficiencies is included. We then present a more complete calculation of the field generated using an optical parametric oscillator, where the down conversion takes place inside an optical cavity. We consider this situation in some detail since the use of a cavity configuration may enable enhancement of the conversion efficiency for signal and idler photons of a particular mode.

Finally considered is the situation where we can have high photodetection efficiencies, but a poor resolution of the photon number due to electronic noise. This result is part of a preliminary investigation applicable to the recent experiment of Smithey et al [24], where quantum photon number correlations are measured between two macroscopic pulses produced by parametric down conversion. The use of photodiodes implies a high detection efficiency. This regime is of particular interest since a strong test of the Bell inequality not limited by auxiliary assumptions [25, 26] might be experimentally realisable. However the new limitation provided by electronic noise which will limit the resolution of photon number detected must be considered.

We point out that the multi-particle tests described here are different to those proposed recently by Greenberger et al [19, 20, 27, 28]. In their case the particles are spatially separated so that there is still only one particle incident on each analyser. An extension of the Greenberger-Horne-Zeilinger result as applied to situations of more than one photon per analyser has been considered by us [29], and is presented in Chapter Three.

2.2 The Classical Bell Inequality applied to the Experimental Configurations

The Figures (2.1-2.2) depict schematically experimental configurations which might be used to test for violations of the Bell inequality. In each case there are four input fields which we will denote simply by a_+, a_- and b_+, b_- as indicated in the Figures (2.1-2.2). Figure (2.1) is the arrangement which most closely resembles that considered by Clauser et al [61] and Aspect et al [3, 5]. The inputs undergo the following transformations which are realised by polarisers although they could also be obtained by beam splitters if a_+, a_- are spatially separated inputs. The second interferometric arrangement was considered by Reid and Walls [7].

$$\begin{aligned} c_+ &= a_+ \cos\theta + a_- \sin\theta \\ c_- &= -a_+ \sin\theta + a_- \cos\theta \\ d_+ &= b_+ \cos\phi + b_- \sin\phi \\ d_- &= -b_+ \sin\phi + b_- \cos\phi \end{aligned} \tag{2.1}$$

We also consider the alternative configuration (Figure 2.2) where phase-shifts and beam splitters generate the mixing of the input beams.

$$c_+ = \frac{a_+ + i \exp[i\theta]\, a_-}{\sqrt{2}}$$

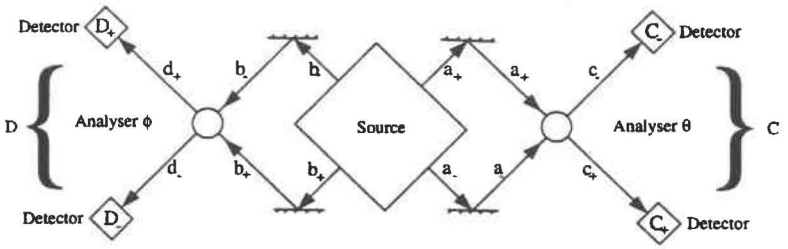

Figure 2.1: Schematic diagram of the transformations involved in the experimental arrangement to test the Bell inequality using polarisers/beam splitters.

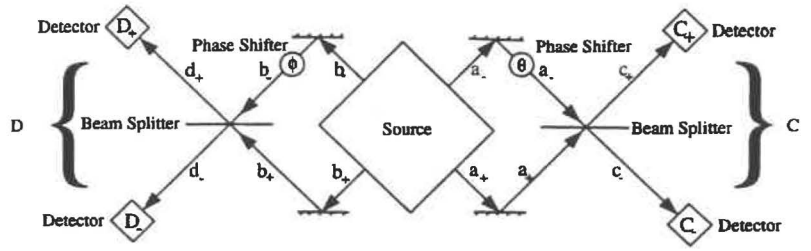

Figure 2.2: Schematic diagram of the transformations involved in the experimental arrangement to test the Bell inequality using phase shifters and beamsplitters.

$$\begin{aligned} c_- &= \frac{ia_+ + \exp[i\theta]\, a_-}{\sqrt{2}} \\ d_+ &= \frac{b_+ + i\exp[i\phi]\, b_-}{\sqrt{2}} \\ d_- &= \frac{ib_+ + \exp[i\phi]\, b_-}{\sqrt{2}} \end{aligned} \tag{2.2}$$

The experiments of Rarity and Tapster [11] obtained violations of the Bell inequality using such phase shifts. Transformations of this type were suggested by Horne et al [8, 72] and also considered by Reid and Walls [7]. The transformation brought about by the analyser apparatus at each of the spatially separated locations C and D is followed by detection. One thus performs a measurement at each of the spatially separated locations, the θ and ϕ indicating the choices made by the experimenter.

It is necessary to summarise the classical prediction for the results of the possible experiments depicted in the Figures (2.1-2.2). This is done by presenting various forms of the Bell inequality adapted for the configurations. Of interest to us is the situation where N quanta are incident on the analysers at each of C and D. We denote the number of quanta detected at C_+ by n_1, and the number of quanta detected at D_+ by n_2. In fact the result is dependent on the angle choices θ and ϕ and we will sometimes write $n_1(\theta)$ and $n_2(\phi)$ to indicate this. The possible values of n_1 and n_2 range in integer steps from 0 to N. In the absence of loss, one has $N - n_1$ and $N - n_2$ photons at C_- and D_- respectively. The measured quantities are the photon numbers $c_+^\dagger c_+$ and $d_+^\dagger d_+$. Introducing the notation

$$\begin{aligned} J_z^{(1)}(\theta) &= \frac{c_+^\dagger c_+ - c_-^\dagger c_-}{2} \\ J_x^{(1)}(\theta) &= \frac{c_+^\dagger c_- + c_-^\dagger c_+}{2} \\ J_y^{(1)}(\theta) &= \frac{c_+^\dagger c_- - c_-^\dagger c_+}{2i} \end{aligned}$$

$$J_z^{(1)} = \frac{a_+^\dagger a_+ - a_-^\dagger a_-}{2} \tag{2.3}$$
$$J_x^{(1)} = \frac{a_+^\dagger a_- + a_-^\dagger a_+}{2}$$
$$J_y^{(1)} = \frac{a_+^\dagger a_- - a_-^\dagger a_+}{2i}$$

one establishes the well-known Schwinger relation between the boson description and angular momentum operators J_x, J_y, J_z. The transformation of the a_+, a_- into the c_+, c_- given by (2.1) is equivalent to a rotation of the angular momentum operators (J_x, J_y, J_z). The boson system with N quanta incident at C and D is equivalent to the $\frac{N}{2}$-spin system. We define $J_z^{(2)}(\phi)$, $J_x^{(2)}(\phi)$, $J_y^{(2)}(\phi)$, $J_z^{(2)}$, $J_x^{(2)}$ and $J_y^{(2)}$ to be the spin operators defined similarly in terms of the operators d_+ and d_- and b_+ and b_- , so that for example $J_z^{(2)}(\phi) = \frac{d_+^\dagger d_+ - d_-^\dagger d_-}{2}$ etc. The result of a measurement of $J_z^{(1)}(\theta)$ and $J_z^{(2)}(\phi)$ at C_+ and D_+ is given respectively by $m_1 = (2n_1 - N)/2$ and $m_2 = (2n_2 - N)/2$. Again, we will sometimes write m_1 as $m_1(\theta)$ and m_2 as $m_2(\phi)$ to indicate the dependence of the measurement on the analyser angles.

One can determine experimentally the joint probability $P(m_1, m_2)$ for the results m_1 and m_2. Mermin [17] has predicted the following Bell inequality for experiments where the set of possible outcomes for m_1 and m_2 are integers between $-N/2$ and $N/2$. The inequality derived from the classical premises of locality and realism is

$$\Delta_N = \langle m_1(\theta) m_2(\phi') \rangle + \langle m_1(\phi) m_2(\phi') \rangle - \frac{N}{2} \langle |m_1(\theta) - m_2(\phi)| \rangle \leq 0 \tag{2.4}$$

More recently Braunstein and Caves [23] have developed a classical information-theory Bell inequality. Following Braunstein and Caves, one defines the information content of the measurements of $J_z^{(1)}(\theta)$ and $J_z^{(2)}(\phi)$ as $I(m_1, m_2) = -\log P(m_1, m_2))$. The information obtained upon measurement of $J_z^{(2)}(\phi)$ at D is

$$I(m_2) = -\log P(m_2),$$

$P(m_i)$ being the probability of obtaining the result m_i. The information obtained when one measures the value m_1, given that one has already measured m_2, is defined as

$$I(m_1/m_2) = -\log P(m_1/m_2)$$

The average value for this conditional information is

$$H\left[J_z^{(1)}(\theta)/J_z^{(2)}(\phi)\right] = \sum_{m_1, m_2} P(m_1, m_2) I(m_1/m_2) \tag{2.5}$$

One abbreviates the notation as follows: $H\left[J_z^{(1)}(\theta)/J_z^{(2)}(\phi)\right] = J(\theta, \phi)$. The Bell-inequality derived by Braunstein and Caves [23] is

$$H(\theta/\phi) \leq H(\theta/\phi') + H(\phi'/\theta') + H(\theta'/\phi) \tag{2.6}$$

The approach taken by Drummond [16] is to consider the joint probability $P(m_1 = N/2, m_2 = N/2)$. This approach is particularly useful for optical experiments of the type considered by Clauser et al [25, 26, 61], where the polarisers are single-channelled and it is not possible to detect photons at the locations C_- and D_-. The Bell inequality considered by Drummond is a modification of that derived by Clauser and Horne, and Clauser-Horne-Shimony-Holt(CHSH) [25, 26, 61]. Let us denote $P(N/2, N/2)$ as $P_N(\theta, \phi)$

to indicate specifically the angular dependence of the measurements. We define more generally $P_n(\theta,\phi)$ as the joint probability of detecting n photons at C_+ and n photons at D_+ to allow for situations where not all of the N photons incident on each analyser are detected. The generalisation of the Bell-Clauser-Horne-Shimony-Holt inequality is

$$B_n = \frac{P_n(\theta,\phi) - P_n(\theta,\phi') + P_n(\theta',\phi) + P_n(\theta',\phi')}{P_n(\theta',-) + P_n(-,\phi)} \leq 1 \tag{2.7}$$

(we outline the derivation of this in Section (2.6) of this chapter). Here $P_n(\theta',-)$ and $P_n(-,\phi)$ are the marginal probabilities for detecting n photons at C_+ and n photons at D_+ respectively. A violation of this inequality corresponds to $B_n > 1$.

We may also consider a 'product' inequality. In many situations $P_N(\theta,\phi)$ is small and hence an experimenter must perform many runs before obtaining sufficient data. It may be advantageous to examine the product inequality defined below where all the data contributes. We assign a value to the variable E_i^θ of $+1$ or -1 if the i^{th}-quantum incident at C is at C_+ or C_- respectively. The variable E_i^ϕ is defined similarly at the location D. If N quanta are incident at each location C and D, we define the product

$$E_N^1(\theta)E_N^2(\phi) \tag{2.8}$$

where $E_N^1(\theta) = \prod_{i=1}^N E_i^\theta$ and $E_N^2(\phi) = \prod_{j=1}^N E_j^\phi$. We now define $E_N(\theta,\phi)$ to be the expected value of this product. Thus

$$E_N(\theta,\phi) = \sum_{i,j=0}^{N} P_{i,N-i,j,N-j}(\theta,\phi)\,(-1)^{2N-i-j}\,(1)^{i+j} \tag{2.9}$$

where $P_{i,N-i,i,N-j}(\theta,\phi)$ is the probability of detecting i, $N-i$, j, $N-j$ photons at C_+, C_-, D_+ and D_- respectively. For the situation where the i^{th} quantum is not detected (due to poor efficiency of detectors for example), one may assign $E_i^\theta = 0$ and generalise the expression (2.9) accordingly. One may also consider more general situations where we select to measure an $E_N(\theta,\phi)$ (defined by (2.9) as above), selecting a total of n photons at both C and D, where n is not necessarily equal to N, the number of photons incident on the analysers. The result for $\left|E_i^\theta\right|$ is always bounded by 1, and a direct application of Bell's 1971 proof leads [1] to the following inequality

$$S_n = \left|E_n(\theta,\phi) - E_n(\theta,\phi') + E_n(\theta',\phi) + E_n(\theta',\phi')\right| \leq 2 \tag{2.10}$$

(the derivation is outlined in Section (2.6) of this chapter).

In order to account for real experiments performed where photon detection efficiencies are very poor, and not all of N quanta incident on each analyser are detected, Clauser and Horne and CHSH derived a modified inequality for the $N = 1$ case, based on additional auxiliary assumptions [1, 25, 26, 61]. The inequalities derived in our case are identical in form to the inequalities (2.7) and (2.10) presented above, except that the probabilities and expectation values are calculated over the subensemble where n quanta are detected at *each* of C and D. The implication of the Clauser and Horne analysis for the inequality (2.7) is that the marginal probabilities are replaced by joint probabilities. The $P_n(\theta,-)$ now becomes the joint probability for detecting n quanta at C_+ *and* n quanta at D, with the analyser at D removed. We will thus also refer to Eqn (2.7) as the Clauser and Horne inequality. The implication for the product inequality (2.10) is the replacement of $E_n(\theta,\phi)$ with the normalised $E_n(\theta,\phi)$ (see Section (2.6)) defined as follows

$$E_n(\theta,\phi) = \frac{\sum_{i,j=0}^{N} P_{i,n-i,j,n-j}(\theta,\phi)\,(-1)^{2n-i-j}\,(1)^{i+j}}{\sum_{i,j=0}^{N} P^{i,n-i,j,n-j}(\theta,\phi)} \tag{2.11}$$

These modified inequalities are weaker since one requires for their derivation the additional auxiliary or supplementary assumptions. These are discussed in Section (2.6).

2.3 Quantum Predictions for Correlated Photon Number States

We first present calculations based on the input state [16]

$$\begin{aligned} |\varphi\rangle &= \frac{\left[a_+^\dagger b_+^\dagger + a_-^\dagger b_-^\dagger\right]^N |0\rangle}{N!\sqrt{N+1}} \\ &= \frac{1}{\sqrt{N+1}} \sum_{r=0}^{N} |r\rangle_{a_+} |r\rangle_{b_+} |N-r\rangle_{a_-} |N-r\rangle_{b_-} \end{aligned} \tag{2.12}$$

where for example $|r\rangle_{b_+}$ is the r-photon number state for b_+. Here we have a total of N quanta at C and N quanta at D. For N = 1, this correlated superposition state (or 'entangled state') is analogous to that generated in the experiments of Aspect et al [3, 5]. In these experiments a_+ and a_- represent orthogonal polarisations.

The input state (2.12) can be expanded in terms of the eigenstates $|m_1, m_2\rangle$ of $J_z^{(1)}(\theta)$ and $J_z^{(2)}(\theta)$

$$|\varphi\rangle = \frac{1}{\sqrt{N+1}} \sum_{r=0}^{N} |\frac{N}{2} - r, \frac{N}{2} - r\rangle_\theta \tag{2.13}$$

where $J_z^{(2)}(\theta)\, J_z^{(1)}(\theta)\, |m_1, m_2\rangle = m_1 m_2 |m_1, m_2\rangle$. The expansion holds regardless of the choice of θ. This state is identical in form to the zero total-spin state considered by Mermin [17] and Caves and Braunstein [23], except that m_2 has changed sign. One can calculate the joint probabilities $P(m_1(\theta), m_2(\phi))$ and expectation values $\langle m_1(\theta) m_2(\phi)\rangle$ and establish a violation of the classical inequalities (2.4), (2.6), (2.7), and (2.10). Since rotation of both sets (a_+, a_-) and (b_+, b_-) by an angle θ in accordance with the transformation (2.1) leaves the state (2.12) invariant, we can select our axes to coincide with the first angle θ associated with the measurement at C. The transformation we consider is then

$$\begin{aligned} c_+ &= a_+ \\ c_- &= a_- \\ d_+ &= b_+ \cos(\varphi) + b_- \sin(\varphi) \\ d_- &= -b_+ \sin(\varphi) + b_- \cos(\varphi) \end{aligned} \tag{2.14}$$

where $\varphi = \phi - \theta$. Calculation of $P(m_1(\theta), m_2(\phi))$ thus proceeds by evaluating $P(m_1(0), m_2(\varphi))$ upon us noting that $|\varphi\rangle$ can be expressed in terms of the measured modes as

$$\begin{aligned} |\varphi\rangle &= \frac{\left[c_+^\dagger d_+^\dagger \cos(\varphi) - c_+^\dagger d_-^\dagger \sin(\varphi) + c_-^\dagger d_+^\dagger \sin(\varphi) + c_-^\dagger d_-^\dagger \cos(\varphi)\right]^N |0\rangle}{N!\sqrt{N+1}} \\ &= \sum_{n_1, n_2 = 0}^{N} C_{n_1 n_2} |n_1\rangle_{c_+} |N-n_1\rangle_{c_-} |n_2\rangle_{d_+} |N-n_2\rangle_{d_-} \end{aligned} \tag{2.15}$$

Now $P(m_1, m_2)$ is the probability of detecting n_1 and n_2 photons at C_+ and D_+ respectively where $n_i = m_i + N/2$. Thus evaluating the relevant coefficients $C_{n_1 n_2}$ we obtain

$$\begin{aligned} P(m_1(\theta), m_2(\phi)) &= \frac{n_1! n_2! (N-n_1)! (N-n_2)!}{N+1} \\ &\times \left[\sum_{r=0}^{\min(n_1, n_2)} \frac{(-1)^{n_1 - r} \cos^{N-n_1-n_2+2r}(\varphi) \sin^{n_1+n_2-2r}(\varphi)}{r!\,(n_1-r)!\,(n_2-r)!\,(N-n_1-n_2-r)!} \right]^2 \end{aligned} \tag{2.16}$$

where $n_1 = m_1(\theta) + N/2$ and $n_2 = m_2(\phi) + N/2$. We note that since the joint probabilities are

$$P(m_1, m_2) = \frac{|C_{n_1 n_2}|^2}{\sum_{n_1,n_2=0}^{N} |C_{n_1 n_2}|^2} \tag{2.17}$$

we can write $P(m_1, m_2)$ in terms of correlation functions

$$P(m_1, m_2) = \frac{\binom{N}{n_1}\binom{N}{n_2} \langle : \left(c_+^\dagger c_+\right)^{n_1} \left(c_-^\dagger c_-\right)^{N-n_1} \left(d_+^\dagger d_+\right)^{n_2} \left(d_-^\dagger d_-\right)^{N-n_2} : \rangle}{\langle : \left(c_+^\dagger c_+ + c_-^\dagger c_-\right)^N \left(d_+^\dagger d_+ + d_-^\dagger d_-\right)^N : \rangle} \tag{2.18}$$

Thus

$$P_N(\theta, \phi) = \frac{\langle : c_+^{\dagger N} c_+^N d_+^{\dagger N} d_+^N : \rangle}{\langle : \left(c_+^\dagger c_+ + c_-^\dagger c_-\right)^N \left(d_+^\dagger d_+ + d_-^\dagger d_-\right)^N : \rangle} \tag{2.19}$$

and

$$P_N(\theta, -) = \frac{\langle : c_+^{\dagger N} c_+^N \left(d_+^\dagger d_+ + d_-^\dagger d_-\right)^N : \rangle}{\langle : \left(c_+^\dagger c_+ + c_-^\dagger c_-\right)^N \left(d_+^\dagger d_+ + d_-^\dagger d_-\right)^N : \rangle} \tag{2.20}$$

The product $E_N(\theta, \phi)$ is written

$$E_N(\theta, \phi) = \frac{\langle : \left(c_+^\dagger c_+ - c_-^\dagger c_-\right)^N \left(d_+^\dagger d_+ - d_-^\dagger d_-\right)^N : \rangle}{\langle : \left(c_+^\dagger c_+ + c_-^\dagger c_-\right)^N \left(d_+^\dagger d_+ + d_-^\dagger d_-\right)^N : \rangle} \tag{2.21}$$

Figures (2.3-2.5) depict the violation of the classical inequalities for varying values of N. The violations predicted in Figures (2.3) and (2.4) have been calculated previously by Mermin [17] and Drummond [16] and are presented here for the sake of comparison. The proposed experiment is potentially one of quantum mechanics at a macroscopic level [16] because the violation is present for N particles incident on each analyser even for N large. We note that the Clauser-Horne experiment where $P_N(\theta, \phi)$ is measured has a potential disadvantage for larger N, since with N photons incident, the actual probability $P_N(\theta, \phi)$ can be small, making the experiment difficult. The product inequalities have the advantage that all outcomes contribute to the data collected for the experiment.

It is important to discuss precisely in what sense our test of quantum mechanics discussed here are macroscopic. We point out that since at each detector one might detect the whole range of N,N-1. .....,0 photons, the final state produced at the detectors is not a simple superposition of macroscopically distinct states (a 'Schrödinger'-cat state [15, 73]). Rather we have a macroscopic (with N large) number of states which are microscopically distinct superposed, so that only some pairs are macroscopically separated. In the tests proposed here the distinction is being made between states which are microscopically distinct in order to gain violations of the Bell inequality, in that we gain the contradiction with classical theories by detecting all N photons. For example, in the Clauser-Horne measurement needed for inequality (2.7) information is gained about all of the N photons in that they are all detected in the + position. The effect of detecting only N-1 photons, so that the location of one photon is not specified, is to decrease or destroy the contradiction with classical theories. This effect was pointed out by Drummond [16] with respect to the case shown in Figure (2.4). We illustrate this effect, in Figures (2.4) and (2.5) by calculating B_N and E_N with $n = N - 1$ so that a total of only $N - 1$ photons are detected. Quantum

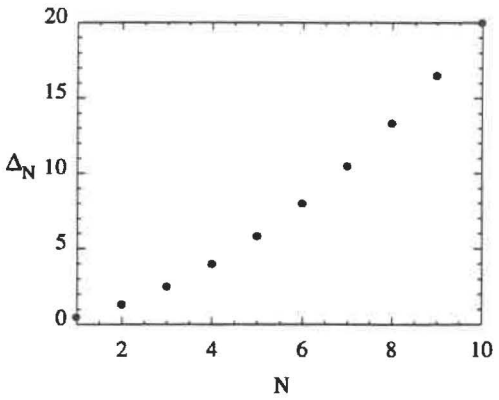

Figure 2.3: Plot of the maximum violation (Δ_N) of Mermin's higher spin inequality for the state $\frac{(a_+^\dagger b_+^\dagger + a_-^\dagger b_-^\dagger)^N}{N!(N+1)^{1/2}}|0\rangle$. A violation of the inequality occurs for $\Delta_N > 0$. The same results occur in both the polariser and phase shifter/beamsplitter arrangement (The angles are chosen for each N to maximise the violation).

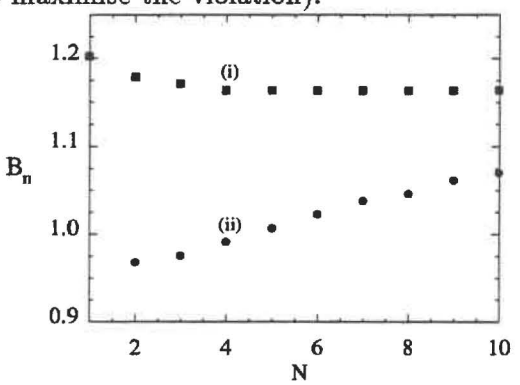

Figure 2.4: Plot of the maximum value of B_n (defined for the Clauser-Horne Bell inequality), versus N, the number of photon pairs in the correlated state $\frac{(a_+^\dagger b_+^\dagger + a_-^\dagger b_-^\dagger)^N}{N!(N+1)^{1/2}}|0\rangle$ for (i) n=N, (ii) n=N-1. A violation of the inequality occurs for $B_n > 1$. The same results occur in the polariser and phase shifter/beamsplitter arrangements (The angles are chosen for each N to maximise the violation).

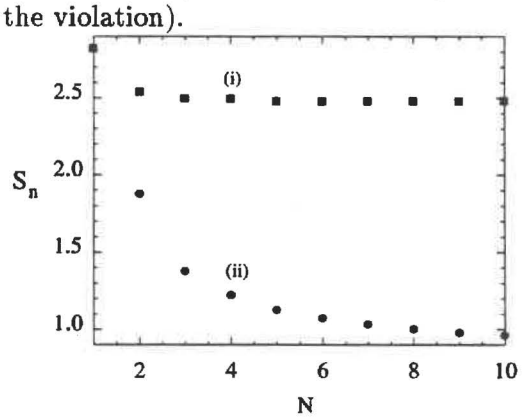

Figure 2.5: Plot of the maximum value of S_n (used in the product Bell inequality), versus N, the number of photon pairs in the correlated state $\frac{(a_+^\dagger b_+^\dagger + a_-^\dagger b_-^\dagger)^N}{N!(N+1)^{1/2}}|0\rangle$ for (i) n=N, (ii) n=N-1. A violation of the inequality occurs for $S_n > 2$. The same results occur in the polariser and phase shifter/beamsplitter arrangement (The angles are chosen for each N to maximise the violation).

mechanics predicts the joint probability functions $P_n(\theta,\phi)$ and $P_n(\theta,-)$ (where n is less than N and no information is obtained about the remaining $N-n$ photons) to be given in this case by the moments $\langle : c_+^{\dagger\, n} c_+^n d_+^{\dagger\, n} d_+^n : \rangle/(n!)^2$ and $\langle : c_+^{\dagger\, n} c_+^n \left(d_+^\dagger d_+ + d_-^\dagger d_-\right)^n : \rangle/(n!)^2$ respectively, so that B_n and $E_n(\theta,\phi)$ are readily calculated. It is noted by comparing Figures (2.4) and (2.5) that the sensitivity of the violation of the Bell inequality to this loss of information about one photon is greater in the case of the product test. In the Clauser-Horne inequality considered by Drummond [16], a violation may be obtained for $n < N$ photons detected, provided a large number N of photons is incident on the detectors. To conclude, the tests proposed here cannot be thought of as a test of macroscopic realism in the sense discussed by Leggett [15] where we always distinguish between two states macroscopically distinct. However the interference generated by the multiple superposition states is sufficient to create contradiction with quantum mechanics at the macroscopic level.

We now need to consider how to generate the state (2.12) or one similar to it which will allow a test of quantum predictions against those of classical theories. In the next few sections we propose the use of parametric down conversion. Experiments with N = 1 have already been performed using parametric down conversion. The experiments of Rarity and Tapster [11] generate an entangled state of the type (2.12) with N=1 using down conversion directly. In the earlier experiments of Shih and Alley [9], and Ou and Mandel [10], the two signal and idler beams generated via down conversion undergo transformations using beam splitters to generate a state similar to the four mode state (2.12). The parametric interaction is used in these experiments to generate the correlated photon number state $|1\rangle|1\rangle$ and hence to demonstrate violation of the Bell inequality in the microscopic regime [9–11, 66–70]. The Figures (2.6-2.8) depict schematically some experimental configurations that are used to test for violations of the Bell inequality in such a twin-beam experiment. The apparatus of Figure (2.6) depicts the following transformations which may be obtained with beam splitters and polarisers. Here a_1 and b_1 represent signal and idler beams respectively.

$$\begin{aligned} a_+ &= \frac{(a_1 + ia_2)}{\sqrt{2}} \\ a_- &= \frac{(b_2 + ib_1)}{\sqrt{2}} \\ b_+ &= \frac{(ia_1 + a_2)}{\sqrt{2}} \\ b_- &= \frac{(ib_2 + b_1)}{\sqrt{2}} \end{aligned} \tag{2.22}$$

The a_+, a_- and b_+, b_- are then combined according to the transformation (2.1). This is essentially the scheme suggested by Reid and Walls [7], and Shih and Alley [9]. Alternative experimental arrangements have also been proposed [8, 72, 75–77]. We have shown previously [21] that the configuration of Figure (2.6) can be used for multiparticle tests of the Bell inequality. The transformations (2.22) are identical to those produced in the experiment of Shih and Alley [9], and Ou and Mandel [10] (Figure 2.7) where the two correlated photons generated via parametric down conversion enter as inputs a_1 and b_1 of the beamsplitter BS. In this arrangement the inputs a_2 and b_2 are orthogonal vacuum states. In the apparatus of Shih and Alley, and Ou and Mandel the non-overlapping modes a_1 and b_1 are thus incident as inputs of the same beamsplitter, and the emerging $a_\pm$ and $b_\pm$ are transformed using two spatially separated polarisers. It is also possible to transform the a_+, a_- and b_+, b_- using phase-shifts as described by the transformation (2.2). This

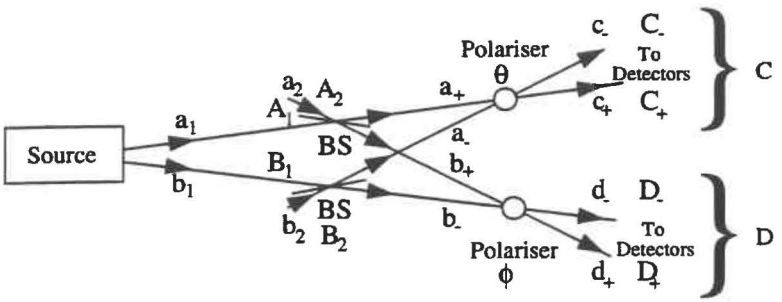

Figure 2.6: Schematic diagram of the transformations involved in the experimental arrangement to test the Bell inequality for the twin beam system using polarisers/beam splitters.

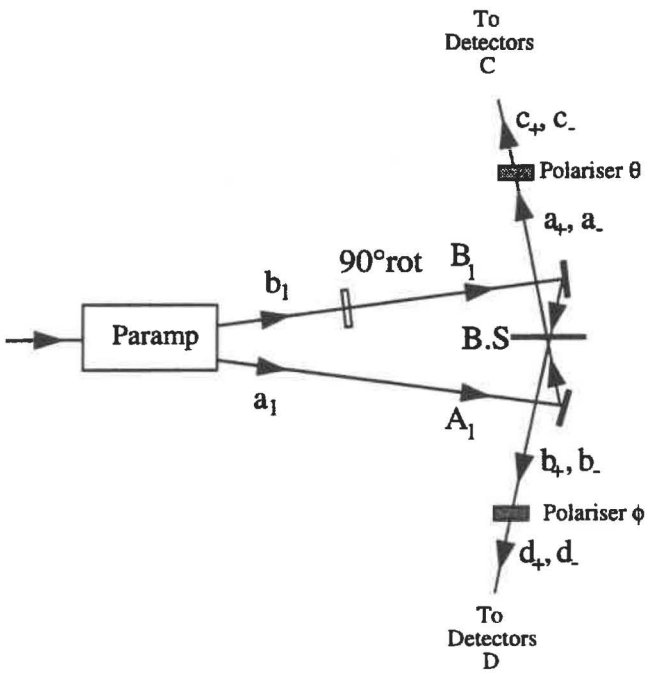

Figure 2.7: Schematic diagram of the transformations used in the experiments of Shih and Alley and Ou and Mandel.

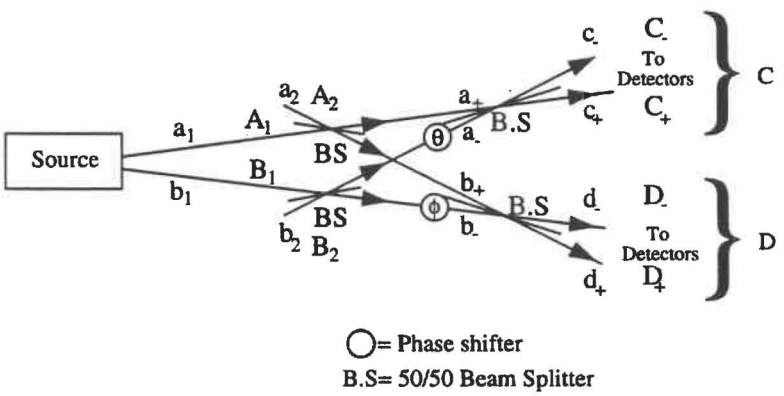

Figure 2.8: Schematic diagram of the transformations involved in the experimental arrangement to test the Bell inequality for the twin beam system using phase shifters and beamsplitters.

arrangement is depicted in Figure (2.8).

We now present calculations with the correlated photon number state $|N\rangle|N\rangle$ at the inputs A_1 and B_1 of Figures (2.6-2.8). The inputs at A_2 and B_2 are vacuum states. It is possible to express (using the transformation (2.22)) the state generated in terms of the a_+, a_-, b_+, b_- fields. One obtains [21]

$$\frac{1}{N!2^N}\sum_{r,r'=0}^{N}(-i)^{r+r'}\begin{bmatrix}N\\r\end{bmatrix}\begin{bmatrix}N\\r'\end{bmatrix}a_+^{\dagger N-r}b_+^{\dagger r}a_-^{\dagger r'}b_-^{\dagger N-r'}|0\rangle \tag{2.23}$$

Here $|0\rangle$ represents the vacuum state for all modes. We see that one does not necessarily have N quanta incident at each of C and D. Use is thus made of the weaker inequalities discussed where the averages are defined only over the reduced subensemble where the selected number of quanta are actually detected at each of the outputs C and D. The terms in the expansion of (2.23) which are relevant for experiments where we select N quanta detected at each of C and D are

$$\frac{1}{N!2^N}\sum_{r=0}^{N}(-1)^r\begin{bmatrix}N\\r\end{bmatrix}^2 a_+^{\dagger N-r}b_+^{\dagger r}a_-^{\dagger r}b_-^{\dagger N-r}|0\rangle \tag{2.24}$$

We see that for N = 1, this reduced state is identical in form to the four-mode state (2.12).

For $N > 1$, relating to the states of higher spin, differences exist. The results predicted for (2.24) will not be identical to those predicted by Mermin for the higher spin state (2.13). The state (2.24) expressed in terms of the eigenstates $|m_1, m_2\rangle$ of $J_z^{(1)}$ and $J_z^{(2)}$ becomes

$$\frac{1}{2^N}\sum_{r=0}^{N}(-1)^r\begin{bmatrix}N\\r\end{bmatrix}|\frac{N}{2}-r,-\frac{N}{2}+r\rangle \tag{2.25}$$

In this case the invariance under rotation to $J_z^{(1)}(\theta)$ and $J_z^{(2)}(\phi)$ is not retained for all N.

The Figures (2.9-2.11) present the quantum predictions of the state (2.23) for the weaker versions of the various classical expressions (2.4) - (2.7) - (2.10). Here we again observe a clear violation of all the different types of the Bell inequality discussed for $N = n$. However in both the Clauser Horne inequality (2.7) and the product inequality (2.10) no violation is seen for $n < N$ (that is, when less photons are detected at the detectors than N the number of photons incident at each of A_1 and B_1). We have previously [21] presented and discussed the predictions for the Clauser-Horne inequality using polarisers (Figure 2.10a).

The calculations presented model two sets of N quanta simultaneously incident on the beam splitters of the apparatus depicted. The need for simultaneity in order to obtain the violation is apparent when we examine the N=1 case. Let us consider the arrangements of the type shown in Figures (2.6-2.8) we consider the ensemble where a single photon is detected at each of the detectors C and D. The state (2.24) is a superposition of two states, the first where the photon detected at C comes from A_1 (the signal field) and the second where the photon at C comes from B_1 (the idler field). With the introduction of a sufficient time delay between the incident signal and idler photons the origin of a particular photon may be inferred. Hence the superposition nature of the state is lost and no violations of the classical predictions will be possible. The parametric down conversion process generates fields with the required correlated photon arrival times [63–65].

2.4 Generation of the Higher-Spin Correlated Quantum States using Parametric Down Conversion

Correlated photon number states of the type we have been considering can be generated using down conversion [21, 22]. We model the process in simple terms by the following Hamiltonian representing pair generation from a non-depleting classical pump field of amplitude ϵ and frequency ω_3

$$H = -\hbar\chi\epsilon\left(a_1 b_1 + a_1^\dagger b_1^\dagger\right) \tag{2.26}$$

Here the a_1, b_1 are the boson operators for orthogonal signal and idler modes of frequency ω_1, ω_2 respectively such that $\omega_3 = \omega_1 + \omega_2$. The χ is proportional to the susceptibility of the medium. This Hamiltonian incorporates only single modes, and hence it will usually apply where the interaction takes place inside a cavity. The model has also been used by Smithey et al [24] to explain experimental observed photon number correlations in the usual nondegenerate parametric down conversion with no cavity. The orthogonal fields may be spatially separated. The state generated after an interaction time t is

$$|\varphi\rangle = \sum_{N=0}^{\infty} c_N |N\rangle|N\rangle \tag{2.27}$$

where

$$c_N = \frac{[-i\tanh r]^N}{\cosh r} \tag{2.28}$$

with $r = \chi\epsilon t$. Here we observe that because the signal and idler are generated in pairs, there is a correlation between the signal and idler photon number. Thus we have a method for generating correlated number states with $N > 1$.

We consider also the twin parametric down conversion process

$$H = \kappa\left(a_+ b_+ + a_- b_-\right) + \kappa^*\left(a_+^\dagger b_+^\dagger + a_-^\dagger b_-^\dagger\right) \tag{2.29}$$

where the entangled states are produced more directly. Here the pairs a_+, b_+ and a_-, b_- may represent down converted photon pairs of differing k-vectors, or different frequencies. The $a_\pm, b_\pm$ here are the inputs to the experimental arrangements considered in Figures (2.1) and (2.2). The advantage of using the four-mode interaction is that it potentially allows a strong test of the Bell inequality, as compared to the arrangements depicted in Figures (2.6-2.11), where, as discussed above, auxiliary assumptions are necessary in deriving the Bell inequality. The experiment of Rarity and Tapster [11] uses parametric amplification in this manner to produce the N=1 entangled state of (2.12), and uses the beam-splitter phase-shifter arrangement of Figure (2.2) to show a violation of the Bell inequality. Violations of the Bell inequality using a twin beam was first presented by Reid and Walls [7, 74]. The state generated after an interaction time t is

$$|\varphi\rangle = \sum_{N=0}^{\infty} \bar{c}_N \sum_{m=0}^{N} |m\rangle|N-m\rangle|m\rangle|N-m\rangle \tag{2.30}$$

where

$$\bar{c}_N = \frac{[-i\tanh r]^N}{\cosh^2 r} \tag{2.31}$$

Assuming initially that the signal and idler may be extracted from the cavity to maintain the correlation given in (2.27) for the two mode system (or (2.30) for the four mode

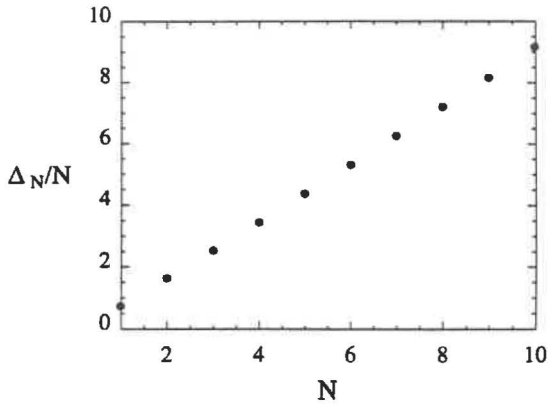

Figure 2.9: Plot of the maximum violation (Δ_N) of Mermin's higher spin inequality for the two mode state $|N\rangle_1|N\rangle_2$. A violation of the inequality occurs for $\Delta_N > 0$. The same results occur in both the polariser and phase shifter/beamsplitter arrangements (The angles are chosen for each N to maximise the violation).

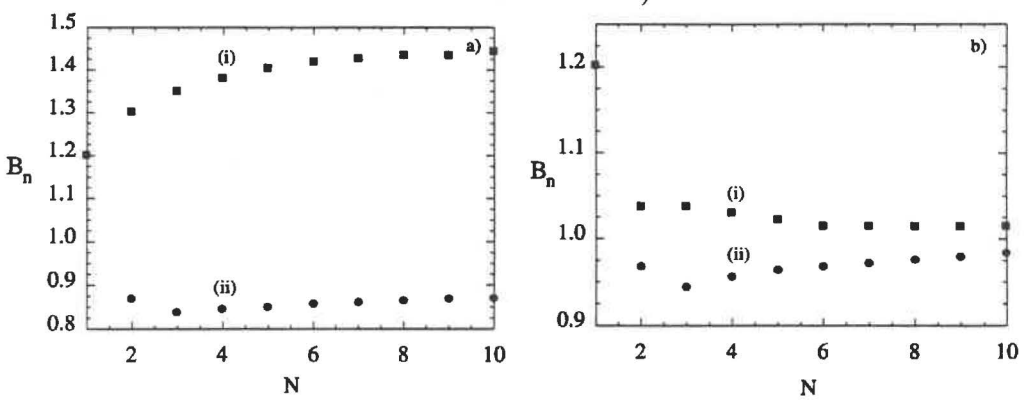

Figure 2.10: Plot of the maximum violation of the Clauser-Horne Bell Inequality. B_n versus N, the number of photons in the correlated two mode state $|N\rangle_1|N\rangle_2$ for
a) The polariser arrangement with (i) n=N, (ii) n=N-1.
b) The phaseshifter/beamsplitter arrangement with (i) n=N, (ii) n=N-1.
A violation of the inequality occurs for $B_n > 1$ (The angles are chosen for each N to maximise the violation) .

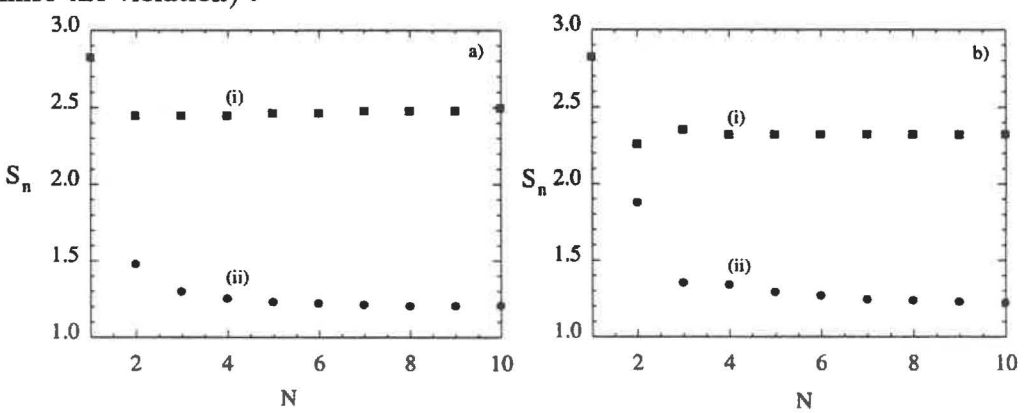

Figure 2.11: Plot of the maximum violation of the product Bell inequality. S_n versus N, the number of photons in the correlated two mode state $|N\rangle_1|N\rangle_2$ for
a) The polariser arrangement with (i) n=N, (ii) n=N-1.
b) The phaseshifter/beamsplitter arrangement with (i) n=N, (ii) n=N-1.
A violation of the inequality occurs for $S_n > 2$ (The angles are chosen for each N to maximise the violation).

system), we observe that we require near perfect photodetection efficiency in order to obtain precisely the violations plotted in Figures (2.4-2.5) for the four mode arrangement, and Figures (2.10-2.11) for the two mode system, for all values of r. The perfect detection allows one to determine precisely the value of N, the number of photons incident on each analyser provided one has beamsplitters or double-sided polarisers so that one can detect photons at all of the locations C_+, C_-, D_+, and D_-. It is then possible in principle restrict measurements to the subensemble where a total of N photons are incident at each analyser. In the Clauser-Horne type experiment, one would need to add detectors at C_- and D_-. The predictions for this experiment in the limit of low efficiency without detectors at the C_- and D_- positions has been presented by us previously [21] and are shown in Figures (2.12) for the four mode arrangement and Figure (2.13). Derivation of the Bell-type inequality in this case requires an extension of the usual auxiliary assumption and is discussed in Section (2.6). Detection of a total of n quanta at each location C and D by inefficient detectors leaves open the possibility that the input state may have been $n+1$ photons or higher and the state $|n+k\rangle|n+k\rangle$ $(k>0)$ contributes to the probability $P_n(\theta,\phi)$. The Figures (2.4), (2.5), (2.10) and (2.11) show for both the Clauser-Horne and product cases that a loss of the violation of the various Bell inequality for B_n where $n=N-1$, indicating detection loss to be an important effect, and particularly relevant where one has poor detector efficiencies.

To calculate this effect, we need to evaluate the appropriate joint probabilities for detection of photons at the four locations. The photon counting probabilities may be expressed in terms of the moments of c_+, c_-, d_+, and d_- by applying the usual photon counting formula derived by Kelly and Kleiner [78]. The probability of detecting N photons at C_+, 0 photons at C_-, N photons at D_+, and 0 photons at D_- is

$$\begin{aligned} P_{N,0,N,0}(\theta,\phi) &= \eta^{2N}\langle: \left\{ \left(c_+^\dagger c_+ d_+^\dagger d_+\right)^N \right. \\ &\quad \left. \times \exp\left[-\eta\left(c_+^\dagger c_+ + c_-^\dagger c_- + d_+^\dagger d_+ + d_-^\dagger d_-\right)\right]\right\} :\rangle \end{aligned} \tag{2.32}$$

while the probability $P_{N,0,N}(\theta,-)$ of detecting N photons at C_+, 0 photons at C_-, and N photons at D with the polariser removed is

$$\begin{aligned} P_{N,0,N}(\theta,-) &= \eta^{2N}\langle: \left\{ \left(c_+^\dagger c_+\right)^N \left(d_+^\dagger d_+ + d_-^\dagger d_-\right)^N \right. \\ &\quad \left. \times \exp\left[-\eta\left(c_+^\dagger c_+ + c_-^\dagger c_- + d_+^\dagger d_+ + d_-^\dagger d_-\right)\right]\right\} :\rangle \end{aligned} \tag{2.33}$$

Here η is the quantum efficiency of the detector. For the product system we can write the appropriate correlation function $E_N(\theta,\phi)$, (where we detect a total of N photons at C, and a total of N photons at D), as

$$\begin{aligned} E_N(\theta,\phi) &= \eta^{2N}\langle: \left\{ \left(c_+^\dagger c_+ - c_-^\dagger c_-\right)^N \left(d_+^\dagger d_+ - d_-^\dagger d_-\right)^N \right. \\ &\quad \left. \times \exp\left[-\eta\left(c_+^\dagger c_+ + c_-^\dagger c_- + d_+^\dagger d_+ + d_-^\dagger d_-\right)\right]\right\} :\rangle \end{aligned} \tag{2.34}$$

It is readily shown (see Section 2.6) that the $P_{N,0,N,0}(\theta,\phi)$, $P_{N,0,N}(\theta,-)$, and $E_N(\theta,\phi)$ obey the inequalities (2.7) and (2.10), substituting for $P_n(\theta,\phi)$, $P_n(\theta,-)$ and $E_n(\theta,\phi)$ respectively. This is provided the auxiliary assumption discussed in Section (2.5) are made.

The results obtained upon evaluating B_N for various efficiencies are plotted in Figure (2.14) for the Clauser-Horne inequality with the four mode parametric interaction (here one has additional detectors at C_- and D_-), Figure (2.15) for the product inequality with the four mode parametric interaction, Figure (2.16) for the Clauser-Horne inequality with

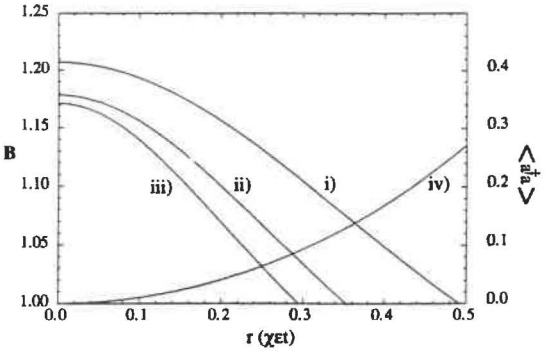

Figure 2.12: Plot of the maximum violation of the product Bell inequality using four parametric down conversion in the low efficiency limit. B_N versus r ($\chi\epsilon t$) for i) N=1, ii) N=2, iii) N=3. Curve (iv) is the mean photon number $\langle a_+^\dagger a_+ \rangle$. The same results occur for both the polariser and phaseshifter arrangements. A violation of the inequality occurs for $B_N > 1$ (The angles are chosen for each N to maximise the violation).

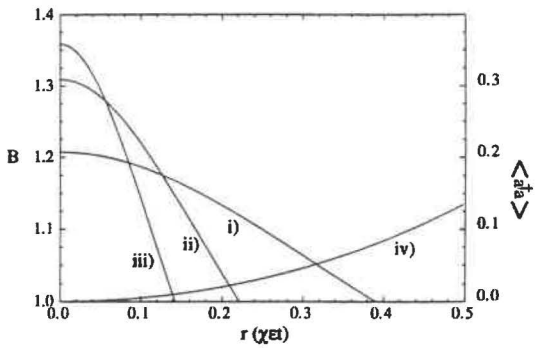

Figure 2.13: Plot of the maximum violation of the product Bell inequality using two parametric down conversion in the low efficiency limit. B_N versus r ($\chi\epsilon t$) for i) N=1, ii) N=2, iii) N=3. Curve (iv) is the mean photon number $\langle a_+^\dagger a_+ \rangle$. The same results occur for both the polariser and phaseshifter arrangements. A violation of the inequality occurs for $B_N > 1$ (The angles are chosen for each N to maximise the violation).

the two mode interaction, and in Figure (2.17) for the product inequality. Where the loss is significant a violation of the Bell inequality is obtained only for fields where the probability of higher ($N > n$) photon number states being generated is negligible. For the parametric solution (2.27), (2.30) we are required to operate at low intensities. Unfortunately this reduces the probability of actually detecting N photons at each set of detection apparatus (whether it be N photons at C_+, D_+ for the Clauser-Horne inequality or N photons at C, D for the product inequality), making the experiment difficult for large N. In this limit of small η we are required in the parametric case, in order to obtain a violation of the $N = 2$ inequality, to operate in a regime where the probability of the two-photon state is $\frac{1}{20}$ that of the one photon state. This result has been discussed by us previously [21, 22] for the two mode interaction. The results in this low detection efficiency limit are not improved by the additional detectors suggested in the Clauser-Horne case. This is because in the low intensity regime, the probability of states with higher photon numbers is very small. We note however that the weaker Clauser-Horne inequality (where the marginal probability is replaced by a joint probability) will not be applicable in the higher r regime without the use of the additional detectors at C_- and D_-, since the auxiliary assumption will break down in this case, (This is discussed in Section 2.6).

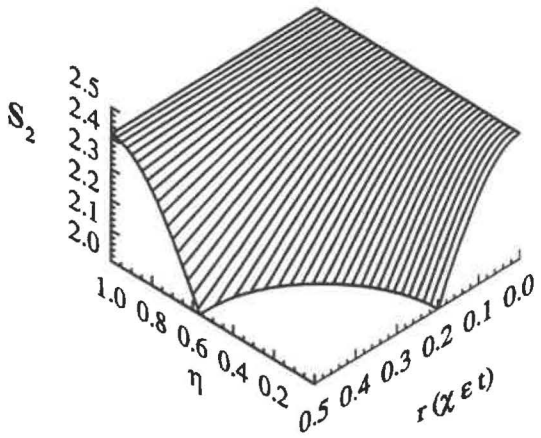

Figure 2.14: Plot of the maximum violation of the Clauser-Horne Bell inequality using four mode parametric down conversion. B_2 versus r, with varying photodetection efficiency η for a) The polariser arrangement (angles chosen such that φ=0.277),
b) The phaseshifter/beamsplitter arrangement (angles chosen such that φ=2.586),
A violation of the inequality occurs for $B_2 > 1$. The same results occur in the polariser and phase shifter/beamsplitter arrangements

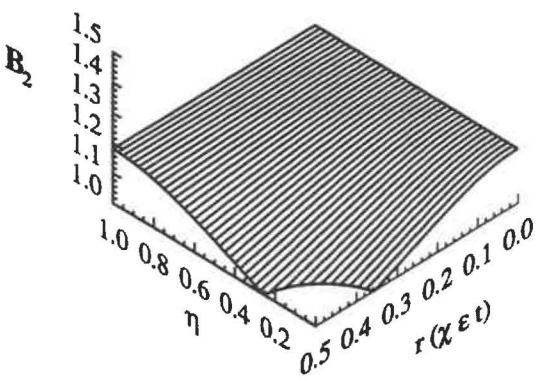

Figure 2.15: Plot of the maximum violation of the product Bell inequality using four parametric down conversion. S_2 versus r ($\chi\epsilon t$), with varying photodetection efficiency η for a) The polariser arrangement (angles chosen such that φ=0.3925),
b) The phaseshifter/beamsplitter arrangement (angles chosen such that φ=2.749)
A violation of the inequality occurs for $S_2 > 2$. The same results occur in the polariser and phase shifter/beamsplitter arrangements.

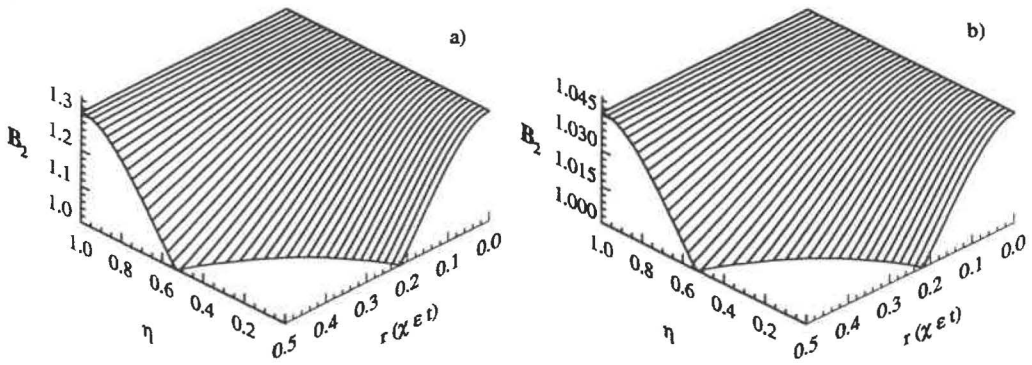

Figure 2.16: Plot of the maximum violation of the Clauser-Horne Bell inequality using parametric down conversion. B_2 versus r, with varying photodetection efficiency η for
a) The polariser arrangement (angles chosen are $\theta = 0.365$, $\theta' = 3.050$, $\phi = -1.662$, $\phi' = 1.955$),
b) The phaseshifter/beamsplitter arrangement (angles are chosen such that $\varphi = \theta - \phi = \theta' - \phi = \theta' - \phi' = (\theta - \phi')/3 = 0.627$).
A violation of the inequality occurs for $B_2 > 1$.

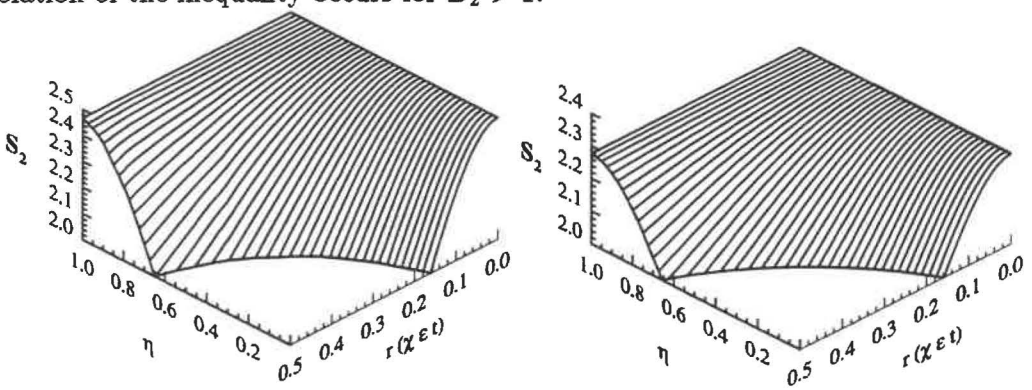

Figure 2.17: Plot of the maximum violation of the product Bell inequality using parametric down conversion. S_2 versus r, with varying photodetection efficiency η for
a) The polariser arrangement (angles chosen are $\theta = 1.290$, $\theta' = 0.666$, $\phi = 0.522$, $\phi' = 1.443$),
b) The phaseshifter/beamsplitter arrangement (angles are chosen such that $\varphi = \theta - \phi = \theta' - \phi = \theta' - \phi' = (\theta - \phi')/3 = 0.393$).
A violation of the inequality occurs for $S_2 > 2$.

Higher detection efficiencies allow violation of the Bell inequality for greater values of r, proportional to the pump intensity and the parametric interaction time. For higher r values, the mean intensities of the signal and idler fields become greater. Violation of the N-order Bell inequality is predicted in this regime, However, while the average photon number may be high, the parametric down conversior with a classical non-depleting pump as modelled here by (2.26), (2.29) has a super-Poissonian photon number distribution for the signal and idler fields. This means that the probability of actually detecting precisely N photons at C and D will be small. Also, because we consider here the reduced ensemble, auxiliary assumptions are used, making a strong test of the Bell inequality not possible, even in the high detection efficiency limit.

2.5 Generation of the Higher-Spin Correlated Quantum States using Parametric Oscillation

The correlated photon number states of the type (2.12) and $|N\rangle|N\rangle$ have been generated for $N = 1$ using parametric down conversion [9–11, 24, 66–70]. Generation of the N quanta wavepacket using parametric down conversion is made difficult because of the poor conversion efficiency of pump to signal photons. One possibility might be to improve the efficiency by employing nondegenerate parametric oscillation where the parametric process takes place inside a cavity. One can resonate the cavity in two orthogonal modes so that the parametric oscillation is modelled by the Hamiltonian

$$H = i\hbar\epsilon\left(c^{\dagger} - c\right) + i\hbar g\left(ca^{\dagger}b^{\dagger} - c^{\dagger}ab\right) + \sum_{i}\left(a_i^{\dagger}\Gamma_{Ri} + a_i\Gamma_{Ri}^{\dagger}\right) \tag{2.35}$$

Alternatively, we could consider four resonant modes

$$\begin{aligned} H &= i\hbar\epsilon\left(c^{\dagger} - c\right) + i\hbar g\left[c\left(a_{+}^{\dagger}b_{+}^{\dagger} + a_{-}^{\dagger}b_{-}^{\dagger}\right) - c^{\dagger}\left(a_{+}b_{+} + a_{-}b_{-}\right)\right] \\ &\quad + \sum_{i}\left[a_{i_{+}}^{\dagger}\Gamma_{Ri_{+}} + a_{i_{-}}^{\dagger}\Gamma_{Ri_{-}}\right] + \sum_{i}\left[a_{i_{+}}\Gamma_{Ri_{+}}^{\dagger} + a_{i_{-}}\Gamma_{Ri_{-}}^{\dagger}\right] \end{aligned} \tag{2.36}$$

as a means of generating the four mode state originally considered by Drummond [16]. Here ϵ is proportional to the classical pump amplitude. The modes c, a and b are the pump, signal and idler modes at the frequencies $\omega_1 + \omega_2$, ω_1 and ω_2 respectively. We also use the notation $a = a_1$, $b = a_2$ and $c = a_3$ for convenience. The loss of the field a_i through the cavity mirrors is modelled by the coupling to an external reservoir Γ_{Ri}. It is the field external to the cavity which is measurable and of interest to us here. We consider the situation where losses occur through just one of the cavity mirrors and denote the signal and idler fields transmitted through it by a_{ext} and b_{ext} respectively. The cavity photon loss rate is assumed equal for signal and idler and is denoted by 2κ. The external operators are related to the internal a and b operators by the boundary condition at the end-mirror. The model describing the interaction involving four cavity modes has been studied previously by Graham [79, 80] and Reid and Walls [7].

2.5.1 The Four Mode System

We present calculations for this case because the use of the four-mode as compared to the two-mode system may allow one to test at least in principle the stronger original form of the Bell inequality. In order to evaluate the quantum predictions for the classical inequalities (2.4) - (2.10) we consider the configurations discussed in Section (2.2) and calculate the joint probabilities such as that for detecting n_1 photons at C_+ and n_2 photons at D_+, in a particular detection time. The input fields denoted by a_+, b_+ in the Figures (2.1-2.2) are

now replaced by the external fields $a_{+\,ext}$, $b_{+\,ext}$. We will consider here only the situation where the photon detection time is much shorter than the field coherence time. Our initial objective is to demonstrate the possibility of obtaining violations of the Bell inequality using correlated states generated via cavity configurations [74]. For detection times much shorter than the field coherence time the probabilities are directly proportional to the normally-ordered correlation functions of the field. Thus for example the probability of detecting n_1 photons at C_+ and n_2 photons at D_+ is given by

$$P(m_1(\theta), m_2(\phi)) \sim \langle : c_{+ext}^{\dagger\, n_1} c_{+ext}^{n_1} d_{+ext}^{\dagger\, n_2} d_{+ext}^{n_2} : \rangle \tag{2.37}$$

where

$$n_1 = m_1(\theta) + N/2 \tag{2.38}$$

$$n_2 = m_2(\phi) + N/2 \tag{2.39}$$

The constant of proportionality is $(\eta T)^{n_1+n_2}$ and is the effective detection efficiency factor, taken here to be small. Here the $c_{\pm\, ext}$, $d_{\pm\, ext}$ are defined in terms of the external signal and idler fields $a_{\pm\, ext}$ and $b_{\pm\, ext}$ in accordance with the transformations (2.1) or (2.2). The detection time T is assumed here to be short so that the n_1 and n_2 quanta are detected simultaneously on the time-scale of the passage time for the photons through the beam-splitter/polariser or interferometric apparatus.

In order to test the classical inequalities for a fixed value of spin N/2, we would like to focus attention on situations where a total of N quanta are incident and detected at each location C and D. Because we consider here a low efficiency limit, it becomes necessary in practice to consider the weaker versions of the classical inequalities, where we only record events for the subensemble where N photons are detected at both C and D. Thus we calculate the probability of detecting n_1 photons at c_+, $N - n_1$ photons at c_-, n_2 photons at D_+, and $N - n_2$ photons at D_- . The probability $P_N(\theta, \phi)$ defined for the Clauser-Horne-type inequality (2.7), becomes

$$P_N(\theta,\phi) = \frac{\langle : c_{+ext}^{\dagger\, N} c_{+ext}^{N} d_{+ext}^{\dagger\, N} d_{+ext}^{N} : \rangle}{\langle : \left[c_{+ext}^{\dagger} c_{+ext} + c_{-ext}^{\dagger} c_{-ext}\right]^N \left[d_{+ext}^{\dagger} d_{+ext} + d_{-ext}^{\dagger} d_{-ext}\right]^N : \rangle} \tag{2.40}$$

The 'marginal' probability defined in the inequality becomes

$$P_N(\theta,-) = \frac{\langle : c_{+ext}^{\dagger\, N} c_{+ext}^{N} \left[d_{+ext}^{\dagger} d_{+ext} + d_{-ext}^{\dagger} d_{-ext}\right]^N : \rangle}{\langle : \left[c_{+ext}^{\dagger} c_{+ext} + c_{-ext}^{\dagger} c_{-ext}\right]^N \left[d_{+ext}^{\dagger} d_{+ext} + d_{-ext}^{\dagger} d_{-ext}\right]^N : \rangle} \tag{2.41}$$

The spin-product expectation value defined for inequality (2.10) becomes

$$E_N(\theta,\phi) = \frac{\langle : \left[c_{+ext}^{\dagger} c_{+ext} - c_{-ext}^{\dagger} c_{-ext}\right]^N \left[d_{+ext}^{\dagger} d_{+ext} - d_{-ext}^{\dagger} d_{-ext}\right]^N : \rangle}{\langle : \left[c_{+ext}^{\dagger} c_{+ext} + c_{-ext}^{\dagger} c_{-ext}\right]^N \left[d_{+ext}^{\dagger} d_{+ext} + d_{-ext}^{\dagger} d_{-ext}\right]^N : \rangle} \tag{2.42}$$

The moments required are directly related through the transformations (2.1) and (2.2) to moments involving the external flux operators $a_{\pm\, ext}$ and $b_{\pm\, ext}$. The correlation functions for the external operators are related to those of the cavity modes $a_\pm$ and $b_\pm$ as determined by the cavity boundary condition. This has been considered previously [81–83] and one obtains relations such as

$$\langle : a_{ext}^{\dagger i} a_{ext}^{j} b_{ext}^{\dagger\, k} b_{ext}^{l} : \rangle = (2\kappa)^{\frac{i+j+k+l}{2}} \langle : a^{\dagger i} a^{j} b^{\dagger\, k} b^{l} : \rangle \tag{2.43}$$

The normally ordered moments are directly related through the constant of proportionality which is the appropriate power of $\sqrt{2\kappa}$. The cavity moments have been derived previously [7] for the case where $\kappa_3 \gg \kappa$ where κ_3 is the cavity loss rate for the pump mode c. The approach used was to derive a Fokker-Planck equation for the generalised P representation [84] of the density operator.

$$\hat{\rho} = \int P\left[\left(\alpha_i^\dagger, \alpha_i\right)\right] \frac{|(\alpha_i)\rangle\langle\left(\alpha_i^\dagger\right)|}{\langle\left(\alpha_i^\dagger\right)|(\alpha_i)\rangle} d\mu \tag{2.44}$$

Here $|(\alpha_i)\rangle = |\alpha_+\rangle|\alpha_-\rangle|\beta_+\rangle|\beta_-\rangle$ and $d\mu$ is an integration measure. Here $\alpha_\pm$, $\alpha_\pm^\dagger$, $\beta_\pm$, $\beta_\pm^\dagger$ are c-numbers corresponding to operators $a_\pm$, $a_\pm^\dagger$, $b_\pm$, $b_\pm^\dagger$ respectively. The α_i and $\alpha_i^\dagger$ are independent complex variables. The equation for $P\left[\left(\alpha_i^\dagger, \alpha_i\right)\right]$ is derived using standard methods from the master equation for the density operator. The Fokker-Planck equation is equivalent to the following c-number equations in the stochastic amplitudes, where the pump has been eliminated adiabatically

$$\dot{\alpha}_+ = -\kappa\alpha_+ + \frac{g\beta_+^\dagger}{\kappa_3}\left[\epsilon - g\alpha_+\beta_+ - g\alpha_-\beta_-\right] + F_{\alpha_+}(t) \tag{2.45}$$

$$\dot{\beta}_+ = -\kappa\beta_+ + \frac{g\alpha_+^\dagger}{\kappa_3}\left[\epsilon - g\alpha_+\beta_+ - g\alpha_-\beta_-\right] + F_{\beta_+}(t) \tag{2.46}$$

The equations for $\alpha_+^\dagger$ and $\beta_+^\dagger$ are obtained by exchanging $\alpha_\pm$ and $\alpha_\pm^\dagger$, and $\beta_\pm$ and $\beta_\pm^\dagger$ and taking the complex conjugate of the other terms. Similarly the equation for α_-, β_-, $\alpha_-^\dagger$ and $\beta_-^\dagger$ are obtained by exchanging α_+ and α_-, β_+ and β_-, $\alpha_+^\dagger$ and $\alpha_-^\dagger$, and $\beta_+^\dagger$ and $\beta_-^\dagger$. The nonzero noise correlations are

$$\langle F_{\alpha_\pm}(t)F_{\beta_\pm}(t')\rangle = g\epsilon\delta(t-t') \tag{2.47}$$

$$\langle F_{\alpha_\pm^\dagger}(t)F_{\beta_\pm^\dagger}(t')\rangle = g\epsilon^*\delta(t-t') \tag{2.48}$$

Reid and Walls [7] derived a potential solution for P in the steady state. An appropriate contour of integration was defined. Normally-ordered moments are calculated directly by integrating over the P-solution. For example

$$\langle : a_+^{\dagger N} a_+^N b_+^{\dagger N} b_+^N : \rangle = \int P\left(\left[\alpha_i^\dagger, \alpha_i\right]\right) \alpha_+^{\dagger N}\alpha_+^N\beta_+^{\dagger N}\beta_+^N d\mu \tag{2.49}$$

The stochastic equations reduce to the classical equations if one ignores the quantum noise terms and uses $\alpha_i^\dagger = \alpha_i^*$. The classical threshold condition is readily derived by examining the steady state solutions for the classical amplitudes. Here $g\epsilon/\kappa_3\kappa = 1$ corresponds to threshold. Here we are concerned only with the system operating below threshold where the classical steady state solution is $\alpha_+ = \alpha_- = \beta_+ = \beta_- = 0$.

In all current experiments the threshold photon number is very large and the effect of the quantum noise is to perturb about the classical solutions. In this limit, predictions may be obtained from a linearisation of the fluctuations. One may choose to linearize operator equations derived directly from (2.35) or to linearize the stochastic equations (2.47) and (2.49). It is particularly convenient to note that, as is the case with the state (2.13) the equations are invariant under rotations of the stochastic variables $\alpha_\pm$, $\beta_\pm$ to the new variables $c_\pm$ and $d_\pm$

$$\begin{aligned} c_+ &= \alpha_+\cos\theta + \alpha_-\sin\theta \\ c_- &= -\alpha_+\sin\theta + \alpha_-\cos\theta \\ d_+ &= \beta_+\cos\theta + \beta_-\sin\theta \\ d_- &= -\beta_+\sin\theta + \beta_-\cos\theta \end{aligned} \tag{2.50}$$

The stochastic variables $c_\pm$, $d_\pm$ determine directly the moments of the measured $c_{\pm ext}$ and $d_{\pm ext}$ fields in accordance with the relation of the type (2.44). Thus it is convenient to rotate the $\alpha_\pm$ and $\beta_\pm$ by θ, the angle determined by the measurement made at C. One then evaluates the prediction of $P_N(\theta, \phi)$ by considering correlations of the type $\langle : c_+^{\dagger N} c_+^N d_+^{\dagger N} d_+^N : \rangle$ where

$$\begin{aligned} c_+ &= \alpha_+ \\ c_- &= \alpha_- \\ d_+ &= \beta_+ \cos\varphi + \beta_- \sin\varphi \\ d_- &= -\beta_+ \sin\varphi + \beta_- \cos\varphi \end{aligned} \tag{2.51}$$

and here $\varphi = \phi - \theta$. The Figure (2.18) depicts the violation of the classical inequality (2.7), for N = 1 and N = 2, while Figure (2.19) depicts the results for the product inequality (2.10). Here we have used linearized solutions.

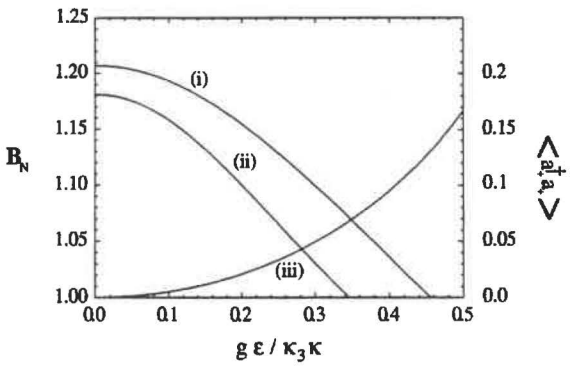

Figure 2.18: Plot of the violation of the four-mode Clauser-Horne Bell inequality, B_N versus $g\epsilon/\kappa_3\kappa$ for parametric oscillation. Here we have $\kappa_3/\kappa = 10$ and plot for (i) N=1, (ii) N=2. Curve (iii) is the mean photon number $\langle a_+^\dagger a_+ \rangle$. The same results occur for both the polariser and phaseshifter arrangements. A violation of the inequality occurs for $B_N > 1$ (The angles are chosen for each N to maximise the violation).

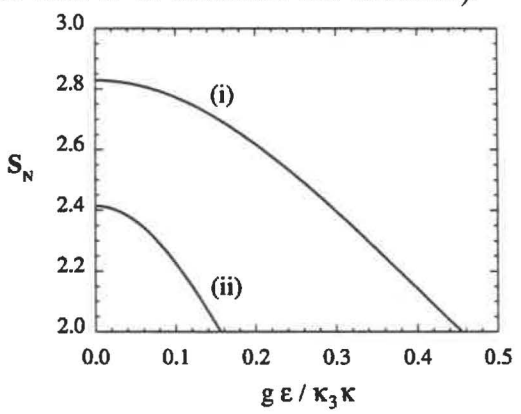

Figure 2.19: Plot of the violation of the four-mode product Bell inequality, S_N versus $g\epsilon/\kappa_3\kappa$ for parametric oscillation. Here we have $\kappa_3/\kappa = 10$ and plot for (i) N=1, (ii) N=2. The same results occur for both the polariser and phaseshifter arrangements. A violation of the inequality occurs for $S_N > 2$ (The angles are chosen for each N to maximise the violation).

2.5.2 The Two Mode Results

So far we have investigated the four mode results. It is also possible to do the two mode calculation. Using a similar procedure to before we can write down the following c number equations

$$\dot{\alpha} = -\kappa\alpha + \frac{g\beta^\dagger}{\kappa_3}[\epsilon - g\alpha\beta] + F_\alpha(t) \tag{2.52}$$

$$\dot{\beta} = -\kappa\beta + \frac{g\alpha^\dagger}{\kappa_3}[\epsilon - g\alpha\beta] + F_\beta(t) \tag{2.53}$$

The equation for $\alpha^\dagger$ and $\beta^\dagger$ are obtained by exchanging α and $\alpha^\dagger$, and β and $\beta^\dagger$ and taking the complex conjugate of the other terms. The nonzero noise correlations are

$$\langle F_\alpha(t)F_\beta(t')\rangle = g\epsilon\delta(t-t') \tag{2.54}$$

$$\langle F_{\alpha^\dagger}(t)F_{\beta^\dagger}(t')\rangle = g\epsilon^*\delta(t-t') \tag{2.55}$$

It is then possible to linearize these equations and hence calculate the expectation values and correlation functions needed for the Clauser-Horne and product Bell inequality. It is also possible to solve the nonlinear equations in the regime where $\kappa_3 \gg \kappa$ [85]. In Figure (2.20-2.21) we present results for the two mode case, using a linearized analysis.

2.5.3 Discussion

Results for N = 1 have been derived previously Reid and Walls [7] for the four-mode case. It is seen that violation of the Bell inequality is possible only if one operates sufficiently far below threshold. The reason for the loss of violation when at higher pump powers becomes apparent when one considers the following simple model Hamiltonian for the four-or two-mode parametric down conversion below threshold, where the pump mode is essentially undepleted and may be modelled as a classical pump.

$$H = -\hbar\chi\epsilon\left\{(a_+b_+ + a_-b_-) + \left(a_+^\dagger b_+^\dagger + a_-^\dagger b_-^\dagger\right)\right\} \tag{2.56}$$

$$H = -\hbar\chi\epsilon\left(ab + a^\dagger b^\dagger\right) \tag{2.57}$$

This model has been discussed above in Section (2.6). For finite ϵ, one generates a superposition of the N-quanta states of the type given by (2.12). At low pump powers only the N = 1 state contributes significantly and the violation of the inequalities is obtained. As ϵ increases the higher-N states are more important. Let us suppose we are interested in the $\frac{N_o}{2}$-spin experiment. At higher-pump values, the states with $N > N_o$ give a finite contribution to moments such as $\langle : c_+^{\dagger N_o} c_+^{N_o} d_+^{\dagger N_o} d_+^{N_o} : \rangle$. Thus in the situation we examine here of low photon-detection efficiency, these higher-N states contribute to the joint photodetection probabilities. Their effect is to decrease or destroy the violation of the $\frac{N_o}{2}$-spin classical inequality. It is seen from the results for $N_o = 2$ that the N_o-state can be made to dominate and thus to give the violation similar to that predicted by the higher spin quantum states (2.12) provided the pump amplitude is sufficiently low. In situations where the detection time T is greater and the detection efficiency increased, one would expect to recover results similar to that described in Section (2.6).

2.6 Derivation of the N-particle Bell inequality

We summarise the derivation of the Clauser-Horne and Clauser-Horne-Shimony-Holt-Bell inequality used in this chapter. The derivations are straightforward extensions of the original derivations by Bell [1] and Clauser-Horne-Shimony and Holt [61], (as pointed out by Drummond [16]).

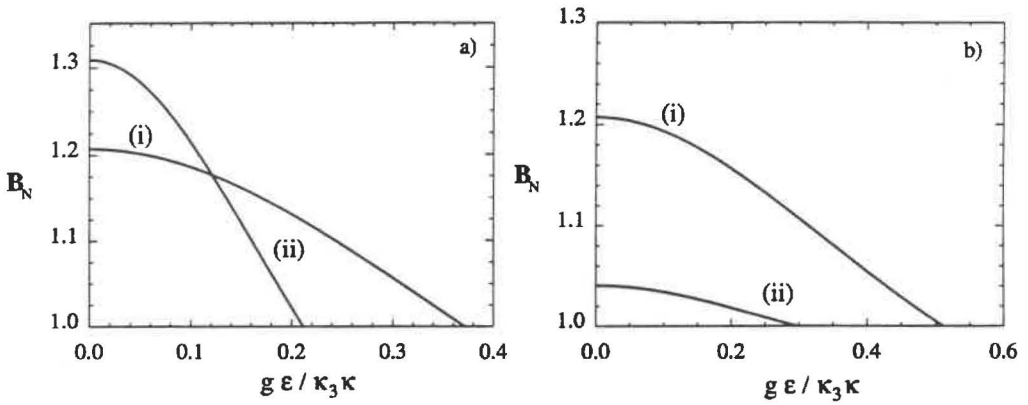

Figure 2.20: Plot of the violation of the two mode Clauser-Horne Bell inequality, B_N versus $g\epsilon/\kappa_3\kappa$ for parametric oscillation. Here we have $\kappa_3/\kappa = 10$ and plot for
a) The polariser arrangement with (i) N=1 (ii) N=2.
b) The phaseshifter/beamsplitter arrangement with (i) N=1 (ii) N=2.
A violation of the inequality occurs for $B_N > 1$ (The angles are chosen for each N to maximise the violation).

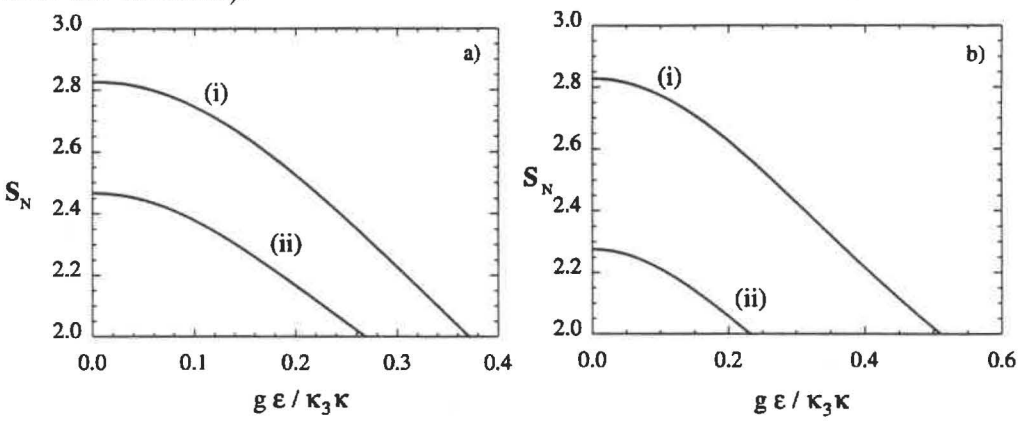

Figure 2.21: Plot of the violation of the two mode product Bell inequality, S_N versus $g\epsilon/\kappa_3\kappa$ for parametric oscillation. Here we have $\kappa_3/\kappa = 10$ and plot for
a) The polariser arrangement with (i) N=1 (ii) N=2.
b) The phaseshifter/beamsplitter arrangement with (i) N=1 (ii) N=2.
A violation of the inequality occurs for $S_N > 2$ (The angles are chosen for each N to maximise the violation).

2.6.1 The N-particle Clauser-Horne Inequality derivation

The set of "hidden" variables which we will denote collectively by the symbol λ is introduced. For given λ, the values of all observables are specified as the values of appropriate real-valued functions defined over the domain Λ of all possible values for the hidden variables. Now denoting the probability density function for the hidden variables in the state $|\psi\rangle$ by ρ we have that $\rho(\lambda)d\lambda$ measures the probability that the collective hidden variable lies in the range λ to $\lambda + d\lambda$. The probability density function is normalised such that

$$\int_\Lambda \rho(\lambda)d\lambda = 1 \tag{2.58}$$

Also it is required that

$$\rho(\lambda) \geq 0 \tag{2.59}$$

We now examine the situations described by Figures (2.1) and (2.2). Applying this hidden variable description to the marginal probability $P_1^N(\theta)$ for detecting a total of N photons at C_+, we may write

$$P_N^1(\theta) = \int_\Lambda P_N^1(\lambda,\theta)\rho(\lambda)d\lambda \tag{2.60}$$

where $P_N^1(\lambda,\theta)$ is the probability given the state described by λ. Similarly we have

$$P_N^2(\phi) = \int_\Lambda P_N^2(\lambda,\phi)\rho(\lambda)d\lambda \tag{2.61}$$

where $P_N^2(\phi)$ is the marginal probability for detecting a total of N photons at D_+, and $P_N^2(\lambda,\phi)$ is the probability of detecting N photons D_+, given λ and ϕ. The joint probability of simultaneously detecting N photons at both C_+ and D_+ is

$$P_N^{12}(\theta,\phi) = \int_\Lambda P_N^{12}(\lambda,\theta,\phi)\rho(\lambda)d\lambda \tag{2.62}$$

where $P_N^{12}(\lambda,\theta,\phi)$ is the probability of detecting N photons at both locations, given λ, θ and ϕ. Mathematically the locality assumption is written

$$P_N^{12}(\lambda,\theta,\phi) = P_N^1(\lambda,\theta).P_N^2(\lambda,\phi) \tag{2.63}$$

and therefore Eqn (2.62) reduces to

$$P_N^{12}(\theta,\phi) = \int_\Lambda P_N^1(\lambda,\theta)P_N^2(\lambda,\phi)\rho(\lambda)d\lambda \tag{2.64}$$

Next we have the following lemma:

Lemma:

If x, x', y, y' and X, Y are real numbers such that

$$0 \leq x \quad , \quad x' \leq X \qquad \text{and} \qquad 0 \leq y \quad , \quad y' \leq Y \tag{2.65}$$

Then the inequality given by

$$0 \geq xy - xy' + x'y + x'y' - x'Y - yX \geq -XY \tag{2.66}$$

holds. Choosing $x = P_N^1(\lambda,\theta)$, $y = P_N^2(\lambda,\phi)$, $X = Y = 1$, we have

$$\begin{aligned} -1 \leq P_N^{12}(\lambda,\theta,\phi) - P_N^{12}(\lambda,\theta,\phi') &+ P_N^{12}(\lambda,\theta',\phi) + P_N^{12}(\lambda,\theta',\phi') \\ &- P_N^1(\lambda,\theta') - P_N^2(\lambda,\phi) \leq 0 \end{aligned} \tag{2.67}$$

Integrating inequality (2.67) over λ with distribution $\rho(\lambda)d\lambda$ the RHS of the inequality can be written as

$$B_N = \frac{P_N^{12}(\theta,\phi) - P_N^{12}(\theta,\phi') + P_N^{12}(\theta',\phi) + P_N^{12}(\theta',\phi')}{P_N^1(\theta') + P_N^2(\phi)} \leq 1 \tag{2.68}$$

To date no situation that violates the Clauser-Horne inequality has been experimentally realised, because of poor photodetection efficiencies. With an auxiliary assumption [25, 26, 61], realisable experiments have been predicted and shown experimentally to yield a violation of the Bell inequality. We consider the apparatus depicted in Figures (2.1) and (2.2), but now select to measure only joint probabilities where a total of N photons are detected at both C and D. One measures the joint probability $P_N^{12}(\theta,\phi)$ as before, and also the one-sided joint probability $P_N^{12}(\theta,-)$, which corresponds to the probability of measuring N photons at C_+ and N photons at D where the analyser (polariser or beamsplitter) at D is removed. The $P_N^{12}(-,\phi)$ is the joint probability of detecting N photons at D_+ and N photons at C with the analyser at C removed. In terms of a hidden variable theory the one-sided probabilities are written

$$P_N^{12}(\theta,-) = \int_\Lambda \rho(\lambda) P_N^1(\lambda,\theta) P_N^2(\lambda) d\lambda \tag{2.69}$$

where the one sided state described by λ has been factorised using the locality assumption and we have defined $P_N^2(\lambda)$ as the probability of detecting N photons at D with the analyser at D removed given λ. One defines $P_N^1(\lambda)$ as the probability of detecting N photons at C with the analyser at C removed. Thus

$$P_N^{12}(-,\phi) = \int_\Lambda \rho(\lambda) P_N^1(\lambda) P_N^2(\lambda,\phi) d\lambda \tag{2.70}$$

and as before

$$P_N^{12}(\theta,\phi) = \int_\Lambda \rho(\lambda) P_N^1(\lambda,\theta) P_N^2(\lambda,\phi) d\lambda \tag{2.71}$$

One can now choose (note the $P_N^1(\lambda)$ and $P_N^2(\lambda)$ do not depend on θ and ϕ)

$$x = \frac{P_N^1(\lambda,\theta)}{P_N^1(\lambda)} \quad \text{and} \quad y = \frac{P_N^2(\lambda,\theta)}{P_N^2(\lambda)} \tag{2.72}$$

and introduce the auxiliary assumption

$$P_N^1(\lambda,\theta) \leq P_N^1(\lambda), \qquad P_N^2(\lambda,\theta) \leq P_N^2(\lambda) \tag{2.73}$$

One selects $X = Y = 1$. Thus one can use the lemma to derive the inequality

$$B_N = \frac{P_N(\theta,\phi) - P_N(\theta,\phi') + P_N(\theta',\phi) + P_N(\theta',\phi')}{P_N(\theta',-) + P_N(-,\phi)} \leq 1 \tag{2.74}$$

where the marginal probabilities are replaced by the one-sided joint probabilities. We have dropped the superscripts for simplicity.

The weaker inequality (2.74) derived with the auxiliary assumption (2.73) has been traditionally used where only a single photons pair is emitted from the source at a time and there is a small probability of actually detecting both photons. One can make measurements and inferences only on the detected ensemble. Our use of the inequality (2.74) in Section (2.6) is slightly broader than this, and special care needs to be taken with the auxiliary assumptions. We examine the parametric down conversion in the regime where r can be large. If attempting to test the N-particle inequalities, we measure the joint probability $P_N(\theta,\phi)$ and the one-sided joint probability $P_N(\theta,-)$ where no polariser is present

at D. Now for larger r, there is a significant probability that more than N photons are emitted by the source in each signal and idler field. Let us imagine $N+1$ photons incident at each of the analysers at C and D. If all photons are detected, this emission will not contribute to the experimenters measurement of $P_N(\theta,-)$. It will however contribute to $P_N(\theta,\phi)$, since it can give a nonzero probability for precisely N photons being detected at C_+. The auxiliary assumption (2.73) thus is not so reasonable in this case, particularly where higher detection efficiencies are considered. In the next section, we consider another situation where the auxiliary assumption (2.73) will not be valid.

In the situations of parametric down conversion with arbitrary r, the Clauser-Horne-type experiment suggested employs additional detectors at C_- and D_- to select the subensemble where a total of N photons are detected at C and D. We consider the derivation of a suitably modified Clauser-Horne inequality. The one-sided probability $P_N^{12}(\theta,-)$ in equations (2.69)-(2.74) now becomes $P_{N,0,N}^{12}(\theta,-)$, the joint probability of detecting N photons at D (with the analyser at D removed), N photons at C_+ and zero photons at C_-. $P_N^{12}(-,\phi)$ becomes $P_{N,N,0}^{12}(-,\phi)$, the joint probability of detecting N photons at C (with the analyser at C removed), N photons at D_+ and zero photons at D_-. The $P_N^1(\lambda,\theta)$ becomes $P_{N,0}^1(\lambda,\theta)$ the probability for detecting N photons at C_+ and zero photons at C_-, given λ. $P_N^2(\lambda,\phi)$ becomes $P_{N,0}^2(\lambda,\phi)$ the probability of detecting N photons at D_+ and zero photons at D_-, given λ. The $P_N^1(\lambda)$ and $P_N^2(\lambda)$ remain as defined previously. The probability $P_N^{12}(\theta,\phi)$ becomes $P_{N,0,N,0}^{12}(\theta,\phi)$, the joint probability for detecting N photons at C_+, zero photons at C_-, N photons at D_+ and zero photons at D_-. With the auxiliary assumption now being

$$\begin{aligned} P_{N,0}^1(\lambda,\theta) &\leq P_N^1(\lambda) \\ P_{N,0}^2(\lambda,\phi) &\leq P_N^2(\lambda), \end{aligned} \tag{2.75}$$

the derivation of the following inequality follows

$$B_N = \frac{P_{N,0,N,0}(\theta,\phi) - P_{N,0,N,0}(\theta,\phi') + P_{N,0,N,0}(\theta',\phi) + P_{N,0,N,0}(\theta',\phi')}{P_{N,0,N}(\theta,-) + P_{N,N,0}(-,\phi)} \leq 1 \tag{2.76}$$

This is the inequality tested in Section (2.4) and (2.5). The auxiliary assumption becomes: for every λ, the probability of detecting N photons at C_+ and zero photons at C_- is always less than the probability of detecting N photons with the analyser at C removed (and similarly for D). The additional detectors at C_- and D_- make the assumption much stronger.

2.6.2 The Nth-Order Product Bell Inequality Derivation

We now derive the Nth-order product Bell inequality. This is a straightforward generalisation of previous proofs of Bell and CHSH [61]. We may write the measured quantity $E_N(\theta,\phi)$ defined in (2.8) and (2.9) in terms of the hidden variables as follows

$$\begin{aligned} E_N(\theta,\phi) &= \int \rho(\lambda)\, E_N^1(\lambda,\theta) E_N^2(\lambda,\phi) d\lambda \\ &= \int \rho(\lambda) \left\{ P_N^1(\lambda,\theta) - P_{N-1}^1(\lambda,\theta) + P_{N-2}^1(\lambda,\theta) - \ldots \right\} \\ &\qquad \times \left\{ P_N^2(\lambda,\phi) - P_{N-1}^2(\lambda,\phi) + P_{N-2}^2(\lambda,\phi) - \ldots \right\} d\lambda \end{aligned} \tag{2.77}$$

where $E_N^1(\lambda,\theta)$ and $E_N^2(\lambda,\phi)$ are the products defined in (2.8) at positions C and D respectively, given the state specified by λ. These products may be defined in terms of the probabilities $P_{N-i}^1(\lambda,\theta)$ and $P_{N-i}^2(\lambda,\phi)$ where $i = 0 \ldots N$. Here $P_{N-i}^1(\lambda,\theta)$ is the

probability of detecting $N-i$ photons at C_+ and i photons at C_-, given the state specified by λ. The $P^2_{N-i}(\lambda,\phi)$ is the probability of detecting $N-i$ photons at D_+ and i photons at D_-, given λ. Since

$$\left|E^1_N(\lambda,\theta)\right|, \left|E^2_N(\lambda,\phi)\right| \leq 1 \tag{2.78}$$

one can derive the following Bell inequality along the lines of Bell's original proof for $N=1$.

$$S_N = |E_N(\theta,\phi) - E_N(\theta,\phi') + E_N(\theta',\phi) + E_N(\theta',\phi')| \leq 2 \tag{2.79}$$

For realisable situations to date involving photodetectors, the probability of detecting a total of N photons at C and D is small even where one has precisely N photons incident on each analyser, because of the detection inefficiencies. Thus $E_N(\theta,\phi)$ is small and the inequality not violated. We may introduce an auxiliary assumption to allow a testable experiment by considering only measurements over the subensemble where a total of N photons are detected at both C and D. We define

$$S^1_N(\lambda,\theta) = \frac{P^1_N(\lambda,\theta) - P^1_{N-1}(\lambda,\theta) + P^1_{N-2}(\lambda,\theta) - \ldots}{P^1_N(\lambda,\theta) + P^1_{N-1}(\lambda,\theta) + P^1_{N-2}(\lambda,\theta) + \ldots} \tag{2.80}$$

and

$$S^2_N(\lambda,\theta) = \frac{P^2_N(\lambda,\theta) - P^2_{N-1}(\lambda,\theta) + P^2_{N-2}(\lambda,\theta) - \ldots}{P^2_N(\lambda,\theta) + P^2_{N-1}(\lambda,\theta) + P^2_{N-2}(\lambda,\theta) + \ldots} \tag{2.81}$$

Rearranging we obtain

$$E_N(\theta,\phi) \;=\; \int f(\lambda) S^1_N(\lambda,\theta) S^2_N(\lambda,\phi) d\lambda \tag{2.82}$$

where

$$f(\lambda) = \rho(\lambda)\left\{P^1_N(\lambda,\theta) + P^1_{N-1}(\lambda,\theta) + \ldots\right\}\left\{P^2_N(\lambda,\phi) + P^2_{N-1}(\lambda,\phi) + \ldots\right\} \tag{2.83}$$

is the probability distribution for the subensemble. With the assumption $|S^1_N(\lambda,\theta)| \leq 1$ and $|S^2_N(\lambda,\phi)| \leq 1$, and assuming $f(\lambda)$ is independent of θ and ϕ (this is the auxiliary assumption), one can derive the normalised inequality

$$\bar{S}_N = |\bar{E}_N(\theta,\phi) - \bar{E}_N(\theta,\phi') + \bar{E}_N(\theta',\phi) + \bar{E}_N(\theta',\phi')| \leq 2 \tag{2.84}$$

where $\bar{E}_N(\theta,\phi)$ is the product $E_N(\theta,\phi)$ calculated over the reduced ensemble.

Previously the weaker inequality (2.84) has been used for situations where a precise number of photons are (assumed) incident on each analyser at C and D, but because of poor detector efficiencies the probability of all the photons being detected and hence contributing to the measured subensemble, is actually small. Our use of the inequality in Sections (2.4) and (2.5) is somewhat broader. Let us select to measure the Nth order correlation $\bar{S}_N$ or S_N. For higher r values, there is a significant probability that the source emits greater than N ($k>0$) photons into each signal and idler field. We thus consider the measured subensemble to be one where not necessarily all of the photons are detected. The standard auxiliary assumption still applies here: that for every λ, the probability of detection of a total of N photons at C (and a total of N photons at D) is independent of the analyser angle θ (and ϕ).

2.7 The Validity of Auxiliary Assumptions in the case of Noisy Detection

In the recent nondegenerate parametric down conversion experiment of Smithey et al [24], subshot noise photon number correlations for twin pulses each with approximately 10^6 photons was demonstrated. Here one was able to use photodiodes with $85-90\%$ quantum efficiency. Thus it is possible to work in a truly macroscopic regime with the high efficiencies indicated in Figures (2.16-2.17). However a new limitation does become apparent. Electronic noise limits the resolution available in determining N the number of photoelectrons. In the experiment demonstrating subshot noise performed by Smithey et al with $N = 10^6$ photons the uncertainty in this photon number was of order $\Delta N = 324$ photoelectrons.

We need to examine the effect of this reduction in resolution of photon number detected on the Bell-inequality experiments we have proposed. Let us consider the N-th order Clauser-Horne experiment as seen in Figure (2.22.a) for the $P_N(\theta,\phi)$ measurement and Figure (2.22.b) for the $P_N(-,\phi)$ case. In the Clauser-Horne inequality we have the auxiliary assumption that requires

$$\begin{aligned} P_N^1(\lambda,\theta) &\leq P_N^1(\lambda,-) \\ P_N^2(\lambda,\phi) &\leq P_N^2(\lambda,-) \end{aligned} \tag{2.85}$$

If one requires to use extra detectors at C_- and D_- as in the down conversion experiments for higher r, one has the auxiliary assumption (2.75). This condition must be satisfied for the inequality to be valid. These assumptions are reasonable when dealing with inefficient detectors. What happens when we have poor resolution instead of inefficient detectors?

An Idealised Situation using Correlated Photon Number States

Consider the case where we have a correlated photon number state $|N\rangle|N\rangle$ source. Let us consider our poor resolution to mean that our detectors could detect $N\pm\Delta N$ photons. Here we use the notation $N\pm\Delta N$ to mean the subset of $N-\Delta N$, $N-\Delta N+1$, ..., $N+\Delta N-1$, $N+\Delta N$ which is zero or positive. We would measure the quantities $P_{N\pm\Delta N}(\theta,\phi)$ and $P_{N\pm\Delta N}(-,\phi)$. For the case $N=3$, $\Delta N=1$ we have (Figure (2.22.c) and Figure (2.22.d)) (Here we do not add the additional detectors at C_-, D_-).

$$\begin{aligned} P_{3\pm1}(\theta,\phi) &= P_{3,3}(\theta,\phi)+P_{3,2}(\theta,\phi)+P_{2,3}(\theta,\phi)+P_{2,2}(\theta,\phi) \\ P_{3\pm1}(-,\phi) &= P_{3,3}(-,\phi)+P_{3,2}(-,\phi)+P_{2,3}(-,\phi)+P_{2,2}(-,\phi) \end{aligned} \tag{2.86}$$

where here $P_{i,j}(\theta,\phi)$ is the probability of detecting (with perfect resolution) i photons at C_+ and j photons at D_+. The $P_{i,j}(-,\phi)$ is similarly defined but with no analyser at C. According to a local hidden variable theory, we can write the generalisations of (2.69), (2.70), and (2.71). Thus for example

$$P^{12}_{N\pm\Delta N}(\theta,\phi) = \int \rho(\lambda)P^1_{N\pm\Delta N}(\lambda,\theta)P^2_{N\pm\Delta N}(\lambda,\phi)d\lambda \tag{2.87}$$

$$P^{12}_{N\pm\Delta N}(-,\phi) = \int \rho(\lambda)P^1_{N\pm\Delta N}(\lambda)P^2_{N\pm\Delta N}(\lambda,\phi)d\lambda \tag{2.88}$$

and where the auxiliary assumption (2.73) becomes

$$0 \leq P^1_{N\pm\Delta N}(\lambda,\theta) \leq P^1_{N\pm\Delta N}(\lambda) \tag{2.89}$$

$$0 \leq P^2_{N\pm\Delta N}(\lambda,\theta) \leq P^2_{N\pm\Delta N}(\lambda), \tag{2.90}$$

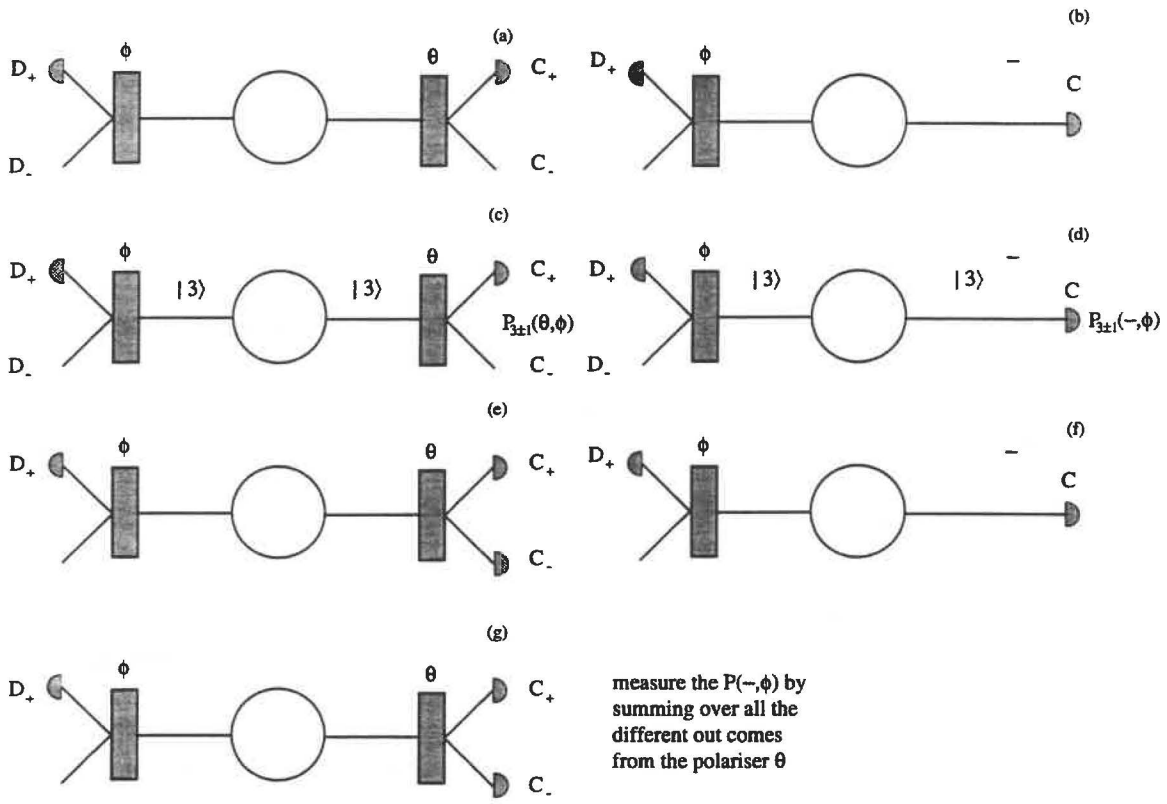

Figure 2.22: Possible experimental configurations for a test of the CHSH inequality for a) A measurement of the joint probability $P_N(\theta, \phi)$ with two detectors and two analysers. b) A measurement of the joint probability $P_N(-, \phi)$ with two detectors and one analyser. c) A measurement of the joint probability $P_{3\pm1}(\theta, \phi)$ with two detectors and two analysers for the case of a $|3\rangle|3\rangle$ correlated photon number state input. The outcomes where three photons and two photons are detected at each detector, will both contribute to the experimenter's calculation of $P_{3\pm1}(\theta, \phi)$.
d) A measurement of the joint probability $P_{3\pm1}(-, \phi)$ with two detectors and one polarisers for the case of a $|3\rangle|3\rangle$ correlated photon number state input. The situations where three photons and two photons are detected at each detector, will both contribute to the experimenters calculation of $P_{3\pm1}(\theta, \phi)$.
e) A measurement of the joint probabilities with three detectors and two analysers for the case of parametric down conversion.
f) A measurement of the one-sided joint probabilities with two detectors and one polarisers for the case of the parametric down conversion.
g) A measurement of the one-sided joint probabilities with three detectors and two polarisers for the case of parametric down conversion.

The assumption is that for every emission λ, the probability of detecting $N \pm \Delta N$ photons is never greater than that without a polariser. Let us consider our example, where three photons (in both signal and idler) are emitted by the source. The assumption that the probability of detecting three photons at C_+ is always less than that of detecting three photons at C with analyser removed seems reasonable. However, recalling that we wish to allow for the situation of good detection efficiencies, it is not reasonable to assume that the probability of detecting precisely two photons at C_+ is less than that of detecting two photons at C with analyser removed (according to quantum mechanics the second probability is actually zero if one has perfect efficiency). Thus the auxiliary assumptions are no longer so reasonable, and the corresponding weaker inequality could not be used in a test of local realism versus quantum mechanics.

Importantly, however, because situations of poor photon number resolution will actually correspond to high N situations where detector efficiencies may be high, it may not be necessary to use weaker inequalities. One could still consider testing the stronger inequality in the poor resolution situation. Here we define the marginal probabilities for example, $P^2_{3\pm1}(\phi) = P^2_3(\phi) + P^2_2(\phi)$, and $P^1_{3\pm1}(\phi) = P^1_3(\phi) + P^1_2(\phi)$ as the extensions of the probabilities defined in (2.60)-(2.62). Derivation of the stronger Clauser-Horne inequality can be derived

$$B_{N\pm\Delta N} = \frac{P^{12}_{N\pm\Delta N}(\theta,\phi) - P^{12}_{N\pm\Delta N}(\theta,\phi') + P^{12}_{N\pm\Delta N}(\theta',\phi) + P^{12}_{N\pm\Delta N}(\theta',\phi')}{P^1_{N\pm\Delta N}(\theta') + P^2_{N\pm\Delta N}(\phi)} \leq 1 \quad (2.91)$$

The Parametric Amplifier

One can calculate the effect of noisy resolution in the case of correlated photon number states. We assume the detection, while noisy, is perfectly efficient. However in the parametric amplifier case the system is a summation of many correlated photon number states, as given by Eqn (2.27). In this case we (for both Clauser-Horne and product inequalities) use an extra detector in an attempt to prepare the $|N\rangle|N\rangle$ state by ensuring that the sum of the photons at both C_+, C_- and at D_+, D_- was equal to N. Because of the limited resolution, the state preparation will not be precise. Such an experiment is depicted in Figure (2.22.e). Now for this arrangement, one still requires use of auxiliary assumptions, even though one may have perfect detectors, because we are restricting measurements to a particular subensemble. The question that must be asked is whether the auxiliary assumptions (2.85) are reasonable. As also discussed above, the assumptions will break down. Let us examine again the case of $N = 3$, $\Delta N = 1$. The possible states contributing to the measurement are $|2\rangle$, $|3\rangle$, $|4\rangle$, $|5\rangle$ which can be seen from the following analysis of what detections will be interpreted by the experimenter within the limits of his resolution as contributing to the relevant subensemble.

$$\begin{aligned}
&C_+ \quad \text{detects } 3 \pm 1 \text{ while } C_- \text{ detects } 0 \pm 1 \text{ photons} \\
&C_+ \quad \text{detects } 2 \pm 1 \text{ while } C_- \text{ detects } 1 \pm 1 \text{ photons} \\
&C_+ \quad \text{detects } 1 \pm 1 \text{ while } C_- \text{ detects } 2 \pm 1 \text{ photons} \\
&C_+ \quad \text{detects } 0 \pm 1 \text{ while } C_- \text{ detects } 3 \pm 1 \text{ photons}
\end{aligned} \quad (2.92)$$

$$C_+ \text{ and } C_- \text{ can detect } 2,\ 3,\ 4, \text{ or } 5 \text{ photons} \quad (2.93)$$

For example the outcome which the experimenter records as 3 photons at C_+ and 0 photons at C_- may arise from detection of 3 ± 1 and 0 ± 1 photons at C_+ and C_- respectively. First we notice from the case where we detect 3 photons at C_+ and 2 photons at C_- that

the state $|5\rangle$ does contribute to the required subensemble. However the outcome where we detect 5 photons at C_+ and 0 photons at C_- is not included by the experimenter as contributing. Hence we can see that the probability distribution for detection will have to depend on θ, ϕ, and hence the auxiliary assumptions used in the derivation of the usual Bell inequality (2.84) are not valid. The total number of counts for a particular θ and ϕ is not independent of θ and ϕ.

The addition of the extra detector in the Clauser-Horne-type experiment also causes a breakdown of the auxiliary assumptions (2.90) and (2.91). Let us consider now the experiment used to determine $P_{N\pm\Delta N}(-,\phi)$ (shown in Figure (2.22.f). It can be seen that on the side with no-polariser (and hence only one detector) the state $|5\rangle$ does not contribute at all, whereas it will contribute to the measurement of $P_{N\pm\Delta N}(\theta,\phi)$. Thus the auxiliary assumption is not valid. We might consider modifying the scheme to include two detectors for this "no-polariser" measurement (Figure (2.22.g)). We would leave the second θ polariser in and measure with two photon detectors both channels of the output from the polariser. Now the probability $P_N(-,\phi)$ would be interpreted as the joint probability of detecting N photons at D_+ and a total of N photons at the C_+ and C_- detectors (Figure 2.1). The auxiliary assumptions here would be that of the product case discussed above in Section (2.6.2). At the C polariser we have the following outcomes (2.93) and (2.94) as relevant by the experimenter for the $N = 3$, $\Delta N = 1$ case. Now the experimenter would want to measure $P_{3,0,3}$ (3 photons at C_+, 0 photons at C_-, 3 photons at D_+) say, but because of the poor resolution ($\Delta N = 1$), he would be actually monitoring the outcomes 3 ± 1 photons at C_+, 0 ± 1 photons at C_-, and 3 ± 1 photons at D_+. The experimenter then counts the number of times (measures the rate of such outcomes) the reading $(3,0,3)$ appears but this is really the number of times he/she measures $(3,0,3)$, $(2,1,3)$, $(3,0,2)$, $(3,1,2)$ at the output since the experimenter can't distinguish between these. To determine the probability $P_{3\ at\ C_+,\ 0\ at\ C_-,\ 3\ at\ D_+}(\theta,\phi)$ we could have perfect event-ready detectors which tell us when there is an emission. Then the probability

$$P_{3\ at\ C_+,\ 0\ at\ C_-,\ 3\ at\ D_+}(\theta,\phi) = \frac{\text{Number of times the results } (3,0,3) \text{ occurs}}{\text{Number of emissions}} \tag{2.94}$$

Next he/she will wish to measure the result $P_{2\ at\ C_+,\ 1\ at\ C_-,\ 3\ at\ D_+}(\theta,\phi)$. If we examine the probabilities calculated we observe that detecting two photons at C_+, one photon at C_- contributes to both the (3,0) result and the (2,1) result. Hence it will be calculated twice and so our calculated 'probabilities' would add to greater than one. Alternatively one could 'normalise', by calculating the probabilities as follows

$$P_{i,j,k} = \frac{P_{i,j,k}}{\sum_{i,j,k} P_{i,j,k}} \tag{2.95}$$

Here the sum of all probabilities $\sum_{i,j,k} P_{i,j,k}$ will contain terms such as $P_{2,1,3}$ twice, and hence will be dependent on the analyser angles θ and ϕ. This prevents the derivation of the usual 'weaker' Bell inequality. Thus one must be careful when determining a measurement scheme for the $P_{i,j,k}$. The difficulty is that the experimenter must channel each detection into one of the distinct $P_{i,j,k}$, even where some random choice is made since he does not possess the resolution to distinguish properly between (for ΔN=1) adjacent N. Note that experiments designed to test the product Bell inequality proposed here require the same care with auxiliary assumptions, since these also, in the case of the parametric amplifier, require more than one detector at C and the measurement of more than one $P_{i,j,k}$.

To conclude, testing the proposed Nth-order Bell inequality with a poor resolution of photon number detected can pose more problems in the case where the incident state is generated by parametric amplification. This is because here states of n, where n is not

necessarily equal to N, photon number can be incident on the analysers and cause a failing of the usual auxiliary assumptions which are introduced in this case, (even where there is a high detection efficiency), to restrict measurements to the case $n = N$. This problem may be overcome where one has incident on the analysers only the $|N\rangle|N\rangle$ state itself, so that the state preparation is done before passage through analysers rather than after. There is however another situation in which a violation of the Bell inequality may be obtained with poor detection resolution. This is the strong test of the Bell inequality where no auxiliary assumptions are made.

2.8 The Strong Bell inequality

In the previous section we found that a test of the weak Bell inequality was not always possible in the regime of poor detection resolution. In this regime the breakdown of the auxiliary assumptions made it impossible to derive the usual classical Bell inequality. However the weaker Bell inequality with the use of auxiliary assumptions was only necessary historically because of the poor detection efficiencies. The use of highly efficient photodiode detectors may enable the use of the strong Bell inequality where auxiliary assumptions are not needed. We investigate this possibility, modelling poor detection resolution but assuming perfect efficiencies.

In this section we thus investigate the strong Bell inequality given by Eqn (2.68). To begin we will again consider the ideal correlated state $\frac{\left(a_+^\dagger b_+^\dagger + a_-^\dagger b_-^\dagger\right)^N}{N!(N+1)^{1/2}}|0\rangle$ with perfect detection efficiency and perfect resolution[1]. From (2.68) as discussed in Section (2.3) we need to calculate the joint probability $P_{n,n}(\theta,\phi)$ of detecting n photons at C_+ and n photons at D_+ and the marginal probabilities $P_n(\theta)$ and $P_n(\phi)$ of detecting n photons at C_+ and D_+ respectively. We assume perfect detection efficiency throughout ($\eta = 1$). Thus automatically for the input state given above we know that if for example n photons are detected at C_+, there will be $N - n$ photons at C_-. The joint probability $P_{n,n}(\theta,\phi)$ is given by

$$P_{n,n}(\theta,\phi) = \langle : \left\{ \left(c_+^\dagger c_+ d_+^\dagger d_+ \right)^n \exp\left[-c_+^\dagger c_+ - d_+^\dagger d_+ \right] \right\} : \rangle \tag{2.96}$$

while the probability $P_n(\theta)$ of detecting n photons at C_+ is

$$P_N(\theta) = \langle : \left\{ \left(c_+^\dagger c_+ \right)^n \exp\left[-c_+^\dagger c_+ \right] \right\} : \rangle \tag{2.97}$$

and the probability $P_n(\phi)$ of detecting n photons at D_+ is

$$P_n(\phi) = \langle : \left\{ \left(d_+^\dagger d_+ \right)^n \exp\left[-d_+^\dagger d_+ \right] \right\} : \rangle \tag{2.98}$$

Figures (2.23-2.24) depict the violation of the classical strong Clauser-Horne-Bell inequality for various values of n and N. It is clearly seen from these figures that for all n, there is a violation of the Bell inequality. For an initial state with $N = 10$, it can be seen that there is a violation even if only one photon is detected at C_+ and D_+. This is unlike the case of Drummond [16] (for the low detection efficiency limit) where the violation was lost. The results for the strong test however are not surprising because in this case no information is lost about the photon path with perfect efficiency. If only one photon is detected at C_+ then nine photons will be detected at C_-.

Having observed a potential strong violation of the Bell inequality for perfect resolution, let us now consider the poor resolution regime. We will however stay with our four mode

[1] It is not possible to consider the initial state $|N\rangle|N\rangle$ for a test of the strong inequality due to the action of the beamsplitter

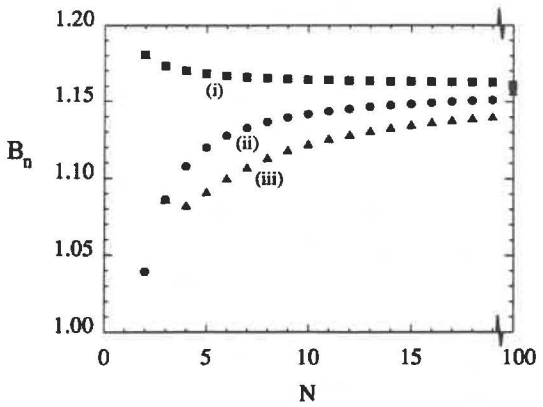

Figure 2.23: Plot of the maximum value of B_n (defined for the strong Clauser-Horne Bell inequality), versus N, the number of photon pairs in the correlated state $\frac{(a_+^\dagger b_+^\dagger + a_-^\dagger b_-^\dagger)^N}{N!(N+1)^{1/2}}|0\rangle$ for (i) n=N, (ii) n=N-1, (iii) n=N-2. A violation of the inequality occurs for $B_n > 1$. (The angles are chosen for each N to maximise the violation).

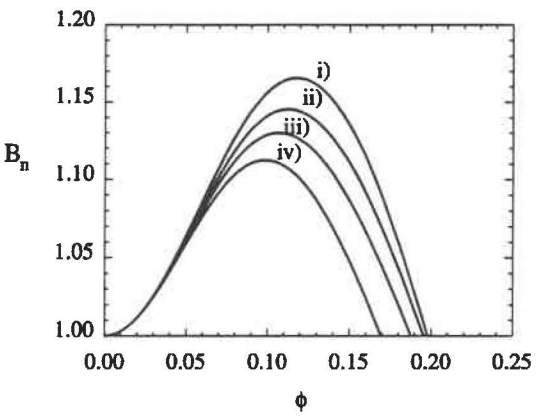

Figure 2.24: Plot of the violation of the strong Bell inequality (with an initial correlated state $\frac{(a_+^\dagger b_+^\dagger + a_-^\dagger b_-^\dagger)^{10}}{10!11^{1/2}}|0\rangle$) as a function of the angle ϕ for (i) n=10, (ii) n=9, (iii) n=8, (iii) n=5. A violation of the inequality occurs for $B_n > 1$.

initial state given above. In this case we need to consider the strong Bell inequality given by Eqn (2.91). Here $P_{n\pm\Delta n}(\theta,\phi)$ is the joint probability of detecting $n \pm \Delta n$ photons at C_+ and $n \pm \Delta n$ photons at D_+. $P_{n\pm\Delta n}(\theta)$ represents the marginal probability of detecting $n \pm \Delta n$ photons at C_+. According to quantum mechanics the joint probability $P_{n\pm\Delta n}(\theta,\phi)$ may be written as

$$P_{n\pm\Delta n}(\theta,\phi) = \sum_{n_1=n-\Delta n}^{n+\Delta n} \sum_{n_2=n-\Delta n}^{n+\Delta n} P_{n_1,n_2}(\theta,\phi) \tag{2.99}$$

where

$$P_{n_1,n_2}(\theta,\phi) = \frac{1}{n_1!n_2!}\langle : \left\{ \left(c_+^\dagger c_+\right)^{n_1} \left(d_+^\dagger d_+\right)^{n_2} \exp\left[-c_+^\dagger c_+ - d_+^\dagger d_+\right] \right\} : \rangle \tag{2.100}$$

The marginal probability $P_{n\pm\Delta n}(\theta)$ is given by

$$P_{n\pm\Delta n}(\theta) = \sum_{n_1=n-\Delta n}^{n+\Delta n} P_{n_1}(\theta) \tag{2.101}$$

where

$$P_{n_1}(\theta,\phi) = \frac{1}{n_1!}\langle : \left\{ \left(c_+^\dagger c_+ \right)^{n_1} \exp\left[-c_+^\dagger c_+ \right] \right\} : \rangle \tag{2.102}$$

A similar expression exists for the other marginal probability $P_{n\pm\Delta n}(\phi)$.

In Figure (2.25-2.26) we present results for various $n = N$ and Δn. Figure (2.25) clearly shows that the effect of having a fixed poor resolution (Δn fixed) decreases as n increases. The results for $n = 10$ with various Δn are presented in Figure (2.26). Hence we observe a violation of the Bell inequality to be possible even in the case of very poor resolution ($\Delta n = 5$). If we examine the special case of $\Delta n = n = N$ then it is found that $B_{n\pm\Delta n} = 1$. For $n = N$ with $\Delta n < n$ a violation of the Bell inequality seems possible even though the violation may be small. The effect of poor resolution is to decrease the magnitude of the violation. It is not logical to consider the case of $\Delta n = n$ because this implies that the experimenter has no detection resolution, and thus the experimenter cannot resolve zero photons from n photons.

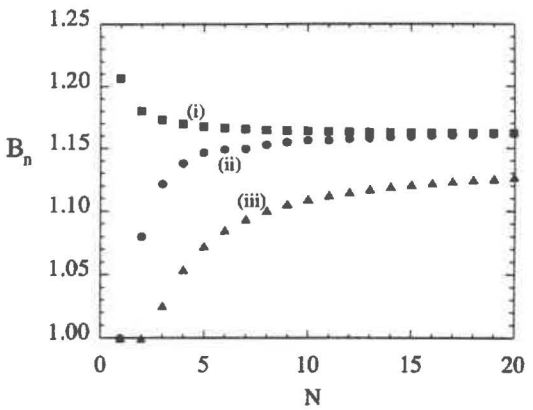

Figure 2.25: Plot of the maximum value of $B_{n\pm\Delta n}$ (defined for the strong Clauser-Horne-Bell inequality), versus N, the number of photon pairs in the correlated state $\frac{\left(a_+^\dagger b_+^\dagger + a_-^\dagger b_-^\dagger\right)^N}{N!(N+1)^{1/2}}|0\rangle$ for (i) n=N, $\Delta n = 0$, (ii) n=N, $\Delta n = 1$, (iii) n=N, $\Delta n = 2$. A violation of the inequality occurs for $B_n > 1$. (The angles are chosen for each N to maximise the violation of B_n).

So far in this section we have considered an initial state with a fixed N. In a real experiment it may not be possible to generate such an ideal state. Hence we now consider the case where the initial state is a summation of several four mode states

$$|\varphi\rangle = \frac{1}{\sqrt{(2\Delta N+1)(N+1)}} \sum_{m=N-\Delta N}^{N+\Delta N} \frac{\left(a_+^\dagger b_+^\dagger + a_-^\dagger b_-^\dagger\right)^m}{m!}|0\rangle \tag{2.103}$$

where the factor outside the summation sign is the normalisation constant such that $\langle\varphi|\varphi\rangle = 1$. Results for a range of ΔN with fixed $n = N = 10$ are presented in Figure (2.27). We clearly observe that even in a superposition of correlated states, a violation of the Bell inequality is still possible. The generation of a finite superposition of correlated states given in (2.103) is however still difficult and needs further investigation.

The result of this section shows that a violation of a strong Bell inequality is possible even in the presence of poor detection resolution of photon number. We have only so far considered ideal correlated states, or finite superpositions of them, and we have not yet considered a truly macroscopic pulse, where N is of the macroscopic order. Nevertheless,

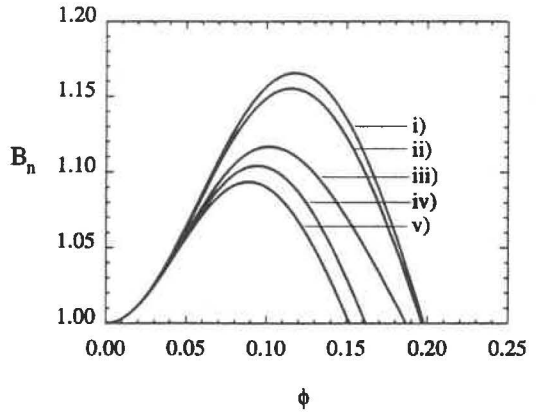

Figure 2.26: Plot of the violation of the strong Bell inequality as a function of the angle ϕ for (i) n=10, $\Delta n = 0$, (ii) n=10, $\Delta n = 1$, (iii) n=10, $\Delta n = 2$ (iv) n=10, $\Delta n = 3$, (v) n=10, $\Delta n = 5$. A violation of the inequality occurs for $B_n > 1$. Here the initial state is the correlated state $\frac{(a_+^\dagger b_+^\dagger + a_-^\dagger b_-^\dagger)^{10}}{10!11^{1/2}}|0\rangle$.

the results here indicate a violation of strong Bell inequality for quite significant percentage reductions in photon resolution. These results suggest a way to perform a strong test of the Bell inequality in macroscopic regimes using photodiode detectors.

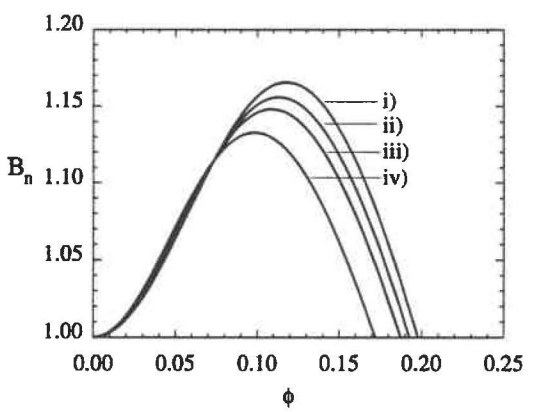

Figure 2.27: Plot of the violation of the strong Bell inequality as a function of the angle ϕ for (i) $n = N = 10$, $\Delta N = 0$, (ii)$n = N = 10$, $\Delta N = 1$, (iii) $n = N = 10$, $\Delta N = 2$ (iv) $n = N = 10$, $\Delta N = 5$. A violation of the inequality occurs for $B_n > 1$.

2.9 Conclusion

We have shown how multiparticle and potentially macroscopic states predicted to violate a Bell inequality may be generated from the correlated photon number states $\sum_{m=0}^{N} |m\rangle|N-m\rangle|m\rangle|N-m\rangle$ (the four mode system) or $|N\rangle|N\rangle$ (the two mode system).The proposed experiment is also a test of quantum mechanics for states of higher spin, and the experiments are extensions of those using parametric down conversion to test quantum mechanics where one photon is incident on each analyser. The inequality is tested by measurement of joint probabilities where n photons are detected at one space-time point. The violation is evident for $n = N$ photons but reduces dramatically for $n < N$, where one looses information about the $n - N$ photons.

The correlated photon number states may be generated via parametric down conversion. For poor detector efficiencies the sensitivity of the violation to the value of n means that at larger gains the direct output of the parametric amplifier gives no violation. This is because the probability of the amplifier generating $|n+i\rangle|n+i\rangle$ (where $i > 0$), rather than $|n\rangle|n\rangle$, is significant. Hence violations are predicted only for regimes where the probability of actually generating the $|n\rangle|n\rangle$ state where n is large is very small. Nevertheless consideration of experiments with $N = 2$ would not seem unreasonable. For higher detector efficiencies, it is possible to "prepare" the $|n\rangle|n\rangle$ state by restricting attention to the subensembles where only n photons are detected at each of the spatially separated locations. Here auxiliary assumptions of the usual type are required. In this case, violations are obtained for all values of parametric gain. Unfortunately, the probability of actually detecting the appropriate $|n\rangle|n\rangle$ state is small, because of the super-poissonian photon number distribution of the output signal and idler beams. Here we have limited our consideration to a classically pumped parametric down conversion.

Finally, we have included a discussion and calculation for the situation corresponding to the Smithey et al experiment. Prior to this experiment, it seemed that the preparation using parametric down conversion of the type of correlated photon states we consider would have been difficult for more than two or three photons in each beam. Yet in their recent experiment, Smithey et al have demonstrated subshot noise photon number correlations for twin pulses each with 10^6 photons. Here one was able to use photodiodes with $85 - 90\%$ quantum efficiency. In terms of the Bell inequality the new limitation is electronic noise which limits the resolution available in determining n the number of photoelectrons. Unfortunately in the case of parametric down conversion, with the form of 'state preparation' we suggest here, the auxiliary assumptions used in the formulation of the classical inequality break down. However if we could prepare a correlated photon number system with only a small number of significant states, then a strong classical Bell inequality formulated without using auxiliary assumptions may be violated and hence provide a possible test of quantum mechanics in the truly macroscopic regime.

Chapter 3

Macroscopic Boson States Exhibiting the Greenberger, Horne and Zeilinger Contradiction with Local Realism

Abstract

It is shown that the recent Greenberger, Horne and Zeilinger "all or nothing" contradiction of quantum mechanics with local realism can be exhibited on a macroscopic scale where a large number of particles are incident on each analyser. We present a formulation of the all or nothing paradox in terms of boson fields, and suggest how the paradox might be realised using a correlated photon triplet. The suggested experiment might be readily extended to test for the first time to our knowledge quantum mechanics against local realism for situations of more than one quanta per wavepacket incident on each measurement apparatus.

3.1 Introduction

There has been much interest recently in quantum states described by Greenberger, Horne and Zeilinger [19, 20, 27, 86, 87] (GHZ) which give predictions contrary to those of all classical theories, based as they are on the Einstein-Podolsky-Rosen [62] (EPR) premises of local realism. The new unexpected feature is that the contradiction with classical theory can be accomplished in a single run or set of measurements. This is not the case with the traditional Bell inequality tests [1] where the contradiction is necessarily statistical and requires data to be collected over many runs.

To begin this chapter we present the original formulation of the Greenberger, Horne, and Zeilinger inequality [19, 20, 27, 86, 87] as presented by Mermin [86]. Let us consider three spin $\frac{1}{2}$ particles which we will conveniently label 1, 2 and 3. These particles originated in a spin-conserving Gedanken decay and fly apart along three different straight lines in the x, y plane. Mermin considered the complete set of Hermitian operators

$$\sigma_x^1\sigma_y^2\sigma_y^3 \quad \sigma_y^1\sigma_x^2\sigma_y^3 \quad \sigma_y^1\sigma_y^2\sigma_x^3 \tag{3.1}$$

where σ_x^i and σ_y^i represent the spin along the vertical and horizontal directions. These are orthogonal to the trajectory. Each of the operators in (3.1) commute with each other, hence the three operators can be provided with simultaneous eigenstates.

For simplicity Mermin choose to consider the symmetric eigenstate in which all of the operators of (3.1) have the eigenvalue $+1$. The state vector may be written as

$$|\varphi\rangle = \frac{1}{\sqrt{2}}\left[|1,1,1\rangle - |-1,-1,-1\rangle\right] \tag{3.2}$$

where the 1 or -1 specifies the spin up or down along the appropriate z axis. Now because the spin vectors of distinct particles commute component by component, we can simultaneously measure the x component of one particle and the y components of the remaining two. Since the particles are in an eigenstate of all three operators, given by (3.1), with an eigenvalue of $+1$, the product of the results of the three spin measurements has to be $+1$. This is regardless of which particle we singled out for the x measurement. For example, if both y components turned out to be the same, then the x component when measured must yield the value $+1$.

The EPR reality criterion says that *If, without in any way disturbing a system, we can predict with certainty the value of a physical quantity, then there exists an element of physical reality corresponding to that physical quantity.* This therefore asserts the existence of elements of reality m_x^1, m_x^2, m_x^3, each having a value of ± 1, each waiting to be revealed by the appropriate pair of far away y component measurements.

The value of the operators $\sigma_x^1\sigma_y^2\sigma_y^3$, $\sigma_y^1\sigma_x^2\sigma_y^3$, and $\sigma_y^1\sigma_y^2\sigma_x^3$ are given by the values of the corresponding products

$$m_x^1 m_y^2 m_y^3 \quad m_y^1 m_x^2 m_y^3 \quad m_y^1 m_y^2 m_x^3 \tag{3.3}$$

We know from considering the symmetrical case that the value of these products is one and hence the combined product must be $m_x^1 m_x^2 m_x^3$. If we were to measure the x component of all three spin particles, then the product must be unity.

The value of the product $m_x^1 m_x^2 m_x^3$ can also be determined without invoking the elements of reality by a simple quantum mechanical calculation. The result we require may be obtained by measuring the Hermitian operator

$$\sigma_x^1\sigma_x^2\sigma_x^3 \tag{3.4}$$

Not only does this commute with each of the operators of (3.1), but it is minus the product of all the three of them. This means the eigenvalue is opposite in sign to that required by the existence of the elements of reality and hence provides a definite test of local reality versus quantum mechanics.

In a realistic experimental situation the ideal correlations predicted by the GHZ state would not be attainable and hence the conflict with the classical EPR arguments would not in fact be revealed so directly. However Mermin [28] has recently shown that the contradiction with classical theories is still stronger than that of traditional Bell inequality tests. The violation of Bell-type inequalities derived by Mermin from classical EPR assumptions is predicted by quantum mechanics to be much greater for the GHZ experiment.

We show in this chapter that the remarkable GHZ prediction can be exhibited on a macroscopic level in the following sense. We consider experiments performed using only three analysers (six detectors) but where there is an arbitrarily large number of particles incident simultaneously on each analyser. One thus makes measurements on three spatially separated wave packets each consisting of N (where N can be large) quanta. This is in contrast with the multi-particle states discussed recently by Mermin [28] where the individual quanta emitted are spatially separated so that there is still only one particle per

analyser. For the situations discussed in this chapter, the EPR "elements of reality" are thus ascribed to a macroscopic system at each spatially separated analyser or measurement apparatus. The "elements of reality" refer to the predetermined parameters which according to classical premises must exist irrespective of the measurement). The strong GHZ violation of the classical predictions is even more surprising at this macroscopic level[1].

To date local realism has not been proved experimentally incorrect for any system of greater than one particle per analyser. It is suggested here how to realise the original microscopic GHZ paradox using a single correlated photon triplet[2]. We suggest that it may be feasible to extend this proposed experiment to test quantum mechanics versus local realism for these new situations involving more than one particle per analyser.

3.2 The GHZ Inequality postulated with photons

We choose to formulate the arguments presented by GHZ in terms of boson fields. This is relevant in view of the fact that the most successful experiments confirming quantum predictions against those of classical theory have to date used correlated photon pairs. Because of the poor efficiency of photon detectors we discuss the GHZ paradox in terms of Clauser-Horne-Shimony-Holt [25,26] modifications of the inequalities derived by Mermin.

Firstly, we consider a simple modification of the triple-correlation experiment suggested by Greenberger, Horne and Zeilinger [19,20,27,86,87] and Mermin [28]. We will show initially that the predictions of the following quantum state are in contradiction with the predictions of all classical (local realistic) theories.

$$|\varphi\rangle = \frac{\left(a_{1+}^{\dagger}a_{2+}^{\dagger}a_{3+}^{\dagger} + a_{1-}^{\dagger}a_{2-}^{\dagger}a_{3-}^{\dagger}\right)^{N}|0\rangle}{N!\sqrt{\sum_{r=0}^{N} r!\,(N-r)!}} \tag{3.5}$$

Here the $a_{j+}^{\dagger}$, $a_{j-}^{\dagger}$ ($j = 1$, 2 or 3) are boson creation operators for six orthogonal field modes. Typically the a_j are of distinct energies, while the $+$ and $-$ refers to orthogonal polarisations at the same energy. Alternatively the $+$ and $-$ might refer to quanta emitted in different directions [19,20,27,86,87]. The $|0\rangle$ symbolises the vacuum state. Here we have N quanta generated in each of the a_1, a_2, a_3 energies. This state may describe N atoms emitting photon triplets in a cooperative fashion so that the quanta are incident on the analysers simultaneously. The distinct energies may be spatially separated into three regions A_j. At each position A_j the polarisation is measured (Figure 3.1). Let us suppose that the detected outputs of the analysers correspond to the following transformed modes

$$d_{j\pm}(\phi_j) = \pm a_{j+} + \exp[i\phi_j]a_{j-} \tag{3.6}$$

If the $+$ and $-$ refer to different directions, this measurement may be realised by providing phase shifts of the a_{j-} with respect to the a_{j+}, and combining the two with a 50/50 beam splitter. If the $+$ and $-$ are different polarisations, the coupling would be achieved by a polariser. Photodetectors measure how many of the N quanta incident on each analyser are deflected 'up' or 'down'. If a particle is detected "up" or "down" we

[1] The violation of the traditional Bells inequalities for situations of more than one particle per analyser (or equivalently for higher spin states) has been shown possible by P.D. Drummond, Phys. Rev. Lett. **50**, 1407 (1983) N.D. Mermin, Phys. Rev. **D22**, 356 (1980); S.L. Braunstein and C.M. Caves, Phys. Rev. Lett. **61**, 662 (1988), B. Oliver and C. Stroud, J. Opt. Soc. Am. **B4**, 1426 (1987)). However, in some sense in these situations the strength of the violations is reduced with larger particle numbers N.

[2] It is suggested by D. Greenberger, M. Horne, A. Shimony and A. Zeilinger, Am. J. Phys. **58**, 1131 (1990), that one might realise the GHZ state using interferometric arrangements similar to the one we propose.

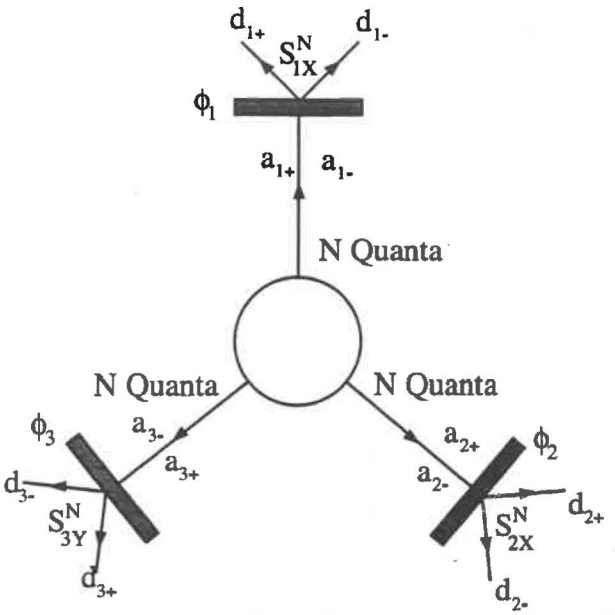

Figure 3.1: A schematic diagram of the GHZ experiment with N quanta in each spatial region A_j. Here one measures the spin products S_{1y}^N, S_{2x}^N, S_{3x}^N respectively at each polariser. A value of "+1" is assigned for 'up', "−1" for down, "0" for not detected.

assign to it a spin value of $+1$ and -1 respectively. We define the spin product $S_j^N(\phi_j)$ as the product of the spins of each of the N particles, detected at position A_j.

Following Greenberger et al we restrict attention to two choices for each of the polariser angles. We consider $\phi = 0$ corresponding to

$$d_{j\pm}(0) = \frac{(\pm a_{j+} + a_{j-})}{\sqrt{2}} \tag{3.7}$$

and $\phi = -\pi/2$ corresponding to

$$d_{j\pm}\left(-\frac{\pi}{2}\right) = \frac{(\pm a_{j+} + i a_{j-})}{\sqrt{2}} \tag{3.8}$$

We shall denote $d_{j\pm}(0)$ and $d_{j\pm}\left(-\frac{\pi}{2}\right)$ as $d_{j\pm}^x$ and $d_{j\pm}^y$ respectively, and the measurements $S_j^N(0)$ and $S_j^N\left(\frac{-\pi}{2}\right)$ as S_{jx}^N and S_{jy}^N respectively. We now consider the predictions of the quantum state (3.5) for the following spin products:

$$S_{1y}^N S_{2y}^N S_{3x}^N, \quad S_{1y}^N S_{2x}^N S_{3y}^N, \quad S_{1x}^N S_{2y}^N S_{3y}^N, \quad \text{and} \quad S_{1x}^N S_{2x}^N S_{3x}^N \tag{3.9}$$

It is convenient to rewrite $|\varphi\rangle$ in terms of the detected modes $d_{j\pm}^x$ and $d_{j\pm}^y$. To calculate

$$\left\langle S_{1x}^N S_{2y}^N S_{3y}^N \right\rangle \tag{3.10}$$

for example we rewrite $|\varphi\rangle$ as follows (using the inverse of the relation (3.6)).

$$|\varphi\rangle = \frac{(d_{1+}^x d_{2-}^y d_{3+}^y + d_{1+}^x d_{2+}^y d_{3-}^y + d_{1-}^x d_{2+}^y d_{3+}^y + d_{1-}^x d_{2-}^y d_{3-}^y)^{\dagger N} |0\rangle}{N!\left(-\sqrt{2}\right)^{3N} \sqrt{\sum_{r=0}^N r!(N-r)!}} \tag{3.11}$$

It is apparent that if N is odd the product $S_{1x}^N S_{2y}^N S_{3y}^N$ will *always* be -1. Similar transformations reveal the same results for $S_{1y}^N S_{2x}^N S_{3y}^N$ and $S_{1y}^N S_{2y}^N S_{3x}^N$, as one would expect from

the symmetry of the state $|\varphi\rangle$. To calculate $\left\langle S_{1x}^N S_{2x}^N S_{3x}^N \right\rangle$ we transform to the $d_{j\pm}^x$. We obtain

$$|\varphi\rangle = \frac{\left(d_{1+}^x d_{2+}^x d_{3+}^x + d_{1+}^x d_{2-}^x d_{3-}^x + d_{1-}^x d_{2-}^x d_{3+}^x + d_{1-}^x d_{2+}^x d_{3-}^x\right)^{\dagger N} |0\rangle}{N! \left(-\sqrt{2}\right)^{3N} \sqrt{\sum_{r=0}^N r!\,(N-r)!}} \tag{3.12}$$

The product $S_{1x}^N S_{2x}^N S_{3x}^N$ is *always* $+1$, for all N.

Now we follow the original argument of GHZ and Mermin to establish the classical predictions for the spin products. If we select N to be odd quantum mechanics predicts that the $S_{1x}^N S_{2y}^N S_{3y}^N$ is *always* -1. Because the three polarisers are spatially separated, the EPR premises of local realism apply [1, 62]. In short, local realistic theories will assign to each of the states at A_j before measurement a value for S_{jx}^N and S_{jy}^N , $\tilde{S}_{jx}^N$ and $\tilde{S}_{jy}^N$ say, where this value must $+1$ or -1, and we have that

$$\tilde{S}_{1x}^N \tilde{S}_{2y}^N \tilde{S}_{3y}^N = \tilde{S}_{1y}^N \tilde{S}_{2x}^N \tilde{S}_{3y}^N = \tilde{S}_{1y}^N \tilde{S}_{2y}^N \tilde{S}_{3x}^N = -1 \tag{3.13}$$

Therefore if we examine the prediction for $S_{1x}^N S_{2x}^N S_{3x}^N$, since we can write (recalling that each $\left(\tilde{S}_{jy}^N\right)^2 = 1$)

$$\tilde{S}_{1x}^N \tilde{S}_{2x}^N \tilde{S}_{3x}^N = \left(\tilde{S}_{1x}^N \tilde{S}_{2y}^N \tilde{S}_{3y}^N\right)\left(\tilde{S}_{2x}^N \tilde{S}_{1y}^N \tilde{S}_{3y}^N\right)\left(\tilde{S}_{3x}^N \tilde{S}_{1y}^N \tilde{S}_{2y}^N\right) = -1 \tag{3.14}$$

the classical prediction must be that $S_{1x}^N S_{2x}^N S_{3x}^N$ is *always* -1. This is in strong disagreement with the quantum result predicted from (3.5) with N odd, that $S_{1x}^N S_{2x}^N S_{3x}^N$ is *always* $+1$! The contradiction is distinct for arbitrary large N, provided N is odd. This is the startling new GHZ "all or nothing" distinction between quantum and classical which we have now shown may apply to macroscopic systems where large numbers of particles are incident on each detector!

3.3 An Experiment using Correlated Photons

We now consider how to realise the GHZ state experimentally using a correlated photon source. To account for experimental situations, where the absolute -1 prediction for the quantity $S_{1x}^N S_{2y}^N S_{3y}^N$ will never be achieved in the first place, we follow the approach of Mermin [28] and derive the following inequality based on classical (local realistic) arguments

$$F = \left|\left\langle S_{1x}^N S_{2y}^N S_{3y}^N \right\rangle + \left\langle S_{1y}^N S_{2x}^N S_{3y}^N \right\rangle + \left\langle S_{1y}^N S_{2y}^N S_{3x}^N \right\rangle - \left\langle S_{1x}^N S_{2x}^N S_{3x}^N \right\rangle\right| \leq 2 \tag{3.15}$$

According to local realistic or hidden variable theories, the averages are expressible in the following form

$$\left\langle S_{1x}^N S_{2y}^N S_{3y}^N \right\rangle = \int \rho(\lambda)\, d\lambda\; S_{1x}^N(\lambda)\, S_{2y}^N(\lambda)\, S_{3y}^N(\lambda) \tag{3.16}$$

where $S_{jx}^N(\lambda)$, $S_{jy}^N(\lambda)$ represent the spin products of the N quanta detected at A_j given the particular set of hidden variables λ describing the state. The $\rho(\lambda)$ is a probability distribution over the hidden parameters λ. Because $\left|S_{jx}^N(\lambda)\right| \leq 1$ the derivation of (3.15) follows in a straightforward manner along the lines given by Mermin. Clearly, the quantum prediction of the state (3.5) for N odd violates the classical inequality, giving $|F| = 4$.

It is well known [25, 26] that inequalities of the type (3.15) will not in fact be violated for optical systems, with which we are primarily concerned here, because of the very poor photodetector efficiencies. Let us select to detect the N quanta incident on each polariser,

assigning a value to the spin of each quanta as follows: $+1$ for up, -1 for down, and 0 if not detected. Clearly with very small detection efficiency factors, the magnitudes of the $\left\langle S_{1x}^N S_{2x}^N S_{3x}^N \right\rangle$ etc. diminish and the inequality (3.15) is satisfied. The strength of the quantum predictions for the GHZ system is counterbalanced by increased sensitivities to the detection inefficiencies (three detectors now being involved). However it is well known that one can violate a weaker version [25, 26] of the Bell-type inequality even in the presence of weak detector efficiencies. Here we follow arguments similar to Clauser and Horne [25, 26] and present a weaker version of the Mermin inequality [25, 26].

Let us define the modified spin product for the N quanta at detector A_j. Let

$$\bar{S}_{j\phi}^N(\lambda) = \frac{S_{j\phi}^N(\lambda)}{P_j^N(\lambda)} \tag{3.17}$$

where $S_{j\phi}^N(\lambda)$ is the spin product of the N quanta for a given set of hidden variables, where we assign a value of zero to the spin for quanta not detected. Now $P_j^N(\lambda)$ is the probability, for the set of hidden parameters λ, that the N quanta of A_j are all detected. In fact $S_{j\phi}^N(\lambda) = P_{+j}(\lambda) - P_{-j}(\lambda)$ where $P_{\pm j}(\lambda)$ is the probability of an arrangement of the N quanta at A_j giving a spin product ± 1 respectively and $P_j^N(\lambda) = P_{+j}^N(\lambda) - P_{-j}^N(\lambda)$. Thus $\left|\bar{S}_{j\phi}^N(\lambda)\right| \leq 1$. Now one makes the important auxiliary assumption that the probability $P_j^N(\lambda)$ of detecting all the N quanta is independent of the choice of analyser angles ϕ_j. We may now rearrange (3.16) to obtain

$$\left\langle S_{1x}^N S_{2y}^N S_{3y}^N \right\rangle_R = \frac{\left\langle S_{1x}^N S_{2y}^N S_{3y}^N \right\rangle}{N_0} = \int \bar{\rho}(\lambda) d\lambda \bar{S}_{1x}^N(\lambda) \bar{S}_{2y}^N(\lambda) \bar{S}_{3y}^N(\lambda) \tag{3.18}$$

where

$$\bar{\rho}(\lambda) d\lambda = \frac{\left(\rho(\lambda) P_1^N(\lambda) P_2^N(\lambda) P_3^N(\lambda)\right)}{N_0} \tag{3.19}$$

and we define

$$N_0 = \int \rho(\lambda) P_1^N(\lambda) P_2^N(\lambda) P_3^N(\lambda) \tag{3.20}$$

which is the proportion of runs where all $3N$ quanta are detected. Thus $\bar{\rho}(\lambda)$ is the normalised probability distribution redefined with respect to the subensemble where all $3N$ photons are detected. The $\left\langle S_{1x}^N S_{2y}^N S_{3y}^N \right\rangle_R$ is thus the product of the spin products calculated at each detector, but where the average is calculated only over those runs where all of the $3N$ quanta are detected. The derivation given by Mermin [28] now applies (as above) to the reduced $\bar{\rho}(\lambda)$ and spin products $\bar{S}_{j\phi}^N(\lambda)$. We have the weaker version of the inequality (3.15) involving averages calculated only over the detected subensemble.

$$F_R = \left|\left\langle S_{1x}^N S_{2y}^N S_{3y}^N \right\rangle_R + \left\langle S_{1y}^N S_{2x}^N S_{3y}^N \right\rangle_R + \left\langle S_{1y}^N S_{2y}^N S_{3x}^N \right\rangle_R - \left\langle S_{1x}^N S_{2x}^N S_{3x}^N \right\rangle_R\right| \leq 2 \tag{3.21}$$

We give a brief discussion of how a state violating $F_R \leq 2$ may be prepared using correlated photon states of the type generated in parametric down conversion. We consider a three mode multi-photon state $a_1^{\dagger N} a_2^{\dagger N} a_3^{\dagger N} |0\rangle$ input on the apparatus sketched in the Figure (3.2). We thus have N quanta incident at each input port associated with a_j. The modes generated after the first set of beam splitters are

$$a_{1+} = \frac{(a_3 + ic_3)}{\sqrt{2}} \qquad a_{1-} = \frac{(ia_1 + c_1)}{\sqrt{2}} \tag{3.22}$$

$$a_{2+} = \frac{(a_1 + ic_1)}{\sqrt{2}} \qquad a_{2-} = \frac{(ia_2 + c_2)}{\sqrt{2}} \tag{3.23}$$

$$a_{3+} = \frac{(a_2 + ic_2)}{\sqrt{2}} \qquad a_{3-} = \frac{(ia_3 + c_3)}{\sqrt{2}} \tag{3.24}$$

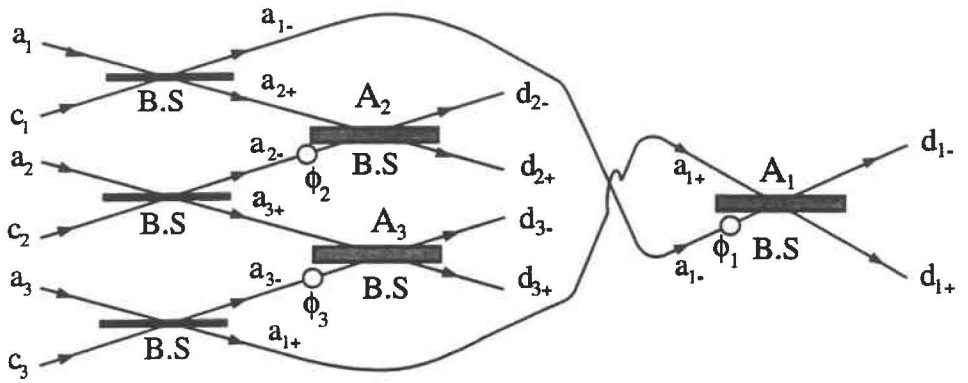

Figure 3.2: A possible realisation of the GHZ state. The B.S. denotes a 50/50 beam splitter or coupler. The detected modes are the $d_{j\pm}$. The a_{j-} may be phase shifted either $\phi = 0$ or $\frac{\pi}{2}$ relative to the a_{j+}. Experiments with photons will involve additional auxiliary assumptions because of poor photodetection efficiencies. The diagram is a schematic depiction only, in that the real distances from the initial sources a_1,a_2,a_3 to the final detectors at the $d_{j\pm}$ are the same.

where the modes corresponding to c_j denote the second vacuum-state inputs to the beam splitters and the a_j are boson operators for the input number state modes. Thus the outgoing state after the beam splitter is

$$|\varphi\rangle = \frac{a_1^{\dagger N} a_2^{\dagger N} a_3^{\dagger N} |0\rangle}{\sqrt{N!^3}} \tag{3.25}$$

$$= \frac{\left(-ia_{1-}^{\dagger} + a_{2+}^{\dagger}\right)^N \left(-ia_{2-}^{\dagger} + a_{3+}^{\dagger}\right)^N \left(-ia_{3-}^{\dagger} + a_{1+}^{\dagger}\right)^N |0\rangle}{\sqrt{2^{3N} N!^3}} \tag{3.26}$$

The transformations due to the second set of beam splitters for (or equivalent couplers) and phase shifts of the a_j relative to a_{j+} at the spatially separated regions A_j generate final detected modes $d_{j\pm}(\phi_j)$ given by $d_{j+}(\phi_j) = a_{j+} + \exp[i\phi_j] a_{j-}$ and $d_{j-}(\phi_j) = -a_{j+} + \exp[i\phi_j] a_{j-}$. We define the $d_{j\pm}^y = d_{j\pm}(-\frac{\pi}{2})$ and $d_{j\pm}^x = d_{j\pm}(0)$ and S_{jy}^N and S_{jx}^N as the "spin" products with the appropriate choices $\phi_j = -\frac{\pi}{2}$ and $\phi_j = 0$ respectively. The subensemble relevant to the weaker inequality (3.21) is where exactly N quanta are detected at each spatial region A_j. The auxiliary assumption involved in the derivation of the weaker Clauser-Horne-type inequality (3.21) is that the probability of detecting N quanta at each A_j will be independent of the angle choice ϕ_j. We note that the use of the beam splitters in this particular configuration requires the use of weaker inequality even in the presence of perfectly efficient photodetectors. The terms in the expansion (10) which are relevant are

$$\sum_{r=0}^{N} \binom{n}{r}^3 i^r \left(a_{1-}^{\dagger} a_{2-}^{\dagger} a_{3-}^{\dagger}\right)^r \left(a_{1+}^{\dagger} a_{2+}^{\dagger} a_{3+}^{\dagger}\right)^{N-r} |0\rangle \tag{3.27}$$

These terms are identical to those produced from the state (3.5) although with different weightings. On substituting the $a_{j\pm}$ for the detected modes $d_{j\pm}^x$ and $d_{j\pm}^y$, it is revealed that the spin products $S_{1y}^N S_{2y}^N S_{3x}^N$, $S_{1x}^N S_{2y}^N S_{3x}^N$ and $S_{1y}^N S_{2x}^N S_{3y}^N$ are always $+1$. This is seen by noting that the $r = N - x$ term in the expansion (11) may be obtained from the $r = x$ term by simply replacing the d_{j-} with $-d_{j-}$. The result is that terms of odd powers of d_{j-} will not contribute, and the spin product must thus be $+1$. Similar substitution and

examination for the $S_{1x}^N S_{2x}^N S_{3x}^N$ case reveal that for N odd the product $S_{1x}^N S_{2x}^N S_{3x}^N$ is always -1. Thus quantum mechanics predicts a violation of the weaker inequality (3.21) for the system depicted in Figure (3.2), provided N is odd.

Of course for $N = 1$ we have the original microscopic version of the GHZ paradox. This may be a useful realisation of the GHZ state, since photon experiments provide good analyser efficiencies and sources of correlated particles. Highly correlated photon pairs generated via parametric down conversion have already been predicted [7, 71, 75, 76] and used [9–11] to demonstrate violation of the traditional weaker Bell inequality using a scheme similar to that of Figure (3.2) (refer footnote 2). Here we require a correlated photon triplet. The paradox would be as follows: given that N quanta are detected at each A_j, the spin products $S_{1y}^N S_{2y}^N S_{3x}^N$, $S_{1y}^N S_{2x}^N S_{3y}^N$, $S_{1x}^N S_{2y}^N S_{3y}^N$ would be observed to always be -1; the product $S_{1x}^N S_{2x}^N S_{3x}^N$ is predicted to be always $+1$ according to quantum mechanics, but always -1 according to the classical EPR premises.

Although three-photon emitting atomic systems seem more natural, generation of the photon triplet may be possible using parametric down conversion in a way that is readily extended to test quantum mechanics for the new situation discussed here of more than one quanta per wavepacket. A single photon state has been prepared experimentally using down conversion by Hong and Mandel [88, 89]. This is possible because detection of a photon in an idler field $a(k)$ implies that a photon is present in the corresponding signal field $a(k')$. Thus one can prepare a correlated triplet $|1\rangle|1\rangle|1\rangle$ in the three signal fields k_j by detection of a photon in each of the corresponding idler fields $k_{j'}$. We point out however that the calculations presented correspond to situations where the three photons are incident on the apparatus simultaneously. Recent work by Yurke and Slusher [90] suggest the use of three independent parametric amplifiers to produce the photon triplet. Here the three photon state being prepared is conditional on the simultaneous detection of a photon in each idler mode k_j'. One can then test for the situations of N (N is odd) photons per analyser by preparing N photons in each of the three k_j directions. This is done by detecting N photons in each of the corresponding idler fields $a_{k_j'}$. Since the parametric down conversion produces signal-idler pairs, the signal and idler photon numbers are correlated. The generation of larger signal-idler photon numbers is more likely at higher pump intensities, or alternatively one may use a cavity to enhance conversion into the selected modes. The feasibility of the experiment for larger N values is however currently limited by the effect of poor detector efficiencies. If N_0 photons are detected by an inefficient detector, one cannot exclude the possibility that there are actually $N_0 + 1$ photons incident on the analyser. The presence of the $N_0 + 1$ state will tend to destroy the GHZ effect anticipated with just N_0 photons incident (see the next section). Thus if one chooses to do the above experiments with $N = N_0$, the parametric down conversion needs to be operated at sufficiently low intensities to ensure that the N_0+1 state is not generated with appreciable probability. This makes generation of the N_0 state itself difficult if N_0 is large[3]. Nevertheless, $N_0 = 3$ should be possible in the near future and would signify a new test of quantum mechanics.

3.4 The Effect of Poor Detection Efficiencies

So far in this chapter we have considered the case where if we had the initial state $|N\rangle|N\rangle|N\rangle$, then at each of our detectors in the GHZ setup we were required to detect

[3] A simplistic treatment of parametric down conversion assumes the signal and idler to be single modes. The state generated is $\sum_{n=0}^{\infty} c_n |n\rangle|n\rangle$ where $c_n = \frac{(-i \tanh r)^n}{\cosh r}$ and r is proportional to the parametric coupling and interaction time. It is seen that in order to ensure the probability of obtaining $n = 4$ is 0.1 that of $n = 3$, we must operate in a regime where the probability of generating the three-photon state is 0.01 that of the one-photon state.

N photons. We allowed for detector losses, by restricting attention to the subensemble, where all N photons were detected at each spatial region A, B and C. The contradiction with local realism is still observable, but one requires auxiliary assumption and working with a subensemble means a low event rate. In this section we investigate further the effect of poor detection, that is where we lose information about which path the individual photons take. We consider the specific case of where we can determine that of the N photons in each mode of the initial triplet $|N\rangle|N\rangle|N\rangle$ m are detected. No information is known about the remaining photons, that is we do not know which path they took. Thus we are examining the potential for observing the GHZ phenomenon with various m, where one is in the limit of very small detector efficiency.

Previously in (3.1) we derived a classical inequality, involving triple correlation functions, that determined whether our initial quantum state was inconsistent with the principles of local reality. This inequality was derived for the case of detecting all the photons in the initial triplet $|N\rangle|N\rangle|N\rangle$. The result can be generalised to the case where only m photons in each mode are detected. In this case the GHZ inequality can be written as

$$F_R = \left|\left\langle S_{1x}^m S_{2y}^m S_{3y}^m \right\rangle_R + \left\langle S_{1y}^m S_{2x}^m S_{3y}^m \right\rangle_R + \left\langle S_{1y}^m S_{2y}^m S_{3x}^m \right\rangle_R - \langle S_{1x}^m S_{2x}^m S_{3x}^m \rangle_R\right| \leq 2 \quad (3.28)$$

Using the relations (3.22-3.24) with the initial state given by (3.26) the triple correlation function $\left\langle S_y^m S_x^m S_x^m \right\rangle_R$ can be determined. More specifically we find

$$\left\langle S_y^m S_x^m S_x^m \right\rangle_R = \frac{1}{(n-m)!^3} \sum_{r=0}^{m} \binom{m}{r}^3 / \text{Norm} \quad (3.29)$$

where this normalisation constant Norm is given by

$$\text{Norm} = \sum_{r_1,r_2,r_3=0}^{m} \frac{\binom{m}{r_1}\binom{m}{r_2}\binom{m}{r_3}}{(n-r_1-r_2)!\,(n-m+r_2-r_3)!\,(r_1-r_3-m)!} \quad (3.30)$$

Similarly it can be shown that

$$\langle S_x^m S_x^m S_x^m \rangle_R = (-1)^m \left\langle s_y^m s_x^m s_y^m \right\rangle \quad (3.31)$$

Hence evaluating the GHZ inequality given by (3.28) we have

$$F_R = \frac{3-(-1)^m}{\text{Norm}\,(n-m)!^3} \sum_{r=0}^{m} \binom{m}{r}^3 \quad (3.32)$$

A careful examination of (3.32) (or Figure (3.3)) reveals that unless all the photons are detected, then $F_R \leq 2$ and hence there is no contradiction with local reality. More specifically we plot in Figure (3.3) F_R versus N (the number of photons in each mode the the triplet $|N\rangle|N\rangle|N\rangle$) for $m = N$ (where all the photons are detected) and $m = N-1$ (here only $N-1$ are detected). For the case where all of the initial photons are detected, we have the results of the previous section. However for the case where information is lost about only a single photon ($m = N-1$) the GHZ inequality is not violated. Loss of a single photon, (that is the photon not being detected), destroys the contradiction with local reality. This effect was also found for the macroscopic product Bells inequality and has been discussed in the previous chapter. As discussed there, a main consequence of this result is a difficulty in obtaining a contradiction with local realism if the input state $|N\rangle|N\rangle|N\rangle$ is "contaminated" with higher states $|n\rangle|n\rangle|n\rangle$ (where $n > N$) and we have poor detector efficiencies. Such a "contamination" can be present if one uses parametric down conversion as a source.

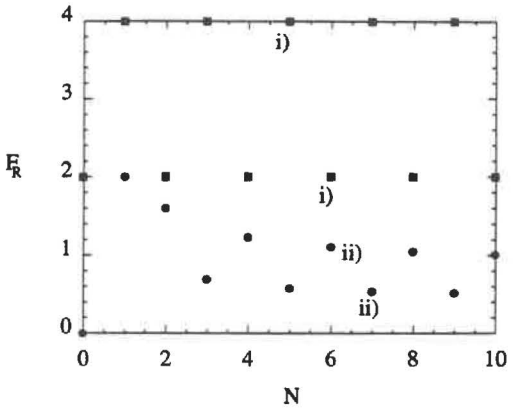

Figure 3.3: Plot of the maximum value of F_R , versus N, the number of photon pairs in the correlated state $|N\rangle|N\rangle|N\rangle$ for (i) m=N, (ii) m=N-1.
A violation of the inequality occurs for $F > 2$.

3.5 Discussion and Conclusion

Presently there are two avenues for the experimental verification of the remarkable features of the triple correlations, both of which are generalizations of previous experiments with pairs of photons. The first consideration must be in generating a single photon triplet state. An atom cascading through two intermediate levels could be used to produce three photons. The second possibility would be to exploit the momentum and energy correlations among three photons emitted in the process of parametric down conversion.

Recently there has been a proposal by Yurke and Stoler [90] to use three independent parametric oscillators to produce the photon triplet. The advantage of this scheme is that for higher pump powers, a multiple photon triplet is formed. Their scheme involves three independent parametric down converters for which the signal and idler modes can be separated. Photons are emitted as a signal idler pair from such sources, and by monitoring the idler mode one can determine when a photon is present in the signal mode. Hence, if all three detectors on the idler modes of the three parametric down converters were to detect single photons, then we would have a photon triplet that would violate the GHZ inequality. It is also know that parametric down converters produce multi-photon pairs (although with a low probability as n increases) and these could be used to violate the higher order GHZ test of local reality. The scheme of Yurke and Stoler provides a definite way to experimentally test the GHZ inequality, but it is difficult because of the need to detect three photons simultaneously at three detectors.

Finally, to conclude, we have presented new aspects of the all-or-nothing GHZ contradiction of quantum mechanics with local realism. The paradox is formulated in terms of boson fields and is shown to hold even for situations where large numbers of particles are incident on a single analyser. We have suggested an appropriate experiment. It is apparent however that if we loose information about even a single photon from the triplet $|N\rangle|N\rangle|N\rangle$, then the contradiction with local reality is lost. Experimentally a state needs to be prepared with an absolute photon number and the subensemble where all the photons are detected should be investigated.

This may be difficult but because of the non-statistical nature of the test, we need only one run where all n photons from the triplet are detected at each detector to validate quantum theory. Experiments with such low event rates should be possible.

Chapter 4

Transient Macroscopic Quantum Superposition States in Degenerate Parametric Oscillation

Abstract

Recent work by Wolinsky and Carmichael [31, 32] suggests that a superposition of two macroscopically distinct coherent-states (a "Schrödinger-cat" state) may be produced in degenerate parametric oscillation in a transient regime. For simplicity we consider a cavity which is single ended with respect to the signal field. This means that one of the mirrors is totally reflecting and cannot act as an input-output port. The intracavity mode is coupled to the external modes through this mirror. The transmission of signal photons from the cavity to the external field through this mirror is considered to be the major source of signal loss. In the usual configuration, the ingoing external field transmitted through the mirror is a vacuum, the second input port of this mirror being unused. This may be thought of as a source of vacuum fluctuations to the intracavity signal mode. To investigate the possibility of "Schrödinger-cat" states in degenerate parametric oscillation we perform numerical simulations of quantum stochastic equations derived using the positive P-representation. The equations allow for finite signal cavity loss. Interference fringes which indicate the existence of the macroscopic superposition states are indeed predicted in regimes where the parametric nonlinearity is sufficiently large compared to the signal cavity losses. Experimental criteria needed for the generation of macroscopic quantum superposition states using parametric oscillation are thus established. The nonlinearity is too large to be experimentally viable and hence motivated by the work of Mecozzi and Tombesi [33] and Kennedy and Walls [34] who showed a definite improvement of the interference fringes visibility to be possible in a χ^3 nonlinearity medium in which the vacuum is replaced with a squeezed input. We analyse the effect of replacing the signal-mode vacuum input with a squeezed input and predict the fringes to be observable for lower nonlinearity values provided the squeezed field is sufficiently intense.

4.1 Introduction

In this thesis so far we have considered various quantum phenomena that have no classical analogy. More specifically we have considered two specific tests of quantum mechanics versus local reality, namely tests of Bell's theorem and the Greenberger-Horne-Zeilinger phenomenon.

In recent years there has been interest in tests of quantum mechanics at the macroscopic or mesoscopic level [16, 21, 22, 91]. Schemes considered in this thesis [21, 22, 91] and by others [16] have shown a violation of the Bell's inequality and also the GHZ phenomenon at the macroscopic level. These are two potential tests of macroscopic quantum mechanics. It is however important to discuss precisely in what sense our proposed tests of quantum mechanics are macroscopic. We point out that since at each set of detectors one might detect the whole range of N, N-1, ..., 0 photons, the final state produced at the detectors for the test of the Bell inequality and the GHZ phenomena that we have discussed so far in this thesis is not a simple superposition of macroscopically distinct states. Rather we have a macroscopic (with N large) number of states which are microscopically distinctly superposed, so that only some pairs or triplets are macroscopically separated. A more simplistic macroscopic quantum state, and one in which the deviation from classical interpretations is striking, was that considered by Schrödinger in his famous *Schrödinger Cat* paradox [30]. A *Schrödinger Cat* state is a quantum superposition of two macroscopic states which are also macroscopically distinct.

We first present an outline of the *Schrödinger Cat* paradox [30]. In a thought experiment, Schrödinger considered the consequence of using a quantum mechanical measurement which has two possible outcomes to determine whether or not a gun is fired in the direction of a cat. If the gun is fired the cat will be killed. The whole apparatus is enclosed in a box which is opened at a later time and the state of the cat (live or dead) examined. Now if the object being measured, the quantum measuring device, the lethal arrangement and the cat are not subject to external loss, then the total system can be considered to be a single quantum system. Hence the state of the system would be a linear combination of the state with the cat alive and the state with the cat dead, where the action of examining the contents of the box determines which state the system is in. Hence the quantum system is described as a superposition of two macroscopically distinct states.

The important point made by Schrödinger is that its seems possible within quantum mechanics to have systems which are quantum mechanically described as superpositions of macroscopically distinct states (these are often coined *Schrödinger cat states*). Now as Schrödinger pointed out the physical interpretation of such a state becomes a problem. For example in the above case, surely the cat must be alive or dead, whether or not one chooses to examine the contents of the box. Surely, macroscopic objects exist in a particular state prior to measurement.

Whether or not these *Schrödinger cat* states exist in a real physical system is still an open question. So far, no macroscopic superposition states have ever been observed experimentally. Theoretical schemes have been suggested [13–15, 31–52]. Leggett and coworkers [36] suggested that SQUID rings may be used to generate macroscopic superpositions states. More recently there have been suggestions to prepare similar states in optical devices [14, 39]. For example Yurke and Stoler [14], and Milburn and Holmes [39] showed that a nonlinear χ^3 medium might be used to generate a "Schrödinger Cat" state. They showed that a coherent state propagating through an amplitude-dispersive medium can evolve into a superposition state of two coherent states which are π out of phase with each other. The calculations of Yurke and Stoler [14] showed that the inference fringes present in one of the quadrature measurements (in conjunction with the observation of twin isolated peaks in the conjugate phase amplitude quadrature) are indicative of "Schrödinger

Cat" like states. Such states are analogous to those considered by Schrödinger in his famous "Schrödinger cat" paradox, and hence defy all classical interpretations[1]. These calculations are ideal in the sense that they were done without loss. Unfortunately the effect of loss is to destroy the macroscopic superposition states [14, 36, 54] and whether or not such cat states exist in the real physical world is not therefore clear.

In this chapter we focus our attention on the use of parametric oscillation to generate "Schrödinger cat" like states. Recent proposals for the generation of superposition states have included the use of both degenerate [31, 32, 38] and nondegenerate [43] parametric oscillation schemes. In this chapter we will only consider degenerate parametric oscillation. The majority of previous theoretical and experimental treatments of the DPO have focussed attention on the semiclassical regimes where the quantum noise is small. The effect of quantum noise is to perturb about stable semi-classical solutions. This is the regime relevant to the majority of optical experiments, including the squeezing experiments of Wu et al [92] and Grangier et al [93], where the parametric nonlinearities are small. This mode of operation of the DPO is characterised by very large photon numbers at threshold.

The usual theoretical approach in the small quantum noise regime is to linearize the quantum fluctuations about the leading classical terms [94–97]. An exception to this are the recent nonlinear calculations of Kinsler and Drummond [98, 99].

The degenerate parametric oscillator above threshold displays a bistability [100]. One finds two stable classical field amplitudes differing in phase by 180°. Associated with the bistability is a switching time for the system change amplitude. Thermal noise can induce a movement from one state to the other. This has been calculated in optical parametric oscillation by Landauer and Woo [101], and in Josephson parametric amplifiers by Bryant, Weisenfield, and McNamara [102]. However even in the absence of thermal fluctuations the system many tunnel from one amplitude to the other because of the presence of quantum noise. Kinsler and Drummond [98, 99] have calculated this tunnelling time due to quantum noise only. Although nonlinear, their calculations still restrict attention to the case of small quantum noise.

There is another mode of operation of the degenerate parametric oscillator where the nonlinearity is sufficiently strong that threshold may be reached at very small photon numbers [98, 99]. This is the regime where quantum noise is very large and solutions deviate strongly from the classical description. Previously considered an unrealisable mode of operation, such regimes may become accessible with the continued development of small scale devices. Yurke et al [103] have used a Josephson parametric amplifier to squeeze the radiation field at microwave frequencies and here greater nonlinearities are possible.

Although the threshold photon number would be very small in these extreme nonlinear quantum oscillators, it is still possible in principle to reach significant intracavity intensities by increasing the input pump power. This raises the question of what new physical properties such macroscopic yet distinctly quantum devices will exhibit, and what theories might be used to model them.

Recent work by Reid and Yurke [53] has shown that "Schrödinger Cat" states are not present in the steady state field of the optical degenerate parametric oscillator in the limit where the pump losses are much greater than signal losses. However this is not necessarily the case for other regimes of parametric oscillation, and it has been suggested by Carmichael and Wolinsky [31] that "Schrödinger Cat" states may be present in a transient regime. In order to establish the predicted existence of the Schrödinger cat states and whether the criteria for the macroscopic quantum superposition states can be met experi-

[1] A possible weakness with the design of this type experiments is that, although certain results, namely the observation of fringes provide evidence for a macroscopic quantum state, it is not clear whether the results exclude all alternative classical theories in the way that a Bell-inequality test does.

mentally, one needs to model the transient evolution of the quantum parametric oscillator in regimes of large quantum noise. This is the prime objective of this chapter.

In this chapter we present a treatment of the degenerate parametric oscillator valid for arbitrary strength quantum noise. Nonlinear steady state analytical solutions valid for a degenerate parametric oscillator of arbitrary quantum noise strength have been derived previously by Drummond et al [94] and by Wolinsky and Carmichael [38]. These solutions were obtained in the adiabatic limit where the pump cavity decay rate is much greater than that of the signal. Subsequent work by Carmichael [38] has indicated that in the absence of all signal loss (this corresponds to the limit of extremely large quantum noise) a signal mode originally in the vacuum will evolve into a quantum superposition of two coherent states with amplitudes 180° out of phase. For sufficient pump intensities, the intracavity photon number becomes large and the system is predicted to be in a superposition of two macroscopically distinct coherent states. The homodyne detection of an appropriate phase amplitude then shows interference fringes, which are a signature of the superposition state. Our aim is to examine the effect of finite signal loss cavity loss and to see quantitatively how damaging this loss is to the formation of the superposition state. This allows us to ascertain whether such states will be experimentally accessible.

A fundamental problem associated with the observation and formulation of "Schrödinger-cat" type states are that macroscopic objects are not isolated, but are coupled to their environment. The environment causes the quantum coherences to be destroyed [34] (that is the interference fringes will be washed away). This occurs on a very fast time scale for a macroscopic object [54]. In this case losses to the system make the observations indistinguishable from that expected of a classical mixture of states, and no superposition states are present. Proposals by Mecozzi and Tombesi [33] and Kennedy and Walls [34] have shown that the use of a squeezed vacuum input rather than the usual vacuum input to model the dissipation has distinct advantages in decreasing the rate of decoherence. A large enough degree of squeezing reduces the diagonal dispersion below the vacuum level and provides a means to prepare states with very small diagonal and off-diagonal dispersions in one quadrature [34] [2]. For the degenerate parametric oscillator, signal cavity loss destroys the formation of the "Schrödinger Cat" state. This means experimental realisation is difficult, being limited to systems with sufficiently small loss. The second objective of this chapter is to study the effect of substituting the vacuum input for the signal input/output cavity mirror with a squeezed vacuum input.

The calculations in this chapter are performed using two methods. The first method involves the careful application of the positive P-representation, developed originally by Drummond and Gardiner [84]. The key feature of the representation is the positivity of the distribution function. This enables direct numerical simulation of stochastic equations which resemble classical equations for field amplitudes except that the dimensions are doubled. Such quantum simulation techniques have successfully been applied to many problems involving small quantum noise [98, 99]. The second method is the numerical solution of the master equation in a number state basis. Results using both methods are compared to confirm agreement.

It is important to realise that the stochastic equations obtained from the positive P representation are derived from a master equation with the assumption that certain boundary terms vanish [104]. It is not always the case that these terms do in fact vanish [105]. The problem [106, 107] generally manifests itself most strongly in the large quantum noise regime. Work by Smith and Gardiner [107] focussed on a system in a large quantum noise limit where boundary terms had not been checked. They showed that the results predicted from the incorrect stochastic equations used in this case were wrong. For the case

[2] The calculations of Kennedy and Walls [34] indicate that the squeezed bath homodyne detection is a better quantum measurement of the quadrature phase operator X_1, than the vacuum of the thermal bath

of the parametric oscillator where thermal noise is absent, there is a bounded manifold [38] within which the trajectories starting originally from the origin (an initial condition for the vacuum state) are confined. On this manifold, it can be shown that the relevant boundary terms vanish for arbitrary quantum noise strength [108]. Hence if we restrict our attention to the evolution described within this manifold, we can be sure in this case that the stochastic equations are correct [38]. For the squeezed vacuum system however no such simple bounded manifold is present and hence care must be taken with the stochastic simulations.

To summarize, this chapter is divided into a number of sections. In the first section of the chapter we present a treatment for the degenerate parametric oscillator valid for arbitrary noise. Next we examine the ideal steady state solutions of the degenerate parametric oscillator using the positive P representation and show how homodyne detection can be used to indicate whether superposition states are present. Most of the latter calculations were originally presented by Wolinsky and Carmichael [38] and dealt with the ideal case where loss is absent. Next we derive the stochastic equations necessary for the numerical simulations, and perform stochastic simulations in the large noise regime. An analysis of a set of stochastic simulations is performed to estimate the errors associated with such a method. These calculations are then repeated using a number state basis approach. Finally we examine the superposition states present in the degenerate parametric oscillator with a squeezed vacuum input to the signal cavity mode. These calculations are presented using the number state method only as the bounded manifold present in the unsqueezed case is not present.

4.2 The Model

4.2.1 The Hamiltonian

We present a simple model of the degenerate parametric oscillator. One has an optical cavity and two quantised modes a and b, the signal mode and the pump mode respectively. The mode a is at a frequency ω, while b is at a frequency 2ω. These modes interact via a second order non-linearity. The interaction Hamiltonian for this two mode system (depicted diagrammatically in Figure 4.1) can be written as

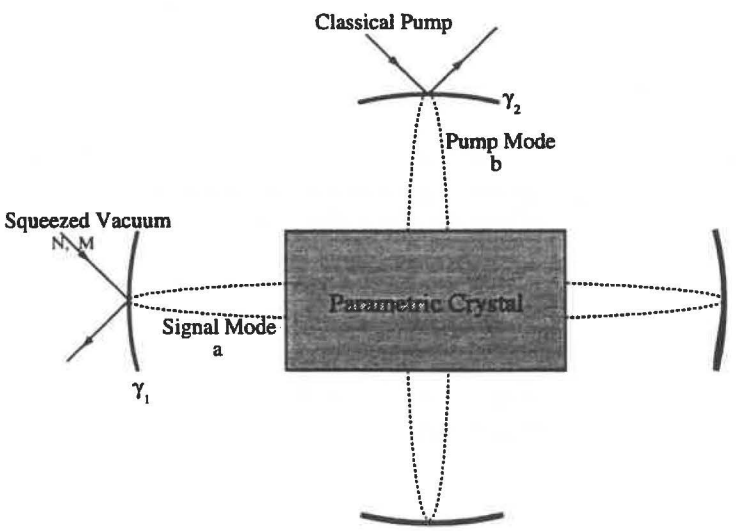

Figure 4.1: Schematic diagram representing the Degenerate Parametric Oscillator.

$$H = H_1 + H_2 + H_3 \tag{4.1}$$

where

$$H_1 = i\hbar\left[\kappa^* a^2 b^\dagger - \kappa a^{\dagger 2} b\right] \tag{4.2}$$

$$H_2 = i\hbar\left[\epsilon b^\dagger - \epsilon^* b\right] \tag{4.3}$$

$$H_3 = a\Gamma_a^\dagger + a^\dagger\Gamma_a + b\Gamma_b^\dagger + b^\dagger\Gamma_b \tag{4.4}$$

The model was used by Drummond, McNeil and Walls [94]. In Eqn (4.2-4.4) a, $a^\dagger$ and b, $b^\dagger$ are the destruction and creation operators for the signal and pump modes respectively. κ is the intermode coupling constant, while the decay of the cavity modes to the external modes of the field outside the cavity is described by the reservoirs Γ_a, Γ_b (with damping constants γ_1, γ_2 respectively). We assume that the modes decay into distinct uncorrelated reservoirs. The signal mode may be driven by a squeezed vacuum, while the classical pump amplitude ϵ is fed into the pump mode. For a bath with squeezed fluctuations around the frequency ω, Gardiner and Collett [83] showed that

$$\langle\Gamma^\dagger(t)\Gamma(t')\rangle = 2\gamma_1 N\delta(t-t') \tag{4.5}$$

$$\langle\Gamma(t)\Gamma^\dagger(t')\rangle = 2\gamma_1(N+1)\delta(t-t') \tag{4.6}$$

$$\langle\Gamma(t)\Gamma(t')\rangle = 2\gamma_1 M\exp[-i\omega t]\,\delta(t-t') \tag{4.7}$$

$$\langle\Gamma^\dagger(t)\Gamma^\dagger(t')\rangle = 2\gamma_1 M^*\exp[i\omega t]\,\delta(t-t') \tag{4.8}$$

The quantities N and M are the parameters used to represent the input squeezed vacuum. Here N will be taken to be real and $M = |M|\exp[i\varphi]$. These quantities satisfy the relation $|M|^2 \leq N(N+1)$, with equality corresponding to a maximally squeezed bath. When $M = 0$ we recover the usual thermal bath, where N plays the role of the mean thermal photon number. In Eqn (4.1) the Hamiltonian term H_1 represents the interaction between the two modes while H_2 represents the pumping of the b mode by the classical pump. H_3 represents the losses of the two modes with the cavity mirrors.

Let us consider the case where the pump mode decays rapidly compared with the signal mode. In this case the Hamiltonian can be simplified to

$$H = -i\hbar\left[\frac{\kappa^*\epsilon^*}{2\gamma_2}a^2 - \frac{\kappa\epsilon}{2\gamma_2}a^{\dagger 2}\right] + a\Gamma_a^\dagger + a^\dagger\Gamma_a + \frac{\kappa^*\kappa}{4\gamma_2^2}a^2\Gamma_b^\dagger + \frac{\kappa^*\kappa}{4\gamma_2^2}a^{\dagger 2}\Gamma_b \tag{4.9}$$

Here we notice that the Hamiltonian includes both a two-photon coherent pump term, and a two photon decay process for the signal mode, in addition to the usual single photon decay process with the damping constant of γ_1. In the above Hamiltonian the two photon pump strength is $\kappa\epsilon/2\gamma_2$ while the two photon damping rate is $\kappa^*\kappa/4\gamma_2^2$. It has been shown by Kinsler and Drummond [98, 99] that the Hamiltonian (excluding the squeezed input) given by Eqn (4.9) is equivalent to Eqn (4.1) in the adiabatic limit.

4.2.2 The Master equation

Using standard techniques [109] it is possible to show that the master equation corresponding to Eqn (4.9) is given in the interaction picture by

$$\frac{d\rho}{dt} = L\rho = \left[\left(\frac{\kappa\epsilon}{2\gamma_2}\right)a^{\dagger 2} - \left(\frac{\kappa^*\epsilon^*}{2\gamma_2}\right)a^2, \rho\right] + \left(\frac{\kappa^*\kappa}{4\gamma_2}\right)\left[2a^2\rho a^{\dagger 2} - a^{\dagger 2}a^2\rho - \rho a^{\dagger 2}a^2\right]$$

$$
\begin{aligned}
&+\gamma_1 (N+1)\left[2a\rho a^\dagger - a^\dagger a\rho - \rho a^\dagger a\right] \\
&+\gamma_1 N\left[2a^\dagger \rho a - aa^\dagger \rho - \rho aa^\dagger\right] \\
&+\gamma_1 M\left[2a\rho a - a^2\rho - \rho a^2\right] \\
&+\gamma_1 M^*\left[2a^\dagger \rho a^\dagger - a^{\dagger\,2}\rho - \rho a^{\dagger\,2}\right]
\end{aligned}
\tag{4.10}
$$

where L is the superoperator describing the time evolution of the density matrix. Next we introduce the scaled variables [38] (so all our quantities are measured with respect to cavity lifetimes)

$$\tau = \gamma_1 t \tag{4.11}$$

$$g^2 = \frac{\kappa^*\kappa}{2\gamma_1\gamma_2} \tag{4.12}$$

$$\lambda = \frac{|\kappa\epsilon|}{\gamma_1\gamma_2} \tag{4.13}$$

We have chosen the phase of κ to insure $\kappa\epsilon$ is real with no loss of generality [110]. Hence with these scaled variables we obtain the following master equation

$$
\begin{aligned}
\frac{d\rho}{d\tau} = &\frac{\lambda}{2}\left[a^{\dagger\,2} - a^2, \rho\right] + \frac{g^2}{2}\left[2a^2\rho a^{\dagger\,2} - a^{\dagger\,2}a^2\rho - \rho a^{\dagger\,2}a^2\right] \\
&+(N+1)\left[2a\rho a^\dagger - a^\dagger a\rho - \rho a^\dagger a\right] \\
&+N\left[2a^\dagger \rho a - aa^\dagger \rho - \rho aa^\dagger\right] \\
&+M\left[2a\rho a - a^2\rho - \rho a^2\right] \\
&+M^*\left[2a^\dagger \rho a^\dagger - a^{\dagger\,2}\rho - \rho a^{\dagger\,2}\right]
\end{aligned}
\tag{4.14}
$$

We now have the master equation required to examine the large noise behaviour of the DPO. This master equation can now be solved using a coherent state basis [94] to give c-number equation or using a number state basis [99][3].

4.2.3 The Coherent State Representation

The first means we choose of solving this master equation is to convert Eqn (4.14) to a Fokker-Planck equation using the Positive P representation, and from there to stochastic equations. The advantage in this case of the stochastic equations is that they can be readily solved, either numerically or analytically.

The positive P representation is defined by [84]

$$\rho = \int\int P(\alpha,\alpha^\dagger)\frac{|\alpha\rangle\langle\alpha^{\dagger\,*}|}{\langle\alpha^{\dagger\,*}|\alpha\rangle}d^2\alpha d^2\alpha^\dagger \tag{4.15}$$

where $|\alpha\rangle$ is a coherent state and the α and $\alpha^\dagger$ are independent complex variables in phase space. From this expansion, the master equation given by Eqn (4.14) can be converted into an equivalent Fokker-Planck equation. Assuming the boundary conditions vanish [4]

[3] In terms of the calculations involving number states we must notice that Eqn (4.14) represents the evolution of a Hilbert space operator on a phase space of infinite dimensions.

[4] For the DPO with a vacuum input ($N = M = 0$) in the signal mode, it has been shown by C.W. Gardiner [108] that the boundary terms do indeed vanish (this proof is shown in Appendix A). For the case of $M \neq 0$ it has not been proved that the boundary terms vanish.

we have

$$\begin{aligned}\frac{\partial P(\alpha,\alpha^\dagger)}{\partial\tau} &= \left\{\frac{\partial}{\partial\alpha}\left[\alpha-\alpha^\dagger\left(\lambda-g^2\alpha^2\right)\right]+\frac{\partial}{\partial\alpha^\dagger}\left[\alpha^\dagger-\alpha\left(\lambda-g^2\alpha^{\dagger\,2}\right)\right]\right.\\ &+\frac{\partial^2}{\partial\alpha^2}\left[\lambda-g^2\alpha^2+M\right]+\frac{\partial^2}{\partial\alpha^{\dagger\,2}}\left[\lambda-g^2\alpha^2+M^*\right] \qquad (4.16)\\ &\left.+2N\frac{\partial^2}{\partial\alpha\partial\alpha^\dagger}\right\}P(\alpha,\alpha^\dagger)\end{aligned}$$

Eqn (4.11) is equivalent to a pair of Ito Stochastic differential equation [104]

$$\frac{\partial}{\partial\tau}\begin{bmatrix}\alpha\\ \alpha^\dagger\end{bmatrix}=\begin{bmatrix}-\alpha+\alpha^\dagger\left[\lambda-g^2\alpha^2\right]\\ -\alpha^\dagger+\alpha\left[\lambda-g^2\alpha^{\dagger\,2}\right]\end{bmatrix}+\begin{bmatrix}\lambda-g^2\alpha^2+M & N\\ N & \lambda-g^2\alpha^{2\,\dagger}+M^*\end{bmatrix}^{\frac{1}{2}}\begin{bmatrix}\eta(\tau)\\ \eta^\dagger(\tau)\end{bmatrix} \qquad (4.17)$$

The $\eta(\tau)$ and $\eta^\dagger(\tau)$ are independent delta correlated real noise variables with a Gaussian probability distribution.

4.3 The Superposition Signature: Interference Fringes in a Quadrature Phase Amplitude

To determine whether superposition states are present in the DPO, we will evaluate the quadrature phase amplitude probability distribution functions $P(z)$ and $P(p)$. $P(z)$ and $P(p)$ are the probability distributions for obtaining the results z and p upon measurement of the quadrature phase amplitude operators X_1 and X_2, respectively. The phase of a local oscillator field can be chosen so that one of the two quadrature phase amplitude operators can be measured

$$X_1 = \left(a+a^\dagger\right)/2 \qquad (4.18)$$

$$X_2 = \left(a^\dagger-a\right)/2i \qquad (4.19)$$

We note that the operators a and $a^\dagger$ can be written in terms of the position and momentum operators $\hat{z}$ and $\hat{p}$ respectively. Choosing our units such that $\omega=\hbar=1$, then it can be shown that the momentum and position are related to the quadrature amplitudes X_1 and X_2 as follows $\hat{p}=X_1$ and $\hat{z}=X_2$.

The probability distribution for z is given by $P(z)=\langle z|\rho|z\rangle$ while the probability distribution for p is $P(p)=\langle p|\rho|p\rangle$. These probability distributions can be calculated using the positive P distribution. The probability distributions $P(p)$ and $P(z)$ can be written respectively as

$$P(p)=\int P(\alpha,\alpha^\dagger)\frac{\langle p|\alpha\rangle\langle\alpha^{\dagger*}|p\rangle}{\langle\alpha^{\dagger*}|\alpha\rangle}d^2\alpha d^2\alpha^\dagger \qquad (4.20)$$

$$P(z)=\int P(\alpha,\alpha^\dagger)\frac{\langle z|\alpha\rangle\langle\alpha^{\dagger*}|z\rangle}{\langle\alpha^{\dagger*}|\alpha\rangle}d^2\alpha d^2\alpha^\dagger \qquad (4.21)$$

where the range of integration is from $-\infty$ to ∞ in both cases. We use here the positive P representation and hence the appropriate measure of integration is the element $d^2\alpha d^2\alpha^\dagger$.

Using the relation given by Louisell [109], we have

$$\langle z|\alpha\rangle = \pi^{-1/4}\exp\left\{-\frac{z^2}{2}+\sqrt{2}z\alpha-\frac{\alpha^2}{2}-\frac{|\alpha|^2}{2}\right\} \qquad (4.22)$$

$$\langle p|\alpha\rangle = \pi^{-1/4}\exp\left\{-\frac{p^2}{2}-i\sqrt{2}p\alpha+\frac{\alpha^2}{2}-\frac{|\alpha|^2}{2}\right\} \qquad (4.23)$$

with units such that $\omega = \hbar = m = 1$. The denominator term in Eqn (4.20) and (4.21) is given by

$$\langle \alpha^{\dagger *} | \alpha \rangle = \exp\left[\frac{1}{2}\left(|\alpha|^2 + |\alpha^\dagger|^2\right) + \alpha\alpha^\dagger\right] \tag{4.24}$$

Evaluating the momentum probability distribution $P(p)$, we find

$$P(p) = \mathcal{N} \int P(\alpha, \alpha^\dagger) \exp\left[-p^2 + \frac{1}{2}\left(\alpha - \alpha^\dagger\right)^2 \cos\left[\sqrt{2}p\left(\alpha - \alpha^\dagger\right)\right]\right] d^2\alpha d^2\alpha^\dagger \tag{4.25}$$

where the sine term arising from the imaginary exponential part of the integral is an odd function in p and thus integrates out. The constant obtained from the integration over α, $\alpha^\dagger$ has been included in the normalisation constant which can now be defined as:

$$\mathcal{N}' = \left[\int_{-\infty}^{\infty} P(p) dp\right]^{-1} \tag{4.26}$$

Similarly, an expression for $P(z)$ can be derived

$$P(z) \;=\; \mathcal{N} \int P(\alpha, \alpha^\dagger) \exp\left\{-\left[\frac{z - (\alpha + \alpha^\dagger)}{\sqrt{2}}\right]^2\right\} d^2\alpha d^2\alpha^\dagger \tag{4.27}$$

4.4 The Degenerate Parametric Oscillator: A Review of the Work of Carmichael and Wolinsky

In this case we will consider our signal mode to be coupled through the cavity mirror to a vacuum ($N = 0$). Here our stochastic differential equation reduces to

$$\frac{\partial}{\partial \tau}\begin{bmatrix} x \\ y \end{bmatrix} = \begin{bmatrix} -x + y\left[\lambda - x^2\right] \\ -y + x\left[\lambda - y^2\right] \end{bmatrix} + \begin{bmatrix} \lambda - g^2x^2 & 0 \\ 0 & \lambda - g^2y^2 \end{bmatrix}^{\frac{1}{2}} \begin{bmatrix} \eta(\tau) \\ \eta^\dagger(\tau) \end{bmatrix} \tag{4.28}$$

where we have used new scaled variables $x = g\alpha$ and $y = g\alpha^\dagger$. The semiclassical stable states of Eqn (4.28) are $x = y = 0$ below threshold, while the above threshold solutions are $x = y = \pm\sqrt{\lambda - 1}$ and $x = y = \pm i\sqrt{1 - \lambda}$. A further nonclassical stable state is $x = -y = \pm\sqrt{\lambda + 1}$. The latter two stable states are nonclassical ($y \neq x^*$) and their presence can lead to anomalous behaviour (unstable trajectories) in numerical simulations.

Consider the manifold $\Lambda(x, y)$ given by $|x|, |y| \leq \sqrt{\lambda}$ with x and y both real. Stochastic trajectories starting within this manifold must remain within the manifold for all time, since x and y must remain real. To escape from the manifold one of the square roots must obtain a negative argument which is possible only if the point lies outside the boundary (either $x > \sqrt{\lambda}$ or $y > \sqrt{\lambda}$).

Steady state analytical solutions for the density operator in the adiabatic limit $\gamma_2 \gg \gamma_1$ have been derived by Drummond et al [94] and Wolinsky and Carmichael [38]. By deriving the Fokker-Planck equation equivalent to the stochastic equation in (6.1), one obtains the following steady-state solution

$$P_{ss}(x, y) \;=\; \mathcal{N}''[(\lambda - x^2)(\lambda - y^2)]^{1/g^2 - 1} \exp(2xy/g^2) \tag{4.29}$$

where $\mathcal{N}''$ is the normalisation constant. Plots of the steady state solution P function $P_{ss}(x, y)$ are given in Figures (4.2) for various values of λ and g. We observe that as the noise becomes large, all the stochastic trajectories are driven to the boundary of the manifold, and then along to the boundary corners.

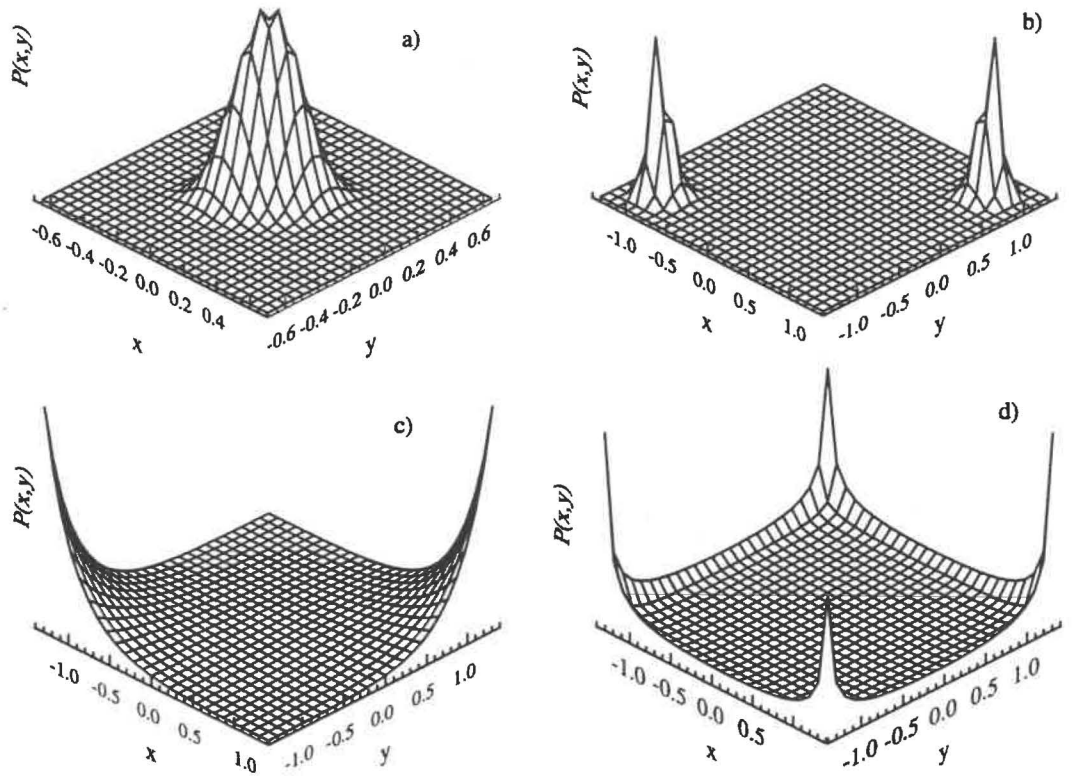

Figure 4.2: Plot of the normalised steady state positive P function $P_{ss}(x, y)$ over the bounded manifold $\Lambda(x, y)$ for a) $g = 0.2$, $\lambda = 0.5$, b) $g = 0.2$, $\lambda = 2.0$, c) $g = 1.0$, $\lambda = 2.0$, d) $g = 5.0$, $\lambda = 2.0$.

4.4.1 The Steady State

In the limit of large noise $g \gg 1$ with $\lambda/g^2 \ll 1$ it has been shown by Wolinsky and Carmichael [38] that the steady state distribution $P_{ss}(x, y)$ approaches a sum of four delta functions (Fig(4.2.d)), with every delta function located at the corner of the manifold. In this case the corresponding density operator can be expressed as the following classical mixture

$$\rho = P_+|\varphi_+\rangle\langle\varphi_+| + P_-|\varphi_-\rangle\langle\varphi_-| \tag{4.30}$$

where $|\varphi_\pm\rangle = |\sqrt{\lambda}/g\rangle \pm |-\sqrt{\lambda}/g\rangle$ and

$$P_+ = \frac{1 + \exp[2\lambda/g^2]}{8\cosh[2\lambda/g^2]} \tag{4.31}$$

$$P_- = -\frac{1 - \exp[2\lambda/g^2]}{8\cosh[2\lambda/g^2]} \tag{4.32}$$

The states $|\varphi_+\rangle$ and $|\varphi_-\rangle$ are quantum coherent state superpositions. For large $\sqrt{\lambda}/g$ the states are a superposition of two macroscopically distinct coherent states. Thus the parametric oscillator operating in the large quantum noise and steady state limits becomes a classical mixture of two "Schrödinger cat" states. The $|\varphi_+\rangle$ has an even number of photons while the $|\varphi_-\rangle$ state has an odd number. A method has been suggested by Yurke and Stoler [14] for detecting these superpositions states. Here one measures the probability distribution $P(z)$ and $P(p)$ for obtaining results z and p upon measurement of the quadrature phase amplitudes X_1 and X_2 respectively.

For the classical mixture the momentum probability distribution is given by [53]

$$P(p) = \mathcal{N}' \exp\left[-p^2\right]\left(\exp\left[\frac{2\lambda}{g^2}\right] + \cos\left[\frac{2\sqrt{2\lambda}}{g}p\right]\right) \tag{4.33}$$

while the position probability distribution is

$$\begin{aligned} P(z) &= \mathcal{N}'\left[\exp\left[\frac{2\lambda}{g^2}\right]\left\{\exp\left[-\left(z+\sqrt{2\lambda}/g\right)^2\right] + \exp\left[-\left(z-\sqrt{2\lambda}/g\right)^2\right]\right\}\right] \\ &\quad +2\exp\left[\frac{2\lambda}{g^2}\right]\exp\left[-z^2\right] \end{aligned} \tag{4.34}$$

A careful examination of the momentum probability distribution indicates that no interference fringes are present for any λ/g^2 value [53] (In Figure (4.3.a) we have plotted $P(p)$ versus p for $g = 2.5$ with $\lambda/g^2 = 100$). There are no superposition states observable in the steady state. In fact, Reid and Yurke [53] have shown that no fringes are present in the steady state for any finite g.

4.4.2 The Pure Superposition State

Above we have shown that the degenerate parametric oscillator in the classical mixture (4.30) of the states $|\varphi_+\rangle$ and $|\varphi_-\rangle$, will give no interference fringes in the $P(p)$ distribution. Let us now consider the state of the system to be a pure superposition state (where the + indicates the even state)

$$|\varphi_+\rangle = |\sqrt{\lambda}/g\rangle + |-\sqrt{\lambda}/g\rangle. \tag{4.35}$$

In this case the unnormalised density operator ρ may be expressed as

$$\rho = |\varphi_+\rangle\langle\varphi_+| \tag{4.36}$$

With $\alpha = x/g$ and $\alpha^{\dagger *} = y/g$ it can be shown that the steady state positive P distribution function $P(x,y)$ is of the form

$$P(x,y) = \frac{e^{\lambda/g^2}}{4\cosh\left[\lambda/g^2\right]}\left[\delta_{--} + \delta_{++}\right] + \frac{e^{-\lambda/g^2}}{4\cosh\left[\lambda/g^2\right]}\left[\delta_{-+} + \delta_{+-}\right] \tag{4.37}$$

The momentum and position probability distributions, $P(p)$ and $P(z)$ respectively, are given by

$$P(p) = \mathcal{N}'\exp(-p^2)[1+\cos(2p\sqrt{2\lambda}/g)] \tag{4.38}$$

$$\begin{aligned} P(z) &= \mathcal{N}'\left[\exp(\lambda/g^2)\exp[-(z+\sqrt{2\lambda}/g)^2]\right. \\ &\quad \left. +\exp(\lambda/g^2)\exp[-(z-\sqrt{2\lambda}/g)^2] + 2\exp(-\lambda/g^2)\exp[-z^2]\right] \end{aligned} \tag{4.39}$$

If the field is in a coherent state superposition such as $|\varphi_+\rangle$, the position probability distribution $P(z)$, for λ/g^2 large, becomes two Gaussian peaks centred at $\sqrt{\lambda}/g$ and $-\sqrt{\lambda}/g$. The distribution $P(p)$ exhibits interference fringes which are a consequence of the coherent superposition nature of the state $|\varphi_+\rangle$. Plots of $P(p)$ versus p are shown in Figure (4.3) for various values of λ/g^2. These are analogous to the interference fringes pointed out by Yurke and Stoler [14]. As expected, the peaks of these plots lie at the points $p = g\pi/(2\sqrt{2}\sqrt{\lambda})$.

So far we have considered only the superposition state $|\varphi_+\rangle$. Another pure superposition state formed by the DPO is

$$|\varphi_-\rangle = |\sqrt{\lambda}/g\rangle - |-\sqrt{\lambda}/g\rangle. \tag{4.40}$$

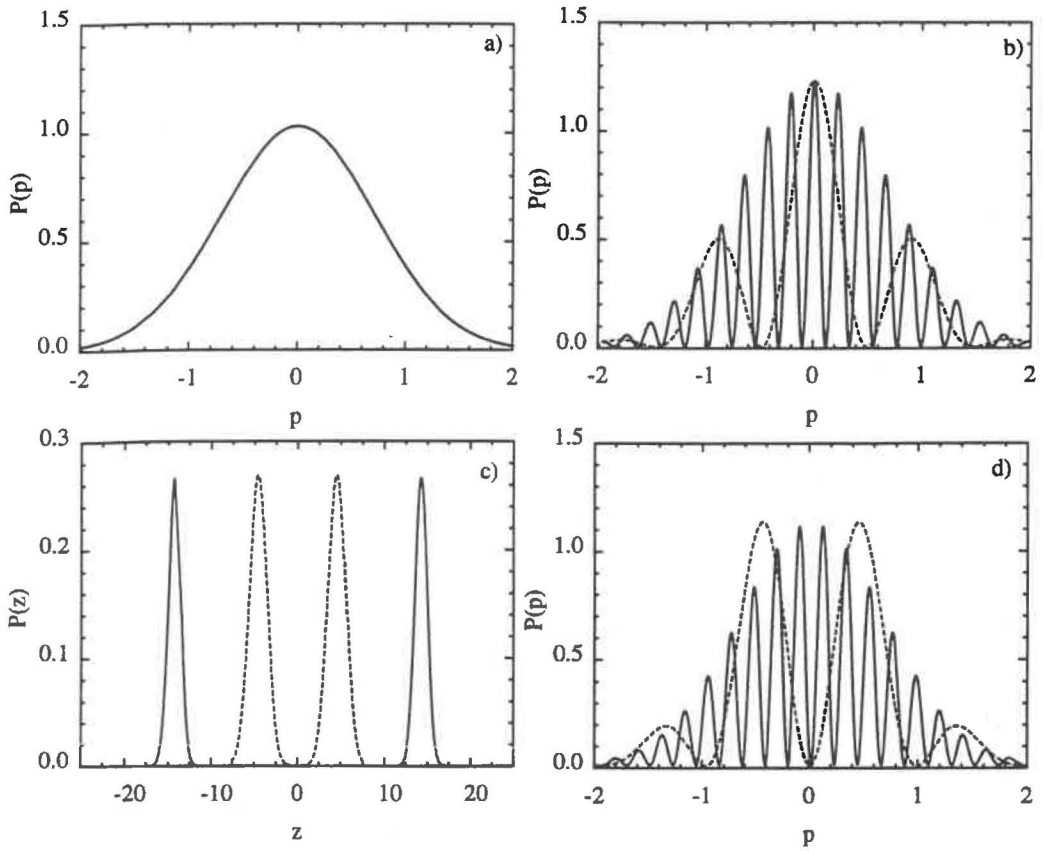

Figure 4.3: Plots of the momentum probability distribution $P(p)$ and position probability distribution $P(z)$.
a) Plot of $P(p)$ versus p for the steady state intracavity field of the parametric oscillator state (4.30) with $g = 2.5$ and $\lambda/g^2 = 100$. The same result is obtained for a 50/50 mixture of the superposition states $|\varphi_+\rangle$, $|\varphi_-\rangle$.
b) Plot of $P(p)$ versus p for the superposition state $|\varphi_+\rangle$. Here $g = 2.5$ and $\lambda/g^2 = 100$ for the solid line; $g = 2.5$ and $\lambda/g^2 = 5$ for the dotted line.
c) Plot of $P(z)$ versus z for the superposition state $|\varphi_+\rangle$. Here $g = 2.5$ and $\lambda/g^2 = 100$ for the solid line; $g = 2.5$ and $\lambda/g^2 = 5$ for the dotted line.
d) Plot of $P(p)$ versus p for the superposition state $|\varphi_-\rangle$. Here $g = 2.5$ and $\lambda/g^2 = 100$ for the solid line; $g = 2.5$ and $\lambda/g^2 = 5$ for the dotted line.

This state does exhibit similar fringes in the momentum probability distribution.

Previously we have discussed that the steady state positive P function obtained from the DPO is a classical mixture of the two superposition states $|\varphi_+\rangle$ and $|\varphi_-\rangle$ and that no interference fringes are observed. However recent work by Carmichael indicates to us that the pure superposition state $|\varphi_+\rangle$ may be observable in transient times.

4.4.3 Transient Superposition States

The work of Carmichael is suggestive of the formation of transient superposition states. The large g limit for which the expansion is valid corresponds also to the limit of no single-photon loss, $\kappa \to 0$. A model Hamiltonian for the oscillator in the fast-decaying pump limit and in the absence of single-photon cavity loss is

$$H = -i\hbar\left[\frac{\kappa^*\epsilon^*}{2\gamma_2}a^2 - \frac{\kappa\epsilon}{2\gamma_2}a^{\dagger 2}\right] + \frac{\kappa^*\kappa}{4\gamma_2^2}a^2\Gamma_b^\dagger + \frac{\kappa^*\kappa}{4\gamma_2^2}a^{\dagger 2}\Gamma_b \tag{4.41}$$

One has a two-photon pumping and a two-photon loss, brought about by the parametric interaction. It is seen that the signal mode, which is coupled to the pump only via the down conversion process, can only absorb or emit photons in pairs. Thus, in the absence of cavity loss, if the signal mode is initially in a vacuum state it can evolve only to a coherent superposition $|\varphi_+\rangle$ which has even photon number. The time needed for this evolution will be determined by the strength of the two-photon nonlinearity. The loss of photons from the cavity through the end-mirrors allows the formation of the odd-photon number-state. The final steady state formed over a number of cavity lifetimes is thus the mixture of the two superposition states. It might be expected however that the macroscopic superposition state $|\varphi_+\rangle$ is generated in a transient regime, provided that the signal cavity lifetime is sufficiently long, corresponding to the regime of large g. We will demonstrate that this is the case.

4.5 Stochastic Simulations

So far we have seen that the degenerate parametric oscillator can, in certain idealised regimes, produce superposition states. Now the full coupled quantum stochastic differential equations (QSDE) can be solved via stochastic simulation. Remembering that our equations were of the form

$$dx = \left[-x + y\left(\lambda - x^2\right)\right] d\tau + g\sqrt{\lambda - x^2}\, dW_1 \tag{4.42}$$

$$dy = \left[-y + x\left(\lambda - y^2\right)\right] d\tau + g\sqrt{\lambda - y^2}\, dW_2 \tag{4.43}$$

we need to decide the method of stochastic simulation. Choosing a fully implicit simulation method we need to write our Ito QSDE's in Stratonovich form (see Appendix B). In this case our fully implicit Stratonovich QSDE's are

$$dx = \left[x\left(\frac{g^2}{2} - 1\right) + y\left(\lambda - x^2\right)\right] d\tau + g\sqrt{\lambda - x^2}\, dW_1(t) + \frac{g^2 x}{2}\, dW_1^2(t) \tag{4.44}$$

$$dy = \left[y\left(\frac{g^2}{2} - 1\right) + x\left(\lambda - y^2\right)\right] d\tau + g\sqrt{\lambda - y^2}\, dW_2(t) + \frac{g^2 y}{2}\, dW_2^2(t) \tag{4.45}$$

The numerical simulations of these stochastic equations are then performed using the weak semi-implicit method of integration. A boundary condition is incorporated into the numerical algorithm to ensure trajectories do not escape the manifold. The results obtained from the stochastic simulations produced for each run at a time t, are a value for x and y. If we then accumulate the x, y results over many runs, the probability distribution $P(x, y)$ can be determined. From eqn (4.25) and (4.27) the momentum and position probability distributions $P(p)$ and $P(z)$ respectively can be calculated. An alternative method for calculating the momentum and probability distributions is to take the x, y obtained from each run and directly calculate the required value from eqn (4.25) and (4.27). The final momentum and position distribution can then be calculated by averaging over all the distributions obtained from each single run. As expected both results give consistent results. The method chosen was the second one discussed as this was computationally more efficient. Because the size of the noise terms scale as g, large ensemble sizes were required to obtain convergence for the larger g values. In the case of $g = 10$ in excess of one million simulations were required.

The results plotted in the Figures (4.4-4.8) reveal the presence of the interference fringes which are the signature of the coherent quantum superposition state. As a comparison, the quadrature phase amplitude distributions $P(z)$ and $P(p)$ for the (ideal) quantum

superposition state ($|\varphi_+\rangle$) are plotted in Figure (4.4-4.8). In agreement with analytical calculations, the steady-state or long-time distributions for the parametric oscillator reveal no interference fringes. For g greater than or of the order of 1.45, interference fringes become apparent in the transient evolution of the oscillator. The fringes (for fixed λ/g^2) become more pronounced as g increases. This is consistent with the earlier analytical conclusions, which were based on calculations performed in the large g limit where the strength of the two-photon nonlinearity is much greater than the single-photon cavity loss rate. The results of the simulations indicate the appearance of visible fringes for $g \sim 5$.

Lastly in this section we need to consider the errors associated with this method. In order to estimate the sampling error associated with the finite limitation of ensemble sizes, a calculation was performed with n subensembles of N trajectories each. The mean and standard error in the mean was evaluated over the subensembles and a graph showing the error bounds is plotted in Figure (4.9). We notice in this figure for $g = 2.5$ that the errors are quite large. The interference fringes however are still quite observable.

In the next section we investigate an alternative method for calculating the momentum and position probability distributions .

4.6 The Number State Calculations

An alternative method for modelling the degenerate parametric oscillator is via direct solution of the master equation in a number state basis. For systems where the mean photon number is not too large (mean photon number < 100), this is viable for calculating the probability distribution. The master equation method involves projecting the master equation onto a number state basis. Strictly, in this case, the master equation reduces to a matrix of infinite order. To allow for numerical calculations, one must establish a finite cut-off, putting a finite limit on the number of Fock states used in the basis. Care must be taken to ensure that the truncation of the number state basis is done correctly so the population of the higher order states is small. In our calculations the effect on increasing the number of basis states by one produced an error of less than 0.001 percent. Such a procedure is practical for systems of small or moderate photon number. With large numbers of photons, the number of Fock states required to adequately span the basis is large, and hence the method can become computationally intensive. For systems with large photon number other techniques such as stochastic simulations may provide an easier method of solution.

Let us expand the density matrix in the number state basis as follows

$$\rho_{nm} = \langle n|\rho|m\rangle \tag{4.46}$$

Previously, without a squeezed input into the signal mode of the degenerate parametric oscillator, we had the master equation given by

$$\begin{aligned} \frac{d\rho}{d\tau} &= \frac{\lambda}{2}\left[a^{\dagger 2} - a^2, \rho\right] + \frac{g^2}{2}\left[2a^2\rho a^{\dagger 2} - a^{\dagger 2}a^2\rho - \rho a^{\dagger 2}a^2\right] \\ &\quad + \left[2a\rho a^\dagger - a^\dagger a\rho - \rho a^\dagger a\right] \end{aligned} \tag{4.47}$$

Here the last term in square brackets (proportional to γ_1 in real time t) represents the signal cavity loss. The remaining terms proportional to λ and g^2 are the two-photon pump and two photon loss terms, respectively, resulting from the coupling via the parametric nonlinearity to the adiabatically eliminated pump cavity mode. The validity of this master equation has been investigated rigorously by Mortimer and Risken [111], and the correspondence to the stochastic equations (4.28) may be established by expanding in terms of

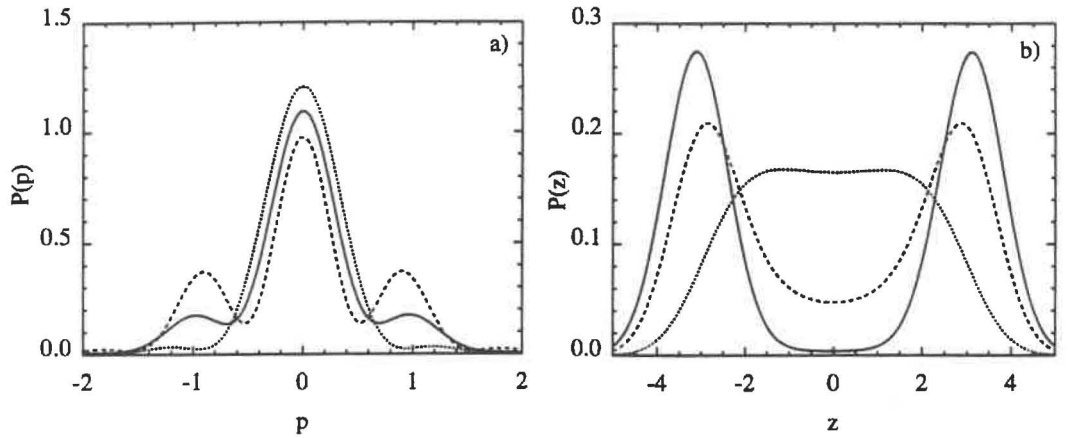

Figure 4.4: Plot of the momentum probability distribution $P(p)$ (Figure (a)) and the position probability distribution $P(z)$ (Figure (b)) for the stochastic simulations at times $t = 0.0025\tau$(dotted), $t = 0.0050\tau$(dashed), $t = 0.0100\tau$(solid) . Here $g = 10.0$ and $\lambda/g^2 = 5.0$.

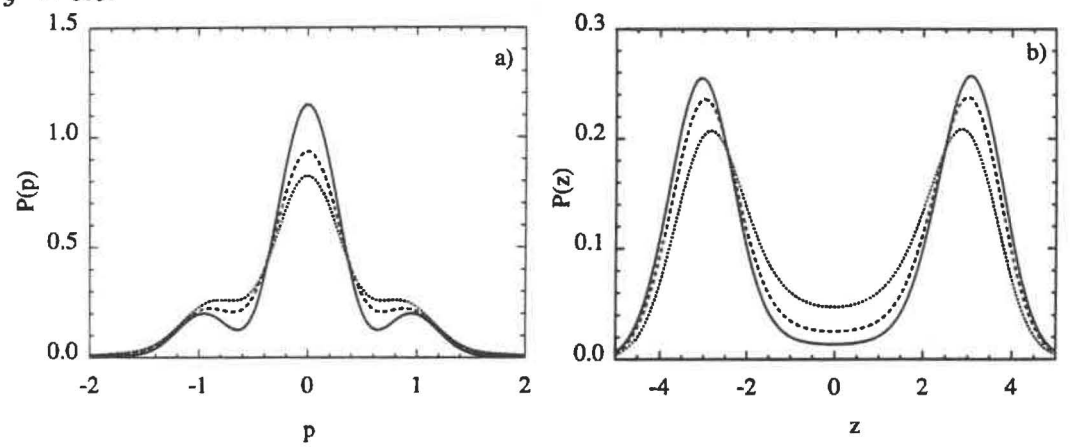

Figure 4.5: Plot of the momentum probability distribution $P(p)$ (Figure (a)) and the position probability distribution $P(z)$ (Figure (b)) for the stochastic simulations at times $t = 0.015\tau$(dotted), $t = 0.020\tau$(dashed), $t = 0.025\tau$(solid). Here $g = 5.0$ and $\lambda/g^2 = 5.0$.

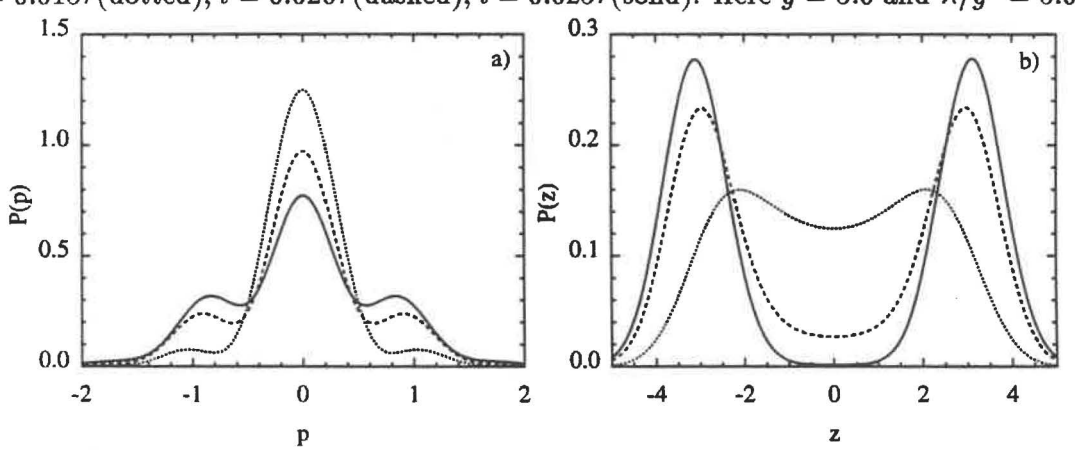

Figure 4.6: Plot of the momentum probability distribution $P(p)$ (Figure (a)) and the position probability distribution $P(z)$ (Figure (b)) for the stochastic simulations at times $t = 0.050\tau$(dotted), $t = 0.100\tau$(solid), $t = 0.200\tau$(dashed). Here $g = 2.5$ and $\lambda/g^2 = 5.0$.

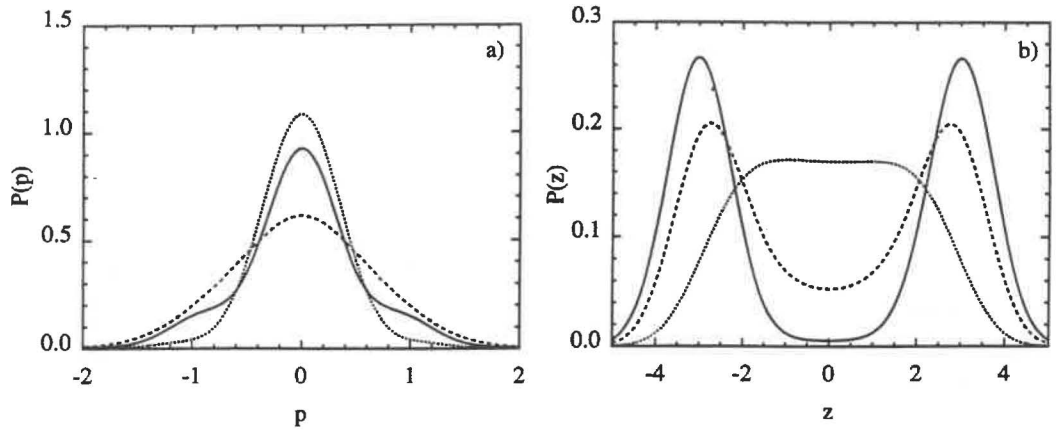

Figure 4.7: Plot of the momentum probability distribution $P(p)$ (Figure (a)) and the position probability distribution $P(z)$ (Figure (b)) for the stochastic simulations at times $t = 0.125\tau$(dotted), $t = 0.250\tau$(solid), $t = 0.500\tau$(dashed). Here $g = 1.45$ and $\lambda/g^2 = 5.0$.

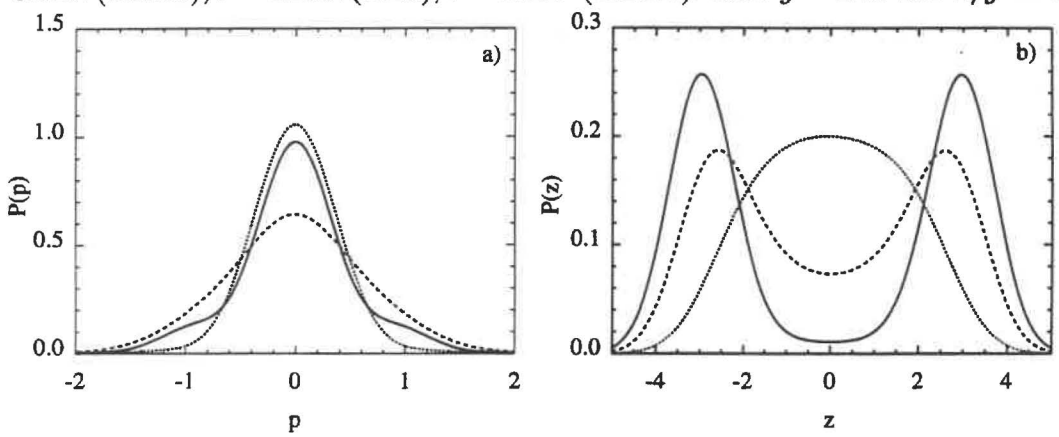

Figure 4.8: Plot of the momentum probability distribution $P(p)$ (Figure (a)) and the position probability distribution $P(z)$ (Figure (b)) for the stochastic simulations at times $t = 0.125\tau$(dotted), $t = 0.250\tau$(solid), $t = 0.500\tau$(dashed). Here $g = 1.35$ and $\lambda/g^2 = 5.0$.

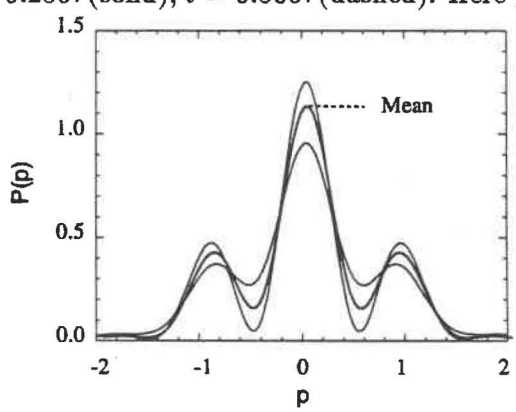

Figure 4.9: Plot of the error estimate for the momentum probability distribution $P(p)$. Here $g = 2.5$ and $\lambda/g^2 = 5$. The time has been set to $t = 0.1\tau$. The thick curve corresponds to the mean of 10 subensembles of 100000 runs. The thin curves correspond to the standard error in this mean.

the positive P-representation using standard procedures. The two-photon loss and pump terms associated with the above master equation are derivable from the model Hamiltonian (4.41). Expanding over the number state basis we may express the time evolution of the system as follows

$$\frac{\partial}{\partial \tau}\rho_{nm} = \langle n|\frac{\partial}{\partial \tau}\rho|m\rangle = \mathcal{L}_{ij}^{nm}\rho_{nm} \tag{4.48}$$

where this supermatrix $\mathcal{L}_{ij}^{nm}$ is given by

$$\begin{aligned}
\mathcal{L}_{ij}^{nm} &= \frac{\lambda}{2}\sqrt{i\,(i-1)}\,\delta_{i,j}^{n+2,m} + \frac{\lambda}{2}\sqrt{j\,(j-1)}\,\delta_{i,j}^{n,m+2} \\
&\quad -\frac{\lambda}{2}\sqrt{(i+1)\,(i+2)}\,\delta_{i,j}^{n-2,m} - \frac{\lambda}{2}\sqrt{(j+1)\,(j+2)}\,\delta_{i,j}^{n,m-2} \\
&\quad -[i+j]\,\delta_{i,j}^{n,m} + 2\sqrt{(i+1)\,(j+1)}\,\delta_{i,j}^{n-1,m-1} \\
&\quad -g^2\,[i\,(i-1)+j\,(j-1)]\,\delta_{i,j}^{n,m} \\
&\quad +2\sqrt{(i+1)\,(i+2)\,(j+1)\,(j+2)}\,\delta_{i,j}^{n-2,m-2}
\end{aligned} \tag{4.49}$$

Here the dirac delta function is given

$$\delta_{i,j}^{n,m} = \begin{cases} 1 & \text{if i = n and j = m} \\ 0 & \text{otherwise} \end{cases} \tag{4.50}$$

Previously we discussed how interference fringes in the momentum probability distribution were suggestive of the formation of "Schrödinger Cat" like states. Hence for the number state method we need to determine the probability distribution functions $P(p)$ and $P(z)$. We may write

$$P(z) = \langle z|\rho|z\rangle \tag{4.51}$$

$$P(p) = \langle p|\rho|p\rangle \tag{4.52}$$

which can be written in terms of the density matrix element ρ_{nm} (obtained by direct solution of the master equation in the number state basis) as

$$P(z) = \sum_{n=0}^{n_{max}}\sum_{m=0}^{n_{max}}\langle z|n\rangle\rho_{nm}\langle m|z\rangle \tag{4.53}$$

$$P(p) = \sum_{n=0}^{n_{max}}\sum_{m=0}^{n_{max}}\langle p|n\rangle\rho_{nm}\langle m|p\rangle \tag{4.54}$$

In Eqn (4.53) and Eqn(4.54), the quantities $\langle z|n\rangle$ and $\langle p|n\rangle$ are given by

$$\langle z|n\rangle = (2^n n!)^{-\frac{1}{2}}\left(\frac{\eta}{\pi}\right)^{\frac{1}{4}}\exp\left[-\frac{1}{2}\eta z^2\right]H_n\left(z\sqrt{\eta}\right) \tag{4.55}$$

$$\langle p|n\rangle = (2^n n!)^{-\frac{1}{2}}(-i)^n\left(\frac{\hbar^2}{\pi\eta}\right)^{\frac{1}{4}}\exp\left[-\frac{1}{2}\eta p^2\right]H_n\left(\frac{\hbar p}{\sqrt{\eta}}\right) \tag{4.56}$$

where $\eta = \sqrt{\frac{km}{\hbar}}$ and $H_n(z)$ is the Hermite polynomial. To compare the results of equations (4.51) and (4.52) with our stochastic calculations we need to set $\eta = 1$. Now once the master equation has been solved numerically in the number state basis to give $\rho_{n,m}$ we can easily determine the probability distribution functions $P(p)$ and $P(z)$. In Fig (4.10) we plot $P(p)$ and $P(z)$ for various parameters. We observe that the results are almost identical

to those obtained for the stochastic simulations. The differences can be associated with the errors involved in the stochastic simulations.

The mean photon number for the superposition states considered so far is small (being about 5). For these cases we can hardly call them macroscopic (or even mesoscopic) superposition states. To this end we re-examine the case of $g \sim 2.5$ with a mean photon number of 100. We present these results in Figure (4.11). Here fringes are quite observable, and the mean photon number is large enough so at the very least we may say mesoscopic superposition states have been detected. Of importance to confirm the generation of the "Schrödinger Cat"state is the position distribution $P(z)$. For a genuine superposition state we need the two position peaks in $P(z)$ (Figure 4.11.b) to be well separated with little or no overlap between them. Figure (4.11) clearly shows no overlap in the position probability distribution and hence we can be confident that a superposition state has been generated.

We have previously commented that these superpositions states occur in the transient evolution of the parametric oscillator. To show this, in Fig (4.12), we plot the time development of the momentum probability distribution for $g = 2.5$ and $\lambda/g^2 = 10$. The probability distribution $P(p)$ originally starts off as a Gaussian but then rapidly narrows and begins to develop the interference fringes indicative of the superposition states. As we evolve further these fringes are washed out as the system develops into the equal mixture of even and odd superposition states. Once the cavity lifetime has been reached no superposition signatures are observed. For $g = 2.5$, the interference fringes are washed out by $t = 0.2\tau$.

In this section we have shown that number state calculations are as efficient as stochastic simulations. Computationally the number state method can be more efficient for low to medium photon numbers.

4.7 Discussion of the Degenerate Parametric Oscillator Results

The results obtained for $P(z)$ and $P(p)$ upon simulation of Eqn (4.28) and numerical solution of the master equation have been presented. These represent the predictions for the signal field of the degenerate parametric oscillator in the adiabatic limit with $\gamma_2 \gg \gamma_1$, where the signal is initially in a vacuum state. As predicted from analytical calculations, the steady-state or long-time distributions for the parametric oscillator reveal no interference fringes. The formation of fringes with the evolution of the signal field from the vacuum state, is clearly evident in Figure (4.12), where $g = 2.5$. The first minimum appearing at approximating $p = \pi g/\sqrt{8\lambda}$ for $\lambda/g^2 = 5$ is consistent with the formation of the state $|\varphi_+\rangle$. Also evident from the Figures is the washing out of the interference pattern as the oscillator evolves further. The $|\varphi_-\rangle$ state which is generated from $|\varphi_+\rangle$ with the loss of a cavity photon, contributes more significantly as time increases, and the fringes are lost in this case well before steady state is reached.

Our complete solutions indicate that values of $g \sim 2.5$ will give clear interference fringes for $\lambda/g^2 \sim 5$. In this case the probability distribution for the orthogonal quadrature phase amplitudes z is clearly bimodal with minimal overlap between the two peaks. Typical optical degenerate parametric oscillators to date have very small g values. The nonlinearity to cavity loss ratio is thus much too small to anticipate observation of the fringes discussed here. A possible scheme is discussed in the next section by which the nonlinearity to cavity loss rate can be decreased while maintaining the superposition signature.

Our calculations here have focussed on the generation of the superposition state within a cavity. Hence the moments we have considered are the intracavity ones. The intracavity moments may be measurable if one uses a Q-switched cavity to suddenly "dump" the cavity

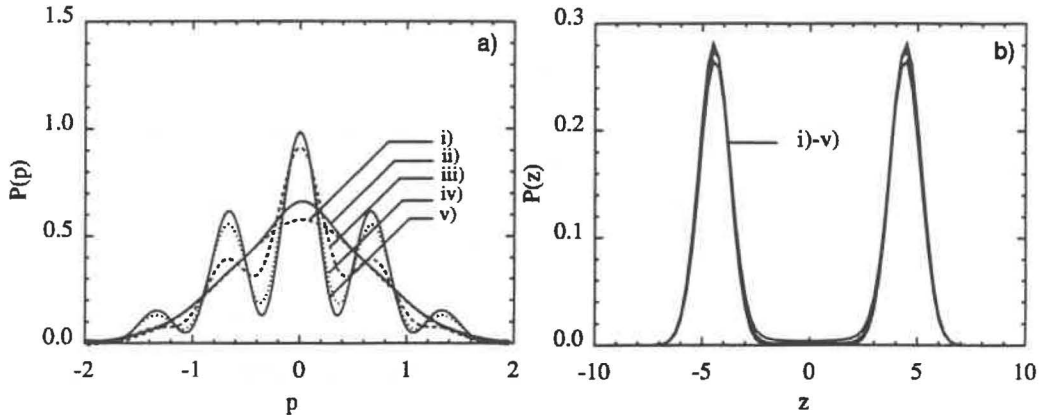

Figure 4.10: Plot of the momentum probability distribution $P(p)$ (Figure a) and the position probability distribution $P(z)$ (Figure b). These number state calculations are plotted for
i) $g = 1.25$ with $\lambda/g^2 = 5$ and $t = 0.4\tau$.
ii) $g = 1.45$ with $\lambda/g^2 = 5$ and $t = 0.250\tau$.
iii) $g = 2.5$ with $\lambda/g^2 = 5$ and $t = 0.100\tau$.
iv) $g = 5.0$ with $\lambda/g^2 = 5$ and $t = 0.020\tau$.
v) $g = 10.0$ with $\lambda/g^2 = 5$ and $t = 0.010\tau$.

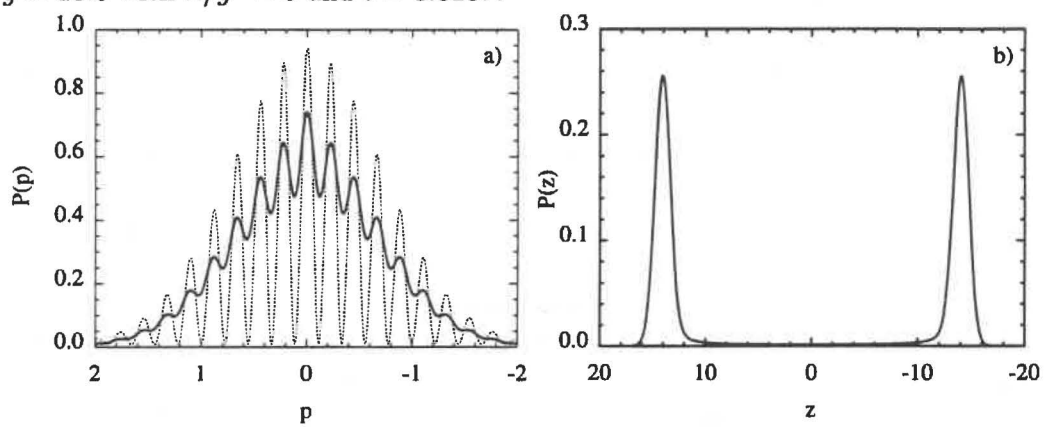

Figure 4.11: Plot of the momentum probability distribution $P(p)$ (Figure a) and the position probability distribution $P(z)$ (Figure b). These calculations are plotted for $g = 2.5$, $\lambda/g^2 = 100$ and $t = 0.01\tau$. We have also plotted (dotted line) in Figure (a) the pure superposition state $|\varphi_+\rangle$.

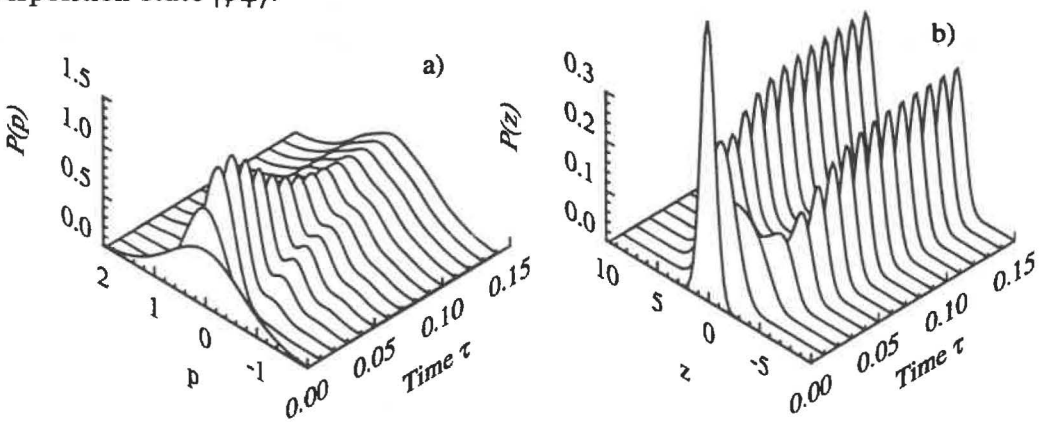

Figure 4.12: Plot of the evolution of the momentum probability distribution $P(p)$ (Figure (a)) and the position probability distribution $P(z)$ (in Figure (b)). Here $g = 2.5$, $\lambda/g^2 = 10$, and τ is the cavity decay time for the signal mode.

field externally, at the appropriate time. One can use a homodyne measurement scheme to measure external quadrature phase amplitudes. In fact the instantaneous intracavity moments are directly related to the external moments by $\langle a_{ext}^{\dagger} a_{ext} \rangle = 2\gamma_1 \langle a^{\dagger} a \rangle$ for the vacuum input case [82]. Alternatively a homodyne measurement should in principle be able to detect the presence of the superpositions states by making measurements on the external field. Since superposition states have a short life span, one may have to be careful that detection times are not too long.

4.8 The Degenerate Parametric Oscillator with a Squeezed Input to the Signal Mode of the Cavity

In the previous sections we showed that without a squeezed vacuum, superposition states were exhibited in degenerate parametric oscillation only for systems with high nonlinear coupling to linear loss ratio.

It has been shown that a macroscopic superposition of coherent states may be preserved in the presence of dissipation if quantum fluctuations of the bath are reduced below the quantum limit in one quadrature (this was the suggestion of Mecozzi and Tombesi [33] and Kennedy and Walls [34]). Kennedy and Walls considered a system initially in a superposition state of two macroscopically distinct coherent states. The system is coupled to a bath, modelling loss to an external environment, and calculations showed the fringes to be destroyed if the losses are sufficiently high. In particular they showed that a specific factor $\left|\langle\sqrt{\lambda}/g| - \sqrt{\lambda}/g\rangle\right|^{\eta}$ (with $\eta = 1 - \exp[-2\gamma_1 t]$) in the momentum probability distribution suppresses the interference fringes unless $\eta \sim 0$. As the system evolves the term $\exp[-2\gamma_1 t] < 1$ and hence the specific factor contributes, destroying the fringes. Kennedy and Walls [34] then examined the effect of coupling to a squeezed bath. They found for $2\gamma t \ll \ln N$, that the specific factor $\left|\langle\sqrt{\lambda}/g| - \sqrt{\lambda}/g\rangle\right|^{\eta}$ is very small, and hence interference fringes persist due to squeezing of the quantum fluctuations.

In this section we investigate the use of a squeezed vacuum input into the signal mode of the cavity (refer Fig (4.1)). Our aim is to examine whether the use of a squeezed vacuum allows the interference fringes to be preserved for lower g values. We will use the number state basis expansion of the master equation over the stochastic simulations approach, because with the inclusion of a squeezed input the simple two dimensional bounded manifold is destroyed. Other manifolds may exist but these cannot be easily found. Hence with no guarantee of boundary terms vanishing, we may have simulation problems with trajectories escaping to infinity.

With the inclusion of a squeezed vacuum into the signal mode of the degenerate parametric oscillator the time evolution of the master equation in the number state basis is given by

$$\frac{\partial}{\partial \tau}\rho_{nm} = \langle n|\frac{\partial}{\partial \tau}\rho|m\rangle = \mathcal{L}_{ij}^{nm}\rho_{nm} \tag{4.57}$$

where this supermatrix $\mathcal{L}_{ij}^{nm}$ is given by

$$\begin{aligned}
\mathcal{L}_{ij}^{nm} \;=\; & \frac{\lambda}{2}\sqrt{i\,(i-1)}\;\delta_{i,j}^{n+2,m} + \frac{\lambda}{2}\sqrt{j\,(j-1)}\;\delta_{i,j}^{n,m+2} \\
& -\frac{\lambda}{2}\sqrt{(i+1)(i+2)}\;\delta_{i,j}^{n-2,m} - \frac{\lambda}{2}\sqrt{(j+1)\,(j+2)}\;\delta_{i,j}^{n,m-2} \\
& -g^2\left[i\,(i-1)+j\,(j-1)\right]\delta_{i,j}^{n,m} + 2\sqrt{(i+1)(i+2)(j+1)(j+2)}\;\delta_{i,j}^{n-2,m-2} \\
& +\gamma\left[N+1\right]\left[2\sqrt{(i+1)(j+1)}\;\delta_{i,j}^{n-1,m-1} - [i+j]\,\delta_{i,j}^{n,m}\right]
\end{aligned} \tag{4.58}$$

$$+\gamma N\left[2\sqrt{ij}\,\delta_{i,j}^{n+1,m+1}-[i+j+2]\,\delta_{i,j}^{n,m}\right]$$
$$+\gamma M\left[2\sqrt{(i+1)\,j}\,\delta_{i,j}^{n-1,m+1}-\sqrt{(i+1)\,(i+2)}\,\delta_{i,j}^{n-2,m}-\sqrt{j\,(i-1)}\,\delta_{i,j}^{n,m+2}\right]$$
$$+\gamma M^{*}\left[2\sqrt{(j+1)\,i}\,\delta_{i,j}^{n+1,m-1}-\sqrt{i\,(i-1)}\,\delta_{i,j}^{n+2,m}-\sqrt{(j+1)\,(j+2)}\,\delta_{i,j}^{n,m-2}\right]$$

This master equation can be straight-forwardly solved by numerical techniques. Using the procedure discussed in the previous section, we can determine the position and momentum probability distributions. However in this case there are two other significant parameters to be considered: N and M. We choose $|M|=\sqrt{N\,(N+1)}$, which leaves us an arbitrary choice of phase ϕ. The optimal phase was found to be $\phi=0$.

Initially to keep the mean photon number small we choose $N\sim 1$ (this corresponds to 70% squeezing). The results are plotted in Figures (4.13-4.16) for various g and λ. The figures definitely reveal the presence of interference fringes in the momentum probability distribution. As we have previously discussed, these fringes are the signature of the coherent quantum superposition state. In particular we have plotted in Fig (4.13) the momentum and position probability distributions for $N=1$ and $N=0$ (the unsqueezed vacuum). It can be seen that the inclusion of only a moderately squeezed vacuum into the signal port improves the interference fringes. Figure (4.13) shows that interference fringes are observable in the $g\sim 1$ regime for $N=1$. No fringes are observable for similar parameters with $N=0$. We observe clearer fringes with the inclusion of only a moderately squeezed input.

In the results presented so far we have considered only a moderately squeezed vacuum input to the signal port of the degenerate parametric oscillation. We need the effect of N, our principle squeezing parameter. To this end we plot in Figure (4.14) the momentum and position probability distributions versus the squeezing parameter N for $g=2.5$. In this Figure we observe that better interference fringes are observed as N increases. The effect on the interference fringes in going from $N=1$ to $N=2$ (71 percent squeezing to 89 percent squeezing) is slight but observable.

The plots in Figures (4.13-4.14) are for a relatively low photon number (determined by λ/g^2). In Figure (4.13) we present the results of a calculation with $\lambda/g^2=100$. These results indicate that the fringes are definitely better resolved with the use of the squeezed input.

Above we discussed the results of a calculations of Kennedy and Walls [34]. They showed that with $|M|=\sqrt{N\,(N+1)}$ and $\phi=\pi$ that the interference fringes were preserved. Thus we have good fringes in the presence of dissipation if quantum fluctuations of the bath are reduced below the quantum limit. There results compare well with our results presented above. However in our case we found the optimum angle of ϕ was zero not π as in Kennedy and Walls case. This however can be attributed to the fact that we are generating a slightly different superposition state from the state considered by Kennedy and Walls [34]. The DPO generates the superposition state $|\sqrt{\lambda}/g\rangle+|-\sqrt{\lambda}/g\rangle$, while Kennedy and Walls choose the initial superposition state $|\sqrt{\lambda}/g\rangle+i\,|-\sqrt{\lambda}/g\rangle$. Thus there is a π phase difference between the two superposition states.

Finally in this section we investigate whether lower values of the crystal nonlinearity to cavity loss ratio g can be used to generate "Schrödinger Cat" like states. To this end we present in Figure (4.16) the results of a calculation with $g=0.1$, $\lambda/g^2=100$ and $N=20$. The plot clearly indicates than the fringes characteristic of "Schrödinger Cat" states are present. Hence we can achieve fringes for $g=0.1$ but we need a highly squeezed input field.

In this section we have observed that with the inclusion of only a moderately squeezed field, the value of g can be significantly lowered, while still maintaining an interference

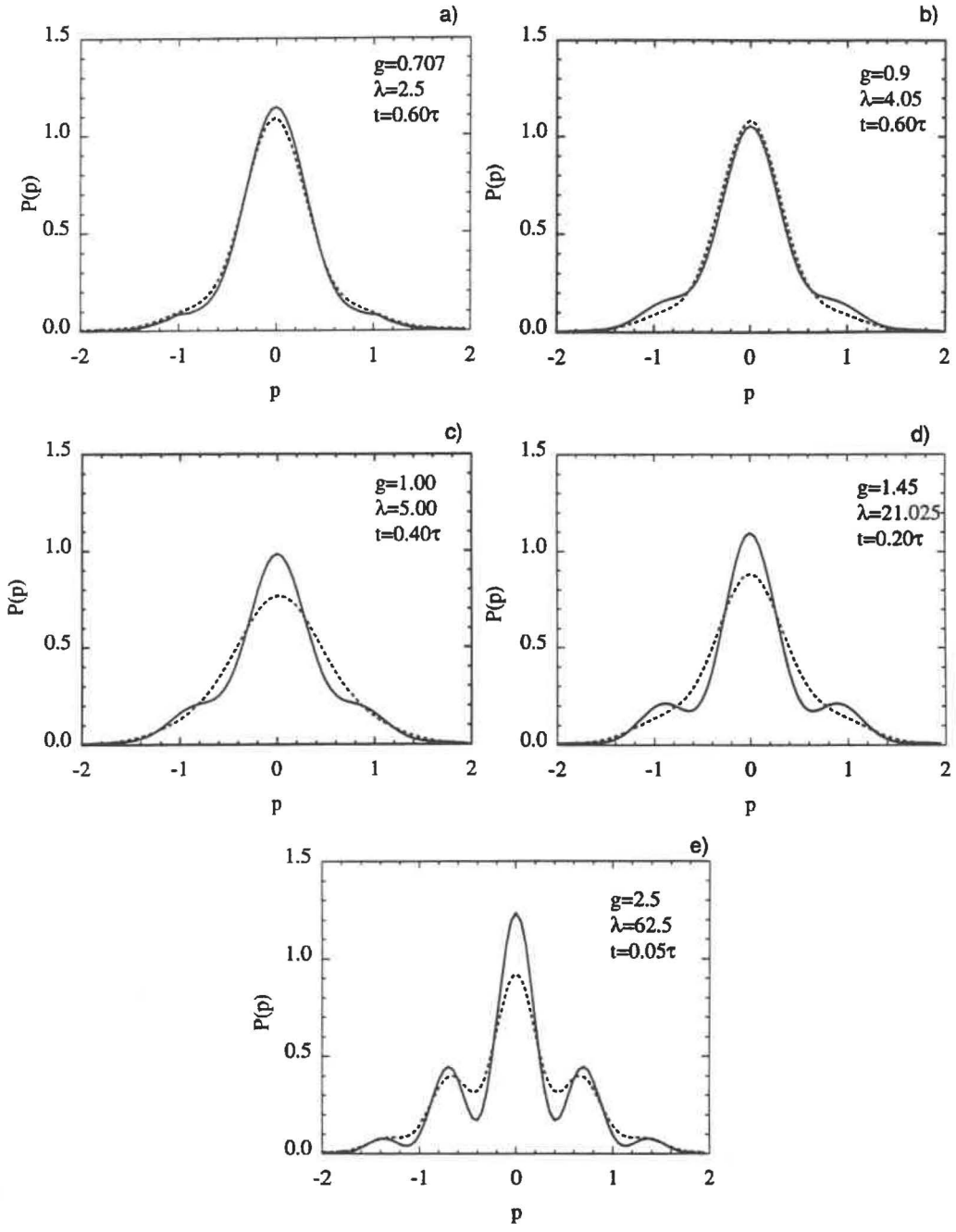

Figure 4.13: Plot of the momentum probability distribution $P(p)$ for
a) $g = 2.50$, $\lambda/g^2 = 10$ and $t = 0.05\tau$.
b) $g = 1.45$, $\lambda/g^2 = 10$ and $t = 0.200\tau$.
c) $g = 1.00$, $\lambda/g^2 = 10$ and $t = 0.400\tau$.
d) $g = 0.90$, $\lambda/g^2 = 10$ and $t = 0.600\tau$.
e) $g = 0.707$, $\lambda/g^2 = 10$ and $t = 0.600\tau$.
The dashed line represent $N = 0$ (unsqueezed) while the solid line represents squeezing with $N = 1$.

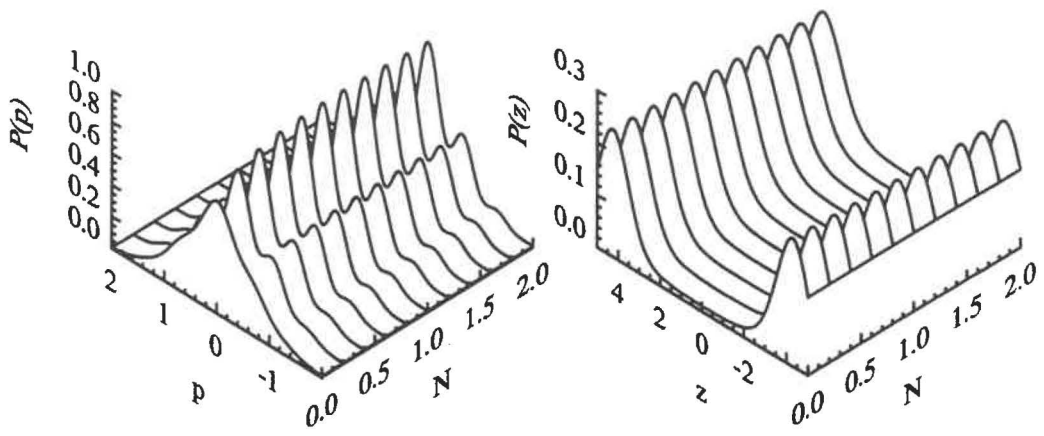

Figure 4.14: Plot of the variation of the momentum probability distribution $P(p)$ (Figure (a)) and the position probability distribution $P(z)$ (in Figure (b)) with N. Here $g = 2.5$ with $\lambda/g^2 = 10$, and $\tau = 0.1$.

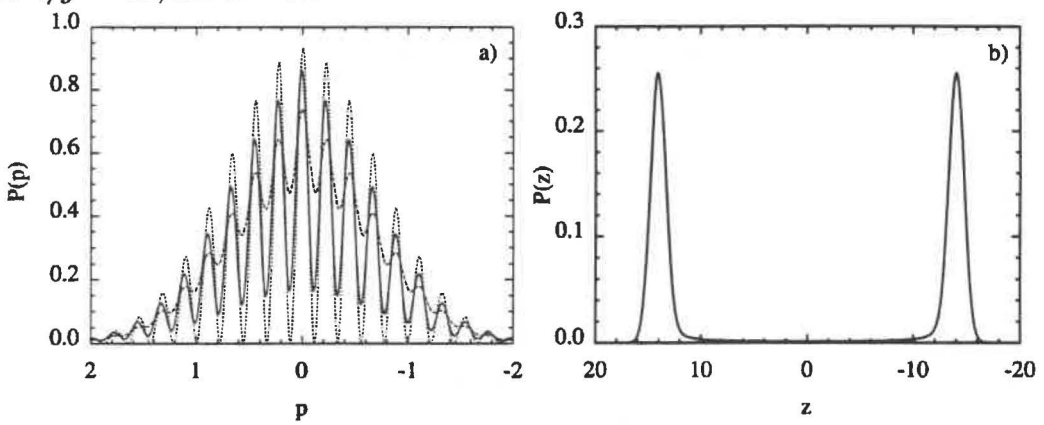

Figure 4.15: Plot of the momentum probability distribution $P(p)$ (Figure a) and the position probability distribution $P(z)$ (Figure b). These calculations are plotted for $N = 1$, $g = 2.5$, $\lambda/g^2 = 100$ and $t = 0.01\tau$. The dashed line in Figure (a) corresponds to the $N = 0$ case, while the dotted line corresponds the pure superposition state $|\varphi_+\rangle$.

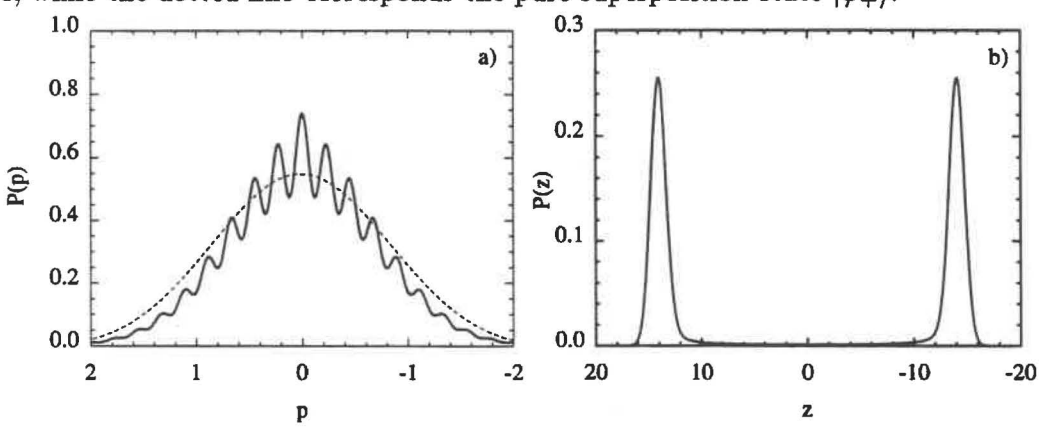

Figure 4.16: Plot of the momentum probability distribution $P(p)$ (Figure a) and the position probability distribution $P(z)$ (Figure b). These calculations are plotted for $N = 20$, $g = 0.1$, $\lambda/g^2 = 100$ and $t = 0.2\tau$. The dashed line in Figure (a) corresponds to the $N = 0$ case.

fringe in the momentum probability distribution. Increasing the degree of squeezing does make the interference fringes more pronounced.

4.9 Discussion and Conclusion

We have obtained numerical predictions for the evolution from a vacuum state of the intracavity signal mode of the degenerate parametric oscillator. The solutions are obtained in the adiabatic oscillator limit where the decay of the pump cavity mode is much greater than that of the signal. Above the semiclassical threshold and for sufficiently large λ/g^2, the probability distribution for one of the quadrature phase amplitudes (z say), becomes clearly bimodal. For sufficiently large g ($g \geq 1$), the corresponding probability distribution for the orthogonal quadrature phase amplitude (p say) develops transient interference fringes. The experimental observation of such fringes would be evidence for the formulation of a coherent superposition of two distinct coherent states well separated in phase space. Such states for very large λ/g^2 values, are analogous to the "Schrödinger-Cat" states discussed by Schrödinger in his famous paradox. Our results have been limited for practical numerical reasons to values for λ/g^2 of the order 5. Nevertheless the observation of superpositions of mesoscopically distinct states would still be a significant advance.

The analysis of arbitrarily large λ/g^2 given by Carmichael and Wolinsky applies to the large g limit. Our complete solutions indicate that values of $g \sim 2.5$ will give clear interference fringes for $\lambda/g^2 \sim 5$. In this case the probability distribution for the orthogonal quadrature phase amplitude z is clearly bimodal with minimal overlap between the two peaks. Typical optical degenerate parametric oscillators to date have very small g values, at least several orders of magnitude lower than what we require. The nonlinearity to cavity loss ratio is thus much to small too anticipate observation of the fringes discussed here. Nevertheless our work showing clear fringes to be predicted for moderate g values not much greater than 1 is encouraging. While the distinction in phase space between the two states associated with z is at most mesoscopic, the observation of such fringes would be a first step towards the observation of true "Schrödinger cat" states, where the two states are microscopically separated. Systems obtaining values of g of this order would not seem out of the question, and may be obtainable using Josephson nonlinearities.

Finally we investigated using a squeezed field as an input to the intracavity signal mode. This allows the nonlinearity of the crystal medium to be decreased while still allowing the fringes to remain. We found that the interference fringes are observable for quite small values of g ($g < 1$), but this required a large degree of squeezing (N large).

We note that in our calculations γ_1 is the loss of the signal cavity mode. We have specified that the sole source of signal loss was through the cavity mirror. Realistically a loss will also occur in the nonlinear medium. We note that the results of the simulations presented here for the DPO are also valid if we simply extend γ_1 to include all signal losses. The main point in generating "Schrödinger-cat" states is that to obtain a system which has a sufficiently large nonlinearity compared to linear losses. We also note that in the hypothetical absence of medium losses it should be possible to improve the method of the superposition states in the following way. As the system evolves, the signal cavity photons are lost through the mirror that acts as the single input-output port. We put a detector behind this mirror, and assume we can collect and count all such photons as they escape the cavity. The detection of an even number number of photons will simply imply generation (at least in the large g limit) inside the cavity of $|\varphi_+\rangle$, while detection of an odd number of photons will imply generation (in the large g limit) of $|\varphi_-\rangle$. Thus, if we restrict our attention to the subensemble where an even number of photons have been lost, we expect that an improvement in the fringe pattern should be obtained. We have

not evaluated numerically such a fringe pattern, since in practice it would be difficult to collect all photons lost, given the loss that occurs inside a realistic nonlinear medium. It is conceivable however that some improvement in fringe visibility may be obtained upon collection of some of the photons lost from the system. Such a calculation has yet to be performed, but involves consideration and simulation of the field external to the cavity.

As we have commented previously our calculations have focussed on the intracavity system. It may be possible in principle to measure the intracavity statistics by using a Q-switched cavity to suddenly dump the field. This involves a sudden increase in the signal cavity relaxation rate, at the time at which the superposition state is formed. Because the intracavity moments are directly related to the external fields it may be possible to alternatively infer intracavity moments by measuring the cavity Q. This method would require a finite nonzero signal cavity decay rate. In measuring the external field, one can also use different detection times to gain information about the different spectral components of the quadrature phase amplitudes. We may obtain better fringes at a particular frequency. In later work, we plan to investigate more fully the predictions for the external field moments.

Part II

The Quantum Brownian Motion Master Equation

Chapter 5

Quantum Brownian Motion: The Validity of the Quantum Brownian Motion Master Equation

Abstract

There has been much recent discussion of problems and unphysical results occurring from the study of the quantum Brownian motion (QBM) master equation. These can occur because the QBM master equation is not of the Lindblad form. The aim of this chapter is to gain an understanding of the limitations of the quantum Brownian motion master equation. To this end we examine two simple examples, the damped free particle and the two level atom, where under certain conditions unphysical results occur. More specifically, in the case of the evolution of a free particle, we show that the equation of motion for the Wigner function (which is exactly the same as the Fokker-Planck equation for classical Brownian motion) gives unphysical results provided the initial position distribution is well localised. We then discuss where the quantum Brownian motion master equation breaks down, and the likely assumptions being violated. The two level atom is then shown to display even more dramatic unphysical results. Under suitable conditions it can be shown that various diagonal matrix elements for the two level atom exceed one even in the steady state.

5.1 Introduction

The introduction of the concept of a quantum mechanical master equation during the last thirty years has led to a relatively straightforward and very useful method of treating damped quantum systems [55, 112–115]. The most notable field in which master equations are used is in quantum optics, where the calculations carried out have now been verified experimentally so many times that there can be no doubt about the validity and practicality of the method.

Central to the success of the master equations of quantum optics is the fact that they are of the "Lindblad form" [55–57], that is, there is an equation of motion for the density

operator of the system under study which can be written in the form

$$\frac{d\rho}{dt} = -\frac{i}{\hbar}[H,\rho] + \sum_J \left\{2A_J^\dagger \rho A_J - \rho A_J A_J^\dagger - A_J^\dagger A_J \rho\right\} \tag{5.1}$$

where H is a (Hermitian) Hamiltonian operator and the A_J are certain operators which depend upon the problem under consideration. The form (5.1) was shown by Lindblad [56] to be the only possible form of the first order linear differential equation for ρ which will preserve the positive semidefinite nature of ρ, that is, the property that $\langle\varphi|\rho|\varphi\rangle \geq 0$ for all $|\varphi\rangle$ as ρ evolves in time.

Although the form of (5.1) is thus rendered very attractive, from the point of view of physics it is *not* an exact equation. Its validity for quantum optical situations arises because in such systems we have a description in terms of well defined energy levels, coupled rather weakly to the myriads of modes of the electromagnetic field. The derivations of equations of this form [55, 58, 104, 112–114] make it clear that the equation for ρ is valid only on a coarse grained time scale, which can average over many cycles of the optical electromagnetic field. This is the "rotating wave approximation" in which the damping is very slow compared to the motion at optical frequencies.

In practice the Hamiltonian part of the quantum optical master equation can be written

$$H = H_0 + H_I \tag{5.2}$$

where H_I is a small perturbation to H_0, and where

$$[H_0, A_J] = \hbar\omega_J A_J. \tag{5.3}$$

The requirement means that H_0 is the Hamiltonian which describes the energy levels of the system, and the operator A_J are transition operators, which take the system from one energy level to another.

The quantum optical master equation has been successfully applied to many physical systems, for example the physical processes occurring in parametric oscillation (see for example [98, 99]). Recently Stenholm et al [116] considered a wave packet model for the study of fast phenomena in atoms, molecules, and solids. More specifically they considered a physical setup as depicted in Figure (5.1). In this model the laser couples the ground state 1 to an excited state 2, so that the the energy of the photon brings the two levels into near resonance at the position of the wavepacket. The coupling allows the resting wave packet to transfer partly from level 1 to level 2, and from there the wavepacket begins sliding down the slope and away from its position in the ground state. When the laser pulse is over the transfer ceases. Now such a model would allow the theoretical calculations of fast phenomena in real atomic systems and hence is very important. Master equations techniques here would prove a useful calculational aid. The quantum optical master equation based on the rotating wave approximation may however not be used to describe all the physical processes occurring. Such a master equation distributes the dissipation equally between the position and momentum variables and we know physically that no damping occurs on the position variable. Also though initially in the Stenholm model the levels 1 and 2 are well separated, (this is a requirement for the derivation of the optical master equation), the sliding of the wavepacket down level two can bring it close to level 1 at large separations from the origin. In such a regime we do not necessarily have well defined energy levels and the approximations present in the derivation of the optical master equation may be violated.

In order to extend the success of the master equation approach to more general situations it is possible to consider situations in which H_0 is not overwhelmingly the dominant term in the equation of motion for ρ. In this case the approximations used to derive the

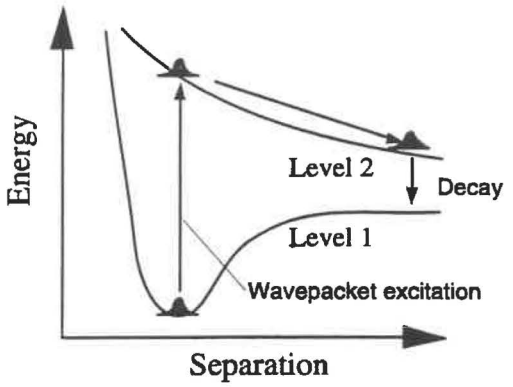

Figure 5.1: Schematic representation of a ultrashort laser pulse exciting a wave packet from the lower level 1 to the upper level 2. The pulse then begin to slide down surface 2 which can bring it close to surface 1.

master equation are of quite a different kind, and we get the so-called "quantum Brownian motion master equation [114, 117–120]", which takes the form

$$\frac{\partial \rho(t)}{\partial t} = -\frac{i}{\hbar}[H_{sys}, \rho(t)] - \frac{i\gamma}{2\hbar}\left[X, \left[\dot{X}, \rho\right]_+\right] - \frac{\gamma kT}{\hbar^2}[X, [X, \rho(t)]] \tag{5.4}$$

in which

$$\dot{X} = \frac{i}{\hbar}[H_{sys}, X], \tag{5.5}$$

and H_{sys} and X are in principle arbitrary. The particular form written in (5.4) assumes coupling to a heat bath of temperature T.

The point of immediate interest is that the quantum Brownian motion master equation (5.4) is not of the Lindblad form [118, 121, 122], and this must inevitably lead to situations in which an unphysical density operator will arise. This is not necessarily a reason to abandon this equation, but it does mean that we must face the fact that in applying the equation, more care must be taken than is necessary when using the quantum optical master equation. In order to put the problem in perspective, one should point out that the basic situation is this: if one uses the quantum optical master equation outside the region of validity of its derivation, one will get incorrect results, but not unphysical results such as negative probabilities; on the other hand using the quantum Brownian motion master equation outside the region of validity of its derivation, the results may be both incorrect and unphysical.

The aim of this chapter is to gain an understanding of the limitations of the quantum Brownian motion master equation. To do this we first review the derivation of the QBM master equation given by Gardiner [58]. We follow this derivation with several specific examples of the kind of unphysical solution which may be obtained, investigating in particular two extreme cases. The first is a particle for which H_{sys} is purely a kinetic term; this gives the true analogue of classical Brownian motion– in fact the equation of motion for the Wigner function is exactly the same as the Fokker-Planck equation for classical Brownian motion. We can show that unphysical results will be obtained for all temperatures provided the initial distribution corresponds to a sufficiently well localised wavefunction. However, at reasonable temperatures this gives rise to a very rapid and rather small transient. The other model is a simple two level system, which perhaps might model a bistable SQUID system [59, 60].

5.2 Derivation and Validity of the Quantum Brownian Motion Master Equation

There have been many approaches used to derive the quantum Brownian motion master equation. The approach we will take in this derivation will be to use the Langevin equation, the particular form used having been presented by Gardiner et al [58, 123, 124, 137]. There are other approaches such as projection operator techniques that can be used to derive the master equation [138]. We choose to use an approach which uses the Langevin equation explicitly with the cumulant expansion [138, 139] as this technique most clearly demonstrates the assumption in the derivation.

5.2.1 The Equations of Motion

Let us consider our heat bath as an ensemble of harmonic oscillators. For a general system where we have a coupling between the system and the heat bath, we may write the Hamiltonian as

$$H = H_{sys}(\mathbf{Z}) + \frac{1}{2}\sum_n \left\{(p_n - \kappa_n X)^2 + \omega_n^2 q_n^2\right\} \tag{5.6}$$

where $H_{sys}(\mathbf{Z})$ represents the system Hamiltonian. At this stage the system Hamiltonian is left arbitrary. We write the system variables as the vector $\mathbf{Z}$. X is one of the particular system operators $\mathbf{Z}$ (As an example, let us consider the two level atom. The possible system operators are σ_x, σ_y, and σ_z). The coupling between the system and bath is achieved by harmonically binding the q_n to the X.

The equation of motion for an arbitrary system operator Y is

$$\dot{Y} = \frac{i}{\hbar}[H_{sys}, Y] + \frac{i}{2\hbar}\sum_n [[Y, \kappa_n X], p_n - k_n X]_+ \tag{5.7}$$

where the + sign at the end of Eqn (5.7) is used to represent an anticommutation relation. (Eqn (5.7) has a direct dependence on the harmonic oscillator's momentum operator p_n, but this can be eliminated, leaving only a dependence on the initial values $p_n(t_0)$ at some initial time t_0 as follows. From Eqn (5.6), equations of motion for the position and momentum operators q_n, p_n are

$$\dot{q}_n = p_n - \kappa_n X \tag{5.8}$$

$$\dot{p}_n = -\omega_n^2 q_n \tag{5.9}$$

These equations are readily solvable and upon substituting their solution into Eqn (5.7), we obtain in the limit $t_0 \to -\infty$ (where we drop the initial transient) the general quantum Langevin equation

$$\begin{aligned}\dot{Y} &= \frac{i}{\hbar}[H_{sys}, Y] - \frac{i}{2\hbar}[[X, Y], \xi(t)]_+ \\ &\quad -\frac{i}{2\hbar}\left[[X, Y], \int_{t_0}^{t} f(t - t')\dot{X}(t')dt'\right]_+\end{aligned} \tag{5.10}$$

where X is the particular system operator harmonically bound to the heat bath, Y is an arbitrary system operator, and H_{sys} is the system Hamiltonian. $\xi(t)$ is an operator function of time given by

$$\xi(t) = \sum_n \kappa_n \sqrt{\frac{\hbar\omega_n}{2}}\left[\frac{p_n(t_0)}{2\hbar\omega_n}\cos[\omega_n(t - t_0)] - \frac{q_n(t_0)}{2\hbar}\sin[\omega_n(t - t_0)]\right] \tag{5.11}$$

We observe that $\xi(t)$ is not however a system operator, but an externally specified operator determined by the initial values of the bath variables. Since $\xi(t)$ is determined directly in terms of heat bath operators at a time t_0, the nature of the bath is significant. For our study of quantum Brownian motion we have assumed that $\xi(t)$ obeys thermal statistics. If the problems under consideration do not have thermal noise characteristics, then this assumption will need to be re-evaluated. For the majority of problems under consideration this approximation is reasonably valid.

To derive the equations so far it has been necessary to assume that the system and bath are initially statistically independent. This allows a factorization of the total density operator ρ into system and bath parts. In some quantum mechanical cases however the system and bath are initially interlinked, and hence there is no natural way of generating a factorised density operator. Assuming a factorised initial density operator in these cases will cause initial transient behaviours.

In Eqn (5.10) $f(t)$ is a memory function (since it makes the equation of motion for a time t dependent on previous values of p_n) defined by

$$f(t) = \sum_n \kappa_n^2 \cos[\omega_n \tau] \tag{5.12}$$

One of the crucial assumptions present in the derivation of the master equation is that we assume that the memory function $f(t)$ has no previous memory, but only remembers the present, (this is commonly called Ohmic dissipation). For this special case we can write

$$f(t) = \delta(t) \tag{5.13}$$

This is a rather dramatic approximation, but has been commonly used in a variety of quantum optical problems. The importance of this result is that our Langevin equation reduces to a simple first order differential equation. All the future time dependence of the operators is determined simply by the present system operators, however the equations of motion for various averages do depend on their values in the past. This is due to the fact that $\xi(t)$ has a nonzero correlation time. In numerical simulations of the quantum Brownian motion adjoint equation, done by Parkins and Gardiner for the two level atom, the above assumptions are present and they give reasonable results when compared with other methods [59, 60].

Although a direct consequence of our choice of memory function, we must also assume that the system has no memory of the infinite past, that is

$$f(t_0) \to 0 \text{ in the limit that } \quad t_0 \to -\infty. \tag{5.14}$$

This assumption is commonly included in the adjoint equation derivation, and for the majority of optical problems is valid.

The operator $\dot{X}$ is given by substituting X for Y in Eqn (5.7), which leads to

$$\dot{X} = \frac{i}{\hbar}[H_{sys}, X] \tag{5.15}$$

so that $\dot{X}$ is simply another system operator. In the derivation process for the quantum Langevin equation so far the only major assumption present is that $f(t) = \delta(t)$. Hence Eqn (5.10) may still be considered as exact, subject to the validity of the Ohmic dissipation assumption. This Ohmic assumption is not necessary when the rotating wave approximation is made in the derivation of the quantum optical master equation. Here only the nature of the couplings within a narrow bandwidth of transition frequencies are involved in the damping constants.

5.2.2 Conversion of the Langevin Equation to a Master Equation

The conversion of the Langevin equation to the master equation has been done previously, and for a complete derivation we refer the reader to [58]. Here we will present a brief outline of the relevant parts of the conversion process. Defining the adjoint operator $\mu(t)$ as

$$\mu(t) = \sum_i \mathrm{Tr}_{sys}\left\{e_i(t)\rho_{sys}\right\} e_i^\dagger \tag{5.16}$$

where e_i represents a complete set of Schrödinger picture system projection operators, and $e_i(t)$ are the corresponding Heisenberg picture system operators. It can be shown that the adjoint equation obtained from Eqn (5.10) is

$$\frac{\partial \mu}{\partial t} = \left[A_0 + \alpha(t)A_1\right]\mu(t) \tag{5.17}$$

where

$$A_0\mu(t) = -\frac{i}{\hbar}\left[H_{sys}, \mu(t)\right] + \frac{i}{2\hbar}\left[\left[\dot{X}, \mu(t)\right]_+, X\right] \tag{5.18}$$

$$A_1\mu(t) = -\frac{i}{\hbar}\left[\mu(t), X\right], \tag{5.19}$$

$\dot{X}$ is given by (5.15) and $\alpha(t)$ is defined by the relation

$$\alpha(t)\mu(t') = (1/2)\left[\xi(t), \mu(t')\right]_+ \tag{5.20}$$

Of interest from Eqn (5.20) is the anticommutator correlation function given by

$$\left\langle\left[\xi(t), \xi(t')\right]_+\right\rangle = \frac{2\gamma\hbar}{\pi}\int_0^\infty d\omega\omega \coth\left(\frac{\hbar\omega}{2KT}\right)\cos\omega(t-t') \tag{5.21}$$

which is strictly divergent. Breaking Eqn (5.21) into non-divergent and divergent parts, the frequency integrals can be performed, where for the divergent part a lower limit time constant λ is introduced. We obtain

$$\begin{aligned}\left\langle\left[\xi(t), \xi(t')\right]_+\right\rangle &= \frac{2\gamma\hbar}{\pi}\left[-\left(\frac{\pi kT}{\hbar}\right)^2 \mathrm{cosech}^2\left(\frac{\pi KT}{\hbar}(t-t')\right) + \frac{1}{(t-t')^2}\right] \\ &\quad + \frac{2\gamma\hbar}{\pi}\frac{\lambda^2 - (t-t')^2}{\left[\lambda^2 + (t-t')^2\right]^2}\end{aligned} \tag{5.22}$$

where the third term in (5.22) is from the divergent part of (5.21). Now integrating (5.22) between zero and infinity, we have in the limit $\lambda \to 0$

$$\int_{-\infty}^{\infty} dt\left\langle\left[\xi(t), \xi(t')\right]_+\right\rangle = 4\gamma kT \tag{5.23}$$

In converting the Langevin equation into an adjoint equation and performing the anti-commutation correlation functions time integrals, no further assumptions have been made. There have been many different methods used to treat equations of the form (5.17), some of these including the eigenfunction method of Ritsch and Zoller [140, 141] and the stochastic simulations of Parkins and Gardiner [137]. A commonly used method is the application of van Kampen's cumulant expansion [138, 139] which yields an equation of motion for

$\rho(t) = \langle \mu(t) \rangle$ in the form of a perturbation expansion in a smallness parameter (this parameter is discussed later in more detail). The equation to second order in this smallness parameter is

$$\frac{\partial \rho(t)}{\partial t} = A_0 \rho(t) + \int_0^t d\tau \langle \alpha(t) A_1 \exp[A_0 \tau] \alpha(t-\tau) A_1 \exp[-A_0 \tau] \rangle \rho(t) \tag{5.24}$$

This equation can be significantly simplified if we assume that the factor $\exp[A_0\tau]$ changes very little in a correlation time τ_c, that is we assume $\exp[A_0\tau] \sim 1$ for $\tau < \tau_c$ (This is a crucial approximation and its validity with these assumptions will be discussed later). Hence equation (5.24) simplifies to

$$\frac{\partial \rho(t)}{\partial t} = -\frac{i}{\hbar}[H_{sys}, \rho(t)] - \frac{i\gamma}{2\hbar}\left[X, \left[\dot{X}, \rho\right]_+\right] - \frac{\gamma kT}{\hbar^2}[X, [X, \rho(t)]] \tag{5.25}$$

where $\int_0^\infty d\tau \langle \alpha(t)\alpha(t-\tau) \rangle$ is obtained from Eqn (5.23). This is the generalised quantum Brownian motion master equation for an arbitrary system with system operators $\mathbf{Z}$ coupled via one particular system operator X to heat bath of harmonic oscillators.

5.2.3 Comments on the Validity of the Quantum Brownian Motion Master Equation

We now make several comments about the quantum Brownian motion master equation and the application of van Kampen's cumulant expansion.

1. Firstly, the cumulant expansion [138, 139] uses a perturbative expansion in the smallness parameter defined by

$$||\alpha||\, ||A_1||\, \tau_c \tag{5.26}$$

which should be much less than one. In equation (5.26) $||\alpha||$ is the root mean square amplitude of $\alpha(t)$, $||A_1||$ is a measure of the magnitude of the operator A_1 and τ_c is the correlation time of α_c. For a Brownian particle (which may be in a potential well) the thermal correlation time is given by $\tau_c = \hbar/2\pi kT$, while the root mean square amplitude of α is given by the square root of the coefficient of the exponential in the asymptotic form for the correlation function, that is $||\alpha|| = 2kT\sqrt{\gamma\pi/\hbar}$ [58]. The exact estimates used for $||A_1||$ are very problem specific because in many cases the operator A_1 may be unbounded. However if we consider the Brownian particle to be near thermal equilibrium, then we can estimate the magnitude of A_1 as [58]

$$||A_1|| = \frac{1}{2\sqrt{mkT}} \tag{5.27}$$

With these estimates we find

$$||\alpha||^2\, ||A_1||^2 \tau_c = \frac{\gamma}{2m} \qquad \text{a constant, independent of temperature} \tag{5.28}$$

Basically Eqn (5.28) can be interpreted as saying that the damping can be arbitrarily large but the temperature T must also be large. Now in the quantum Brownian motion limit we assume that the correlation time of the noise is much shorter than the typical time scales associated with damping and systematic motion, that is, the QBM limit is

$$\tau_c \to 0 \tag{5.29}$$

With the requirement on the system that the smallness parameter $||A_1||||\alpha||\tau_c \ll 1$ we have using the previous estimates that

$$\frac{\hbar\gamma}{m} \ll kT \tag{5.30}$$

or in the general notational usage

$$\tau_c \ll \tau_D \equiv \gamma/m \tag{5.31}$$

where τ_D is the damping constant of the system. Re-examining Eqn (5.30), we could interpret γ/m as an imaginary "frequency", and hence Eqn (5.30) means that the thermal energy given by kT must be much greater than the quantum of energy associated with the imaginary frequency.

In our general derivation process of a master equation from a Langevin equation, only second order terms in the cumulant expansion are retained. If this quantity $A_1\alpha\tau$ becomes large (this can occur as $T \to 0$), then the perturbative approach can break down, and hence higher order terms in the perturbation need to be included (Fourth order terms have been included in an analysis done by Collett [118]).

2. One of the most critical assumptions present in the derivation of the quantum Brownian motion master equation, is approximating

$$\exp[A_0\tau] \sim 1 \tag{5.32}$$

for some time $\tau < \tau_c$. In this case Eqn (5.24) reduces to

$$\frac{\partial\rho(t)}{\partial t} = A_0\rho(t) + \int_0^t d\tau\langle\alpha(t)A_1\alpha(t-\tau)A_1\rangle\rho(t) \tag{5.33}$$

from which the usual quantum Brownian motion master equation can be obtained. As long as the correlation time τ_c is short this is quite a reasonable assumption. However as we have previously discussed, the thermal correlation time is given by $\tau_c = \hbar/(2\pi kT)$, and as the temperature approaches zero, this thermal correlation time becomes large, violating the assumption given in Eqn (5.32). This breakdown will be investigated in the next two sections.

In several derivations of a modified quantum Brownian motion master equation [118] an auxiliary assumption is imposed, that is the damping is weak compared to the systematic motion. Hence in the derivation process the approximation given by (5.32) is modified to

$$\exp[A_0\tau] \to \exp[A_{sys}\tau] \tag{5.34}$$

This allows the derivation of a modified quantum Brownian motion master equation which has been discussed by Collett [118]. However with the addition of an auxiliary assumption the region of validity of any master equations derived would be different from the original master equation. The type of assumption given by (5.34) is commonly used in the derivation of the quantum optical master equation.

3. It is also possible to obtain the quantum optical master master equation from the Langevin approach. In this case we resolve the operator X in eigen-operators of H_{sys}, that is

$$X = \sum_i \left(X_i^+ + X_i^-\right) \tag{5.35}$$

where

$$\left[H_{sys}, X_i^{\pm}\right] = \pm\hbar\omega_i X_i^{\pm} \tag{5.36}$$

Now in the quantum optical master equation we then assume $\omega_i \gg \gamma$. Hence

$$\exp\left[\pm A_0\tau\right] X_i^{\pm} \rightarrow \exp\left[\pm\omega_i\tau\right] X_i^{\pm} \exp\left[\pm A_0\tau\right] \tag{5.37}$$

Using Eqn (5.37), the usual quantum optical master equation can be derived. In the optical case we assume the damping is very weak compared to the systematic motion. In this case we do not assume that $\exp\left[A_0\tau\right] \sim 1$, rather we examine the limit in which $\exp\left[A_0\tau\right]$ is a rapid oscillation.

4. Lastly we need to re-emphasise the point that Eqn (5.25) is not of the Lindblad form. It is clearly evident that the third expression in Eqn (5.25) (namely, $[X,[X,\rho(t)]]$) is of the appropriate form, however the second term is not (only in the special case where $\dot{X} = 0$ is the Lindblad form obtained).

5.3 A Damped Free Particle

Probably the simplest example that could be considered is the motion of a free damped particle [142]. The system Hamiltonian is given by

$$H_{sys} \rightarrow \frac{p^2}{2m} \tag{5.38}$$

We have a choice of two operators that can be used to couple the system to the environment, namely the position and momentum operators. The natural choice, which corresponds to the classical case, is the position operator, that is we set $X = x$. In this case our Brownian motion master equation is

$$\frac{d\rho}{dt} = -\frac{i}{\hbar}\left[H_{sys},\rho\right] - \frac{i\gamma}{2\hbar m}\left[x,[p,\rho]_+\right] - \frac{\gamma kT}{\hbar^2}\left[x,[x,\rho]\right] \tag{5.39}$$

If we consider our system to be initially in a pure state $|\varphi\rangle$, then initially the expectation value

$$\langle\varphi|\rho(0)|\varphi\rangle = 1. \tag{5.40}$$

Now we can derive from our master equation

$$\langle\varphi|\frac{d\rho}{dt}|\varphi\rangle\Big|_{t=0} = \frac{\gamma}{2m}\langle\varphi|\rho|\varphi\rangle\Big|_{t=0} - \frac{\gamma kT}{\hbar^2}\left[\langle\varphi|x^2|\varphi\rangle - \langle\varphi|x|\varphi\rangle^2\right]\Big|_{t=0} \tag{5.41}$$

where the second part, proportional to $[\langle\varphi|x^2|\varphi\rangle - \langle\varphi|x|\varphi\rangle^2]$, must always be negative. If we consider our system to be in a near eigenstate of position, that is $[\langle\varphi|x^2|\varphi\rangle - \langle\varphi|x|\varphi\rangle^2]$ is very small, then the first term in Eqn (5.41) dominates (We do not consider the system to be in a perfect eigenstate because the position wavefunction is not normalisable). It is always possible to choose $|\varphi\rangle$ so that the second term is less than the first, and under these circumstances, $\langle\varphi|\rho(t)|\varphi\rangle$ will initially increase. Since $\langle\varphi|\rho(t)|\varphi\rangle$ is initially 1, this must yield the unphysical result $\langle\varphi|\rho(t)|\varphi\rangle > 1$ for some time t near 0.

However this is only a transient behaviour as can be seen from the following argument. When the system is in a near position eigenstate, because the uncertainty principle requires

$\Delta x \Delta p = i\hbar$, and because initially we have little or no uncertainty in x, we have a very large uncertainty in the momentum. Now the position operator x evolves as

$$x \rightarrow x + p/m\, dt \tag{5.42}$$

which, because of the large uncertainty in p, will drive the system from its near position eigenstate, and hence the second term in Eqn (5.41) proportional to γkT will make a larger contribution. This will force the density matrix elements $\langle \rho(t) \rangle$ back below one.

We notice that the analysis given above is only valid near $t = 0$. There is an alternative approach by which the free particle problem can be considered. Defining the Wigner function by [58]

$$W(x,p) = \frac{1}{\hbar\pi} \int dy \langle x + y|\rho|x - y\rangle \exp\left[-2iyp/\hbar\right], \tag{5.43}$$

our quantum Brownian motion master equation for the free particle can be converted to the following Wigner function equation

$$\frac{\partial W}{\partial t} = \left\{ -\frac{\partial}{\partial x}\frac{p}{m} + \frac{\partial}{\partial p}\gamma\frac{p}{m} + \gamma kT\frac{\partial^2}{\partial p^2} \right\} W. \tag{5.44}$$

This equation for the Wigner function is identical with the corresponding classical Fokker Planck equation [58]. The probability of the system being in the state $|\varphi\rangle$ is

$$P = \langle \varphi|\rho(t)|\varphi\rangle = \int \phi(x)\phi^*(y)\langle x|\rho|y\rangle dx dy \leq 1 \tag{5.45}$$

where $\phi(x)$ is the initial position wavefunction, and $\langle x|\rho|y\rangle$ is determined from the Fourier transform of the Wigner function given by (5.43). There are exact Gaussian solutions to equation (5.44), which can be used to give exact solutions of the master equation. The time evolution of the Wigner function can be specified by the covariance matrix, formed by the solution of the equations of motion of the second order moments (for example the position and momentum variances). Initially setting the position wavefunctions to be a Gaussian with a known variance, the momentum wavefunction was chosen so as to give a minimum uncertainty state. Thus the probability could be determined and must be less than one for all times. However when the initial Gaussian wavefunctions are chosen such that the variance in the position is very small, the probability P may exceed one for very short times.

In Figure (5.2) we observe the probability exceeding one. Figure (5.2.a) plots the probability P versus time (for various parameters that may be experimentally realised, $T \sim 1\text{K}$, $m \sim 10^{-26}\text{kg}$). We have set the initial variance in the position to be $\langle \Delta x^2 \rangle = \sigma^2$, while the initial variance in the momentum is chosen to give a minimum uncertainty state, that is, $\langle \Delta p^2 \rangle = \hbar^2/(4\sigma^2)$. There is no initial correlation chosen between position and momentum, so $\langle \Delta x \Delta p \rangle = 0$.

In Figure (5.2), with σ varied between $10^{-12} - 10^{-9}\text{m}$, we observe on the time scale of nanoseconds that the probability P exceeds one for the cases (ii-iv) but not for case (i) ($\sigma = 10^{-12}\text{m}$) and case (v) ($\sigma = 10^{-9}\text{m}$). For the cases (ii-iv) we observe that the probability peaks at a value greater than one (for $\sigma \sim 5 \times 10^{-11}\text{m}$ (case iii) the probability reaches a maximum value of approximately 1.4) and then decreases such that in the long time regime it is below one. In Figure (5.2b) we re-plot the various cases considered in Figure (5.2a) but on a time scale of picoseconds. Case (i) according to Eqn (5.41) has an initial positive gradient and hence, with the initial condition $\langle \varphi|\rho(0)|\varphi\rangle = 1$, the probability must exceed one. In Figure (5.2 a and b) this behaviour has not been observed. It is not however an anomalous behaviour, but a question of the time scales on which the Figures

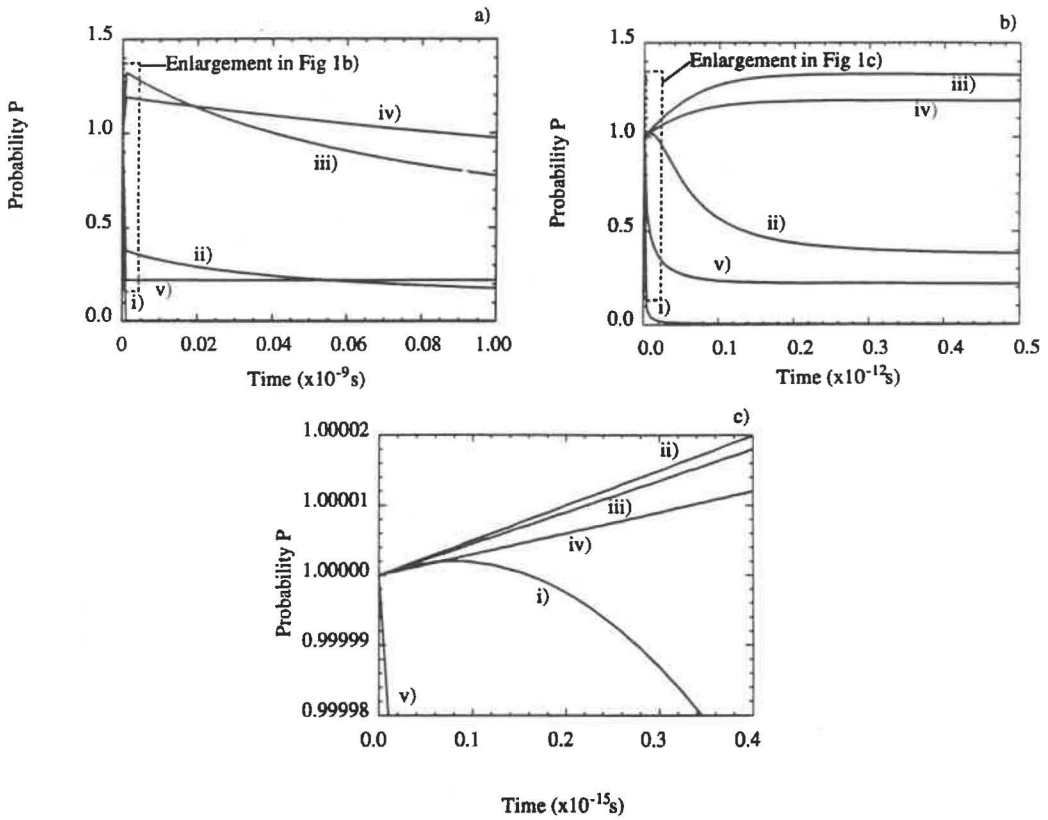

Figure 5.2: Plot of the Probability P versus time t for the damped free particle with $T = 1\text{K}$, $\gamma \sim 10^{-13}\text{kgs}$, and $m \sim 10^{-26}\text{kg}$. For the parameters chosen above the magnitude of the smallness parameter is $||A_0||||\alpha||\tau_c \sim 1$. The time scales for the plots are
a) nanoseconds, i) $\sigma = 10^{-12}\text{m}$, ii) $\sigma = 10^{-11}\text{m}$, iii) $\sigma = 5 \times 10^{-11}\text{m}$, iv) $\sigma = 10^{-10}\text{m}$, v) $\sigma = 10^{-9}\text{m}$.
b) picoseconds, i) $\sigma = 10^{-12}\text{m}$, ii) $\sigma = 10^{-11}\text{m}$, iii) $\sigma = 5 \times 10^{-11}\text{m}$, iv) $\sigma = 10^{-10}\text{m}$, v) $\sigma = 10^{-9}\text{m}$.
c) femtoseconds, i) $\sigma = 10^{-12}\text{m}$, ii) $\sigma = 10^{-11}\text{m}$, iii) $\sigma = 5 \times 10^{-11}\text{m}$, iv) $\sigma = 10^{-10}\text{m}$, v) $\sigma = 10^{-9}\text{m}$.

are plotted. In Figure (5.2c) we again re-plot the parameter set used in Figures (5.2a and b) but on a much shorter time scale. In case (i) ($\sigma = 10^{-12}$) the probability does exceed one on this short time scale but then rapidly decreases below one. For $\sigma >\sim 10^{-10}$ (case (v) in Figure (5.2)), the probability never exceeds one.

In the cumulant expansion [138, 139] used to convert the Langevin equation to the master equation, there is a requirement in the perturbation theory that the quantity $A\alpha\tau$ is small. Thus for the free particle case this leads to the condition

$$\tau_c \ll \tau_{\text{damping}} \tag{5.46}$$

where $\tau_{\text{damping}} = m/\gamma$. Eqn (5.46) specifies that all the time scales associated with damping, etc. must be very much slower than the thermal correlation time τ_c. For the parameters considered above, the thermal correlation is of the order of magnitude $\tau_c = 10^{-12}\text{s}$, that is of the picosecond time scale. The time scale associated with damping is given by $\tau_{\text{damping}} \approx 10^{-13}\text{s}$, that is about 0.1ps. Hence in this regime where we observed the master equation breaking down, we have $\tau_{\text{damping}} < \tau_c$, and thus the cumulant expansion's validity must be questioned. The analysis used to give the constraints in Eqn (5.46) is only valid for the free particle case or where the particle is bound in a potential well.

Let us consider another set of parameters ($\gamma/m = 10^{11}\text{s}^{-1}$ (with $m \sim 10^{-26}\text{kg}$) and $T \sim 1\text{K}$). With this parameter set we find that the smallness parameter is of the size $|A_1\alpha\tau| \sim 0.2$. This would seem to indicate that the cumulant expansion is valid based on the estimates for $||A_1||$ given in section (5.2). In Figures (5.3 a-c), we plot the probability on three different time scales. The first is on the time scale associated with the damping time, while the second is on a time scale associated with the thermal correlation time, and the third is on a time much less than τ_c. We observe in Figure (5.3b-c) that the probability can exceed one for certain σ values. This violation of probability however is very small (for this parameter set, less than one part in a millon), and occurs on time scales less than the thermal correlation time.

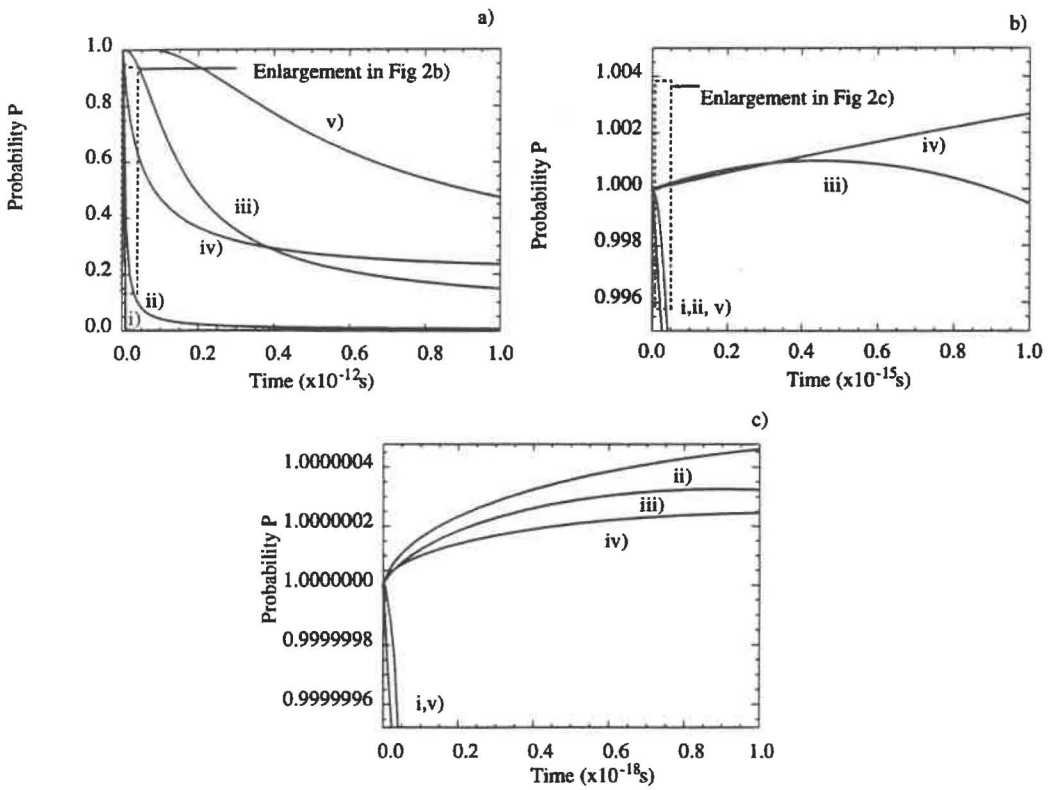

Figure 5.3: Plot of the Probability P versus time t for the damped free particle with $T = 1\text{K}$, $\gamma \sim 10^{-15}\text{kgs}$, and $m \sim 10^{-26}\text{kg}$. For the parameters chosen above the magnitude of the smallness parameter is $||A_0||||\alpha||\tau_c \sim 0.2$. The time scales for the plots are
a) picoseconds, i) $\sigma = 10^{-12}\text{m}$, ii) $\sigma = 10^{-11}\text{m}$, iii) $\sigma = 5 \times 10^{-11}\text{m}$, iv) $\sigma = 10^{-10}\text{m}$, v) $\sigma = 10^{-9}\text{m}$.
b) femtoseconds, i) $\sigma = 10^{-12}\text{m}$, ii) $\sigma = 10^{-11}\text{m}$, iii) $\sigma = 5 \times 10^{-11}\text{m}$, iv) $\sigma = 10^{-10}\text{m}$, v) $\sigma = 10^{-9}\text{m}$.
c) attoseconds, i) $\sigma = 10^{-12}\text{m}$, ii) $\sigma = 10^{-11}\text{m}$, iii) $\sigma = 5 \times 10^{-11}\text{m}$, iv) $\sigma = 10^{-10}\text{m}$, v) $\sigma = 10^{-9}\text{m}$.

Let us consider a third example with $||A_1||||\alpha||||\tau_c|| = 0.001$. For this case a violation is not even seen on time scales of the order of the thermal correlation time (Figure 5.4a), however violations are observed (Figure 5.4b) for very short times ($t \ll \tau_c$) and the magnitude of the violation is even smaller than one part per million. The equation is however clearly not valid on such a time scale, and nor is the unphysical probability anything to worry about. The QBM master equation gives a good representation of the physics, but an approximate representation only, which is not guaranteed to satisfy physical requirements exactly.

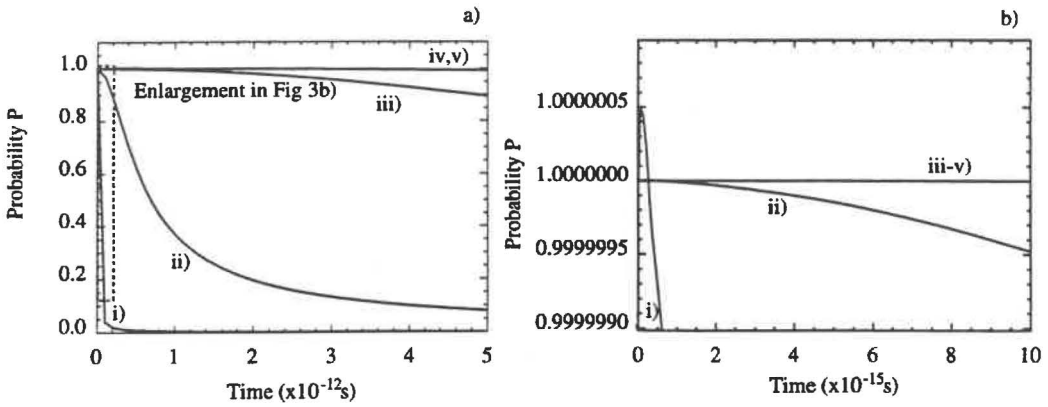

Figure 5.4: Plot of the Probability P versus time t for the damped free particle with $T = 1\text{K}$, $\gamma \sim 10^{-20}$kg s, and $m \sim 10^{-26}$kg. For the parameters chosen above the magnitude of the smallness parameter is $||A_0||||\alpha||\tau_c \sim 0.001$. The time scales for the plots are
a) picoseconds, i) $\sigma = 10^{-12}$m, ii) $\sigma = 10^{-11}$m, iii) $\sigma = 5 \times 10^{-11}$m, iv) $\sigma = 10^{-10}$m, v) $\sigma = 10^{-9}$m.
b) femtoseconds, i) $\sigma = 10^{-12}$m, ii) $\sigma = 10^{-11}$m, iii) $\sigma = 5 \times 10^{-11}$m, iv) $\sigma = 10^{-10}$m, v) $\sigma = 10^{-9}$m.

5.3.1 A Minimum Uncertainty Thermal Distribution

So far we have considered our system to be in a well localised position state. Let us now consider the case, where instead of considering the system to be in a near position state with variance σ, the variance in the momentum is determined by the standard Boltzmann distribution $\exp\left[-p^2/2mkT\right]$. Here $\langle \Delta p^2 \rangle = mkT$. If our system is in a minimum uncertainty state, chosen so that the position variance is smallest, then $\langle \Delta x^2 \rangle = \hbar^2/2mkT$ (we have also set $\langle \Delta x \Delta p \rangle = 0$). Now according to the master equation given in Eqn (5.41) we have

$$\langle \varphi | \frac{d\rho}{dt} | \varphi \rangle \Big|_{t=0} = \frac{\gamma}{4m} \tag{5.47}$$

Given $\langle \varphi | \rho(0) | \varphi \rangle = 1$ at $t = 0$, $\langle \varphi | \rho(t) | \varphi \rangle$ must exceed one for very short times, thus yielding an unphysical result. We note that this violation must occur for all temperatures (not just low temperatures as previously indicated) since Eqn (5.47) is not temperature dependent. Using the expression for the probability generated by the Wigner function it was observed that a violation (the probability being greater than one) always occurs. However this violation is observed only for very short times, again $t \ll \tau_c$, and the magnitude of the violation is very small for reasonable temperatures. We do need however to reconsider the smallness parameter used in the cumulant expansion. For this case the smallness parameter is of the form

$$||A_1||\,||\alpha||\,\tau_c = \sqrt{\left(\frac{\gamma}{2m}\right)\left(\frac{\hbar}{2\pi kT}\right)}. \tag{5.48}$$

Hence in the above consideration we can always choose for a fixed temperature T, the γ/m ratio such that Eqn (5.48) is always much less than one. In this case the cumulant expansion will be valid, however the result given in Eqn (5.47) remains true. The quantum Brownian motion limit is $\tau_c \to 0$. In the example considered above our thermal correlation time is some finite but nonzero number. There is no physical validity in considering time scales shorter than the thermal correlation time because of the coarse grain time scale approach used to derive the master equation.

5.3.2 A Re-Examination of the Quantum Brownian Motion Master Equation

Let us now re-examine our quantum Brownian motion master equation for the free particle. In the previous section we wrote the master equation explicitly as

$$\frac{\partial \rho(t)}{\partial t} = A_0\rho(t) + \int_0^t d\tau \langle \alpha(t) A_1 \exp[A_0\tau]\, \alpha(t-\tau) A_1 \exp[-A_0\tau]\rangle \rho(t) \tag{5.49}$$

For this reconsideration we will consider a weak damping limit, thus approximating A_0 by $A_0 = -\frac{i}{\hbar}[H_{sys}, \ ]$. We will not assume $\exp[A_0\tau] \sim 1$ but carry this explicit dependent through the calculation in the weak damping limit. It can be shown that (5.48) reduces in this limit to

$$\frac{d\rho}{dt} = -\frac{i}{\hbar}[H_{sys}, \rho] - \frac{i\gamma}{2\hbar m}\left[x, [p,\rho]_+\right] - \langle \frac{\int_0^\infty d\tau \alpha(t)\alpha(t-\tau)}{2\hbar^2}[x,[x(\tau),\rho]]\rangle \tag{5.50}$$

We need to examine the effect of the evolution of the position variable $x(\tau)$ on the third term in Eqn (5.50). Now we know that the operator $x(\tau)$ evolves according to Eqn (5.42) and hence putting this momentum dependence directly into Eqn (5.50) we have

$$\frac{d\rho}{dt} = -\frac{i}{\hbar}[H_{sys}, \rho] - \frac{i\gamma}{2\hbar m}\left[x, [p,\rho]_+\right] - \langle \frac{\int_0^\infty d\tau \alpha(t)\alpha(t-\tau)}{2\hbar^2}[x,[x+p/m\,\tau,\rho]]\rangle \tag{5.51}$$

We notice that the last term in Eqn (5.51) involves a double commutator in both x and p, while the second term in (5.51) involves a commutator in x and an anticommutator in p. In evaluating the integrals of (5.51) we obtain

$$\int_\lambda^\infty d\tau \langle \tau \alpha(t)\alpha(t-\tau)\rangle = \frac{2\gamma\hbar}{\pi}\log_e[4\lambda/\tau_c] \tag{5.52}$$

where λ_1 is a cutoff dependence small time constant . Hence our master equation given by Eqn (5.51) can be rewritten as

$$\begin{aligned}\frac{d\rho}{dt} &= -\frac{i}{\hbar}[H_{sys},\rho] - \left(\frac{i\gamma}{2\hbar m} + \frac{\gamma}{\pi\hbar m}\log_e[4\lambda/\tau_c]\right)[xp\rho - p\rho x] \\ &\quad - \left(\frac{i\gamma}{2\hbar m} - \frac{\gamma}{\pi\hbar m}\log_e[4\lambda_1/\tau_c]\right)[x\rho p - \rho p x] \\ &\quad - \frac{\gamma kT}{\hbar^2}[x,[x,\rho]]\end{aligned} \tag{5.53}$$

Several comments need to be made about Eqn (5.53)

1. Firstly we must note that our master equation now contains logarithmic terms of the form $\log_e[4\lambda/\tau_c]$. This term is dependent on the lower cutoff limit λ_1 which must always be less than the thermal correlation time. Hence this logarithmic term is always negative. A careful examination of the first and second order momentum indicates that the contribution from the double commutator in x and p (the logarithmic term) is only present in the equation of motion for the cross momentum, position variance. The logarithmic term is not present in any of the other moments. Hence it does not effect the equations of motion of the position and momentum.

   We must re-emphasise the point that the preceding analysis is only valid in the weak damping limit.

2. If we examine the Wigner function corresponding to Eqn (5.53) we observe that the noise correlation matrix is not positive semidefinite. Hence the system must evolve into regions physically unacceptable according to classical mechanics.

3. Note that (5.53) is still not of the Lindblad form.

5.3.3 Discussion

To conclude this section we have observed that the classical Langevin equations with a quantum initial condition give rise to probabilities greater than one. Thus though the equations of motion for the Wigner function give Langevin equations which look exactly like the classical Brownian motion set, they are not exactly equivalent. The inclusion of a quantum initial condition dramatically alters the properties of the system. We showed that if the Brownian particle is initially well localised, then unphysical results can occur when the quantum Brownian motion master equation is examined. However for reasonable temperatures, this behaviour gives rise to a rather rapid and small transient. Even at high temperatures this behaviour persists.

5.4 A Second Example: The Two Level System

A second simple example that may be considered is the two level system. This may be a purely formal consideration discussed here, but applications of the quantum Brownian motion master equation have been applied to the study of twin well potentials [59, 60]. We consider a two level atom because this has a limited number of basis states available to it and hence explicit solutions for the equations of motion are possible.

For a two level atom only two basis states exist, $|1/2\rangle$ and $|-1/2\rangle$, and the possible states in the density matrix are

$$\rho_{n,m} = \langle n|\rho|m\rangle \tag{5.54}$$

with $n, m = \pm\frac{1}{2}$. The Pauli spin matrices are related to these density matrix elements by the standard relations.

There are a number of possible choices for our operator X that we use to couple to the harmonic oscillator heat baths. There are two principal choices σ_z or σ_x. Here σ_x is chosen for this coupling.

5.4.1 Coupling to σ_x

We have chosen our coupling operator to be $X = \sqrt{\frac{\hbar}{\Omega}}\sigma_x$, which with a system Hamiltonian of the form

$$H_{sys} = \frac{1}{2}\hbar\Omega\sigma_z \tag{5.55}$$

gives the operator $\dot{X}$ as

$$\dot{X} = \frac{i}{\hbar}\left[H_{sys}, X\right] = -\sqrt{\hbar\Omega}\sigma_y \tag{5.56}$$

Thus we have the two level atom quantum Brownian motion Master equation

$$\frac{d\rho}{dt} = -\frac{i}{2}\Omega\left[\sigma_z, \rho\right] - \frac{i\gamma}{2}\left[\sigma_x, \left[\sigma_y, \rho\right]_+\right] - \frac{\gamma kT}{\hbar\Omega}\left[\sigma_x, \left[\sigma_x, \rho\right]\right] \tag{5.57}$$

where we notice that our anticommutation term is still present. Evaluating this expression gives the following two decoupled sets of differential equations

$$\frac{d}{dt}\begin{bmatrix} \rho_{-\frac{1}{2},-\frac{1}{2}}(t) \\ \rho_{\frac{1}{2},\frac{1}{2}}(t) \end{bmatrix} = \begin{bmatrix} \gamma - \frac{2\gamma kT}{\hbar\Omega} & \gamma + \frac{2\gamma kT}{\hbar\Omega} \\ -\gamma + \frac{2\gamma kT}{\hbar\Omega} & -\gamma - \frac{2\gamma kT}{\hbar\Omega} \end{bmatrix}\begin{bmatrix} \rho_{-\frac{1}{2},-\frac{1}{2}}(t) \\ \rho_{\frac{1}{2},\frac{1}{2}}(t) \end{bmatrix} \tag{5.58}$$

and

$$\frac{d}{dt}\begin{bmatrix} \rho_{-\frac{1}{2},\frac{1}{2}}(t) \\ \rho_{\frac{1}{2},-\frac{1}{2}}(t) \end{bmatrix} = \begin{bmatrix} i\Omega - \frac{2\gamma kT}{\hbar\Omega} & \frac{2\gamma kT}{\hbar\Omega} \\ \frac{2\gamma kT}{\hbar\Omega} & -i\Omega - \frac{2\gamma kT}{\hbar\Omega} \end{bmatrix} \begin{bmatrix} \rho_{-\frac{1}{2},\frac{1}{2}}(t) \\ \rho_{\frac{1}{2},-\frac{1}{2}}(t) \end{bmatrix} \tag{5.59}$$

Solving these equations explicitly, we have the following solutions for the diagonal elements

$$\rho_{-\frac{1}{2},-\frac{1}{2}}(t) = \left\{\frac{1}{2}\left(b^{-1}+1\right)\left[1-\exp\left(-2\gamma bt\right)\right] + \rho_{-\frac{1}{2},-\frac{1}{2}}\exp\left(-2\gamma bt\right)\right\} \tag{5.60}$$

$$\rho_{\frac{1}{2},\frac{1}{2}}(t) = 1 - \rho_{-\frac{1}{2},-\frac{1}{2}}(t) \tag{5.61}$$

where

$$b = \frac{2kT}{\hbar\Omega}, \tag{5.62}$$

while the off-diagonal elements have the solution

$$\begin{aligned} \rho_{-\frac{1}{2},\frac{1}{2}}(t) &= \exp\left[-\gamma bt\right]\left[\frac{I\Omega}{\Theta}\sinh\left(\Theta t\right) + \cosh\left(\Theta t\right)\right]\rho_{-\frac{1}{2},\frac{1}{2}} \\ &\quad + \exp\left[-\gamma bt\right]\frac{\gamma b}{\Theta}\sinh\left(\Theta t\right)\rho_{\frac{1}{2},-\frac{1}{2}} \end{aligned} \tag{5.63}$$

$$\rho_{\frac{1}{2},-\frac{1}{2}}(t) = \rho_{-\frac{1}{2},\frac{1}{2}}(t)^* \tag{5.64}$$

where

$$\Theta = \sqrt{\gamma^2 b^2 - \Omega^2} \tag{5.65}$$

Now, with explicit solutions for the various density matrix elements in the two level atom, can we determine if these elements violate the properties of the density operator? For the density matrix elements there are two crucial conditions which must be satisfied, namely we require $\mathrm{Tr}(\rho) = 1$ and that ρ is positive semidefinite. The condition for positive semidefiniteness is

$$\mathrm{Tr}\{\rho(t)\} > 0 \tag{5.66}$$

$$\det\rho(t) > 0 \tag{5.67}$$

is automatically guaranteed by the master equation. The second condition that $\det\rho(t) > 0$ needs to be investigated. A detailed examination of the determinant is considered in Appendix (C) for various parameter regimes. Here we consider only the long time behaviour with the initial conditions chosen such that the off-diagonal elements are not present in the determinant expression. In the long time regime ($\gamma bt \gg 1$) it can be shown that the determinant is given by

$$\det\rho = \frac{1}{4}\left[1 - \left(\frac{\hbar\Omega}{2kT}\right)^2\right] \tag{5.68}$$

which is clearly negative when the thermal energy kT is less than the *zero point* energy $\hbar\Omega/2$. Hence in this long time regime we have an absolute criterion of when the determinant will be less than zero. This conclusion must be questioned. In the derivation process of the master equation we have assumed that the shortest time scale present in the system should be the thermal correlation time (this is necessary so that the $\exp\left[A_0\tau\right] \sim 1$ approximation can be made). There is however a time scale associated with the transition frequency Ω, and in the case of $kT < \hbar\Omega/2$ the time scale associated with Ω is smaller than τ_c. Hence it is no longer valid to assume $\exp\left[A_0\tau\right] \sim 1$, instead we must

write $\exp[A_0\tau] \sim \exp[A_{sys}\tau]$. This leads to the modified master equations considered by Collett [118]. In this case the resulting master equation is still not of the Lindblad form and hence anomalous results can be obtained [118, 125].

In the first example considered, we observed that the master equation broke down in a regime where the cumulant expansion was not valid. For the two level atom, we now need to determine the validity of the cumulant expansion in the regimes we have considered. Using Eqn (5.26) with an estimate for the magnitude of $||A_1||$ as

$$||A_1|| \sim \frac{1}{\sqrt{\hbar\Omega}} \tag{5.69}$$

we have the criteria for the validity of the expansion as

$$\frac{\gamma}{\Omega} \ll 1, \tag{5.70}$$

that is we are required to work in the weak damping limit. In Appendix (C) we test this validity condition, and find as expected that problems occurs in the limit $\gamma \gg \Omega$, the opposite limit in which our equations are valid.

5.5 A Modified Quantum Brownian Motion Master Equation

Previously we have observed that because the quantum Brownian motion master equation is not of the Lindblad form anomalous results occurred. There have been two approaches to modify the master equation, such that the anomalous or unphysical results may be eliminated.

- The first is an *ad-hoc* method by which the necessary terms are added to make the master equation of the Lindblad form [126]. Though these modified master equations then preserve the Lindblad form, it is hard to explain the physical significance of these additional terms.
- The second method is based on altering the physical model. We modify the physical picture to make it look more like the quantum optical master equation. One approach by Collett [118] replaces $\exp[A_0\tau]$ by $\exp[A_{sys}\tau]$. However the physical model has been altered, the resulting modified quantum Brownian motion master [117, 118] is still not of the Lindblad form.

In both approaches discussed above we move away from the physical system originally considered.

5.6 Discussion and Conclusion

It has been noted several times that the quantum Brownian motion master equation is not of the Lindblad form, and hence it may not preserve positivity. This may lead to situations in which unphysical results occur. In the derivation process of a master equation for an open quantum system, the process involves a perturbative approach (an approximation method), and there is nothing in this approximation method to guarantee that the master equation is of the appropriate Lindblad form. Currently both the single photon and the two photon damping master equations used in quantum optical situations are of the Lindblad form, however as discussed previously the quantum Brownian motion master equation is not.

Recent work by Carmichael [127–131] have seen the development of wavefunction simulations. To use this procedure the master equation is required to be of the Lindblad form. However because the quantum Brownian motion master equation is not of this form, an event can occur with negative probability (or probability greater than one), and hence stochastic wavefunction simulations are impossible. Thus an entire calculational method is barred from use in this physical problem.

In this chapter we have discussed the limitations of the quantum Brownian motion master equation. We considered several specific examples of the kind of unphysical solution which can occur, investigating in particular two extreme cases. The first was a particle in which H_{sys} is purely a kinetic term. This gave the true analogue of classical Brownian motion and in fact the equation of motion for the Wigner function is exactly the same as the Fokker-Planck equation for classical Brownian motion. We showed that unphysical results were obtained for all temperatures provided the initial distribution corresponds to a sufficiently well localised wavefunction. However, for situations where the cumulant expansion is valid this gives rise to very rapid, and rather small transients. The second model considered was a simple two level system, which showed anomalous behaviour even in the steady state. However in a more realistic physical model [118] the anomalous results only occurs in the short to medium time regimes.

The quantum Brownian motion master equation is not valid for time scales shorter than the thermal correlation time, because of the coarse grain time scale approach used in its derivation. Hence in these transient time regimes anomalous regimes may occur and has been discussed previously by Ambegaokar [132] and Diosi [133] as well as many other authors [58, 134, 135]. Recent work by Gardiner [58] and Collett [136] however suggest that this transient behaviour may be due to the unrealistic factorization of the system and bath's density operator.

Finally, we point out that the quantum Brownian motion master equation has been used to study many physical problems. However being not of the Lindblad form, anomalous results can occur. A careful application of the cumulant expansion used in the master equations derivation limits these anomalous results to rather rapid transients, which occur on a time scale more rapid than the thermal correlation time.

Chapter 6

The Rate of Decoherence in a Semiconductor Medium

Abstract

Recent years have seen the rise in importance of quantum principles in semiconductor devices. In order to determine whether a semiclassical theory is adequate to model such a system or whether a fully quantum mechanical theory is necessary, we investigate the rate of decay of the off-diagonal elements in a quantum mechanical master equation. These off-diagonal elements contain quantum information such as quantum interference. We choose to use the quantum Brownian motion master equation to describe this semiconductor material as this particular master equation is based on a model close to the physical processes occurring. Choosing the electron probability density as the observable we couple to the phonon heat bath, we initially consider a single electron system. For such a system no electron-electron scattering is possible. Extending the calculations to a two electron system we show, that with electron-electron scattering neglected, the two electron solution is simply the product of the one electron solution. More importantly we show that the many electron solution with electron-electron scattering neglected is again simply a product of the one electron solutions. The effect of electron-electron scattering is an important physical effect and hence in the last part of this chapter we provide a brief discussion of how this effect can be modelled.

6.1 Introduction

Recent miniaturization of semiconductor and solid state devices has meant that quantum mechanical principles are playing an increasingly more important role in the understanding of the transport properties of such devices. There are important considerations to be made where devices reach below the sub-micron limit. In particular when devices reach such a level, the validity of the semiclassical theory used to describe them must be questioned, and a fully quantum theory developed.

A general solid can be modelled as a crystal lattice (with atoms attached to lattice points) with the valence electrons being responsible for the conduction properties. A number of important phenomena such as electrical and thermal conductivity are based on the motion of electrons in a solid. For a metal the interpretation of metallic properties in

terms of the motion of free electrons has long been known. A similar description can be applied to semiconductor devices[1].

The physical properties of such a solid can be divided into those determined by the movement of electrons and those determined by the movement of the atoms. The properties determined by electrons include the majority of the electronic properties of the media while the atomic motion can be responsible for many of the thermodynamic properties.

In modelling a semiconductor device (or more generally electrons bound in a lattice), we need to consider the following physical facts

1. The electrons are Fermions and obey Fermi statistics.
2. There is an electron band structure.
3. There are atoms bound in a lattice.
4. There are electron-lattice interactions which cause an electronic band structure.
5. There is electron-electron scattering.

The above physical model of the semiconductor is very simplistic but it does incorporate the major processes occurring in such devices.

From a theoretical point of view there are a number of ways to model the semiconductor system. The most fundamental way is to take the explicit structure and physical origin of the interactions into account and write the Hamiltonian as follows [145]

$$H_{\text{total}} = H_{\text{el}} + H_{\text{el-lat}} + H_{\text{el-el}} + H_{\text{lat}} \tag{6.1}$$

where H_{el} represents the Hamiltonian associated with the electron itself. $H_{\text{el-lat}}$ represents the Hamiltonian associated with the electron-lattice interaction (This interaction occurs via phonons). $H_{\text{el-el}}$ is the Hamiltonian associated with electron-electron scattering. Finally H_{lat} models the atoms in the lattice. There may be other effects that we have neglected in this simplistic Hamiltonian model, but as a first approximation this model explains many physical effects. We now need to examine the terms in (6.1) in some detail.

Let us consider the electron Hamiltonian H_{el} given in (6.1). To adequately describe this Hamiltonian term we must take into the account the electronic band structure. Though the band structure is a result of the electron-lattice interaction it does affect our electron Hamiltonian. The electron Hamiltonian H_{el} we present here describes the motion in a particular band. In a particular band the electron may be though of as a free particle and hence described by the field theory Hamiltonian [145]

$$H_{\text{el}} = -\frac{\hbar^2}{2m}\int dx\ \Psi^\dagger(x)\nabla^2\Psi(x) \tag{6.2}$$

where $\Psi(x)$ is the electron field operator and m is associated with the mass of the electron. An alternative description for the free electron model would be [145, 146]

$$H_{\text{el}} = \sum_k \frac{\hbar^2 k^2}{2m} b_k^\dagger b_k \tag{6.3}$$

where $b_k^\dagger$, b_k are the creation and destruction operators for the electrons. The free electron model of a metal gives a good insight into various properties of the material. The particular free electron model however fails to explain the difference between metals, semi-metals,

[1]This description of a material has long been known and is covered in most solid state text books (see for Example [143–146]

semiconductors, and insulators. This is caused because the band structure of the electrons in such devices is normally neglected in this model. We have however included the electron structure into our model. There are deficiencies in choosing such a model, but we have chosen it as a first approximation.

The next term in (6.1) to consider is the lattice Hamiltonian denoted by H_{lat}. This Hamiltonian can be written as [145, 146]

$$H_{\text{lat}} = \sum_{\beta} \hbar\omega(\beta) a_{\beta}^{\dagger} a_{\beta} \tag{6.4}$$

where $a_{\beta}^{\dagger}$, a_{β} are the creation and destruction operators for the phonons and $\omega(\beta)$ is the frequency associated with the particular phonon.

The second term in (6.1) is Hamiltonian describing the electron lattice interaction. The primary effect of the electron-lattice interaction is to cause a band structure in the material. We have however already included this effect in obtaining the electron Hamiltonian above. There are a couple of methods for describing this electron-lattice interaction. There are two primary interactions, absorption of a phonon or emission of a phonon (we depict these two process in Fig (6.1)). Most solid state texts (see for example [143–146]) describe this interaction via the following Hamiltonian

$$H_{\text{el-lat}} = \sum_{k,\beta} \left(C_{k,\beta}^{\dagger} a_{\beta}^{\dagger} b_{k-\beta}^{\dagger} b_k + C_{k,\beta} a_{\beta} b_{k+\beta}^{\dagger} b_k \right) \tag{6.5}$$

The first expression $a_{\beta}^{\dagger} b_{k-\beta}^{\dagger} b_k$ in Eqn (6.5) describes the destruction of an electron (b_k) with wavevector k simultaneously followed by the creation of an electron with wavevector $k - \beta$ and the emission of a phonon with wavevector β. The second term in $a_{\beta} b_{k+\beta}^{\dagger} b_k$ describes the destruction of an electron (b_k) followed by the creation of an electron with wavevector $k + \beta$ and the absorption of a phonon with wavevector β. In equation (6.5) $C_{k,\beta}$ and $C_{k,\beta}^{\dagger}$ are temperature dependent constants.

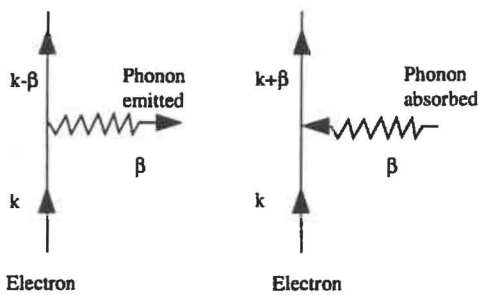

Figure 6.1: The basic processes occurring in electron-phonon interaction.

In considering the Hamiltonian model above we need to explicitly specify every single electron-lattice interaction. This means if we write equations of motion for the system, then we have explicit equations for both the electrons and phonons. This makes the system quite complex to model. An alternative method and slightly easier method for describing the electron-lattice interaction would be to consider the coupling as being an interaction between the electrons and a bath of phonons (The bath of phonons can exchange energy with the electrons, and this leads to a dissipation/fluctuation mechanism). The general quantum optical description of a heat bath coupled to a field mode has the interaction occurring at a specific localised position in space [58, 138]. In a semiconductor system the spatial dependence of the system is important (as there are atoms localised at certain points), and hence to fully describe this spatial dependence of such a system we will require

an infinite number of local heat baths. Using the techniques commonly used in quantum optics [58, 104, 138] we can model this dissipation mechanism (the coupling of a field mode to a heat bath) by the field Hamiltonian term

$$H_{\text{el-lat}} = \int dx \Psi^{\dagger}(x)\Psi(x)\phi(x) \tag{6.6}$$

where $\phi(x)$ is an operator associated with the bath. The exact nature of this operator will not be discussed here in detail but it must be temperature dependant. The electron-lattice interaction given by (6.6) only scatters electrons, it does not create or destroy electrons. Thus it is a scattering mechanism rather than the standard absorption/emission mechanism used in quantum optics. We must emphasise that the electron-lattice interaction given by H_{el-lat} is only an approximate model of the full interaction Hamiltonian given by (6.5).

The Hamiltonian term (6.6) represents a localised coupling of the field mode to the reservoir modes (symbolised by ϕ). $\phi(x)$ as we discussed above was an operator associated with the bath. Generally in quantum optics the correlation function of this bath operator would be written as [58, 104, 138]

$$\langle \phi(x,t)\phi(x',t') \rangle = \delta(x-x')\delta(t-t') \tag{6.7}$$

As can be seen from (6.7) $\phi(x)$ is localised in both time and space. However more realistically in a semiconductor medium this correlation function will not be absolutely localised. In the general band theory of a solid the position can only be localised on a coarse graininess associated with the lattice vibrations, the phonons are known to have rather long wavelengths. Hence in our model we must allow for a degree of delocalisation of the electrons, (Eqn (6.7) represents absolute localisation of the electron). This could be achieved by replacing the delta correspondence with some function that is nonzero in a small region near $x \sim x'$. This is discussed later in Section 6.3.

The last term we need to consider in any semiconductor model is electron-electron scattering represented by the Hamiltonian term $H_{\text{el-el}}$. The general electron-electron field scattering Hamiltonian is given by [145]

$$H_{\text{el-el}} = \frac{1}{2}\int dx dx' \Psi^{\dagger}(x)\Psi^{\dagger}(x')\frac{e^2}{\epsilon_0}V(x-x')\Psi(x)\Psi(x') \tag{6.8}$$

where $V(x-x')$ is the coulombic potential. We notice that this Hamiltonian term is clearly nonlinear in the electron field operators and hence gives equations of motion which are difficult to solve analytically.

In considering a Fermion system, there are two principal approaches that can be used to examine the transport properties from the Hamiltonian. The first treatment is based on a single particle approach where the equations of motion for the momenta and position of each individual Fermion evolve forward in time, the Fermions are also coupled via phonons to the atoms in the lattice. In this approach, the collective variables such as the current density can be obtained by averaging over the entire ensemble of Fermions.

In the single electron approach, Schrödinger's wave equation can be written as

$$i\hbar\frac{d}{dt}|\Psi\rangle = H_{tot}|\Psi\rangle \tag{6.9}$$

where $|\Psi\rangle$ is the total electron wavefunction. The total wavefunction could be simply the single electron wavefunction for a one particle case or a multi electron wavefunction for many electrons. Eqn (6.9) is quite complex in nature and hence difficult to solve analytically, because of the interactions between Fermions and atoms.

The second approach that may be used to describe the transport properties of quantum devices is based on a collective variable theory. Here we examine collective variables such as electron density and current density and solve the system for these collective variables. With this approach it is impossible to obtain any information about the properties of the individual Fermions.

Above we have described two methods by which the properties of the semiconductor system have be examined. In this paper we choose the single particle approach, but instead of using the single electron (or many electron) Schrödinger equation we use the master equation techniques common to the quantum optics field [58, 104, 138]. There are a number of reasons for choosing a master equation approach.

1. The master equation provides an easy method for examining purely quantum effects. These effect will generally manifest themselves in the off-diagonal master equation elements.

2. With an appropriate choice of operator coupling the electron to phonons it is possible to investigate how rapidly the off-diagonal elements of the master equation decay. Work by Gardiner [58] showed that when the coupling operator is coupled to a noise source (a heat bath), the operator itself is diagonalised rapidly. In our electron-phonon scattering Hamiltonian given by (6.6), we have coupled the electron probability density to the phonon bath.

3. Master equations have proved a very useful method of treating damped quantum systems [55, 112–115]

In the field of quantum optics, there are two principal master equations used

- The quantum optical master equation [58], and
- The quantum Brownian motion master equation [58].

These master equations are valid for different physical situations [58, 138].

The quantum optical master equation given by is based on a physical model where we require a description of the system (Fermion in this case) in terms of well defined distinct energy levels, coupled rather weakly to the myriad of modes of the heat bath (for most optical cases this is coupling to the electromagnetic field) [58, 138]. However in the semiconductor material we have a band of energy levels. Thus the model does not correspond to the physical properties of the semiconductor system.

The quantum Brownian motion master equation is however derived for situations in which the energy levels of the system are rather closely spaced [58, 138]. We could for example have a band of energy levels, and hence the choice of model must be the quantum Brownian motion (QBM) master equation.

The QBM master equation takes the form [58, 114, 117–120] [2]

$$\frac{\partial W(t)}{\partial t} = -\frac{i}{\hbar}[H_{\rm sys}, W(t)] - \frac{i\gamma}{2\hbar}\left[X, \left[\dot{X}, W\right]_+\right] - \frac{\gamma kT}{\hbar^2}\left[X, \left[X, W(t)\right]\right] \quad (6.10)$$

in which

$$\dot{X} = \frac{i}{\hbar}[H_{\rm sys}, X], \quad (6.11)$$

and $H_{\rm sys}$ is the system Hamiltonian for the electrons (previously denoted as $H_{\rm el}$) and X is one of the system operators (for example in the free particle Hamiltonian this could be the

[2] There are a number of assumptions implicit in the derivation of eqn (6.10) and for a full discussion of these we refer the reader to Quantum Noise [58].

position or momentum operator). We has used the symbol $W(t)$ to represent the density operator. The particular form written in (6.10) assumes a localised coupling γ between the system operator X and the heat bath is at a temperature T. To model the semiconductor medium fully we will need to modify the master equation to include a near infinite number of localised baths at different points.

Choosing our coupling operator to be the electron probability density, we can solve the master equation (6.10) in a position state basis. This allows us examine the time evolution of the off-diagonal density matrix elements. The off-diagonal elements of the master equation contain quantum information such as the interference effects. When the master equation (6.10) is diagonal no quantum information is retained and the results can be obtained from a classical description.

In this Chapter we began initially in Section (6.2) by modifying the quantum Brownian motion master equation to more fully describe the semiconductor device, that is we generalise the master equation to cases where our electrons are coupled to many different localised heat baths. Choosing the electron probability density as the observable we couple to the phonon heat baths, we initially consider a single electron system in Section (6.3). We examine the rate of decay of the off-diagonal elements in the master equation and show there are two particular time constants, one being associated with frictional damping and the second being that generally associated with classical diffusion process. We also examine the low temperature limit for the single electron system. In Section (6.4) we consider a two electron system, and show how a solution can be obtained when electron-electron scattering is neglected. The method of the two electron solution is then applied to the many electron system. Finally in Section (6.6) we discuss the effect of electron-electron scattering.

6.2 The Quantum Brownian Motion equation

The quantum Brownian motion master equation as discussed previously may be written as [3]

$$\frac{\partial W(t)}{\partial t} = -\frac{i}{\hbar}[H_{\rm sys}, W(t)] - \frac{i\gamma}{2\hbar}\Big[X, \Big[\dot{X}, W\Big]_+\Big] - \frac{\gamma kT}{\hbar^2}\Big[X, \Big[X, W(t)\Big]\Big] \qquad (6.12)$$

where $\dot{X}$ is given by Eqn (6.11). In this formulation of the quantum Brownian motion master equation we are restricted to considering a single variable coupled to a single bath of harmonic oscillators localised to a specific point in space. If we want to formulate a theory for a semiconductor device then we need to allow our system to have an electron coupled to many baths each located at a different point in space. In this case we write the equation for the density operator as[4]

$$\frac{\partial W(t)}{\partial t} = -\frac{i}{\hbar}[H_{\rm sys}, W(t)] - \frac{i}{2\hbar}\sum_i \gamma_i \Big[X_i, \Big[\dot{X}_i, W\Big]_+\Big] - \frac{kT}{\hbar^2}\sum_i \gamma_i \Big[X_i, \Big[X_i, W(t)\Big]\Big] \qquad (6.13)$$

[3] There are various criterion that must be considered when examining the quantum Brownian motion master equation. Because it is not of the Lindblad form [55–57] anomalous results can occur [147]. As discussed in the previous chapter for the damped free particle, we must consider the validity of the cumulant expansion. The cumulant expansion has a smallness parameter associated with it, which for the free particle system has the form

$$\sqrt{\frac{\gamma}{2m}\frac{\hbar}{2\pi kT}} \ll 1$$

The parameters must be chosen such that the relation above is satisfied.

[4] In deriving the equation above we have used an *ad hoc* approach to obtain a master equation with many modes coupled to many heat baths (all the temperature T). The same result can be obtained by starting with the appropriate physical model.

where the damping constant γ_i is associated with the i^{th} heat bath. In the general band theory of solid we can not localise the position of the electron down below the lattice spacing. Hence we can replace these summation signs by integrals, the discrete damping constant γ_i by γ, and X_i by X. Thus the master equation can be written in the form

$$\frac{\partial W(t)}{\partial t} = -\frac{i}{\hbar}\left[H_{\text{sys}}, W(t)\right] - \frac{i\gamma}{2\hbar}\int dX \left[X, \left[\dot{X}, W\right]_+\right] - \frac{\gamma kT}{\hbar^2}\int dX \left[X, \left[X, W(t)\right]\right] \quad (6.14)$$

Critical to the investigation of Eqn (6.14) is the choice of the operator X coupled to the heat baths. For a solid state device there are a number of observables that could be examined. Most commonly associated with the quantum Brownian motion master equation are the position or momentum operators. However work by Gardiner [58] showed that when the coupling operator is coupled to a noise source (a heat bath), the operator itself is diagonalised rapidly. In our electron-phonon scattering Hamiltonian given by (6.6), we have coupled the electron probability density to the phonon bath. Hence the logical choice of operator if we wish to examine the rate the off-diagonal decay would be the electron probability density given by

$$X = \rho(x) = \Psi^\dagger(x)\Psi(x) \quad (6.15)$$

where x is the position operator. Also the majority of transport properties can be determined from the electron probability density. With our choice of X the following master equation Eqn (6.14) reduces to

$$\frac{\partial W}{\partial t} = -\frac{i}{\hbar}\left[H_{\text{sys}}, W\right] - \frac{i\gamma}{2\hbar}\int dx \left[\rho(x), \left[\dot{\rho}(x), W\right]_+\right] - \frac{\gamma kT}{\hbar^2}\int dx \left[\rho(x), \left[\rho(x), W\right]\right] \quad (6.16)$$

where in this problem the kinetic part of the free particle Hamiltonian is written

$$H_{\text{sys}} = -\frac{\hbar^2}{2m}\int dx\, \Psi^\dagger(x)\nabla^2\Psi(x) \quad (6.17)$$

In writing down equation (6.16) we have assumed that bath is exactly delta correlated in position. This however is physically unrealistic and a delocalisation must be incorporated into the model. This is discussed in detail in the next section.

In equation (6.16) T is the temperature of the heat baths (in K), and k is Boltzmann's constant. We have taken m as the mass of the Fermion but in principle this be the effective mass. The damping constant γ is associated with the coupling between the electrons and phonons. The exact nature of this damping constant is quite complex and has an explicit temperature dependence. As the temperature decreases the damping constant must also decrease[5].

6.3 The Single Electron Example

The simplest model for a semiconductor device would be to have a single electron present in a one dimensional material, this is highly unrealistic but provides a convenient way to examine the method of solution. As an operator equation, equation (6.16) is quite

[5] If we assume that γ has at least a linear temperature then the inequality given in the previous footnote is trivially satisfied. The justification for specifying a temperature dependant damping constant is actually quite simple. It has long been known that as the temperature decreases there are fewer phonons available in the bath unless at very low temperatures no phonons are available and no electron-phonon interaction can occur between the electrons and the lattice. Hence the damping constant must be temperature dependent with $\lim_{T\to 0}\gamma(T) \to 0$.

complex, but as an equation for the position space matrix element $\langle a_1|W|b_1\rangle$, the equation is much more easily solved. For the position eigenstate $|b_1\rangle$ given by

$$|b_1\rangle = \Psi^\dagger(b_1)|0\rangle \tag{6.18}$$

the density matrix element $\langle a_1|W(t)|b_1\rangle$ evolves according to the master equation (6.16) as

$$\begin{aligned}\frac{\partial\langle a_1|W|b_1\rangle}{\partial t} = -\frac{i}{\hbar}\langle a_1|\left[H_{\rm sys}, W\right]|b_1\rangle &- \frac{i\gamma}{2\hbar}\int dx\ \langle a_1|\left[\rho(x),[\dot\rho(x),W]_+\right]|b_1\rangle \\ &- \frac{\gamma kT}{\hbar^2}\int dx\ \langle a_1|\left[\rho(x),[\rho(x),W]\right]|b_1\rangle\end{aligned} \tag{6.19}$$

In eqn (6.19) we need to evaluate the action of the operators $\rho(x)$ and $\dot\rho(x)$ on the position state $|b_1\rangle$. More specifically it can be easily shown that

$$\Psi^\dagger(x)\Psi(x')|b_1\rangle = \delta(x'-b_1)|x\rangle. \tag{6.20}$$

To evaluate $\dot\rho(x)|b_1\rangle$ we need to write the operator $\dot\rho(x)$ purely in terms of the electron field operator $\Psi(x)$. We will write $\dot\rho(x)$ as

$$\dot\rho(x) = \frac{i\hbar}{2m}\left[\Psi^\dagger(x)\nabla^2\Psi(x) - \nabla^2\Psi^\dagger(x)\Psi(x)\right] \tag{6.21}$$

We have not derived the expression for $\dot\rho(x)$, rather we have just quoted what it must logically be. It should be however possible to derive the result from our original Hamiltonian.

Now evaluating the action of $\dot\rho(x)$ on $|b_1\rangle$ we have

$$\dot\rho(x')|b_1\rangle = \frac{i\hbar}{2m}\left[\left(\nabla^2_{x'}\delta(x'-b_1)\right) - \delta(x'-b_1)\nabla^2_{x'}\right]|x'\rangle \tag{6.22}$$

We now have the tools to explicitly evaluate the quantum master equation given by (6.19). To this end we will evaluate (6.19) term by term.

Consider the first term of our master equation (6.19). We can obtain the straight forward result

$$\begin{aligned}-\frac{i}{\hbar}\langle a_1|\left[H_{\rm sys}, W\right]|b_1\rangle &= -\frac{i}{\hbar}\int dx dx' \frac{\hbar^2}{2m}\nabla^2_{x'}\delta(x-x')\langle a_1|\left[\Psi^\dagger(x)\Psi(x), W\right]|b_1\rangle \\ &= -\frac{i\hbar}{2m}\left[\nabla^2_a - \nabla^2_b\right]\langle a_1|W|b_1\rangle\end{aligned} \tag{6.23}$$

The second term in (6.19) however needs careful consideration as it contains both a commutator in ρ and an anticommutator in $\dot\rho(x)$. The second term can be explicitly written as

$$-\frac{i\gamma}{2\hbar}\int dx\ \langle a_1|\left[\rho(x),[\dot\rho(x),W]_+\right]|b_1\rangle \tag{6.24}$$

Because our electrons are not fully localised around an individual atoms in the lattice we must allow for their delocalisation. In this case instead of writing $\rho(x)\dot\rho(x)|b_1\rangle$ we will write $\int dx'\zeta(x-x')\,\rho(x)\dot\rho(x')|b_1\rangle$ where we may consider the function $\zeta(x-x')$ as an *"inexact"* delta function which allows for the required delocalisation of the electrons. $\zeta(x-x')$ is a function that is nonzero in a small neighbourhood of $x=y$, but zero everywhere else. The exact choice of mathematical function that could be used to model $\zeta(x-x')$ is left open but we could envisage it as a Gaussian or a Lorenztian function. Allowing for the delocalisation of the electrons equation (6.24) can be rewritten in the form

$$\begin{aligned}-\frac{i\gamma}{2\hbar}\int dx\ &\langle a_1|\left[\rho(x),[\dot\rho(x),W]_+\right]|b_1\rangle \\ &= -\frac{i\gamma}{2\hbar}\int dx dx'\zeta(x-x')\,\langle a_1|\left[\rho(x),[\dot\rho(x'),W]_+\right]|b_1\rangle\end{aligned} \tag{6.25}$$

which using the relations of (6.20) and (6.22) gives

$$
\begin{aligned}
-\frac{i\gamma}{2\hbar}\int dx\langle a_1|\left[\rho(x),[\dot{\rho}(x),W]_+\right]|b_1\rangle &= \frac{\gamma}{2m}\nabla_{b_1}\zeta(a_1-b_1)\nabla_b\langle a_1|W|b_1\rangle \\
&+\frac{\gamma}{2m}\nabla_{a_1}\zeta(b_1-a_1)\nabla_{a_1}\langle a_1|W|b_1\rangle \\
&+\frac{\gamma}{4m}\nabla^2_{b_1}\left[\zeta(a_1-b_1)-\zeta(0)\right]\langle a_1|W|b_1\rangle \\
&+\frac{\gamma}{4m}\nabla^2_{a_1}\left[\zeta(b_1-a_1)-\zeta(0)\right]\langle a_1|W|b_1\rangle
\end{aligned}
\tag{6.26}
$$

Lastly we need to consider the third term in (6.19) which contains a double commutator in $\rho(x)$. Again allowing for the explicit delocalisation of the electrons, the following result can be obtained[6]

$$
\frac{\gamma kT}{\hbar^2}\int dx\langle a_1|\left[\rho(x),[\rho(x),W]\right]|b_1\rangle = \frac{\gamma kT}{\hbar^2}\left[\zeta(0)-\zeta(a_1-b_1)\right]\langle a_1|W|b_1\rangle \tag{6.27}
$$

Using the results (6.21), (6.25) and (6.27), the total quantum Brownian motion master equation may be written as

$$
\begin{aligned}
\frac{\partial\langle a_1|W|b_1\rangle}{\partial t} &= \frac{i\hbar}{2m}\left[\nabla^2_{a_1}-\nabla^2_{b_1}\right]\langle a_1|W|b_1\rangle \\
&+\frac{\gamma}{2m}\left[\nabla_{b_1}\zeta(a_1-b_1)\nabla_{b_1}+\nabla_{a_1}\zeta(b_1-a_1)\nabla_{a_1}\right]\langle a_1|W|b_1\rangle \\
&+\frac{\gamma}{4m}\left[\nabla^2_{b_1}\left[\zeta(a_1-b_1)-\zeta(0)\right]+\nabla^2_{a_1}\left[\zeta(b_1-a_1)-\zeta(0)\right]\right]\langle a_1|W|b_1\rangle \\
&-\frac{\gamma kT}{\hbar^2}\left[\zeta(0)-\zeta(a_1-b_1)\right]\langle a_1|W|b_1\rangle
\end{aligned}
\tag{6.28}
$$

This is a second order partial differential equation, which can be readily solved. It is clear that the solution of our above equation is damped exponentially, with a number of time constants, one which will depend on $[\zeta(0)-\zeta(a_1-b_1)]$. Furthermore this constant has $\hbar^2$ in the denominator, so for $[\zeta(0)-\zeta(a_1-b_1)]$ nonzero, the damping of the off-diagonal elements will be exceedingly fast.

6.3.1 Solution to the Single Electron Quantum Motion Master Equation

The partial differential equation (6.28) can be significantly simplified by the change of variables to

$$a_1 = u+\hbar z \tag{6.29}$$

$$b_1 = u-\hbar z \tag{6.30}$$

where we have also written $P(u,z)=\langle a_1|W|b_1\rangle$. With this notational change the quantum Brownian motion master equation can be written in the form

$$
\frac{\partial P(u,z)}{\partial t} = \left(\frac{i}{2m}\frac{\partial}{\partial u}\frac{\partial}{\partial z}-\frac{\gamma}{2m\hbar}\zeta'(2\hbar z)\frac{\partial}{\partial z}-\frac{2\gamma kT}{\hbar^2}\left[\zeta(0)-\zeta(2\hbar z)\right]\right)P(u,z) \tag{6.31}
$$

[6] We note that if we consider the diagonal terms of the density matrix (that is $(a_1=b_1)$) then eqn (6.27) reduces to

$$\frac{\gamma kT}{\hbar^2}\left[\zeta(0)-\zeta(a_1-b_1)\right]\langle a_1|W|b_1\rangle = 0$$

that is, no damping occurs from the third term on the diagonal terms.

where $\zeta'(x) = \frac{\partial}{\partial x}\zeta(x)$. The solution of Eqn (6.31) can further be simplified by Fourier transforming $P(u,z)$ with respect to u, that is

$$P(u,z) = \int dq \exp(iqu)\hat{P}(q,z) \tag{6.32}$$

In the q Fourier space we have

$$\frac{\partial \hat{P}(q,z)}{\partial t} + \left(\frac{q}{2m} + \frac{\gamma}{2m\hbar}\zeta'(2\hbar z)\right)\frac{\partial \hat{P}(q,z)}{\partial z} = -\frac{2\gamma kT}{\hbar^2}\left[\zeta(0) - \zeta(2\hbar z)\right]\hat{P}(q,z) \tag{6.33}$$

This equation is now ready for solution by the method of characterisation.

6.3.2 The Method of Characteristics

Eqn (6.33) can be solved by the method of characteristics [58, 148], providing $U(z,t,q,P) = a$ and $V(z,t,q) = b$ are two integrals of the subsidiary equation (with a and b are arbitrary constants)

$$dt = \frac{2m dz}{q + \gamma\zeta'(2\hbar z)/\hbar} = \frac{-d\hat{P}}{\frac{2\gamma kT}{\hbar^2}\left[\zeta(0) - \zeta(2\hbar z)\right]\hat{P}}. \tag{6.34}$$

As seen the method of characteristics involves separating the partial differential equation given by (6.33) into one subsidiary equation.

For a solution to Eqn (6.34) to be possible we need to know explicitly the form of $\zeta'(2\hbar z)$. There are many possible choices available for this "inexact" delta function. In Figure (6.1) we show the ideal behaviour that the inexact delta function must have, that is it must be nonzero only in a small region near $x \sim 0$. As a crude approximation we model this parameter simply by

$$\zeta(x) = A - Bx^2 \tag{6.35}$$

where A and B are parameters depending on the exact nature of the inexact delta function[7]. At first glance this may seem a strange choice for our choice of inexact delta function but as shown in Figure (6.1) the quadratic approximation can provide the approximate behaviour we require of $\zeta(x)$ near $x \sim 0$. If x becomes too large then this quadratic approximation will dramatically break down and invalidate the analysis.

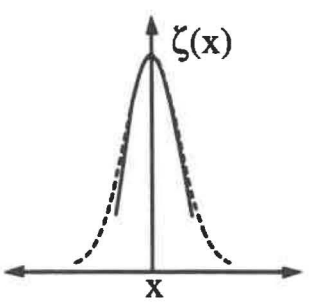

Figure 6.2: Schematic representation of the behaviour of the inexact delta function $\zeta(x)$. The dotted curve represents the ideal behaviour that we require of this function while the solid curve represent the $\zeta(x) = A - Bx^2$ approximation.

[7] In reality there is only one free parameter B say because A is bounded by the requirement for the delta function that $\int \zeta(x)dx = 1$.

Two partial integrals are obtained by integrating the first two and the second two of the equations in (6.34). The first integral

$$\int dt = \int \frac{2mdz}{q + \gamma\zeta'(2\hbar z)/\hbar} \tag{6.36}$$

gives the result

$$U(z,t,q,P) = \left(z + \frac{q}{4\gamma B}\right) \exp\left[-\frac{2\gamma Bt}{m}\right] - \frac{q}{4\gamma B} \tag{6.37}$$

where we have written the constant of integration as $U(z,t,q,P)$. The second equation from Eqn (6.34) written as

$$-\frac{d\hat{P}}{\hat{P}} = \frac{2m\,(8\gamma kTBz^2)\,dz}{q + 4\gamma Bz} \tag{6.38}$$

can be integrated to give

$$\hat{P} = \exp\left[-2mkTz^2 + \frac{mkTqz}{\gamma B}\right](q + 4\gamma Bz)^{-\frac{mkTq^2}{4\gamma^2B^2}}\, V(z,t,q) \tag{6.39}$$

where the constant of integration here is $V(z,t,q)$. Now the general solution to the partial differential equation (6.33) can be written in the form

$$V = F(U) \tag{6.40}$$

where F is an arbitrary function. Hence the complete solution to (6.33) can be written as

$$\begin{aligned} \hat{P} \;=\; & \exp\left[-2mkTz^2 + \frac{mkTqz}{\gamma B}\right](q + 4\gamma Bz)^{-\frac{mkTq^2}{4\gamma^2B^2}} \\ & \times F\left[\left(z + \frac{q}{4\gamma B}\right)\exp\left(-\frac{2\gamma Bt}{m}\right) - \frac{q}{4\gamma B}\right] \end{aligned} \tag{6.41}$$

Assuming that at $t = 0$, $\hat{P} = f(q,z)$ we can deduce that

$$\begin{aligned} \hat{P} \;=\; & f\left[q, z\exp\left(\frac{-2\gamma Bt}{m}\right) - \frac{q\left(1 - \exp\left[\frac{-2\gamma Bt}{m}\right]\right)}{4\gamma B}\right]\exp\left[-2mkTz^2\right] \\ & \times \exp\left[2mkT\left\{z\exp\left(\frac{-2\gamma Bt}{m}\right) - \frac{q}{4\gamma B}\left(1 - \exp\left[\frac{-2\gamma Bt}{m}\right]\right)\right\}^2\right] \\ & \times \exp\left[\frac{mkTq}{\gamma B}\left(z + \frac{q}{4\gamma B}\right)\left(1 - \exp\left[\frac{-2\gamma Bt}{m}\right]\right)\right]\exp\left[-\frac{kTq^2}{2\gamma B}t\right] \end{aligned} \tag{6.42}$$

In Eqn (6.42) the function $f(q,z)$ is highly dependant on the initial conditions chosen for the system.

Our choice of initial condition is highly important to get the physics of the system correct. The motion of a free electron can with a fixed momentum can be described by an infinitely extended plane wave. In describing the motion of electrons in a realistic media we are confronted with finding a method for describing a semi-localised particle from a wave theory point of view. To allow for a degree of localisation of the electron a summation of infinity extended plane waves is necessary. For our initial condition to this single electron situation we consider a system initially in the pure state $|\varphi\rangle$, expressed as a sum of two plane waves so that

$$\langle a_1|\varphi\rangle = \frac{1}{\sqrt{2}}\left\{\exp\left[ik_2a_1\right] + \exp\left[ik_1a_1\right]\right\} \tag{6.43}$$

Initially we have

$$\begin{aligned} f[u,z] &= \langle a_1|\varphi\rangle\langle\varphi|b_1\rangle \\ &= 1/2\exp[ik_1a_1]\exp[-ik_1b_1] + 1/2\exp[ik_1a_1]\exp[-ik_2b_1] \\ &\quad +1/2\exp[ik_2a_1]\exp[-ik_1b_1] + 1/2\exp[ik_2a_1]\exp[-ik_2b_1] \\ &= \exp[2ik_1\hbar z] + \exp[2ik_2\hbar z] + \exp[i(k_1-k_2)u]\exp[i(k_1+k_2)\hbar z] \\ &\quad + \exp[i(k_2-k_1)u]\exp[i(k_1+k_2)\hbar z] \end{aligned} \tag{6.44}$$

Fourier transforming $f[u,z]$ with respect to u we have

$$\begin{aligned} f[q,z] &= \frac{1}{2}\delta(q)\left(\exp[2ik_1\hbar z] + \exp[2ik_2\hbar z]\right) \\ &\quad +\frac{1}{2}\exp[i(k_1+k_2)\hbar z]\left(\delta(q-k_1+k_2)+\delta(q+k_1-k_2)\right) \end{aligned} \tag{6.45}$$

Now that we have an expression for $f[q,z]$ it is possible to perform an inverse Fourier transform on Eqn (6.42) to obtain $P(a_1,b_1)$. Performing this inverse Fourier transform we have

$$\begin{aligned} P(a_1,b_1) &= \frac{1}{2}\{P(a_1,a_1;k_1,k_2) + P(b_1,b_1;k_1,k_2) \\ &\quad + P(a_1,b_1;k_1,k_2) + P(a_1,b_1;k_2,k_1)\} \end{aligned} \tag{6.46}$$

where

$$P(a_1,b_1;k_1,k_2) = P_{oscillation}(a_1,b_1;k_1,k_2)P_{damping}(a_1,b_1;k_1,k_2) \tag{6.47}$$

The other terms such as $P(a_1,a_1;k_1,k_2)$ can be obtained by replacing b_1 with a_1 in Eqn (6.47). In Eqn (6.47) $P_{oscillation}(a_1,b_1;k_1,k_2)$ and $P_{damping}(a_1,b_1;k_1,k_2)$ are given by

$$\begin{aligned} P_{oscillation}(a_1,b_1;k_1,k_2) &= \exp\left[i(k_1-k_2)\left(\frac{a_i+b_j}{2}\right)\right] \\ &\quad \times\exp\left[i\hbar(k_1+k_2)\left(\frac{a_1-b_1}{2\hbar}\right)\exp\left[-\frac{2\gamma Bt}{m}\right]\right] \\ &\quad \times\exp\left[\frac{i\hbar(k_1^2-k_2^2)}{4\gamma B}\left(1-\exp\left[-\frac{2\gamma Bt}{m}\right]\right)\right] \end{aligned} \tag{6.48}$$

and

$$\begin{aligned} P_{damping}(a_1,b_1;k_1,k_2) &= \exp\left[-2mkT\left(\frac{a_1-b_1}{2\hbar}\right)^2\right] \\ &\quad \times\exp\left[2mkT\left\{\left(\frac{a_1-b_1}{2\hbar}\right)\exp\left[-\frac{2\gamma Bt}{m}\right]\right\}^2\right] \\ &\quad \times\exp\left[-\frac{mkT}{\gamma B}\left(\frac{a_1-b_1}{2\hbar}\right)(k_2-k_1)\left(1-\exp\left[-\frac{2\gamma Bt}{m}\right]\right)^2\right] \\ &\quad \times\exp\left[2mkT\left\{\frac{(k_2-k_1)}{4\gamma B}\left(1-\exp\left[-\frac{2\gamma Bt}{m}\right]\right)\right\}^2\right] \\ &\quad \times\exp\left[\frac{mkT}{\gamma B}\left(\frac{(k_2-k_1)^2}{4\gamma B}\right)\left(1-\exp\left[\frac{-2\gamma Bt}{m}\right]\right)\right] \\ &\quad \times\exp\left[-\frac{kT(k_2-k_1)^2}{2\gamma B}t\right] \end{aligned} \tag{6.49}$$

respectively.

Eqn (6.46) contains four distinct terms, the first two given by $P(a_1, a_1; k_1, k_2)$ and $P(b_1, b_1; k_1, k_2)$ representing the diagonal density elements. These can be directly associated with the probability of the system being in a particular state. Figure (6.3) presents a plot of the diagonal elements of the density matrix. It is clearly observable that for $k_2 - k_1$ not zero, these diagonal elements do decay. In (6.46) there are two off-diagonal density matrix elements given by $P(a_1, b_1; k_1, k_2)$ and $P(a_1, b_1; k_2, k_1)$. For these terms we are particularly interested in there rate of decay as this gives an indication as to how fast certain quantum effects vanish.

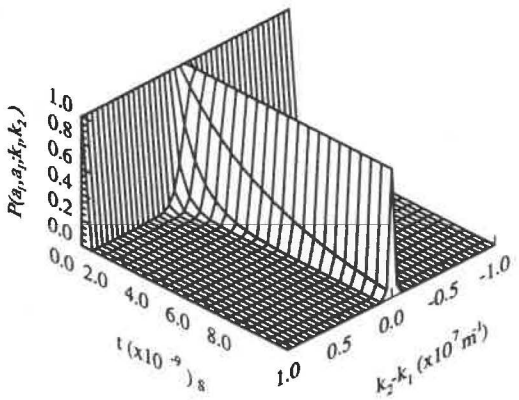

Figure 6.3: Plot of the diagonal density matrix element $P_{damping}(a_1, a_1; k_1, k_2)$ versus the time and $k_1 - k_2$. Here we have set $a_1 = 0\text{m}$ and $k_1 = 10^6\text{m}^{-1}$.

To this end we examine one of the particular terms in (6.46), namely $P(a_1, b_1; k_1, k_2)$. According to (6.47) can be written in two parts: $P_{oscillation}(a_1, b_1; k_1, k_2)$ which causes oscillations in $P(a_1, b_1; k_1, k_2)$ and $P_{damping}(a_1, b_1; k_1, k_2)$ which causes direct damping of the density matrix element $P(a_1, b_1; k_1, k_2)$. In Fig (6.4-6.5) we plot $P_{damping}(a_1, b_1; k_1, k_2)$ for various parameter choices. More specifically in Fig (6.4) we plot $P_{damping}(a_1, b_1; k_1, k_2)$ versus time and the degree of diagonalisation (or off-diagonalisation) $a_1 - b_1$ for fixed values of $k_2 - k_1$. Here is clear evidence under all circumstances that the off-diagonal elements $P_{damping}(a_1, b_1; k_1, k_2)$ decay even for $k_2 = k_1$. Fig (6.5) investigates the effect of $k_2 - k_1$ nonzero on $P_{damping}(a_1, b_1; k_1, k_2)$. In this case we plot $P_{damping}(a_1, b_1; k_1, k_2)$ versus time and $k_2 - k_1$. This is done for fixed $a_1 - b_1$. For $a_1 = b_1$ and $k_2 = k_1$ we have $P_{damping}(a_1, b_1; k_1, k_2) = 1$ for all times, that is the diagonal elements of the density matrix do not decay away with time provided initially the electron wave could be represented as a single plane wave. The off-diagonal terms do however rapidly decay as is easily seen in Figures (6.4-6.5) . For $k_2 - k_1$ nonzero, we observe in Fig(6.5), that we get a rapid decay of the density matrix element, including the diagonal elements. This occurs even for small $k_2 - k_1$.

Associated with (6.47) are a number of time scales and we investigate these in the next subsection.

6.3.3 The Characteristic Time Constants associated with the Master Equation

From our QBM master equation solution given by (6.47) (or more specifically (6.48) and (6.49)) we have noted two distinct time constants

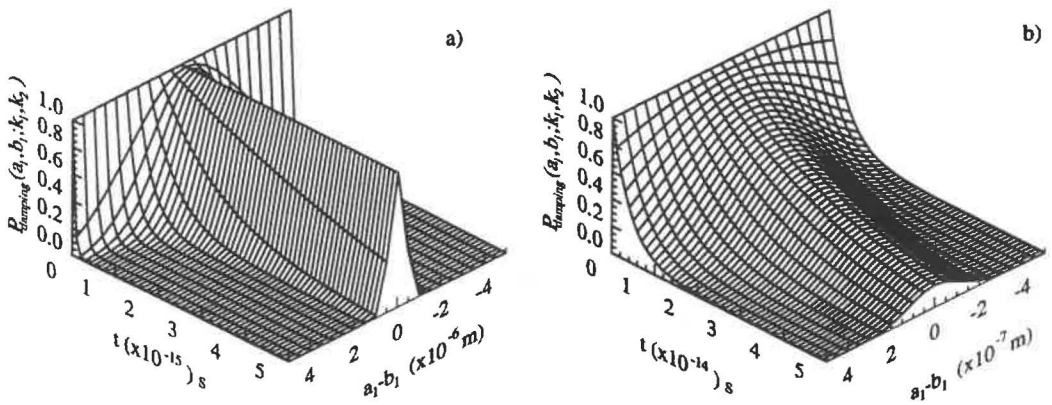

Figure 6.4: Plot of the density matrix element $P_{damping}(a_1, b_1; k_1, k_2)$ versus the time and $a_1 - b_1$ (a measure of the off-diagonality of the system). Here we have a) $k_2 - k_1 = 0\text{m}^{-1}$, and b) $k_2 - k_1 = 3 \times 10^7\text{m}^{-1}$.

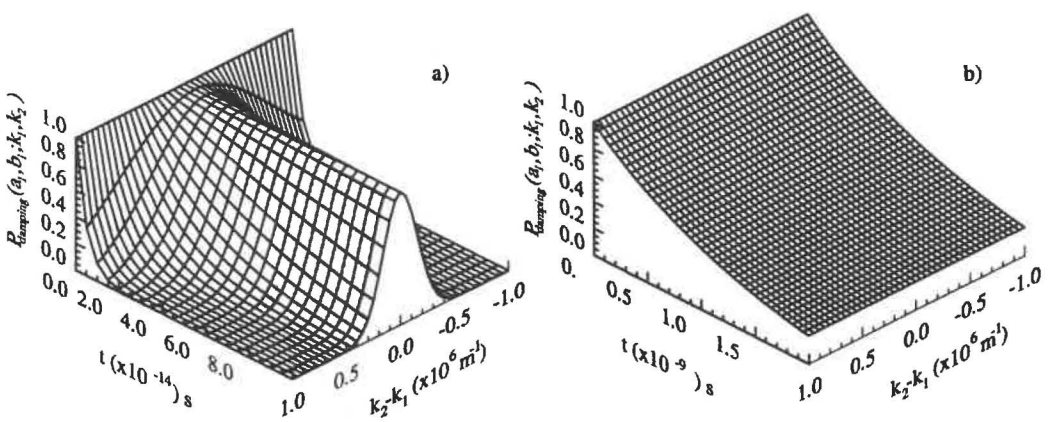

Figure 6.5: Plot of the density matrix element $P_{damping}(a_1, b_1; k_1, k_2)$ versus the time and $k_1 - k_2$. Here we have a) $a_1 - b_1 = 0$ and b) $a_1 - b_1 = 10^{-6}\text{m}$

1. The first time constant is associated with terms like

$$\exp\left[\frac{-2\gamma B}{m}t\right] \tag{6.50}$$

where we say the time constant τ_D is given by

$$\tau_D = \frac{m}{2\gamma B} \tag{6.51}$$

This type of time constant is generally associated with frictional damping.

2. The second time constant

$$\tau_{k_2-k_1} = \frac{2\gamma B}{kT\left(k_2 - k_1\right)^2} \tag{6.52}$$

is much like the terms that appear in classical diffusion theory.

To carefully examine the effect of these two time constants we need realistic estimates for the various parameters. In order to get a estimate for the magnitude of the time constants and hence their range of effect. For a realistic semiconductor system we have the parameters

- $T = 300\text{K}$
- $m = m_e = 9.11 \times 10^{-31}\text{kg}$
- $k_2 - k_1$. k_1 and k_2 are related to the momentum of the electron plane waves. In particular to allow for some delocalisation of the electron wave we have previously modelled it as a sum of two plane wave, the first with k_1 and the second with k_2. The exact choice of $k_2 - k_1$ needs to be determined for the problem under consideration.
- $a_1 - b_1 = \Delta a$ (Δa is a measure of the off-diagonality of the matrix element. $\Delta a = 0$ corresponds to the diagonal elements)
- Another parameter we need to investigate is B which is associated with the delocalisation function. Previously we had

$$\zeta(x) = A - Bx^2 \tag{6.53}$$

as an approximation to a Lorenztian function of the form

$$\zeta(x) = \frac{a'}{a'^2 + x^2} \tag{6.54}$$

Here a' is of the order of magnitude of the phonon interaction distance in the lattice, which could be in the range $10^{-6} - 10^{-10}\text{m}$. For convenience we will for calculation purposes set $a' = 10^{-8}\text{m}$. In the range where $x < a'$ is small eqn(6.54) reduces to

$$\zeta(x) = \frac{1}{a'} - \frac{x^2}{a'^3} \tag{6.55}$$

Comparing this equation with (6.55) we see B is of the order of magnitude 10^{24}m^{-3}.

- The last parameter we need to investigate is the damping constant γ. This parameter can be obtained from the diffusion constant given by $D = \frac{kT}{2\gamma B}$. The exact value of the diffusion constant for electrons in a semiconductor material is unknown (it is known only for specific semiconductor materials), but as a rough figure, let us set $D = 10^{-2}\ \text{m}^2\text{s}^{-1}$. This gives us our damping term γ to be of the order of magnitude $10^{-43}\text{kgm}^3\text{s}^{-1}$

Substituting these estimates for our required parameters into our time constants given by (6.51) and (6.52) we have

$$\tau_D \sim 10^{-12}\text{s} \tag{6.56}$$

$$\tau_{k_2-k_1} \sim 10^{-18}\text{s} \tag{6.57}$$

The first observation about the time constants are that they are very rapid being in the slowest case on the picosecond scale. Thus an immediate conclusion will be that it is going to be very difficult to observe quantum effects since the off-diagonal elements will decay very rapidly.

6.3.4 The One Electron QBM Master Equation at Low Temperatures

At high temperatures it has long been known that quantum effects can be washed out by thermal noise. To this end, we investigate in this section the low temperature regime. In this low temperature limit ($T \to 0$), we must take into account the temperature dependence of our coupling of the electrons to the boson bath. We need to note that the correlation time of the bath gets very large as the temperature approaches absolute zero. However as we have commented previously the cumulant expansion is valid in this low temperature regime for this specific problem, assuming the damping constant γ has at least a linear temperature dependence (see footnote (3,5)).

Explicitly writing $\gamma = \bar{\gamma}T$ to represent the temperature dependance of the coupling constant it can be shown that the off-diagonal element ($P(a_1, b_1; k_1, k_2)$ given by Eqn(6.48) reduces in the limit $T \to 0$ to

$$\lim_{T\to 0} P(a_1, b_1; k1, k2) = \exp\left[ik_1 a - ik_2 b_1\right] \exp\left[i\hbar \frac{(k_1^2 - k_2^2)}{2m} t\right] \tag{6.58}$$

We notice for all times, that at $T = 0$, there is as expected no damping of the off-diagonal elements of the density matrix. More importantly however we see that the solution (6.58) is just our initial plane wave multiplied by the Schrödinger evolution factor

$$\exp\left[i\hbar \frac{(k_1^2 - k_2^2)}{2m} t\right] \tag{6.59}$$

6.4 The Two Electron System

In the previous sections we considered a one electron model. Let us now consider a situation where we have two electrons in a semiconductor medium. With a two electron system there will be electron-electron effects occurring that were not present in the single electron case. However for initial simplicity we will neglect these electron-electron interactions. If we are going to discuss our two electron system in terms of a density matrix element of a master equation, then we need to define our position basis. This is done simply by specifying the position eigenstate $|b_1, b_2\rangle = |b_1\rangle \otimes |b_2\rangle$ where b_1 refers to the first electron and b_2 refer to the position of the second electron. Using the same procedure we had for the one electron case, we can show that the density matrix element $\langle a_1, a_2|W|b_1, b_2\rangle$ evolves according to

$$\begin{aligned}
\frac{\partial \langle a_1, a_2|W|b_1, b_2\rangle}{\partial t} = & \frac{i\hbar}{2m}\left[\nabla_{a_1}^2 + \nabla_{a_2}^2 - \nabla_{b_1}^2 - \nabla_{b_2}^2\right]\langle a_1, a_2|W|b_1, b_2\rangle \\
& -\frac{\gamma}{2m}\nabla_{a_1}\left[\zeta(a_2 - a_1) - \zeta(b_1 - a_1) - \zeta(b_2 - a_1)\right]\nabla_{a_1}\langle a_1, a_2|W|b_1, b_2\rangle \\
& -\frac{\gamma}{2m}\nabla_{a_2}\left[\zeta(a_1 - a_2) - \zeta(b_1 - a_2) - \zeta(b_2 - a_2)\right]\nabla_{a_2}\langle a_1, a_2|W|b_1, b_2\rangle
\end{aligned}$$

$$
\begin{aligned}
&+\frac{\gamma}{2m}\nabla_{b_1}\left[\zeta(a_1-b_1)-\zeta(a_2-b_1)-\zeta(b_2-b_1)\right]\nabla_{b_1}\langle a_1,a_2|W|b_1,b_2\rangle\\
&+\frac{\gamma}{2m}\nabla_{b_2}\left[\zeta(a_1-b_2)+\zeta(a_2-b_2)-\zeta(b_1-b_2)\right]\nabla_{b_2}\langle a_1,a_2|W|b_1,b_2\rangle\\
&-\frac{2\gamma kT}{\hbar^2}\left[\zeta(0)-\zeta(a_1-b_1)-\zeta(a_1-b_2)\right]\langle a_1,a_2|W|b_1,b_2\rangle\\
&-\frac{2\gamma kT}{\hbar^2}\left[\zeta(0)-\zeta(a_2-b_1)-\zeta(a_2-b_2)\right]\langle a_1,a_2|W|b_1,b_2\rangle \qquad (6.60)
\end{aligned}
$$

In Eqn (6.60) the last two terms are responsible for the majority of damping. If they are zero then only minor damping of the density matrix element $\langle a_1,a_2|W|b_1,b_2\rangle$ occurs. A close examination of these last two lines of (6.60) reveal that these terms are only zero in the special case of $a_1\sim b_1$ and $a_2\sim b_2$ or $a_1\sim b_2$ and $a_2\sim b_1$. For these two cases the last two terms of (6.60) vanish and hence the main terms associated with the damping have disappeared. For the case of $a_1\sim b_1$ and $a_2\sim b_2$ we specify that $\zeta(a_2-b_1)\sim\zeta(a_1-b_2)\sim 0$. The case of $a_1\sim b_2$ and $a_1\sim b_2$ requires $\zeta(a_1-b_1)\sim\zeta(a_2-b_2)\sim 0$.

To considerably simplify the solution of (6.60) we now invoke Pauli's exclusion principle. This means both electrons cannot occupy the same spatial location and hence we require $a_1\neq a_2$ and $b_1\neq b_2$. Thus we must enforce the requirement $\zeta(a_1-a_2)=\zeta(b_1-b_2)=0$ for all a_1, a_2, b_1, b_2. This does however assume that a_1, a_2 are spatially separated enough so there is no overlap. The use of the exclusion principle places an anti-symmetrisation on our two electron system. If we specify the electrons to be in the order $a_1<a_2$, $b_1<b_2$, then the last two terms in (6.60) are zero only if $a_1=b_1$, and $a_2=b_2$. In this case there is no damping from the last two terms of (6.60). With this ordering procedure it is not possible to have $a_1=b_2$, and $a_2=b_1$ unless $a_1=a_2=b_1=b_2$ and this is not allowed due to the exclusion principle. Hence we set terms like $\zeta(a_2-b_1)=\zeta(a_1-b_2)=0$. If these terms were not zero then the last two terms of (6.60) would be nonzero for all a_i, b_i and hence we would have rapid decay of even the diagonal elements of the master equation. Therefore invoking this ordering assumption (6.61) reduces to

$$
\begin{aligned}
\frac{\partial\langle a_1,a_2|W|b_1,b_2\rangle}{\partial t} &= \frac{i\hbar}{2m}\left[\nabla_{a_1}^2+\nabla_{a_2}^2-\nabla_{b_1}^2-\nabla_{b_2}^2\right]\langle a_1,a_2|W|b_1,b_2\rangle\\
&+\frac{\gamma}{2m}\left[2B\left(a_1-b_1\right)\left(\nabla_{b_1}-\nabla_{a_1}\right)\right]\langle a_1,a_2|W|b_1,b_2\rangle \qquad (6.61)\\
&+\frac{\gamma}{2m}\left[2B\left(a_2-b_2\right)\left(\nabla_{b_2}-\nabla_{a_2}\right)\right]\langle a_1,a_2|W|b_1,b_2\rangle\\
&-\frac{2\gamma kT}{\hbar^2}\left[B\left(a_1-b_1\right)^2+B\left(a_2-b_2\right)^2\right]\langle a_1,a_2|W|b_1,b_2\rangle
\end{aligned}
$$

where we have used the explicit form of $\zeta(a_1-b_1)$ given in (6.35). Taking equation (6.61) we make the following change of variables

$$
\begin{aligned}
a_1 &= u_1+\hbar z_1 && (6.62)\\
b_1 &= u_1-\hbar z_1 && (6.63)\\
a_2 &= u_2+\hbar z_2 && (6.64)\\
b_2 &= u_2-\hbar z_2 && (6.65)
\end{aligned}
$$

with $P(u_1,z_1,u_2,z_2)=\langle a_1,a_2|W|b_{1,2}\rangle$. With this notation change equation (6.61) can be rewritten as

$$
\begin{aligned}
\frac{\partial P(u_1,z_1,u_2,z_2)}{\partial t} &= \frac{i}{2m}\left[\frac{\partial}{\partial u_1}\frac{\partial}{\partial z_1}+\frac{\partial}{\partial u_2}\frac{\partial}{\partial z_2}\right]P(u_1,z_1,u_2,z_2)\\
&-\frac{\gamma}{2m}\left[4Bz_1\frac{\partial}{\partial z_1}+4Bz_2\frac{\partial}{\partial z_2}\right]P(u_1,z_1,u_2,z_2) \qquad (6.66)\\
&-8\gamma kTB\left[z_1^2+z_2^2\right]P(u_1,z_1,u_2,z_2)
\end{aligned}
$$

Performing a Fourier transform with respect to both u_1, u_2 we have

$$\begin{aligned}\frac{\partial \hat{P}}{\partial t} = & -\left(\left[\frac{q_1+4\gamma B z_1}{2m}\right]\frac{\partial}{\partial z_1}+8\gamma kTBz_1^2\right)\hat{P} \\ & -\left(\left[\frac{q_2+4\gamma B z_2}{2m}\right]\frac{\partial}{\partial z_2}+8\gamma kTBz_2^2\right)\hat{P}\end{aligned} \tag{6.67}$$

The way this equation has been written clearly indicates that there is no interaction between the first and second electron (that is, there are no cross terms involving z_1 and z_2). Hence writing $\hat{P}$ as the product $\hat{P} = \hat{P}_1(q_1, z_1)\hat{P}_2(q_2, z_2)$, Eqn (6.67) breaks into two uncoupled equations

$$\frac{\partial \hat{P}_1(q_1,z_1)}{\partial t} = -\left(\left[\frac{q_1+4\gamma B z_1}{2m}\right]\frac{\partial}{\partial z_1}+8\gamma kTBz_1^2\right)\hat{P}_1(q_1,z_1) \tag{6.68}$$

$$\frac{\partial \hat{P}_2(q_2,z_2)}{\partial t} = -\left(\left[\frac{q_2+4\gamma B z_2}{2m}\right]\frac{\partial}{\partial z_2}+8\gamma kTBz_2^2\right)\hat{P}_2(q_2,z_2) \tag{6.69}$$

Equation (6.68) and (6.69) are simply the single electron equation and hence there individual solution is simply (6.42). To obtain our solution in terms of a_1, a_2, b_1, b_2, we need to Fourier transform the solution of $\hat{P} = \hat{P}_1(q_1, z_1)\hat{P}_2(q_2, z_2)$. Hence we need to again examine the initial conditions. Choosing the same initial condition for each electron that we did in single electron case, the two electron solution can be written as

$$P(a_1, a_2, b_1, b_2) = P(a_1, b_1)P(a_2, b_2) \tag{6.70}$$

where $P(a_1, b_1)$ is given by Eqn (6.46). $P(a_2, b_2)$ can be obtained by simply substituting a_2, b_2 for a_1, b_1 and k_4, k_3 for k_2, k_1 in (6.46) respectively. This solution has the same time constants as in the one electron case.

6.5 The Many Electron System

The method used in the two electron solution can be applied to the many electron system. Again we choose to neglect the effects of electron-electron interactions. Defining the n electron position basis as $|b_1, \cdots, b_n\rangle = |b_1\rangle \cdots |b_{n-1}\rangle \otimes |b_n\rangle$ we can show that the density matrix element $P = \langle a_1, \cdots, a_n|W|b_1, \cdots, b_n\rangle$ evolves according to

$$\begin{aligned}\frac{\partial P}{\partial t} = & \frac{i\hbar}{2m}\sum_{i=1}^{n}\left[\nabla_{a_i}^2 - \nabla_{b_i}^2\right]P - \frac{2\gamma kT}{\hbar^2}\left[n\zeta(0) - \sum_{i=1}^{n}\sum_{j=1}^{n}\zeta(a_i - b_j)\right]P \\ & -\frac{\gamma}{2m}\sum_{i=1}^{n}\sum_{j=1}^{n}\nabla_{a_i}\left[\zeta(a_j - a_i) - \zeta(b_j - a_i)\right]\nabla_{a_i}P \\ & +\frac{\gamma}{2m}\sum_{i=1}^{n}\sum_{j=1}^{n}\nabla_{b_i}\left[\zeta(a_j - b_i) - \zeta(b_j - b_i)\right]\nabla_{b_i}P\end{aligned} \tag{6.71}$$

As we did in the two electron system we now use our an order procedure. We specify that $a_i < a_{i+1}, b_i < b_{i+1}$ and hence equation (6.71) simplifies to

$$\begin{aligned}\frac{\partial P}{\partial t} = & \frac{i\hbar}{2m}\sum_{i=1}^{n}\left[\nabla_{a_i}^2 - \nabla_{b_i}^2\right]P + \frac{\gamma}{2m}\sum_{i=1}^{n}\left[\nabla_{a_i}\zeta(b_i - a_i)\nabla_{a_i} + \nabla_{b_i}\zeta(a_i - b_i)\nabla_{b_i}\right]P \\ & -\frac{2\gamma kT}{\hbar^2}\left[n\zeta(0) - \sum_{i=1}^{n}\zeta(a_i - b_i)\right]P\end{aligned} \tag{6.72}$$

As in the two electron problem we observe that Eqn (6.72) representing the n electron system factorises into n single electron equations, that is writing $P = \prod_{i=1}^{n} P_i$, Eqn(6.72) can be written as

$$\frac{\partial P_i}{\partial t} = \left(\frac{i\hbar}{2m}\left[\nabla_{a_i}^2 - \nabla_{b_i}^2\right] + \frac{\gamma}{2m}\sum_{i=1}^{n}\left[\nabla_{a_i}\zeta(b_i - a_i)\nabla_{a_i} + \nabla_{b_i}\zeta(a_i - b_i)\nabla_{b_i}\right]\right) P$$
$$- \frac{2\gamma kT}{\hbar^2}\left[\zeta(0) - \zeta(a_i - b_i)\right] P \tag{6.73}$$

which is just the density matrix element equation for the one electron system. Hence the n electron master equations solution is simply a product of the one electron solutions.

$$P = \prod_{i=1}^{n} P(a_i, b_i) \tag{6.74}$$

In the calculations shown in the previous sections we have neglected the effects of electron-electron scattering (these effects do not arise in the single electron case). For a realistic semiconductor system these effects are known to be important and hence we provide a discussion of their effect in the next section.

6.6 The Effect of Electron-Electron Scattering

So far in this paper we have only considered a free particle type approach in which electron-electron scattering has been neglected. In this section we will investigate the effect electron-electron scattering between two electrons. We consider however only the two electron model. In Eqn (6.8) we modelled the electron-electron scattering by the Hamiltonian

$$H_{el-el} = \frac{1}{2}\int dx dx' \Psi^\dagger(x)\Psi^\dagger(x')\frac{e^2}{\epsilon_0}V(x - x')\Psi(x)\Psi(x') \tag{6.75}$$

For this Hamiltonian term we need to specify the Coulombic potential given by $V(x - x')$. The simplest possible potential we could choose for $V(x - x')$ would be a delta function $\delta(x - x')$. However this would be highly unrealistic and instead we choose our inexact delta function $\zeta(x - x')$, that is the Coulombic potential is given by

$$V(x - x') = \zeta(x - x') \tag{6.76}$$

The contribution of (6.75) to the two electron master equation is a term of the form

$$-\frac{i}{\hbar}\left[\frac{1}{2}\int dx dx' \Psi^\dagger(x)\Psi^\dagger(x')\frac{e^2}{\epsilon_0}V(x - x')\Psi(x)\Psi(x'), W(t)\right]. \tag{6.77}$$

This gives a density matrix element for the position basis $|b_1, b_2\rangle$ as

$$-\frac{i}{\hbar}\langle a_1, a_2|\left[\frac{1}{2}\int dx dx' \Psi^\dagger(x)\Psi^\dagger(x')\frac{e^2}{\epsilon_0}V(x - x')\Psi(x)\Psi(x'), W(t)\right]|b_1, b_2\rangle \tag{6.78}$$

Evaluating (6.78) we observe that only terms of the form $\zeta(a_1 - a_2) + \zeta(b_1 - b_2)$ arise. This terms are however set to zero because of the ordering assumptions present in deriving the two electron solution. Thus for our simply choice of the Coulombic potential the electron-electron scattering is negligible.

There are a number of other ways to model this interaction. Of key importance in these calculations is the fact that we are considering only a one dimensional model. This makes the choice of $V(x - x')$ difficult (the standard $1/r$ Coulombic potential is associated with a three dimensional model). Our final comment about electron-electron scattering is that it is an important effect and needs to be modelled in detail. We anticipate that this would be a fruitful area for future research.

6.7 Discussion

The aim of this chapter has been to examine the rate at which quantum effects in a semiconductor device decay away in time. Using the quantum Brownian motion master equation to model such a system we find a number of explicit time constants associated with the decay of the off-diagonal density matrix elements. In particular for a single electron system, where the electron probability density was the operator coupled to the phonon heat bath, we found two time constants. The first we labelled τ_D was temperature independent and was much like the terms generally associated with frictional damping. The second term $\tau_{k_2-k_1}$ was inversely proportional to the temperature. With semi-realistic parameters for the semiconductor we found that the resulting time constants are exceedingly rapid. The shortest time constant is on the pico second time scale. With such fast time constants the off-diagonal elements of the density matrix decay away very rapidly.

The one electron system approach was then applied to a two electron system. Here we found that with the electron-electron interaction neglected (a drastic approximation) the two electron solution is simply a product of the one electron solutions. The same time constants are present. We then showed that the many electron systems solution is also a product of one electron solutions. As mentioned above to obtain these solutions it was necessary to neglect the effects of electron-electron scattering and lastly in Section (6.6) we provide a discussion of the effects of electron-electron scattering. In modelling this interaction it was necessary to explicitly specify the from of the Coulombic potential. Remembering that we have considered only a one dimensional model and that the coulombic potential is a short range effect we choose the "inexact" delta function to model this potential. Here we found that the electron -electron scatter term in the master equation produces only terms of the form $\zeta(a_1 - a_2)$. These terms were then set to zero because of the exclusion principle. Hence in our model there is no effect from electron-electron scattering. This means that our choice of Coulombic potential is inadequate to describe the processes occurring.

The most important comment that can be made about this chapter is that it provides a preliminary investigation into modelling various transport properties of a semiconductor system. The models are crude but they have provided some insight into the time scales on which the quantum information in the off-diagonal elements of the master equation disappear.

Part III

Conclusion and Appendices

Chapter 7

Conclusion

We begin in this thesis by examining systems of significant particle number that violate the generalised Bell inequality. In Chapter (2) we have analysed the ideal two and four-mode correlated photon number states. Our calculations show that the quantum interference produced from the large number of superpositions states is sufficient to contradict all the classical interpretations of the experiment even at large n where large numbers of photons are detected. The correlated photon number states may be generated via parametric down conversion.

In any realistic system, there are going to losses associated with the medium and the photodetection process. We have shown that the ideal photon number-type states required are presently difficult to prepare because of the detection inefficiency. Our calculations reveal that violations of the macroscopic Bell inequality still occur with loss included, but only in a regime where the probability our generating the appropriate state is reduced. Nevertheless consideration of experiments with $N = 2$ would not seem unreasonable. Photocounting measurements are particularly sensitive to poor detector efficiencies, and this again has the effect of diminishing our chance of detecting a truly macroscopic quantum state. For higher detector efficiencies, it is possible to "prepare" the $|n\rangle|n\rangle$ state by restricting attention to the subensembles where only n photons are detected at each of the spatially separated locations. Here auxiliary assumptions of the usual type are required. In this case, violations are obtained for all values of parametric gain. Unfortunately, the probability of actually detecting the appropriate $|n\rangle|n\rangle$ state is small.

A recent experiment of Smithey et al has demonstrated subshot noise photon number correlations for twin pulses each with 10^6 photons. Here one was able to use photodiodes with $85 - 90\%$ quantum efficiency. In terms of the Bell's inequality a new limitation is electronic noise which limits the resolution available in determining n the number of photoelectrons. Here one is unable to formulate the weaker Bell inequality due to a breakdown in the auxiliary assumptions. However if we could prepare a correlated photon number system with only a small number of significant states, then a strong classical Bell inequality formulated without using auxiliary assumptions may be violated. This would provide a possible test of quantum mechanics in the truly macroscopic regime.

In Chapter (3) we explored the Greenberger Horne Zeilinger phenomenon. We have formulated the paradox in terms of boson fields and have shown this to hold even for situations where large numbers of particles are incident on a single analyser. The contradiction only occurs however when the number of particles in the state is odd. We have suggested an experiment using correlated photons to show this paradox (A recent paper by Yurke and Stoler indicate how this correlated photon state may be generated by parametric amplification). It is apparent however that if we lose information about even a single photon from the correlated triplet $|N\rangle|N\rangle|N\rangle$, then the contradiction with local reality is lost. Experimentally to observe the GHZ phenomenon we need to prepare a state with absolute

photon number and to focus on the subensemble where all the photons are detected.

Chapter (4) of this thesis explores another test of macroscopic quantum mechanics, namely the generation and formation of "Schrödinger cat" states. This is done in the limit of large quantum noise in parametric oscillation. Above the semiclassical threshold and for sufficiently large λ/g^2, the probability distribution for one of the quadrature phase amplitudes (z say), becomes clearly bimodal. For sufficiently large g ($g \geq 1$), the corresponding probability distribution for the orthogonal quadrature phase amplitude (p say) develops transient interference fringes. The experimental observation of such fringes would be evidence for the formulation of a coherent superposition of two distinct coherent states well separated in phase space. Such states for very large λ/g^2 values, are analogous to the "Schrödinger-Cat" states discussed by Schrödinger in his famous paradox. Our results have been limited for practical numerical reasons to values for λ/g^2 of the order 5. Nevertheless the observation of superpositions of mesoscopically distinct states would still be a significant advance.

Finally in Chapter (4) we investigated the use of a squeezed field as the input to the intracavity signal mode. We show the inclusion of a squeezed field allows the nonlinearity of the crystal medium to be decreased while still maintaining the interference fringes. More specifically we found that the interference fringes are observable for quite low values of g ($g < 1$), but this require a highly squeezed field.

Part (2) of this thesis considered various aspects of the quantum Brownian motion master equation. The quantum Brownian motion master equation has been used to study many physical problems. However being not of the Lindblad form, anomalous results can occur and hence we began in Chapter (5) with analysis of the validity of such a master equation. More specifically we emphasise that in the quantum Brownian motion master equation there is little validity in considering time scales shorter than the thermal correlation time, because of the coarse grain time scale approach used in its derivation. We consider several specific examples of the kind of unphysical solution which can occur, investigating in particular two extreme cases. The first was a damped free particle in which H_{sys} is purely a kinetic term. In this case the equation of motion for the Wigner function is exactly the same as the Fokker-Planck equation for classical Brownian motion. We have shown here that the unphysical results can be obtained for all temperatures provided the initial position distribution corresponds to a sufficiently well localised wavefunction. However, for situations where the cumulant expansion is valid this gives rise to very rapid, and rather small transients. The second model considered was a simple two level system, which showed anomalous behaviour even in the steady state. This occurs in a regime where the cumulant expansion is invalid.

In Chapter (6) of this thesis we applied the quantum Brownian motion master equation to the study of a semiconductor device. Here we specifically modelled the electron-phonon interaction as a coupling between electrons and a bath of phonons. The master approach is used to get an estimate for the rate of diagonalisation of the off-diagonal elements. In particular we found there were two specific time constants for the single electron system. The first we labelled τ_D was temperature independent and was much like the terms generally associated with frictional damping. The second term $\tau_{k_2-k_1}$ was inversely proportional to the temperature. Of importance to our consideration is that when semi-realistic parameters are examined the resulting time constants are exceedingly rapid. The shortest time constant is on the pico second time scale. With such fast time constants the off-diagonal elements of the density matrix decay away rapidly. Hence any quantum signature quickly disappears. We then considered a two electron system and neglected electron-electron scattering we found that its solution is simply a product of the one electron solutions. Lastly in chapter (6) we provided a brief description of the effect of the electron-electron interaction in the two electron system. We found here that our crude description is not

adequate to describe such an interaction successfully and that this effect needs further consideration.

Appendix A

Boundary Condition Proof for the Degenerate Parametric Oscillator

The boundary condition for the simulation of the degenerate parametric oscillator system needs to meet both the requirements of being a reflecting boundary and also that the diffusion coefficient must vanish on it, if it is to be accurately represented by the Fokker-Planck equation of the system. The proof shown below was first presented by Gardiner [108].

Writing the Fokker-Planck equation in an abbreviated form as

$$\begin{aligned}\frac{\partial P}{\partial t} &= \frac{\partial}{\partial \alpha}\left\{-V(\alpha,\alpha^\dagger)P\right\}+\frac{1}{2}\frac{\partial^2}{\partial \alpha^2}\left\{D(\alpha)P\right\} \\ &+\frac{\partial}{\partial \alpha^\dagger}\left\{-V(\alpha^\dagger,\alpha)P\right\}+\frac{1}{2}\frac{\partial^2}{\partial \alpha^{\dagger 2}}\left\{D(\alpha^\dagger)P\right\} \qquad \text{(A.1)}\end{aligned}$$

where

$$V(\alpha,\alpha^\dagger) = x - y(\lambda - x^2) \qquad \text{(A.2)}$$

$$V(\alpha^\dagger,\alpha) = y - x(\lambda - y^2) \qquad \text{(A.3)}$$

and

$$D(\alpha) = g^2(\lambda - x^2) \qquad \text{(A.4)}$$

$$D(\alpha^\dagger) = g^2(\lambda - y^2) \qquad \text{(A.5)}$$

Using the characteristic function method of definition, the equivalent equation may be written as

$$\chi(\lambda,\lambda^*) = \int_{\mathcal{D}} d^2\alpha d^2\alpha^\dagger P(\alpha,\alpha^\dagger)\exp(\lambda\alpha^\dagger - \lambda^*\alpha) \qquad \text{(A.6)}$$

Hence the real equation is

$$\begin{aligned}\dot{\chi}(\lambda,\lambda^*) &= -\int_{\mathcal{D}} d^2\alpha d^2\alpha^\dagger P(\alpha,\alpha^\dagger)\left\{V(\alpha,\alpha^\dagger)\frac{\partial}{\partial\alpha}+V(\alpha^\dagger,\alpha)\frac{\partial}{\partial\alpha^\dagger}\right\}\exp(\lambda\alpha^\dagger-\lambda^*\alpha) \\ &+\int_{\mathcal{D}} d^2\alpha d^2\alpha^\dagger P(\alpha,\alpha^\dagger)\left\{\frac{1}{2}D(\alpha)\frac{\partial^2}{\partial\alpha^2}+\frac{1}{2}D(\alpha^\dagger)\frac{\partial^2}{\partial\alpha^{\dagger 2}}\right\}\exp(\lambda\alpha^\dagger-\lambda^*\alpha) \qquad \text{(A.7)}\end{aligned}$$

This equation contains two explicit terms, drift terms represent by $V(\alpha)$ and diffusion terms represented by $D(\alpha)$. Evaluating the drift term, using integration by parts, we obtain

$$\int_{\mathcal{D}} d^2\alpha d^2\alpha^\dagger P(\alpha,\alpha^\dagger)\left\{V(\alpha,\alpha^\dagger)\frac{\partial}{\partial\alpha}+V(\alpha^\dagger,\alpha)\frac{\partial}{\partial\alpha^\dagger}\right\}\exp(\lambda\alpha^\dagger-\lambda^*\alpha)$$

$$
\begin{aligned}
&= \int_{\mathcal{D}} d^2\alpha d^2\alpha^\dagger \left\{ \frac{\partial}{\partial \alpha} V(\alpha,\alpha^\dagger) P(\alpha,\alpha^\dagger) \exp(\lambda\alpha^\dagger - \lambda^*\alpha) \right\} \\
&\quad + \int_{\mathcal{D}} d^2\alpha d^2\alpha^\dagger \left\{ \frac{\partial}{\partial \alpha^\dagger} V(\alpha^\dagger,\alpha)) P(\alpha,\alpha^\dagger) \exp(\lambda\alpha^\dagger - \lambda^*\alpha) \right\} \qquad \text{(A.8)} \\
&\quad + \int_{\mathcal{D}} d^2\alpha d^2\alpha^\dagger \left\{ \frac{\partial}{\partial \alpha} V(\alpha,\alpha^\dagger) P(\alpha,\alpha^\dagger) + \frac{\partial}{\partial \alpha^\dagger} V(\alpha^\dagger,\alpha)) P(\alpha,\alpha^\dagger) \right\} \exp(\lambda\alpha^\dagger - \lambda^*\alpha)
\end{aligned}
$$

The first two terms in (A.8) describe one of the boundary terms and can explicitly written as

$$
\begin{aligned}
&\int_{\mathcal{D}} d\alpha^\dagger V(\alpha,\alpha^\dagger) P(\alpha,\alpha^\dagger) \exp(\lambda\alpha^\dagger - \lambda^*\alpha)|_{\alpha=-}^{\alpha=+} \\
&\int_{\mathcal{D}} d\alpha V(\alpha^\dagger,\alpha) P(\alpha,\alpha^\dagger) \exp(\lambda\alpha^\dagger - \lambda^*\alpha)|_{\alpha^\dagger=-}^{\alpha^\dagger=+} \qquad \text{(A.9)}
\end{aligned}
$$

The last two terms in (A.8) correspond to the drift terms remaining in the Fokker Planck equation.

Next we next to consider the diffusion terms in (A.8). In this case these terms can be rewritten in the form

$$
\begin{aligned}
&\int_{\mathcal{D}} d^2\alpha d^2\alpha^\dagger P(\alpha,\alpha^\dagger) \left\{ \frac{1}{2} D(\alpha) \frac{\partial^2}{\partial \alpha^2} + \frac{1}{2} D(\alpha^\dagger) \frac{\partial^2}{\partial \alpha^{\dagger 2}} \right\} \exp(\lambda\alpha^\dagger - \lambda^*\alpha) \\
&= \frac{1}{2} \int_{\mathcal{D}} d^2\alpha d^2\alpha^\dagger \left[\frac{\partial^2}{\partial \alpha^2} P(\alpha,\alpha^\dagger) D(\alpha) + \frac{\partial^2}{\partial \alpha^{\dagger 2}} P(\alpha,\alpha^\dagger) D(\alpha^\dagger) \right] \exp(\lambda\alpha^\dagger - \lambda^*\alpha) \\
&\quad + \frac{1}{2} \int_{\mathcal{D}} d^2\alpha d^2\alpha^\dagger \frac{\partial}{\partial \alpha} \left[P(\alpha,\alpha^\dagger) D(\alpha) \frac{\partial}{\partial \alpha} \exp(\lambda\alpha^\dagger - \lambda^*\alpha) \right] \\
&\quad + \frac{1}{2} \int_{\mathcal{D}} d^2\alpha d^2\alpha^\dagger \frac{\partial}{\partial \alpha^\dagger} \left[P(\alpha,\alpha^\dagger) D(\alpha^\dagger) \frac{\partial}{\partial \alpha^\dagger} \exp(\lambda\alpha^\dagger - \lambda^*\alpha) \right] \\
&\quad - \frac{1}{2} \int_{\mathcal{D}} d^2\alpha d^2\alpha^\dagger \frac{\partial}{\partial \alpha} \left[\frac{\partial}{\partial \alpha} \left(P(\alpha,\alpha^\dagger) D(\alpha) \right) \exp(\lambda\alpha^\dagger - \lambda^*\alpha) \right] \\
&\quad - \frac{1}{2} \int_{\mathcal{D}} d^2\alpha d^2\alpha^\dagger \frac{\partial}{\partial \alpha^\dagger} \left[\frac{\partial}{\partial \alpha^\dagger} \left(P(\alpha,\alpha^\dagger) D(\alpha^\dagger) \right) \exp(\lambda\alpha^\dagger - \lambda^*\alpha) \right] \qquad \text{(A.10)}
\end{aligned}
$$

The first two terms in this equation correspond to the diffusion terms in the Fokker Planck equation. The next four terms are

$$
\begin{aligned}
&\frac{1}{2} \int_{\mathcal{D}} d^2\alpha d^2\alpha^\dagger \frac{\partial}{\partial \alpha} \left[P(\alpha,\alpha^\dagger) D(\alpha) \frac{\partial}{\partial \alpha} \exp(\lambda\alpha^\dagger - \lambda^*\alpha) \right] \\
&+ \frac{1}{2} \int_{\mathcal{D}} d^2\alpha d^2\alpha^\dagger \frac{\partial}{\partial \alpha^\dagger} \left[P(\alpha,\alpha^\dagger) D(\alpha^\dagger) \frac{\partial}{\partial \alpha^\dagger} \exp(\lambda\alpha^\dagger - \lambda^*\alpha) \right] \\
&= \frac{1}{2} \int_{\mathcal{D}} d\alpha^\dagger \left[P(\alpha,\alpha^\dagger) D(\alpha) \frac{\partial}{\partial \alpha} \exp(\lambda\alpha^\dagger - \lambda^*\alpha) \right] |_{\alpha=-}^{\alpha=+} \\
&\quad + \frac{1}{2} \int_{\mathcal{D}} d\alpha \left[P(\alpha,\alpha^\dagger) D(\alpha^\dagger) \frac{\partial}{\partial \alpha^\dagger} \exp(\lambda\alpha^\dagger - \lambda^*\alpha) \right] |_{\alpha^\dagger=-}^{\alpha^\dagger=+} \qquad \text{(A.11)}
\end{aligned}
$$

and

$$
\begin{aligned}
&\frac{1}{2} \int_{\mathcal{D}} d^2\alpha d^2\alpha^\dagger \frac{\partial}{\partial \alpha} \left[\frac{\partial}{\partial \alpha} \left(P(\alpha,\alpha^\dagger) D(\alpha) \right) \exp(\lambda\alpha^\dagger - \lambda^*\alpha) \right] \\
&+ \frac{1}{2} \int_{\mathcal{D}} d^2\alpha d^2\alpha^\dagger \frac{\partial}{\partial \alpha^\dagger} \left[\frac{\partial}{\partial \alpha^\dagger} \left(P(\alpha,\alpha^\dagger) D(\alpha^\dagger) \right) \exp(\lambda\alpha^\dagger - \lambda^*\alpha) \right] \\
&= \frac{1}{2} \int_{\mathcal{D}} d\alpha^\dagger \left[\frac{\partial}{\partial \alpha} \left(P(\alpha,\alpha^\dagger) D(\alpha) \right) \exp(\lambda\alpha^\dagger - \lambda^*\alpha) \right] |_{\alpha=-}^{\alpha=+} \\
&\quad + \frac{1}{2} \int_{\mathcal{D}} d\alpha \left[\frac{\partial}{\partial \alpha^\dagger} \left(P(\alpha,\alpha^\dagger) D(\alpha) \right) \exp(\lambda\alpha^\dagger - \lambda^*\alpha) \right] |_{\alpha^\dagger=-}^{\alpha^\dagger=+} \\
&\qquad \text{(A.12)}
\end{aligned}
$$

The requirement is that the sum of the boundary terms should equal zero on the boundary for stochastic trajectories to be trapped inside the manifold. Collecting together all the boundary terms and equating them to zero we have

$$
\begin{aligned}
&- \int d\alpha^\dagger \left\{ V(\alpha,\alpha^\dagger)P(\alpha,\alpha^\dagger) - \frac{1}{2}\frac{\partial}{\partial\alpha}\left[\left(P(\alpha,\alpha^\dagger)D(\alpha)\right]\right\}\exp(\lambda\alpha^\dagger - \lambda^*\alpha)\right] |_{\alpha=-}^{\alpha=+} \\
&- \int d\alpha \left\{ V(\alpha,\alpha^\dagger)P(\alpha,\alpha^\dagger) - \frac{1}{2}\frac{\partial}{\partial\alpha}\left[\left(P(\alpha,\alpha^\dagger)D(\alpha^\dagger)\right]\right\}\exp(\lambda\alpha^\dagger - \lambda^*\alpha)\right] |_{\alpha^\dagger=-}^{\alpha^\dagger=+} \\
&+ \int d\alpha^\dagger \frac{1}{2}\left[P(\alpha,\alpha^\dagger)D(\alpha)\frac{\partial}{\partial\alpha}\exp(\lambda\alpha^\dagger - \lambda^*\alpha)\right] |_{\alpha=-}^{\alpha=+} \\
&+ \int d\alpha \frac{1}{2}\left[P(\alpha,\alpha^\dagger)D(\alpha^\dagger)\frac{\partial}{\partial\alpha^\dagger}\exp(\lambda\alpha^\dagger - \lambda^*\alpha)\right] |_{\alpha^\dagger=-}^{\alpha^\dagger=+} = 0
\end{aligned}
\tag{A.13}
$$

The first term contains current terms of the form

$$
\begin{aligned}
&V(\alpha,\alpha^\dagger)P(\alpha,\alpha^\dagger) - \frac{1}{2}\frac{\partial}{\partial\alpha}\left[(P(\alpha,\alpha^\dagger)D(\alpha)\right] \\
&V(\alpha,\alpha^\dagger)P(\alpha,\alpha^\dagger) - \frac{1}{2}\frac{\partial}{\partial\alpha^\dagger}\left[P(\alpha,\alpha^\dagger)D(\alpha^\dagger)\right]
\end{aligned}
\tag{A.14}
$$

which can be made zero by imposing a reflecting boundary condition, that is trajectories per unit time reaching the boundary can be made zero by reflecting those trajectories which cross the boundary back into the manifold.

The drift terms $D(\alpha)$ and $D(\alpha^\dagger)$ can only be simultaneously zero if $D(\alpha) = 0$ and $D(\alpha^\dagger) = 0$ on the boundary $\alpha = \pm\sqrt{\lambda}$ and $\alpha^\dagger = \pm\sqrt{\lambda}$. It can be seen from our original equations that these conditions are fulfilled.

Appendix B

Implicit Quantum Stochastic Differential Equations

In Chapter (4) our computer stochastic simulations were done via implicit methods[1]. In deriving the equations of motion the Ito form was used. As our discussions have indicated, for implicit methods we require stochastic equations to be in the Stratonovich form. If the Ito form of the equation is

$$dx = adt + bdW(t) \tag{B.1}$$

then the equivalent Stratonovich SDE [104] is

$$dx = [a - 1/2b\partial_x b]\, dt + bdW(t) \tag{B.2}$$

or more conveniently as

$$dx = A(x)dt + B(x)dW(t) \tag{B.3}$$

where $A(x) = a - 1/2b\partial_x b$ and $B(x) = b$. In order to simulate Eqn (B.1) we must convert the stochastic differential equation to a set of coupled differential equations of the form

$$\Delta x = A(x^{n+\lambda_1})\Delta t + B(x^{n+\lambda_2})\Delta W(t) \tag{B.4}$$

where $\Delta x = x^{n+1} - x^n$. The variables $\lambda_{1/2}$ are parameters that depend on the integration method used. $\lambda_{1/2} = 0$ corresponds to the simpler Euler method, while $\lambda_{1/2} > 0$ corresponds to an implicit method (because the solution at each time step depends on the future). To further simplify Eqn (B.3) we make the following approximations

$$A(x^{n+\lambda_1}) \rightarrow A(x^{n+\lambda_1}) - J_A^{n+1}\,(1-\lambda_1)\,\Delta x \tag{B.5}$$

$$B(x^{n+\lambda_2}) \rightarrow B(x^{n+\lambda_1}) - J_B^{n+1}\,(1-\lambda_2)\,\Delta x \tag{B.6}$$

In Eqn (B.5) J_A^{n+1} is defined by

$$\left(J_A^{n+1}\right)_{ij} = \left[\frac{\delta A_i}{\delta x_j}\right]_{x=x^{n+1}} \tag{B.7}$$

[1]The simulation program shell was originally developed by Prof C.W.Gardiner and later refined by A. Gilchrist. A manual including the source code is available at the Physics Department, University of Waikato, Hamilton, New Zealand. The shell requires the input of the implicit stochastic differential equations as well as the form of the results. In our case the program simply outputs the (x,y) coordinates after a certain time.

Collecting the terms in Δx we have from Eqn (B.4)

$$\Delta x = \left[A(x^{n+1})\Delta t + B(x^{n+1})\Delta W\right]\left[1 + J_A^{n+1}(1-\lambda_1)\Delta t + J_B^{n+1}(1-\lambda_2)\Delta W\right]^{-1} \quad \text{(B.8)}$$

Now using a binomial expansion for the inverse term $\left[1 + J_A^{n+1}(1-\lambda_1)\Delta t + J_B^{n+1}(1-\lambda_2)\Delta W\right]^{-1}$ we have

$$\Delta x = A(x^{n+1})\Delta t + B(x^{n+1})\Delta W - B(x^{n+1})J_B^{n+1}(1-\lambda_2)\Delta W^2 + O(\Delta t^{3/2}) \quad \text{(B.9)}$$

The third term in Eqn (B.9) is the correction term necessary for the implicit simulation of the Stratonovich SDE.

Hence for our original Ito equations given by (4.42-4.43) the implicit form of these equations for simulation is

$$dx = \left[x\left(\frac{g^2}{2} - 1\right) + y\left(\lambda - x^2\right)\right]d\tau + g\sqrt{\lambda - x^2}\, dW_1(t) + \frac{g^2 x}{2} dW_1^2(t) \quad \text{(B.10)}$$

$$dy = \left[y\left(\frac{g^2}{2} - 1\right) + x\left(\lambda - y^2\right)\right]d\tau + g\sqrt{\lambda - y^2}\, dW_2(t) + \frac{g^2 y}{2} dW_2^2(t) \quad \text{(B.11)}$$

Appendix C

The Determinant for the Two Level Atom

In Section (5.4) we discussed the determinant for the two level atom in the long time limit. More generally it can be shown that the determinant is given by

$$\begin{aligned}
\det\rho(t) = & - \left\{\frac{1}{2}\left(b^{-1}+1\right)\left[1-\exp\left(-2\gamma bt\right)\right]+\rho_{-\frac{1}{2},-\frac{1}{2}}\exp\left(-2\gamma bt\right)\right\} \\
& \times\left\{\frac{1}{2}\left(b^{-1}+1\right)\left[1-\exp\left(-2\gamma bt\right)\right]-\left[1-\rho_{-\frac{1}{2},-\frac{1}{2}}\exp\left(-2\gamma bt\right)\right]\right\} \\
& - \exp\left(-2\gamma bt\right)\left\{\cosh^2\left(\gamma bt\sqrt{1-\frac{\Omega^2}{\gamma^2b^2}}\right)+\frac{1+\frac{\Omega^2}{\gamma^2b^2}}{1-\frac{\Omega^2}{\gamma^2b^2}}\sinh^2\left(\gamma bt\sqrt{1-\frac{\Omega^2}{\gamma^2b^2}}\right)\right. \\
& \left. + \frac{1}{\sqrt{1-\frac{\Omega^2}{\gamma^2b^2}}}\sinh\left(2\gamma bt\sqrt{1-\frac{\Omega^2}{\gamma^2b^2}}\right)\right\}\left|\rho_{\frac{1}{2},-\frac{1}{2}}\right|^2 \qquad \text{(C.1)}
\end{aligned}$$

We specify that initially $\det\rho(0) > 0$, that is, the system must start in a physically acceptable state. In Figure (C.1) we plot $\det\rho(t)$ versus the scaled time γt and $b = \frac{\hbar\Omega}{2kT}$. The ratio γ/Ω has been set to one. We notice for $\gamma t > 2$ that the determinant in Figure (C.1) we observe that the determinant becomes negative for various $\frac{2kT}{\hbar\Omega}$ choices.

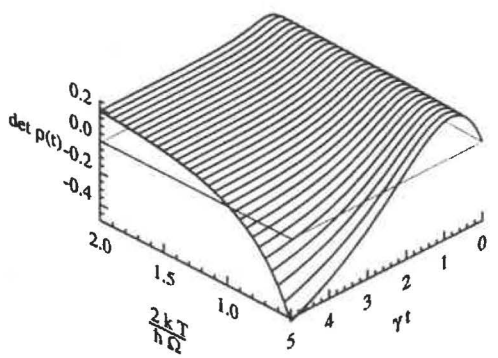

Figure C.1: A three dimensional plot of the determinant $\det\rho(t)$ versus $b = \frac{2kT}{\hbar\Omega}$ and the scaled γt for the two level atom. The temperature has been set to $T = 1K$. $\frac{\gamma}{\Omega}$ is set to one.

In Eqn (C.1) there are two parameter sets of interest, namely $\frac{2kT}{\hbar\Omega}$ and $\frac{\gamma}{\Omega}$. In the first example given below we examine the effect of the $\frac{2kT}{\hbar\Omega}$ ratio in the absence of the $\frac{\gamma}{\Omega}$ ratio.

This is done by setting $\rho_{\frac{1}{2},-\frac{1}{2}} = 0$. In the second example we examine the effect of various $\frac{\gamma}{\Omega}$ ratios.

1. The first case to be examined is when the off-diagonal elements do not contribute to the determinant expression, that is we set $\left|\rho_{\frac{1}{2},-\frac{1}{2}}\right| = 0$. In this case Equation (C.2) reduces to

$$\begin{aligned} \det\rho(t) = \; - \; & \left\{\frac{1}{2}\left(b^{-1}+1\right)\left[1-\exp\left(-2\gamma bt\right)\right] + \rho_{-\frac{1}{2},-\frac{1}{2}}\exp\left(-2\gamma bt\right)\right\} \\ \times \; & \left\{\frac{1}{2}\left(b^{-1}+1\right)\left[1-\exp\left(-2\gamma bt\right)\right] - \left[1-\rho_{-\frac{1}{2},-\frac{1}{2}}\exp\left(-2\gamma bt\right)\right]\right\} \end{aligned} \tag{C.2}$$

We observe that for $\gamma t > 2$ and $kT < \frac{\hbar\Omega}{2}$) the determinant $\det\rho(t) < 0$. In the long time limit Eqn (C.2) reduces to the expression given by Eqn (5.68).

Though we have observed that the determinant criterion for a physically acceptable solution has been violated, we have not seen the exact effect on the density matrix elements themselves. Let us consider a specific example that illustrates this. Consider a system initially in the excited state, that is the only nonzero initial density matrix element is $\langle\phi|\rho(0)|\phi\rangle = \langle\phi|\rho_{\frac{1}{2},\frac{1}{2}}|\phi\rangle = 1$. In this case we have

$$\langle\rho_{\frac{1}{2},\frac{1}{2}}(t)\rangle \;=\; \left\{1-\left(1-\exp\left[-\frac{4\gamma kTt}{\hbar\Omega}\right]\right)\left[\frac{\hbar\Omega}{2kT}+\frac{1}{2}\right]\right\}\rho_{\frac{1}{2},\frac{1}{2}} \tag{C.3}$$

This expression is plotted in Fig (C.2). We observe that in the long time limit $\langle\rho_{\frac{1}{2},\frac{1}{2}}(t)\rangle < 0$ for $kT < \frac{\hbar\Omega}{2}$. We note that these violations are not occurring in transient times as previously, but in the long time regime. The result for the violation when $kT < \frac{\hbar\Omega}{2}$ has been discussed previously in Section (5.4). If we however measure the quantity $\sigma_z(t) = \langle\rho_{\frac{1}{2},\frac{1}{2}}(t)\rangle - \langle\rho_{\frac{-1}{2},\frac{-1}{2}}(t)\rangle$ then it well behaved in the sense that $|\sigma_z(t)| \leq 1$.

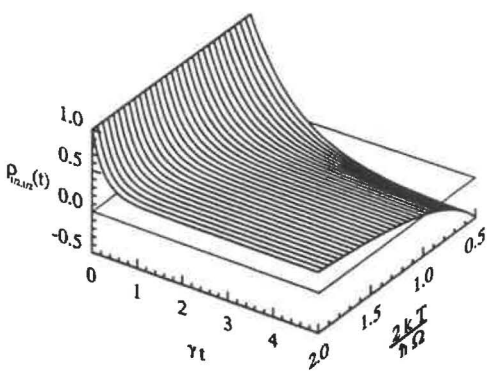

Figure C.2: A three dimensional plot of the expectation value of the density matrix element $\rho_{1,1}(t)$ for the two level atom versus $b = \frac{2kT}{\hbar\Omega}$ and the scaled time γt. $\frac{\gamma}{\Omega}$ is set to one.

2. In this second example we consider nonzero off-diagonal elements. So far we have considered an example where the off-diagonal elements are not present and found a violation for $kT < \frac{\hbar\Omega}{2}$. In this case we will examine the situation of nonzero initial off-diagonal density matrix elements as well as thermal temperatures greater than the zero point energy. This should allow us to examine the effect of the γ/Ω necessary for the validity of the cumulant expansion.

For the determinant to initially start in a valid regime, we require $\left|\rho_{\frac{1}{2},-\frac{1}{2}}\right|^2 < \rho_{-\frac{1}{2},-\frac{1}{2}}\rho_{\frac{1}{2},\frac{1}{2}}$. Setting $2kT/\hbar\Omega = 4$ we plot in Figure (C.3) the determinant $det\rho(t)$ versus the ratio γ/Ω for various γt. We observe that in certain time ranges (not the long time regime) that the determinant goes negative for large γ/Ω values ($\gamma/\Omega > 1$) even with $\hbar\Omega \gg 2kT$.

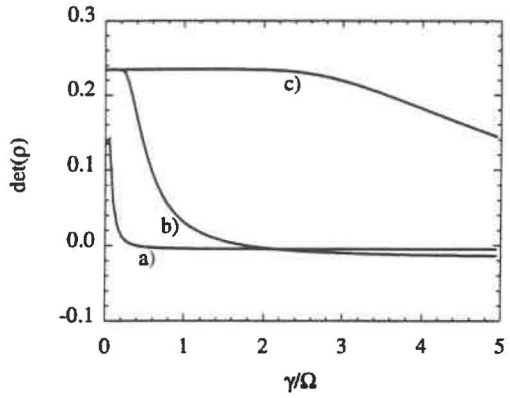

Figure C.3: A plot of the determinant $\det\rho(t)$ versus the ratio γ/Ω for various γt, a) $\gamma t = 0.1$, b) $\gamma t = 1.0$, c) $\gamma t = 100$.

Bibliography

[1] J. S. Bell, Physics (N. Y.) **1**, 195 (1965).

[2] S. J. Freedman and J. F. Clauser, Phys. Rev. Lett**28**, 1938 (1972).

[3] A. Aspect, P. Grangier, and G. Roger, Phys. Rev. Lett**49**, 91 (1982).

[4] A. Aspect, P. Grangier, and G. Roger, Phys. Rev. Lett**47**, 460 (1981).

[5] A. Aspect, J. Dalibard, and G. Roger, Phys. Rev. Lett**49**, 1804 (1982).

[6] A. Aspect, Phys. Rev. D**14**, 1944 (1976).

[7] M. D. Reid and D. F. Walls, Phys. Rev. A**34**, 1260 (1985).

[8] M. A. Horne and A. Zeilinger in *Proc Symp on Foundations of Modern Physics* ed P. Lahti and P. Mittelstaedt, (World Scientific, Singapore, 1985).

[9] Y. H. Shih and C. O. Alley, Phys. Rev. Lett. **61**, 2921 (1988).

[10] Z. Y. Ou and L. Mandel, Phys. Rev. Lett. **61**, 50 (1988).

[11] J. G. Rarity and P. R. Tapster, Phys. Rev. Lett. **65**, 2495 (1990).

[12] T. K. Lo and A. Shimony, Phys. Rev. A**14**, 3003 (1981).

[13] A. J. Leggett, in *Directions in Condensed Matter Physics*, edited by G. Grinstein and G. Mazenko (World Scientific, Singapore, 1985).

[14] B. Yurke and D. Stoler, Phys. Rev. Lett. **57**, 13 (1986).

[15] S. Song, B. Yurke, and C. M. Caves, Phys. Rev. A**41**, 5261(1990).

[16] P. D. Drummond, Phys. Rev. Lett. **50**, 1407 (1983).

[17] N. D. Mermin, Phys. Rev. D**22**, 356 (1980).

[18] B. J. Oliver, and C. R. Stroud, J. Opt. Soc. Am B**4**, 1426(1987).

[19] N. D. Mermin, Am. J. Phys. **58**, 731 (1990).

[20] D. M. Greenberger, M. A. Horne and A. Zeilinger, in Bells Theorem, Quantum Theory and Conceptions of the Universe, edited by M. Kafatos (Kluwer Academic, Dordrecht, The Netherlands, 1989) p. 173.

[21] W. J. Munro and M. D. Reid, Phys Rev A**47**, 4412(1993).

[22] W. J. Munro and M. D. Reid, Quantum Optics Letter **6**, 1 (1994).

[23] S. L Braunstein and C. M. Caves, Phys. Rev. Lett **61**, 662(1988).

[24] D. T. Smithey, M Beck, M. Belsley, and M. G. Raymer, Phys. Rev Lett**69**, 2650(1992).

[25] J. F. Clauser and M. Horne, Phys. Rev. D. **10**, 526 (1974).

[26] J. F. Clauser, M. A. Horne, A. Shimony and R. A. Holt, Phys. Rev. Lett. **23**, 880 (1969).

[27] D. M. Greenberger, M. A. Horne, A. Shimony and A. Zeilinger, Am. J. Phys. **58**, 1131 (1990).

[28] N. D. Mermin, Phys. Rev. Lett. **65**, 1838 (1990).

[29] M. D. Reid and W. J. Munro Phys. Rev. Lett **69**, 997 (1992).

[30] E. Schrödinger, Naturewissenschaften **23**, 812 (1935).

[31] H. J. Carmichael and M. Wolinsky, OSA Annual Meeting, 1989 Technical Digest Series, Vol 18 (Optical Society of America, Washington, D. C, 1989).

[32] M. Wolinsky, Ph. D thesis, Austin, Texas, 1990.

[33] A. Mecozzi and P. Tombesi, Phys. Rev. Lett **58**, 1055 (1987).

[34] T. A. B. Kennedy and D. F. Walls, Phys. Rev. A **37**, 152 (1988).

[35] A. J. Leggett, in *Proceedings of the International Symposium on Foundations of Quantum Mechanics*, edited by S. Kamefuchi et al (Physical Society of Japan, 1983).

[36] A. O. Calderia, and A. J. Leggett, Phys. Rev. A **31**, 1059 (1985).

[37] A. Leggett and C. Gard, Phys. Rev. Lett **54**, 857 (1985).

[38] M. Wolinsky and H. J. Carmichael, Phys. Rev. Lett. **60**, 1836 (1988).

[39] G. J. Milburn, and C. A. Holmes, Phys. Rev. Lett. **56**, 2237 (1986).

[40] H. J. Carmichael, Private communication.

[41] H. J. Carmichael, L. Tian, W. Ren and P. Alsing, in Cavity Quantum Electrodynamics, edited by P. Berman (Academic Press, Boston, 1994).

[42] H. J. Carmichael, , P. Kochan, and L. Tian, in the Proceedings of the International Symposium on Coherent States: Past, Present, and future, Oak ridge, Tennessee, June 14-17 1993 (World Scientific, Singapore).

[43] M. D. Reid and L. Krippner, Phys. Rev. A **47**, 552 (1993).

[44] M. Kitagawa and Y. Yamamoto, Phys. Rev. A **34**, 3974 (1986).

[45] G. J. Milburn, Phys. Rev. A **33**, 674 (1986).

[46] T. A. B. Kennedy and P. D. Drummond, Phys. Rev. A **38**, 1319 (1988).

[47] C. M. Savage and W. A. Cheng, Opt. Comm **70**, 439 (1989).

[48] B. C. Sanders, Phys. Rev. A **44**, 5913 (1989).

[49] P. Meystre, J. Slosser and M. Wilkens, Phys. Rev. A **43**, 6458 (1991).

[50] B. Yurke, W. Schleich and D. F. Walls, ibid **42**, 5261 (1990).

[51] A. La Porta, R. E. Slusher and B. Yurke, Phys. Rev. Lett **62**, 26 (1989).

[52] H. J. Carmichael, J. S. Satchael, and S. Sarkar, Phys. Rev. A **34**, 3166 (1986).

[53] M. D. Reid and B. Yurke, Phys. Rev. A **46**, 4131 (1992).

[54] G. J. Milburn and D. F. Walls, Phys. Rev. A **28**, 2065 (1983).

[55] H. Spohn, Rev. Mod. Phys**52**, 569 (1980).

[56] G. Lindblad, Commun. Mathem. Phys**40**, 147 (1975).

[57] V. Gorini, A. Kossakowski, and E. C. G. Sundarsham, J. Mathem. Phys**17**, 821 (1976).

[58] C. W. Gardiner, *Quantum Noise*, (Springer-Verlag, 1991).

[59] A. S. Parkins, and C. W. Gardiner, *Effect of dissipation on macroscopic quantum coherence in a double well system, in Coherence and Quantum Optics IV*, ed L. Mandel and E. Wolf (Plenum, New York, 1989).

[60] A. S. Parkins, C. W. Gardiner, and M. L. Steyn-Ross, Z Phys B **83**, 413, (1991).

[61] J. F. Clauser and A. Shimony, Rep. Prog. Phys**41**, 1881 (1978).

[62] A. Einstein, B. Podolsky and N. Rosen, Phys. Rev. **47**, 777 (1935).

[63] D. C. Burnham and D. L. Weinberg, Phys. Rev. Lett. **25**, 84 (1970).

[64] S. Friberg, C. K. Hong and L. Mandel, Phys. Rev. Lett. **54**, 2011 (1985).

[65] R. Ghosh and L. Mandel, Phys. Rev. Lett. **59**, 1903 (1987).

[66] Z. Y. Ou, X. Y. Zou, L. J. Wong and L. Mandel, Phys. Rev. Lett. **65**, 321 (1990).

[67] J. G. Rarity, P. R. Tapster, E. Jakeman, T. Larchuk, R. A. Campos, M. C. Teich and B. E. A. Saleh, Phys. Rev. Lett. **65**, 1348 (1990).

[68] P. G. Kwait, W. A. Vareka, C. K. Hong, H. Nathel, R. Y. Chiao, Phys. Rev. A**41**, 2910 (1990).

[69] J. Brendel, E. Mohler, W. Martienssen, Europhysics lett. **20**, 575 (1992).

[70] P. G. Kwait, A. M. Steinberg, R. G. Chiao, Phys. Rev. A**47**, 2472 (1993).

[71] M. A. Horne, A. Shimony and A. Zeilinger, Phys. Rev. Lett. **62**, 2209 (1989).

[72] M. A. Horne, A. Shimony and A. Zeilinger, Phys. Rev. Lett. **62**, 2209 (1989).

[73] A. J. Leggett in 'Directions in Condensed Matter Physics', ed G. Grinstein and G. Mazenko (World Scientific Singapore, 1986).

[74] M. D. Reid and D. F. Walls, Phys. Rev. Lett**53**, 955 (1984).

[75] J. D. Franson, Phys. Rev. Lett. **62**, 2205 (1989).

[76] P. Grangier, M. J. Potasek and B. Yurke, Phys. Rev. A**38**, 3131 (1988).

[77] S. Tan, D. F. Walls and M. J. Collett, Phys. Rev. Lett. **66**, 252 (1991).

[78] P. L. Kelly and W. H. Kleiner, Phys. Rev. **A136**, 316 (1964).

[79] R . Graham, Phys Lett **32 A**, 373 (1970).

[80] R . Graham, Phys Rev. Lett **52** , 117 (1984).

[81] M. J. Collett and D. F. Walls, Phys. Rev. A**32** , 2887(1985).

[82] M. J. Collett and C. W. Gardiner, Phys. Rev. A**30** , 1386(1984).

[83] C. W. Gardiner and M. J. Collett, Phys. Rev. A**31**, 3761(1985).

[84] P. D. Drummond and C. W. Gardiner, J. Phys. A**13**, 2353 (1980).

[85] K. J. McNeil and C. W. Gardiner, Phys. Rev. A**28**, 1560 (1983).

[86] N. D. Mermin, Physics Today, June, p. 11 (1990).

[87] R. K. Clifton, M. L. G. Redhead and J. N. Butterfield, Found. Phys. **21**, 149 (1991).

[88] C. K. Hong and L. Mandel, Phys. Rev. Lett. **56**, 58 (1986).

[89] C. K. Hong, Z. Y. Ou and L. Mandel, Phys. Rev. Lett. **59 b**, 2044 (1987).

[90] B. Yurke and D. Stoler, Phys. Rev. Lett. **68**, 1151 (1992).

[91] W. J. Munro and M. D. Reid, submitted to Phys Rev A.

[92] L. Wu, H. J. Kimble, J. L. Hall and H. Wu, Phys. Lett. **57**, 2520 (1986).

[93] P. Grangier, R. E. Slusher, B. Yurke, and A. LaPorta, Phys. Rev. Lett. **59**, 2153 (1987).

[94] P. D. Drummond, K. J. McNeil, and D. F. Walls, Optica Acta **28**, 211 (1981).

[95] R. Graham and H. Haken, Z. Phys **210**, 276 (1968).

[96] R. Graham, Z. Phys **210**, 319 (1968).

[97] R. Graham, Z. Phys **211**, 469 (1968).

[98] P. D. Drummond and P. Kinsler, Phys. Rev. A **40**, 4813 (1989).

[99] P. Kinsler and P. D. Drummond, Phys. Rev. Lett. **64**, 236 (1989).

[100] R. Graham, *Springer Tracts in modern Physics* **66**, 1 (1973).

[101] R. Landauer and J. Woo, IEEE J. Quantum Electron **7**, 435 (1971).

[102] P. Bryant, K. Weisenfield, and B. McNamara, J. Appl Phys **62**, 2898 (1987).

[103] B. Yurke, P. G. Kaminsky, R. E. Miller, E. A. Whittaker, A. D. Smith, A. H. Silver and R. W. Simon, Phys. Rev. Lett **60**, 764 (1988).

[104] C. W. Gardiner, *Handbook of Stochastic Methods for Physics, Chemistry, and the Natural Sciences*, (Springer-Verlag, Second Edition, 1990)

[105] A. Gilchrist, P. D. Drummond and C. W. Gardiner, to be published (1994).

[106] R. Schack and A. Schenzle, Phys. Rev A **43**, 6303 (1990).

[107] A. M. Smith and C. W. Gardiner, Phys. Rev. A **39**, 3511 (1989).

[108] C. W. Gardiner, to be published.

[109] W. Louisell, *Quantum Statistical Properties of Radiation*, (Wiley, New York, 1974).

[110] H. J. Carmichael and M. Wolinsky, in *Quantum Optics IV*, edited by J. D. Harvey, and D. F. Walls (Springer, Berlin, 1986).

[111] I. K. Mortimer and H. Risken, Phys. Rev. A **44**, 617 (1991).

[112] W. Louisell, *Quantum Optics*, ed S. Kay, A. Maitland, (Academic, New York, 1970).

[113] W. Louisell, *Quantum Statistical Properties of Radiation*, (Wiley, New York, 1974).

[114] F. Haake, *Statistical Treatment of Open Systems by Generalised Master Equations*, (Springer Tracts in Modern Physics, Vol 66, Springer, Berlin, 1973).

[115] B. Davies, *Quantum Theory of Open Systems*, (Academic, New York, 1972).

[116] K. Suominen, B. M. Garraway, and S. Stenholm, Phys. Rev. A **45**, 3060 (1991).

[117] G. S. Agarwal, Phys. Rev. **4**, 739 (1969).

[118] M. J. Collett, *Environmental Correlations in the Theory of Open Quantum Systems*, Ph. D. Thesis(unpublished), University of Essex, 1983.

[119] H. Dekker, Phys. Rev. A**16**, 2126 (1977).

[120] H. Grabert, *Projection Operator Techniques in Nonequilibrium Statistical Mechanics*, (Springer Tracts in Modern Physics, Vol 95, Springer, Berlin, 1982).

[121] S. Stenholm, in Lecture Notes in Physics, ed F. Ehlotzky (Springer Verlag, 1993).

[122] S. Stenholm, submitted for publication to Phys. Rev. A.

[123] C. W. Gardiner, A. S. Parkins and M. J. Collett, J. Opt. Soc. Am. **B4**, 1683 (1987).

[124] C. W. Gardiner, IBM J. Res. Dev. **B32**, 127 (1988).

[125] W. J. Munro and C. W. Gardiner, private communications with M. Collett (1994).

[126] A. Sandulescu and H. Scutaru, Annals of Physics **173**, 277 (1987).

[127] H. J. Carmichael, *ULB Lectures on Quantum Optics* (University of Oregon, Fall 1991).

[128] J. Dalibard, Y. Castin, and K. Mølmer, Phys. Rev. Lett. **68**, 580 (1992).

[129] R. Dum, P. Zoller, and H. Ritsch, Phys. Rev. A **45**, 4879 (1992).

[130] C. W. Gardiner, A. S. Parkins, and P. Zoller, Phys. Rev. A **46**, 4363 (1992).

[131] R. Dum, A. S. Parkins, P. Zoller, and C. W. Gardiner, Phys. Rev. A **46**, 4382 (1992).

[132] V. Ambegaokar, Ber. Bunsenges. Phys. Chem **95**, 400 (1991).

[133] L. Diosi, Europhysics Lett. **22**, 1 (1993).

[134] W. G. Unruh, and W. H. Zurek, Phys. Rev **D40**, 1071 (1989).

[135] F. Haake and R. Reibold, Phys. Rev. A **32**, 488 (1993).

[136] M. J. Collett, private communication.

[137] A. S. Parkins and C. W. Gardiner, Phys. Rev. A**37**, 3867 (1988).

[138] N. G. van Kampen, *Stochastic Processes in Physics and Chemistry*, (North-Hollard Personal Library, 1992).

[139] N. G. van Kampen, Physica**74**, 215 and 239(1974).

[140] H. Ritsch, and P. Zoller, Phys. Rev. Lett **61**, 1097 (1988).

[141] H. Ritsch, and P. Zoller, Phys. Rev. A **38**, 4657 (1988).

[142] V. Hakim and V. Ambegaokar, Phys. Rev. A**32**, 423 (1985).

[143] C. Kittel, *Introduction to Solid State Physics*, Sixth Edition, Wiley, 1986).

[144] H. Ibach and H. Luth, *Solid State Physics: An introduction to Theory and Experiment*, (Springer-Verlag, 1990).

[145] H. Haken, *Quantum Field Theory of Solids: An Introduction*, (North-Holland, 1976).

[146] S. Datta, *Quantum Phenomena*, (Volume VIII, Modular Series on Solid States Devices, edited by R. Pierret, G. Neudeck, Addison-Wesley, 1989).

[147] W. J. Munro and C. W. Gardiner, submitted to Phys. Rev. A

[148] G. E. Uhlenbeck and L. S. Ornstein, Phys. Rev. **36**, 823 (1930).